THE UNIVERSITY OF CHICAGO

NONRECIPROCITY, SYMMETRIES, AND DIAGONALIZATION IN OPEN QUANTUM SYSTEMS

A DISSERTATION SUBMITTED TO
THE FACULTY OF THE DIVISION OF THE PHYSICAL SCIENCES
IN CANDIDACY FOR THE DEGREE OF
DOCTOR OF PHILOSOPHY

DEPARTMENT OF PHYSICS

BY
ALEXANDER MCDONALD

CHICAGO, ILLINOIS
AUGUST 2022

To Matt, whose light always shone bright, even during the darkest of times.

CONTENTS

LIST OF FIGURES

ACKNOWLEDGMENTS

I would like to first and foremost thank my advisor Aash for his guidance, patience and supervision. His approach to science, eagerness to learn, and passion for physics is something I truly admire. His ability to maintain a hands-on research style regardless of group size is remarkable. Recognizing to what extent my capabilities as a writer, public speaker, and physicist have grown as a direct result of the feedback he provides has been very gratifying. Its been an incredible six years, and although it is coming to an end, what I have learned from Aash will undoubtedly stay with me throughout my career. Thank you.

I am grateful to my committee members, Vincenzo, Peter, and Liang, both for their time and feedback they have provided these past years. Putri's help in making sure my thesis submission went smoothly is greatly appreciated, as her quick response to emails has saved me much undue stress.

I would like to express my gratitude to the graduate students and postdocs in Aash's group Yu-Xin, David, Andrew L., Kero, Peter, Setiawan, Martin and Alireza. Not only are they all friendly and passionate about their work, but they have had to endure both my bad jokes and gripes about non-Hermitian Hamiltonians for longer than any person should. I am especially grateful to Ryo, Orazio, and Gideon, all of whom I have had the pleasure of working with directly with, and am especially proud of the science we produced together.

I am thankful for the numerous friends I made during my time at the University of Chicago. In particular I would like to thank Dan, Anora, Sharba, Syrian, Jan and Joe for their companionship. I am grateful to Amanda and Jordan, without whom I would not have a coveted Univesrity of Chicago intramural champion t-shirt. Many thanks to Meg and Gabrielle, my co-coordinators for Forget the Year 2019. Their dedication and efforts to the show are what made it a resounding success. I would like to thank Andrew P. and Anchita both for their friendship and willingness to play ping-pong at a moments notice. I am deeply grateful to Jon and Chloe for their support, warmth and kindness. Their friendship means

the world to me, and I am forever indebted to them for the role they played in making my graduate school experience a positive on. Its crazy to think that a random TA assignment sparked lifelong friendships.

I would like to thank my friends back home Erik, JP, Mart, GB, Chris, Andy, Justin, Émilie and baby Jude. Whenever we get together, regardless of how long it has been since we last saw each other, it feels like no time has passed since our high school and university days. Our friendship has and will persist regardless of physical separation and the realities of daily life, for which I am thankful. There really are no friends like old friends.

I am eternally grateful to my wonderful family, whom I love with all my heart. I never would have come this far without them. I am thankful for my parents, who have always had the best interest of their children at heart. They consistently do whatever it takes to makes us happy, successful and ease life's many burdens. My twin sister and best friend Laura deserves an endless amount of thanks. She consistently brightens my life with her warmth, joie de vivre and sense of humor. Further, her perseverance and resolve in the face of painful and seemingly-insurmountable obstacles is an inspiration to all who know her. I am truly blessed to know that my family will always be there for me.

ABSTRACT

Many familiar notions of classical physics are supplanted by new concepts and intuition in quantum mechanics. This goes doubly so for open quantum systems, where coupling to an external environment leads to the irreversible loss of quantum information. In this thesis, we investigate how non-reciprocity, symmetries and diagonalization procedures in open quantum systems are different than their classical or closed-system counterparts.

We first show that non-reciprocity, the tendency for particles to propagate in a preferred direction, can be used to build a quantum sensor whose signal-to-noise ratio grows exponentially with the size of the sensor. Non-reciprocity also has a marked effect on the quantum steady state of tight-binding models; we find for a representative model that the steady state occupation is characterized by a surprising macroscopically-large length scale.

Shifting gears, we then demonstrate how to diagonalize a large class of Lindbladians, the open quantum system equivalent of a Hamiltonian. We first reformulate third quantization, a technique that is used to diagonalize quadratic Lindbladians. Not only do we make the procedure more physically transparent, but we show that is naturally related to Keldysh field theory, a much more widely-used tool. Finally, we use this technique to show how so-called weak symmetries can be used to diagonalize strongly-interacting dissipative quantum models, despite there being no associated conserved quantities.

CHAPTER 1

INTRODUCTION

This thesis contains a slightly diverse collection of works which are thematically unified asking to what extent quantum mechanics changes in an open-system setting. This is of course a very broad question, and we thus focus on two more concrete topics.

The first two chapters are concerned with quantum non-reciprocity, which for the purposes of this thesis can be defined as the asymmetric spatial propagation of particles. One of the main aims of these chapters is to convince the reader that the seemingly-bizarre properties of non-reciprocity can be explained by thinking about the dynamics of the system as a whole, instead of focusing solely on usual spectral properties such as eigenvalues or eigenvectors like one would in closed systems.

The last two chapters are focused on diagonalizing a Lindbladian of an open quantum systems using either so-called weak symmetries or hidden symmetries of linear quantum systems. The upshot of these works is that even fully quantum models which can be diagonalized in this manner have a surprising connections to well-known classical concepts. The hope is that these works can serve as a starting point to explore more complicated quantum models using e.g. Lindblad perturbation theory.

Each chapter is a self-contained body of work and can be read separately. The organization and content of each chapter is as follows.

Chapter 2 is a paper that attempts to build a useful quantum sensor using non-reciprocity as a resource. Remarkably, we show that one can build a sensor whose signal-to-noise ratio is exponentially-large in system size even if one constrains the total number of photons used to make the measurement. We discuss non-Markovian and non-perturbative effects to the sensing protocol, demonstrating that one still obtains a parametrically-larger advantage over conventional schemes.

Chapter 3 is a paper that shows that the steady state of quantum non-Hermitian tight-

binding model can not simply be understood simply in terms of the spectral information of the underlying non-Hermitian Hamiltonian. For example, we show that the steady state of a quantum realization of the Hatano-Nelson model is described by a macroscopic length scale which is completely different than the localization length of the eigenvectors.

Chapter 4 is a paper that demonstrates that continuous weak symmetries can be used to analytically diagonalize the Lindbladian of a class of open quantum systems. Although weak symmetries do not have a conserved quantities due to the open nature of the problem, we identify a generic structure which nevertheless allows for an exact description of the dissipative eigenvectors and eigenvalues. Our method effectively show a mean-field ansatz becomes exact in this models, and can analogously be understood as a kind of classical-to-quantum mapping.

Chapter 5 is a paper in which we reformulate a well-known technique used to diagonalize quadratic Lindbladians known as third quantization. Our method reveals a surprising symmetry of *all* linear quantum master equations allows one to "gauge" away fluctuations, recovering a result that is well known in a classical setting. We further show that our reformulation allows one to make connections to other well-known open quantum system approaches such as Keldysh field theory and phase-space-based methods.

CHAPTER 2

EXPONENTIALLY-ENHANCED QUANTUM SENSING WITH NON-HERMITIAN LATTICE DYNAMICS

2.1 Overview of Results

Non-Hermitian systems exhibit markedly different phenomena than their conventional Hermitian counterparts. Several such features, such as the non-Hermitian skin effect, are only present in spatially extended systems. Potential applications of these effects in many-mode systems however remains largely unexplored. Here, we study how unique features of non-Hermitian lattice systems can be harnessed to improve Hamiltonian parameter estimation in a fully quantum setting. While the quintessential non-Hermitian skin effect does not provide any distinct advantage, alternate effects yield dramatic enhancements. We show that certain asymmetric non-Hermitian tight-binding models with a $\mathbb{Z}_2$ symmetry yield a pronounced sensing advantage: the quantum Fisher information per photon increases exponentially with system size. We find that these advantages persist in regimes where non-Markovian and non-perturbative effects become important. Our setup is directly compatible with a variety of quantum optical and superconducting circuit platforms, and already yields strong enhancements with as few as three lattice sites.

2.2 Introduction

Quantum metrology and sensing aim to improve measurement precision over classical devices by exploiting uniquely quantum phenomena such as entanglement and squeezing [42, 29, 106]. It is interesting to ask whether distinct effects associated with non-Hermitian dynamics can

also be used to improve sensors operating in quantum regimes [67, 68, 148, 25, 97]. In purely classical settings, mode degeneracies specific to non-Hermitian systems (so-called exceptional points) have been suggested as a means for enhanced parametric sensing [138]. Evidence for enhancement has been demonstrated in several classical-domain experiments involving small coupled mode systems (see e.g. Refs. [26, 54, 140, 66]). Theory suggests that particular kinds of non-Hermitian effects could also be useful in truly quantum settings [68].

To date, both theory and experiment have focused on non-Hermitian sensing schemes that utilize at most a few coupled modes. It is however well known that unusual new phenomena appear when considering genuinely multi-mode non-Hermitian dynamics. The paradigmatic example is the so-called "non-Hermitian skin effect" [145, 70, 85], which occurs in several non-Hermitian tight-binding models [141, 69, 61]. In these systems, all eigenvalues and wavefunctions of the Hamiltonian exhibit a dramatic sensitivity to a change of boundary conditions. This extreme sensitivity would seem to be a potentially powerful resource for parametric sensing [120].

In this work, we show that non-Hermitian lattice dynamics does indeed provide a unique means for constructing enhanced sensors; moreover, this advantage persists even when operating in truly quantum regimes. We study in detail Hamiltonian parameter estimation using a one-dimensional lattice model with asymmetric tunneling (akin to the well-studied Hatano-Nelson model [49]). We find, somewhat surprisingly, that the non-Hermitian skin effect does not provide any advantage over more traditional sensing protocols. Rather, we find another distinct non-Hermitian mechanism that enables a dramatic enhancement of measurement sensitivity: the quantum Fisher information per photon exhibits an exponential scaling with system size. As we discuss, the underlying mechanism makes use of both non-reciprocity and an unusual kind of symmetry breaking.

While our ideas are general, our analysis focuses on a system that uses parametric driving to realize non-Hermitian dynamics; this has the strong advantage of not requiring any

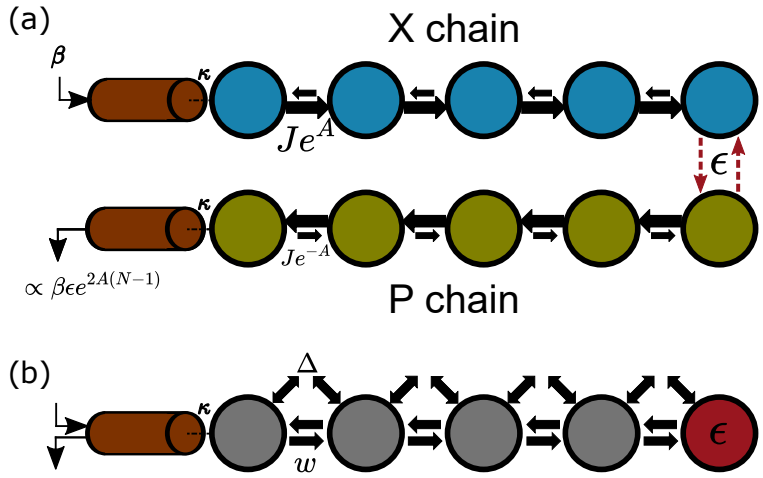

Fig. 2.1: (a) Basic lattice sensor: two N-site non-Hermitian tight binding chains, each with opposite chirality. Each chain has asymmetric hopping: for the top (bottom) chain, hopping to the right is a factor of e^{2A} larger (smaller) than hopping to the left. The two lattices are only coupled via a weak symmetry breaking perturbation ϵ on the rightmost site; the goal is to estimate ϵ. A signal entering the top X chain induces an exponentially large output in bottom P chain, but only if $\epsilon \neq 0$. (b) An array of bosonic cavities coupled via nearest neighbour hopping w and coherent two-photon drive Δ with a small detuning ϵ on the last site. This provides a dissipation-free realization of the setup in (a), where the canonical quadratures $\hat{x}$ and $\hat{p}$ play the role of the top and bottom chains respectively. This system yields an exponentially enhanced SNR even when quantum noise effects are included.

external dissipation or post-selection [85, 136]. Further, we ultimately focus on dispersive sensing, where the parameter of interest shifts the frequency of a resonant mode. This is a ubiquitous sensing strategy, with applications ranging from superconducting qubit measurement [14] to virus detection [135]. Our proposal is also compatible with a number of different experimental platforms in superconducting quantum circuits and quantum optics, and ultimately requires one to make a standard homodyne measurement. We also consider physics that goes beyond the usual limit of strictly infinitesimal parameter sensing. We find that the exponential enhancement of measurement sensitivity persists even when considering limitations associated with the finite propagation time of a large lattice. Even for parameters large enough to invalidate a full linear response analysis, we find that our scheme provides a strong advantage: it achieves a square-root enhancement of the sensitivity (including noise effects). This is similar to what is found in exceptional point sensors in the absence of noise

[138]. Finally, while our discussion focuses on large lattices, the results we present are already interesting in a small system consisting of just three coupled resonators.

2.3 Ingredients for a non-Hermitian lattice sensor

2.3.1 Amplified non-reciprocal response in the Hatano-Nelson model

A key feature that we will exploit in our new sensor is the dramatically large and unidirectional response exhibited by certain non-Hermitian lattice models: perturbing a single lattice site induces a large change at one end of the chain, but not the other (see e.g. [120, 137]). We start by providing a physically-transparent explanation of this effect, based on interpreting non-Hermitian asymmetry in tight-binding matrix elements as directional gain and loss.

The simplest relevant system is the well-known Hatano-Nelson model [49, 48]. This is a 1D tight-binding chain with asymmetric nearest-neighbour hoppings

$$\hat{H} = iJ \sum_n \left(e^{A} \left| n+1 \right\rangle\!\left\langle n \right| - e^{-A} \left| n \right\rangle\!\left\langle n+1 \right| \right) \tag{2.1}$$

where J, A are real and $|n\rangle$ is a position eigenket. The corresponding single-particle Schrödinger equation is ($\hbar = 1$ throughout)

$$\dot{\psi}_n = Je^{A}\psi_{n-1} - Je^{-A}\psi_{n+1}, \tag{2.2}$$

where $\psi_n = \langle n|\psi\rangle$. While A formally plays the role of an imaginary vector potential, it is more usefully thought of as an amplification factor. Assuming A is positive for definiteness, Eq. (2.2) describes a system where a wavefunction's amplitude grows by e^{A} every time a particle hops one site to the right, and decays an equal amount e^{-A} as it travels to the left, regardless of its energy.

With this picture in mind, the form of the real-space susceptibility (i.e. single particle Green's function) $\chi(n, m; t)$ for a finite open chain has an intuitive form. Letting $|m(t)\rangle = e^{-i\hat{H}t}|m\rangle$, a simple calculation yields (see App. 2.9.2):

$$\chi(n, m; t) \equiv \langle n|m(t)\rangle = e^{A(n-m)}\chi_0(n, m; t). \tag{2.3}$$

Here, $\chi_0(n, m; t)$ is the susceptibility matrix when $A = 0$, i.e. the Green's function of a Hermitian tight-binding chain. This quantity is reciprocal, in the sense that $\chi_0(n, m; t) = (-1)^{m-n}\chi_0(m, n; t)$ (i.e. apart from a phase, there is no asymmetry in rightwards versus leftwards propagation). The Green's function $\chi_0(n, m; t)$ both describes how particles propagate in the lattice, and also the response properties of the system (i.e. if you perturb site m at $t = 0$, how does site n respond at some later time?).

The simple factorization in Eq. (2.3) makes it clear that there are two basic processes determining the response. The first is a distance and direction-dependent amplification / deamplification factor, whereas the second encodes the dynamics of the underlying ($A = 0$) Hermitian tight-binding model. We thus have a simple intuitive picture for the susceptibility, without having to make recourse to other seemingly more complicated non-Hermitian features, such as exceptional points, the non-Hermitian skin effect, or the Petermann factor [105, 44]. Note that Eq. (2.3) can be easily derived via a similarity transformation, which is analogous to the gauge transformation one would make if A were imaginary (and hence a real synthetic gauge field) [49, 48].

2.3.2 $\mathbb{Z}_2$ symmetry in non-Hermitian lattice models

The second basic ingredient we will exploit in constructing our sensor is symmetry breaking. The Hatano-Nelson chain breaks reciprocity for any $A \neq 0$; formally, it picks a preferred amplification direction, and does not remain invariant (up to a local gauge change) under a

spatial inversion operation $|n\rangle \to |-n\rangle$. We can trivially restore this symmetry by considering a system with *two* uncoupled Hatano-Nelson chains indexed by $\sigma = \uparrow, \downarrow$ with amplification factors $A_\uparrow, A_\downarrow$. If we pick $A_\uparrow = -A_\downarrow$, then the composite system restores some of the lost symmetry. Formally, the two-chain system is invariant up to a local gauge change under the combined operations $|n\rangle \to |-n\rangle$ (spatial inversion) and $\sigma \to \bar{\sigma}$ (pseudospin inversion). While this may seem trivial, this kind of discrete symmetry can persist even for certain forms of interchain coupling, and has recently been interpreted as a formal $\mathbb{Z}_2$ symmetry class with its own distinct non-Hermitian topological phenomena [101]. We discuss this symmetry more formally in Appendix 2.9.1.

For our purposes, the interesting feature here will be to consider *breaking* this symmetry with an external perturbation whose magnitude we wish to estimate. As we will see, the response to this symmetry breaking can be exponentially large in system size, enabling a new kind of sensor.

2.4 Model and Measurement Protocol

With the motivation of the previous section, we now consider a sensor comprised of two Hatano-Nelson chains with an opposite chirality (see Fig. 2.1(a)). There are a variety of means for such realizing non-Hermitian directional tight-binding models using dissipation [89, 92]; approaches based on feedback control are also possible and have been recently implemented [16]. However, for optimal sensing properties in quantum settings, methods that are both autonomous and avoid the noise associated with dissipation are desirable. We thus focus on a dissipation-free method for realizing non-Hermitian dynamics based on parametric driving [85, 136]. We stress that the response properties of our sensor will be independent of how the non-Hermitian dynamics is implemented, and hence apply equally well to dissipative and feedback based strategies.

We consider an N-site chain of driven, coupled bosonic modes described by the fully

Hermitian Hamiltonian

$$\hat{H}_B = \sum_{n=1}^{N-1} \left(iw\hat{a}_{n+1}^\dagger \hat{a}_n + i\Delta \hat{a}_{n+1}^\dagger \hat{a}_n^\dagger + h.c. \right). \tag{2.4}$$

Here $\hat{a}_j$ is the photon annihilation operator on site j, w is the nearest-neighbour hopping term, Δ is the nearest-neighbour two-photon drive, and we consider open boundary conditions. We take both w and Δ to be positive and $w > \Delta$. This model describes a 1D cavity array subject to parametric drives on each bond (described in a rotating frame set by the external pump frequency). As discussed extensively in Ref. [85], this system could be realized in both quantum superconducting circuits or nonlinear quantum optical systems. Note the lack of any on-site terms corresponds to the parametric driving frequency matching the resonance frequency of each isolated cavity.

Although not immediately obvious, the dynamics generated by $\hat{H}_B$ corresponds to two copies of the Hatano-Nelson model. In the basis of local canonical quadrature operators $\hat{x}_j$ and $\hat{p}_j$, defined via $\hat{a}_j = (\hat{x}_j + i\hat{p}_j)/\sqrt{2}$, the Hamiltonian reads

$$\hat{H}_B = \sum_{n=1}^{N-1} \left(-(w-\Delta)\hat{x}_{n+1}\hat{p}_n + (w+\Delta)\hat{p}_{n+1}\hat{x}_n \right). \tag{2.5}$$

This then yields the Heisenberg equations of motion

$$\dot{\hat{x}}_n = Je^{A}\hat{x}_{n-1} - Je^{-A}\hat{x}_{n+1}, \tag{2.6}$$

$$\dot{\hat{p}}_n = Je^{-A}\hat{p}_{n-1} - Je^{A}\hat{p}_{n+1}, \tag{2.7}$$

where the effective hopping amplitude J and imaginary vector potential A are related to w

and Δ by

$$J = \sqrt{w^2 - \Delta^2}, \tag{2.8}$$

$$e^{2A} = \frac{w + \Delta}{w - \Delta}. \tag{2.9}$$

Comparing against Eq. (2.2), we see that the dynamics of each canonical quadrature corresponds to that of a Hatano Nelson model, with opposite chiralities for $\hat{x}$ and $\hat{p}$ (Fig. 2.1). These orthogonal quadratures correspond to different phases of photonic excitations, and hence the system exhibits phase-dependent non-reciprocal amplification [85]. Note that there is a constraint on our mapping: the complex wavefunction amplitudes in the Hatano-Nelson model have been replaced by Hermitian quadrature operators in our system. This will play no role in what follows.

We now demonstrate how this setup can be used for Hamiltonian parameter estimation. We add a Hermitian perturbation $\epsilon\hat{V}$ to our Hamiltonian where $\hat{V}$ is some system operator; the goal is to estimate ϵ. We also couple the first site of our lattice to an input-output waveguide as a means to probe its properties. The simplest protocol is to use this waveguide to drive the system with a classical tone (i.e. a coherent state), and then measure the outgoing light in the waveguide (see Fig. 2.1(b)). The full Hamiltonian becomes

$$\hat{H}[\epsilon] = \hat{H}_B + \epsilon\hat{V} + \hat{H}_\kappa - i\sqrt{\kappa}\left(\hat{a}_1^\dagger\beta - h.c.\right) \tag{2.10}$$

$\hat{H}_\kappa$ describes damping of the first site at a rate κ, due to coupling to the modes of the waveguide which we treat using standard input-output theory [27]. The last term corresponds to a classical drive with amplitude $\beta = |\beta|e^{i\theta}$. Note that we take the drive frequency to match the resonance frequency of the isolated cavities; this frequency is zero in our rotating frame.

Using the standard input-output boundary condition, the output field in the waveguide

is given by

$$\hat{B}^{(\mathrm{out})}(t) = \left(\beta + \hat{B}^{(\mathrm{in})}(t)\right) + \sqrt{\kappa}\hat{a}_1(t) \tag{2.11}$$

where $\hat{B}^{(\mathrm{in})}$, the operator equivalent of Gaussian white noise, describes the noise entering the lattice through the waveguide. Our goal is to estimate ϵ by making an optimal measurement of the output field. In what follows, we take ϵ to have units of frequency and $\hat{V}$ to be dimensionless.

We further specialize to the usual case where ϵ is so small that it can only be estimated by integrating the output field over a long timescale τ. If we turn on the drive tone at $t = 0$, the relevant temporal mode of the output field to consider is

$$\hat{\mathcal{B}}_\tau(N) = \frac{1}{\sqrt{\tau}} \int_0^\tau dt \hat{B}^{(\mathrm{out})}(t) \tag{2.12}$$

Note that this is a canonical bosonic lowering operator satisfying $[\hat{\mathcal{B}}_\tau(N), \hat{\mathcal{B}}_\tau^\dagger(N)] = 1$. We write an explicit dependence on the chain size N, as we will be interested in understanding how things scale as N is increased.

The maximum amount of information available in $\hat{\mathcal{B}}_\tau(N)$ on ϵ is quantified by the quantum Fisher information (QFI). The QFI provides a lower bound on the root mean square error of any (unbiased) estimate of ϵ regardless of how $\hat{\mathcal{B}}_\tau(N)$ is measured [42]. Calculation of the QFI unfortunately does not in general tell one the form of the optimal measurement. However, in our linear Gaussian system, things are much simpler: for large $|\beta|$, the optimal measurement will always correspond to a standard homodyne measurement [9, 107]. The relevant Hermitian measurement operator has the form

$$\hat{M}_\tau(N) = \frac{1}{\sqrt{2}} \left(e^{-i\phi}\hat{\mathcal{B}}_\tau(N) + e^{i\phi}\hat{\mathcal{B}}_\tau^\dagger(N)\right), \tag{2.13}$$

i.e. a quadrature of the output operator $\hat{\mathcal{B}}_\tau(N)$ along a direction in phase space determined by the angle ϕ.

We will focus throughout on the large-drive limit, and will be interested in characterizing the QFI to leading order in $|\beta|$. In this limit, QFI is determined by the statistics of $\hat{M}_\tau(N)$ via [68, 9]

$$\mathrm{QFI}_\tau(N) = \max_\phi \left[\lim_{\epsilon \to 0} \left(\frac{1}{\epsilon} \frac{\mathcal{S}_\tau(N,\epsilon)}{\mathcal{N}_\tau(N,\epsilon)} \right)^2 \right], \tag{2.14}$$

where

$$\mathcal{S}_\tau(N,\epsilon) = |\langle \hat{M}_\tau(N) \rangle_\epsilon - \langle \hat{M}_\tau(N) \rangle_0|, \tag{2.15}$$

$$\mathcal{N}_\tau(N,\epsilon) = \sqrt{\langle \hat{M}_\tau^2(N) \rangle_\epsilon - \langle \hat{M}_\tau(N) \rangle_\epsilon^2}, \tag{2.16}$$

are the signal and the noise respectively associated with the measurement. Here, $\langle \cdot \rangle_z$ means an average with respect to a state whose dynamics are governed by $\hat{H}[z]$.

This expression for the QFI coincides with the SNR of an optimal homodyne measurement, and scales as $|\beta|^2$; the next-leading order term is independent of $|\beta|$. Note that the QFI only depends on the noise $\mathcal{N}_\tau(N,\epsilon)$ calculated to zeroth order in ϵ. We stress that the expression for the QFI still depends on the drive phase θ as well as the form of the operator $\hat{V}$; in what follows, we will be interested in optimizing these as well.

Given its role as a fundamental performance metric, it is tempting to declare that a better sensor has been built if it increases the QFI. Different measurement strategies however use resources differently, and one must carefully consider which to constrain when making comparisons. In our case, we wish to distinguish a true sensing enhancement from a more trivial effect, where a different protocol simply results in there being more photons in the system available to interact with the perturbation $\hat{V}$ (as occurs with standard exceptional-point based sensing schemes [68, 148]). For this reason, we will take as the relevant metric

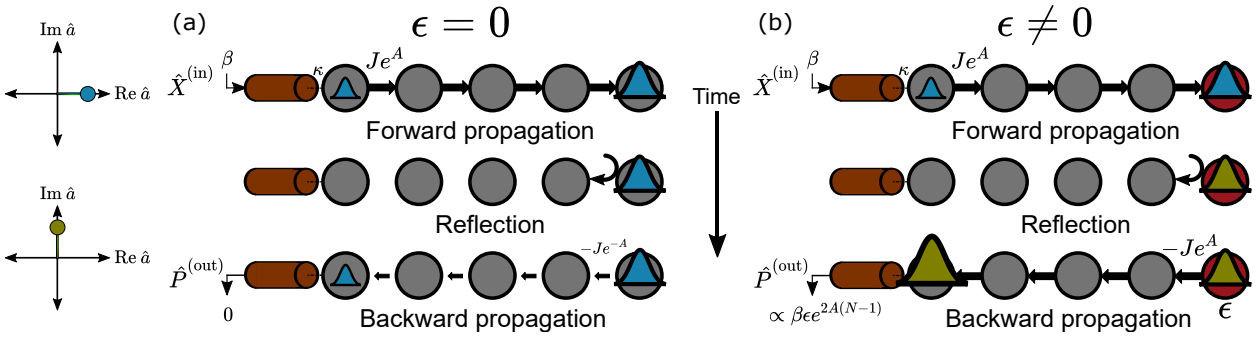

Fig. 2.2: Schematic of measurement dynamics. A classical drive is injected into the leftmost lattice site via a waveguide (coupling rate κ). The drive amplitude is real (blue wavepacket), corresponding to an $\hat{x}$ quadrature excitation. As the wavepacket propagates rightwards, its amplitude grows $\propto e^{A(N-1)}$ until it reaches the last site N. (a) If $\epsilon = 0$, the wavepacket scatters off the open boundary without changing quadrature. It is thus *deamplified* as it propagates back to the first site. As a result, for $\epsilon = 0$ there is no amplification of the drive or of injected noise. (b) For non-zero ϵ, a wavepacket can scatter of the boundary and change quadrature (olive wavepacket). It then is *also* amplified as it propagates back to the waveguide, and leaves the waveguide with a net amplification factor $e^{2A(N-1)}$. The result is a SNR and quantum Fisher information which grow exponentially with system size even when the total intracavity photon number is held fixed.

the QFI scaled by the *total* average photon number $\bar{n}_{\mathrm{tot}}$ [68]:

$$\bar{n}_{\mathrm{tot}} \equiv \sum_n \langle \hat{a}_n^\dagger \hat{a}_n \rangle_0 \simeq \sum_n \langle \hat{a}_n^\dagger \rangle_0 \langle \hat{a}_n \rangle_0 \propto |\beta|^2/\kappa. \tag{2.17}$$

As we consider throughout the large-drive limit, we only keep the leading-order-in-β contribution to $\bar{n}_{\mathrm{tot}}$. This is simply the photon number associated with the drive-induced displacement of each cavity annihilation operator. The additional contribution to $\bar{n}_{\mathrm{tot}}$ due to amplification of vacuum fluctuations is β-independent, hence plays no role in the large-drive limit we consider (see Appendix 2.9.4).

2.5 Exponential SNR and QFI enhancement

We now focus on computing the optimal SNR of the measurement operator $\hat{M}_\tau(N)$ for our N site chain in the $\epsilon \to 0$ limit; via Eq. (2.14), this directly yields the QFI. In this limit, an

SNR ~ 1 will only be achieved for τ much longer than any internal dynamical timescale. We thus consider the long-τ limit, effectively ignoring any transient behaviour and assuming the system is in its steady state. Note that our system is dynamically stable as long as $w > \Delta$ and $\kappa > 0$, ensuring that a steady state exists.

From Eqs. (2.15),(2.13) and (2.11), the first order in ϵ in this limit reads

$$\mathcal{S}_\tau(N,\epsilon) = \sqrt{2\kappa\tau}\left|\,\mathrm{Re}[e^{-i\phi}\delta\langle\hat{a}_1\rangle^{\mathrm{SS}}]\right| \tag{2.18}$$

where

$$\delta\langle\hat{a}_1\rangle^{\mathrm{SS}} \equiv \epsilon \lim_{\epsilon\to 0}\left(\frac{\langle\hat{a}_1\rangle_\epsilon^{\mathrm{SS}} - \langle\hat{a}_1\rangle_0^{\mathrm{SS}}}{\epsilon}\right) \tag{2.19}$$

is the steady state linear response of the site-1 average amplitude to a non-zero ϵ. This response will be determined by the zero-frequency susceptibilities (Green's functions) of the unperturbed system.

It will be convenient to split up $\delta\langle\hat{a}_1\rangle_\epsilon^{\mathrm{SS}}$ into its real and imaginary parts, or equivalently to think of the dynamics in the quadrature picture. There are then four different types of susceptibilities: $\chi^{\alpha\beta}[n,m;\omega]$ is the response of the α quadrature on site n to a force which directly drives the β quadrature on site m. From Eqs. (2.6)-(2.7) and Eq.(2.3), we find that the $\epsilon = 0$ susceptibilities are

$$\chi^{xx}[n,m;\omega] = e^{A(n-m)}\tilde{\chi}^{xx}[n,m;\omega], \tag{2.20}$$

$$\chi^{pp}[n,m;\omega] = e^{-A(n-m)}\tilde{\chi}^{pp}[n,m;\omega], \tag{2.21}$$

$$\chi^{xp}[n,m;\omega] = \chi^{px}[n,m;\omega] = 0. \tag{2.22}$$

Here $\tilde{\chi}^{\alpha\beta}[n,m;\omega]$ the susceptibility of a Hermitian N site tight-binding chain with hopping iJ and amplitude decay rate $\kappa/2$ on the first site (see Appendix 2.9.3). The above structure reflects the fact that the dynamics of the $\hat{x}$ and $\hat{p}$ quadratures correspond to two uncoupled

copies of the Hatano-Nelson chain with opposite signed imaginary vector potential A. Hence, $\hat{x}$ quadrature signals are amplified as they propagate to the right, and deamplified as they traverse to the left, while the opposite is true for $\hat{p}$ quadrature signals. Note that if we started with two explicit Hatano-Nelson chains, the discussion here would be identical; x and p would then just index the two different chains.

To proceed, we need to specify the form of the perturbation Hamiltonian $\hat{V}$. Our system exhibits the the non-Hermitian skin effect (NHSE), implying a strong sensitivity to changes in boundary conditions. As the unperturbed system is an open chain, this suggests that an optimal $\hat{V}$ would induce tunneling between the first and last site, i.e.

$$\hat{V}_{\text{NHSE}} = e^{i\varphi}\hat{a}_1^\dagger \hat{a}_N + e^{-i\varphi}\hat{a}_N^\dagger \hat{a}_1, \tag{2.23}$$

with φ an arbitrary phase. As we show in Appendix 2.9.5, this choice of $\hat{V}$ does not result in an enhanced sensitivity if one uses the proper metric of $\text{QFI}/\bar{n}_{\text{tot}}$ (or equivalently $\text{SNR}/\sqrt{\bar{n}_{\text{tot}}}$). While the signal produced by $\hat{V}_{\text{NHSE}}$ is large, this is simply because our system is an amplifier with a large end-to-end gain. The number of photons on the last site (and hence $\bar{n}_{\text{tot}}$) will be amplified equally by this gain. As a result, $\text{QFI}/\bar{n}_{\text{tot}}$ does not show any enhancement as one increases the system size N, nor any enhancement over a conventional, single-cavity dispersive detector. We are thus left with a depressing conclusion: the non-Hermitian skin effect does not provide any true advantage in sensing. Note also that $\hat{V}_{\text{NHSE}}$ does not break the $\mathbb{Z}_2$ symmetry of the unperturbed system (see App. 2.9.1).

Luckily, this is not the end of the story. Enhanced sensing is possible with our system, if we chose a $\hat{V}$ that fully exploits the opposite chiralities of our two (effective) Hatano-Nelson chains. Consider the innocuous-looking purely local perturbation

$$\hat{V}_N = \hat{a}_N^\dagger \hat{a}_N, \tag{2.24}$$

so that ϵ now corresponds to a small change in the resonance frequency of the last site. This perturbation does indeed break the $\mathbb{Z}_2$ symmetry of the unperturbed system. To understand how $\hat{V}_N$ affects the dynamics of the lattice, it is best to re-examine the equations of motion in the $\hat{x}$ and $\hat{p}$ basis. They remain the same everywhere except the last site N, where they now read

$$\dot{\hat{x}}_N = Je^{A}\hat{x}_{N-1} + \epsilon\hat{p}_N, \tag{2.25}$$

$$\dot{\hat{p}}_N = Je^{-A}\hat{p}_{N-1} - \epsilon\hat{x}_N. \tag{2.26}$$

Recall that without the perturbation present, the dynamics of the $\hat{x}$ and $\hat{p}$ quadratures are completely independent (c.f. Eqs. (2.6) and (2.7)). The dispersive shift ϵ on site N now effectively couples the two non-Hermitian chains, thereby breaking phase-dependent non-reciprocity (see Fig. 2.1). While the intuitive picture of directional amplification remains unchanged in the rest of the lattice, a wavepacket with a well defined global phase can now scatter off of the perturbation ϵ and change its phase in the process. The role of ϵ is reminiscent to that of a magnetic impurity in the quantum spin Hall effect: in both cases the propagation direction of a particle is determined by some internal degree of freedom, which the impurity can change [80].

We next judiciously choose the phase of the drive β to be real and the measurement angle $\phi = \pi/2$. Equivalently, we apply a driving force $-\sqrt{2\kappa}|\beta|$ to $\hat{x}_1$ and consider the corresponding response of its canonically conjugate quadrature $\hat{p}_1$. When $\epsilon = 0$, this off-diagonal susceptibility vanishes, see Eq.(2.22). To first order in ϵ, it becomes non-zero. We further take N to be odd in what follows, as this guarantees (via the chiral symmetry of our unperturbed system) that the lattice will have a resonant mode at zero frequency. This then provides a further resonant enhancement of our system's zero frequency response properties. Note that for an even N, we would still have the same exponential enhancement quoted in Eqs. (2.20)-(2.21); in this case however, there is no resonant mode at zero frequency, causing

a suppression of susceptibilities by a multiplicative factor of $\kappa/(2J)$ (see Eqs.(2.97)-(2.98)).

With these optimized choices, first order perturbation theory yields:

$$\begin{aligned}\mathcal{S}_\tau(N,\epsilon) &= \sqrt{\kappa\tau}|\sqrt{2\kappa}\beta|\Big(|\delta\chi^{px}[1,1;0]|\Big)\\ &= \sqrt{2\kappa\tau}\sqrt{\kappa}|\beta|\Big(|\chi^{pp}[1,N;0]\epsilon\chi^{xx}[N,1;0]|\Big)\\ &= \sqrt{8\kappa\tau\bar{n}_N}\left|\frac{\epsilon}{\kappa}\right|e^{A(N-1)}. \end{aligned} \tag{2.27}$$

Here $\bar{n}_N$ denotes the leading-order-in-β average photon number of the last site in the lattice, and is given by:

$$\bar{n}_N = |\langle\hat{a}_N\rangle_0^{ss}|^2 = \kappa|\beta|^2|\chi^{xx}[N,1,0]|^2 \propto e^{2A(N-1)} \tag{2.28}$$

For large A, the average photon number on site N is exponentially larger than that on other sites. Writing $\bar{n}_N = Z(A)\bar{n}_{\text{tot}}$ we have $Z(A) = 1 - \mathcal{O}(e^{-4A})$ (see App. 2.9.4). We thus obtain:

$$\mathcal{S}_\tau(N,\epsilon) = \sqrt{8Z(A)\kappa\tau\bar{n}_{\text{tot}}}\left|\frac{\epsilon}{\kappa}\right|e^{A(N-1)}. \tag{2.29}$$

Eq. (2.29) is a central result of this work: it shows that even when the total photon number $\bar{n}_{\text{tot}}$ is held fixed, our system exhibits a signal power that grows exponentially with system size.

For an intuitive picture, consider the propagation of x-quadrature photons injected from the waveguide into site 1, as depicted in Fig. 2.2. These photons will propagate to the last site N, with an amplitude $\chi^{xx}[N,1;\omega] \propto e^{A(N-1)}$. Photons that then scatter off the perturbation $\epsilon\hat{V}_N$ will change phase, so that they now correspond to the p quadrature (c.f. Eq. (2.26)). They can then propagate back to the first lattice site with an amplitude $-\epsilon\chi^{pp}[1,N;\omega] \propto e^{A(N-1)}$. This simple scattering process (involving both x and p quadrature propagation) leads to a parametrically large signal in $\hat{p}_1$.

The above heuristic picture also explains why the signal is amplified more than the

average photon number $\bar{n}_{\text{tot}}$: the average photon number only involves amplification along one traversal of the chain, whereas the signal magnitude involves two traversals (forward and back). This directly explains the extra large factor of $e^{A(N-1)}$ in Eq. (2.29). We stress that this exponential signal enhancement would also occur in dissipative realizations of our doubled Hatano-Nelson chain.

The final step in characterizing our sensor is to examine its noise properties. Naively, one might expect that the same dynamics responsible for our signal enhancement would also exponentially amplify fluctuations in the output field. This is not the case: as already discussed, calculating the QFI only requires computing the noise to zeroth order in ϵ, see Eq.(2.14). Without the perturbation, the two effective Hatano-Nelson chains are completely decoupled. Thus, any noise entering through the waveguide will undergo equal amounts of amplification and deamplification before exiting the lattice. For the ideal case of zero internal loss, this means that the noise temperature of the output field will be identical to that of the input field. As a result, the noise in the homodyne current is

$$\mathcal{N}_\tau(N,0) = \sqrt{\bar{n}_{\text{th}} + \frac{1}{2}} \tag{2.30}$$

with $\bar{n}_{\text{th}}$ representing the number of thermal quanta in the input field.

Combining these two results, our signal-to-noise ratio is

$$\begin{aligned} \text{SNR}_\tau(N,\epsilon) &= 4\sqrt{\frac{Z(A)\bar{n}_{\text{tot}}\kappa\tau}{2\bar{n}_{\text{th}}+1}}|\frac{\epsilon}{\kappa}|e^{A(N-1)} \\ &= \sqrt{Z(A)}e^{A(N-1)}\,\text{SNR}_\tau(1,\epsilon), \end{aligned} \tag{2.31}$$

where $\text{SNR}_\tau(1,\epsilon)$ is the signal-to-noise ratio of a ubiquitous single-mode dispersive detector [27, 32]. As we have stressed, $\text{SNR}_\tau(N,\epsilon)$ also represents the QFI of our system. We see that the SNR and QFI can be exponentially enhanced by either increasing system size N or amplification factor A, while all the while maintaining a *fixed* total photon number $\bar{n}_{\text{tot}}$.

This is the central result of our work. The crucial ingredients here are the inherent chiral amplification present in a Hatano-Nelson chain, the effective symmetry breaking that occurs when coupling the two opposite-chirality chains in our sensor, and the lack of any amplified output noise in the unperturbed system.

Several comments are in order. First, note that the large SNR achieved here is not contingent on approaching a parametric instability: our system is dynamically stable for any value of ϵ and A (see Appendix 2.9.7). Second, the mechanism we discuss here is useful even in small systems, as the fixed photon number QFI has an exponential dependence on A; an arbitrarily large QFI can thus be achieved with only three lattice sites. We further emphasize that the spatially-dependent amplification is a crucial aspect of our scheme. Indeed, the signal-to-noise ratio for a single-mode cavity amplifier can never achieve this sort of sensing enhancement, since the signal and noise are amplified in a similar manner [32]. Finally, we stress that this enhanced QFI in no way requires or is even related to the existence of an exceptional point in our dynamical matrix.

It is also worth stressing that our mechanism is completely distinct from other recently introduced methods that use parametric amplifiers to enhance dispersive sensing [11, 32, 102]. These works exploit noise squeezing as the basic mechanism for enhancing the SNR and QFI. Unfortunately, in many practical settings this squeezing is difficult to exploit, as one becomes extremely sensitive to the added noise of amplification stages that follow the primary measurement (i.e. one needs following amplifiers to be quantum limited). In contrast, our scheme does not rely on squeezing the measurement noise, but instead effectively amplifies the signal power at fixed total photon number. The output noise has the same magnitude as the input noise, and hence taking advantage of our enhanced QFI does not need following amplification stages to be quantum limited. This represents a significant practical advantage.

We end this section by pointing out that the N dependence of the QFI in Eq. (2.31) does not violate standard Heisenberg-limit constraints [42], as the setting here is different.

The usual Heisenberg limit applies to N sensor systems which each interact independently with the parameter of interest; the QFI here scales as best as $\propto N$, a result which requires entanglement. In contrast, each of the N modes in our system is not an independent sensor interacting independently with the dispersive perturbation, as the sites are coupled. The enhanced scaling we find is not the result of entanglement: we stress that the input light to our system is just a coherent state. Instead, the enhancement is a consequence of our system's unusual mechanism for non-reciprocal amplification.

2.6 Non-Markovian Effects

We now relax the assumption that the parameter ϵ is infinitely weak. For concreteness, we assume the sensing target is to distinguish the case $\epsilon = 0$ from the case $\epsilon = \epsilon_0 \neq 0$. This kind of discrimination is relevant in many practical situations, for example the dispersive measurement of the state of a qubit [27]. We assume that ϵ_0 is small enough such that linear response is still valid, but not so small that measurement will be infinitely long compared to internal system timescales. We thus need to understand the finite-frequency response and noise properties of our non-Hermitian lattice sensor.

In this section, we will characterize our sensor by its measurement time τ_M: what is the minimum integration time to to achieve an SNR of unity? Heuristically, τ_M is the minimum amount of time required to distinguish between $\epsilon = 0$ and $\epsilon = \epsilon_0$. In the limit $\epsilon_0 \to 0$, τ_M will be much longer than any internal sensor timescale, and we can use the long-time limit SNR expression derived in the previous section (c.f. Eq. (2.31)). We define $\tau_M^*(N)$ to be this $\epsilon_0 \to 0$ expression for the measurement time. Assuming that the input field has only vacuum noise, we find:

$$\tau_M^*(N) = \frac{1}{16 Z(A) \bar{n}_{\text{tot}} \kappa} \left(\frac{\kappa}{\epsilon_0}\right)^2 e^{-2A(N-1)}. \tag{2.32}$$

The obviously attractive feature here is the exponential reduction of τ_M with increasing lattice size N (but at fixed total photon number).

As N or ϵ_0 is increased, $\tau_M^*(N)$ will become increasing smaller, and at some point will become comparable to internal system timescales. At this point, the long-time limit assumption used to derive this expression becomes invalid. There are two distinct relevant timescales that govern the dynamics of our sensor. The first $t_{rt}(N)$ determines the ballistic propagation time to traverse the lattice end to end:

$$t_{rt}(N) = \frac{N}{J}, \tag{2.33}$$

The second $t_{esc}(N)$ involves the coupling to the waveguide: how quickly does a particle that is delocalized in the lattice leak out to the waveguide. A simple Fermi's Golden Rule estimate yields the scale:

$$t_{esc}(N) = \frac{N+1}{\kappa} \tag{2.34}$$

Both these timescales increase with system size. As a result, non-Markovian effects associated with internal dynamics become increasingly important with increasing N. The crucial question is how this physics modified or places a limit on the exponential-in-N measurement enhancement predicted by Eqs. (2.31) and (2.32). For large enough N the measurement will be so fast that these internal timescales matter. Do they simply put a bound on the measurement time, or does performance continue to increase with increasing N?

We first consider the limit $J \gg \kappa$; the only relevant dynamical timescale is then $t_{esc}(N)$, the time it takes a delocalized photon to escape the lattice. In this regime, the level spacing of lattice resonances is much larger than their widths. We can thus accurately approximate the relevant low-frequency behaviour of lattice susceptibilities by the contribution from the zero-frequency resonance (whose width is $1/t_{esc}(N)$). Assuming as always that N is odd,

we have:

$$\chi^{xx}[N,1;\omega] \approx \frac{2i^N}{N+1}\frac{e^{A(N-1)}}{\omega + i\frac{\kappa}{N+1}} \tag{2.35}$$

$$\chi^{pp}[1,N;\omega] \approx \frac{-2i^{-N}}{N+1}\frac{e^{A(N-1)}}{\omega + i\frac{\kappa}{N+1}}. \tag{2.36}$$

Note crucially that the residue at the poles are exponentially large in system size; this directly reflects the amplification physics we have discussed previously. Because of these factors, the above response functions are not simply equivalent to those of a single mode system with a very small linewidth.

With this approximation, we find that the SNR is given by (see Appendix 2.9.6 for details)

$$\mathrm{SNR}_\tau(N,\epsilon,J\to\infty) = \sqrt{\frac{\tau}{\tau_M^*(N)}}\left(1+e^{-\frac{\tau}{t_{esc}(N)}} - \frac{2t_{esc}(N)}{\tau}(1-e^{-\frac{\tau}{t_{esc}(N)}})\right) \tag{2.37}$$

The bracketed factor represents the non-Markovian correction to the long-time limit expression. Note that the correction is only to the magnitude of the signal. As we continue to use linear response, we only need to compute the homodyne current noise to zeroth order in ϵ_0. This noise is thus always vacuum noise regardless of the choice of integration time τ.

Using the above expression, we can then directly compute the measurement time τ_M in the $J \to \infty$ limit. While finding the measurement time analytically is unfeasible, we can

describe its asymptotic behavior in the strong and weak measurement limit (see App. 2.9.6)

$$\tau_M^{J=\infty}(N) = \begin{cases} \tau_M^*(N), & \tau_M^*(N) \gg t_{esc}(N) \\ \sqrt{6} t_{esc}(N) \sqrt[5]{\frac{\tau_M^*(N)}{\sqrt{6} t_{esc}(N)}}, & \tau_M^*(N) \ll t_{esc}(N) \end{cases}$$
$$\propto \begin{cases} e^{-2A(N-1)}, & \tau_M^*(N) \gg t_{esc}(N) \\ (N+1)^{4/5} e^{-2A(N-1)/5}, & \tau_M^*(N) \ll t_{esc}(N). \end{cases} \tag{2.38}$$

We thus find a surprising result: even for fast measurements where the escape time from the lattice plays a role, the measurement time continues to improve exponentially with lattice size N. Intuitively, this is because the deleterious effects of increasing the escape time $t_{esc} = (N+1)/\kappa$ with increasing N is more than offset by the exponentially large number of photons $e^{2A(N-1)}$ that exit through the waveguide when $\epsilon = \epsilon_0$.

We next consider the case where the hopping amplitude J is not infinitely larger than all other scales. In this case, we must also take into account the finite propagation speed $v \propto J$ of particles the lattice. Because an injected wavepacket must make a round trip before acquiring any information about the perturbation ϵ, for times less than $2N/v = N/J = t_{rt}(N)$ we expect the signal to be approximately zero. After this first round trip, the limiting factor in obtaining a large signal is once again the escape rate. Including the effects of a finite J, we find that the SNR is well approximated by simply adding a cutoff to the $J \to \infty$ result in Eq. (2.37):

$$\mathrm{SNR}_\tau(N, \epsilon, J) = \Theta\left(\tau - t_{rt}\right) \mathrm{SNR}_\tau(N, \epsilon, J \to \infty) \tag{2.39}$$

where $\Theta(t)$ is the Heaviside step function. This form reflects the basic intuition that it is impossible to make a measurement faster than the propagation time.

Combining these results, we finally find that including the effects of both internal timescales

$t_{rt}(N)$ and $t_{esc}(N)$, the measurement time (to good approximation) is given by

$$\tau_M(N) = \max(\tau_M^{J=\infty}(N), t_{rt}(N)) \tag{2.40}$$

where $\tau_M^{J=\infty}(N)$ is given in Eq. (2.32). Thus, as a function of increasing system size N, the measurement time first decreases exponentially until it reaches the round-trip time in the lattice, after which it increases with N. The upshot of our analysis is that increasing the lattice size still provides an exponential sensing advantage when including non-Markovian effects. This continues to be true until the measurement time is reduced to being on par with the round-trip propagation time $t_{rt}(N) = N/J$.

In Fig. 2.3, we plot the numerically-calculated measurement time $\tau_M(N)$ versus lattice size N for a fixed total photon number $\bar{n}_{\text{tot}}$ and perturbation size ϵ_0/κ; different curves correspond to different values of the hopping J/κ. We find an excellent agreement with the analytic approximation given in Eq. (2.40). The measurement time follows $\tau_M^{J=\infty}(N)$ (dark solid line) until it reaches the round-trip time $t_{rt}(N)$ (faint dashed lines), after which it increases linearly with N.

2.7 Beyond linear response

In this final section, we again consider the sensing problem of distinguishing $\epsilon = 0$ from $\epsilon = \epsilon_0$; now however, we analyze the regime where (due to amplification effects) ϵ_0 is too large for a linear response analysis to be valid. This is in contrast to the previous section, where ϵ_0 was small enough that linear response was still valid, but large enough that non-Markovian detector effects were important.

For any ϵ_0 the output state of the light leaving the waveguide will be Gaussian, and the statistics of the measured homodyne current will be Gaussian. We can thus again quantify our sensor's performance by calculating the signal-to-noise ratio. We now however need to

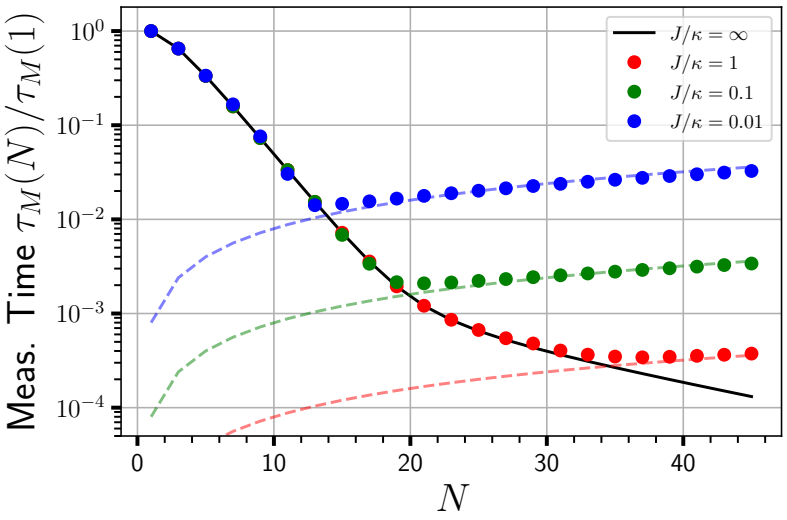

Fig. 2.3: Measurement time $\tau_M(N)$ versus lattice size N, for different choices of the hopping amplitudes J. The solid black line is the measurement time in the $J \to \infty$ limit, $\tau_M^{J=\infty}(N)$. Faint dashed lines are the round trip propagation timescale $t_{rt}(N) \equiv N/J$. The measurement time decays exponentially with increasing N, up until $\tau_M^{J=\infty}(N) \approx t_{rt}(N)$. Further increases of N cause the measurement time to scale with $t_{rt}(N)$, implying that it increases linearly with N. We take $\epsilon_0 = 10^{-8}\kappa$, $\bar{n}_{\rm tot} = 5 \times 10^9$ and $A = 0.2$. We also plot results for odd values of N only, as this guarantees the existence of a zero-frequency lattice eigenstate and thus an additional resonant enhancement of our measurement (c.f. main text before Eq. (2.27)).

account for the fact that the homodyne current noise will also depend on ϵ_0. The definition of the signal-to-noise ratio becomes:

$$\mathrm{SNR}_\tau(N, \epsilon_0) \equiv \frac{|\langle \hat{M}_\tau(N) \rangle_{\epsilon_0} - \langle \hat{M}_\tau(N) \rangle_0|}{\sqrt{\frac{\mathcal{N}_\tau^2(N,0) + \mathcal{N}_\tau^2(N,\epsilon_0)}{2}}} \tag{2.41}$$

This SNR quantifies the distinguishability between the Gaussian homodyne current distributions obtained for $\epsilon = 0$ versus $\epsilon = \epsilon_0$ (see e.g. [27, 65]).

As might be expected, the nonlinear dependence of SNR on ϵ_0 will prevent one from indefinitely improving the measurement with increasing N. The key issue is that beyond linear response, noise amplification will also play a role. We show in what follows that even with this complication, our system yields a strong advantage, allowing one to fundamentally change the scaling of the SNR with ϵ_0.

We will focus on the most interesting situation where $\epsilon_0/\kappa \ll 1$, but where linear response breaks down because of a large amplification factor (i.e. $e^{A(N-1)}\epsilon_0/\kappa$ is not necessarily small). Further, we take the round-trip time $t_{rt}(N) = N/J$ to be small enough that we can ignore the transient dynamics and consider only the steady-state response. Formally, we now need to calculate the output field leaving the waveguide to all orders in ϵ_0. We thus expand the zero frequency quadratures of the output field as a power series in ϵ_0/κ:

$$\hat{X}^{(\text{out})}[0] \equiv \sum_{k=0}^{\infty} \left(\frac{\epsilon_0}{\kappa}\right)^k \hat{X}_k^{(\text{out})} \tag{2.42}$$

$$\hat{P}^{(\text{out})}[0] \equiv \sum_{k=0}^{\infty} \left(\frac{\epsilon_0}{\kappa}\right)^k \hat{P}_k^{(\text{out})} \tag{2.43}$$

To zeroth order in ϵ_0, there is no mixing of quadratures, and input signals are reflected with no net amplification (but just a trivial sign change):

$$\hat{X}_0^{(\text{out})} = -\hat{X}^{(\text{in})}[0], \;\; \hat{P}_0^{(\text{out})} = -\hat{P}^{(\text{in})}[0], \tag{2.44}$$

Note that throughout this section, we associate the coherent drive tone amplitude β with the average value of $\hat{X}^{(\text{in})}[0]$.

In contrast, the first order contributions correspond to a process where input fields scatter once off the “impurity" before returning to the waveguide. This scattering converts one canonical quadrature to the other, and also results in a net amplification or deamplification

$$\hat{X}_1^{(\text{out})} = 4e^{-2A(N-1)}\hat{P}^{(\text{in})}[0] \tag{2.45}$$

$$\hat{P}_1^{(\text{out})} = -4e^{2A(N-1)}\hat{X}^{(\text{in})}[0] \tag{2.46}$$

The amplification of $\hat{X}^{(\text{in})}$ is exactly the process we discussed in Sec. 2.5 that is responsible for the exponentially-enhanced signal. The attenuation of $\hat{P}^{(\text{in})}$ at this order can be understood

analogously.

What about the second order in ϵ_0 contributions? Heuristically, these correspond to input fields scattering off the impurity twice. While we expect such a process to preserve the identity of each canonical quadrature, it also has a more surprising feature: it results in no net amplification or deamplification:

$$\hat{X}_2^{(\text{out})} = 8\hat{X}^{(\text{in})}[0], \quad \hat{P}_2^{(\text{out})} = 8\hat{P}^{(\text{in})}[0] \tag{2.47}$$

This unexpected result can again be traced by to the chiral and quadrature-dependent nature of gain and loss in our system. Interacting with the impurity twice implies that an input signal has performed at least two round-trip traversals of the lattice (partially as an X, partially as a P). The gain and attenuation for each of these roundtrips necessarily cancel.

This pattern continues to higher order, and provides a simple explanation for the full expression we find for the output field: the net amplification / deamplification factor for each kind of quadrature to quadrature scattering process is independent of ϵ_0. We find

$$\hat{X}^{(\text{out})}[0] = R(\epsilon_0)\hat{X}^{(\text{in})}[0] - T(\epsilon_0)e^{-2A(N-1)}\hat{P}^{(\text{in})}[0] \tag{2.48}$$

$$\hat{P}^{(\text{out})}[0] = T(\epsilon_0)e^{2A(N-1)}\hat{X}^{(\text{in})}[0] + R(\epsilon_0)\hat{P}^{(\text{in})}[0] \tag{2.49}$$

where

$$R(\epsilon_0) = -\frac{(\frac{\kappa}{2})^2 - \epsilon_0^2}{(\frac{\kappa}{2})^2 + \epsilon_0^2} \tag{2.50}$$

$$T(\epsilon_0) = \frac{\kappa\epsilon_0}{(\frac{\kappa}{2})^2 + \epsilon_0^2} \tag{2.51}$$

are elements of an orthogonal scattering matrix describing the conversion of quadratures (see Appendix 2.9.7 for details). We see that quadrature-preserving scattering processes never come with amplification factors, whereas the amplification factors for quadrature-

changing scattering are independent of ϵ_0. Crucially, there are no amplification factors in denominators in this expression. This result can be derived via a canonical squeezing transformation which eliminates the anomalous terms in Eq. (2.4); it also reflects the fact that our system is dynamically stable regardless of the strength of ϵ_0.

From these input-output relations, we can readily compute the SNR. Taking the noise of the input field to be vacuum, we have:

$$\begin{aligned}\mathrm{SNR}_\tau(N,\epsilon_0) =& \frac{\sqrt{8\tau}|\beta||T(\epsilon_0)|e^{2A(N-1)}}{\sqrt{1+R^2(\epsilon_0)+T^2(\epsilon_0)e^{4A(N-1)}}} \\ =& \frac{\sqrt{2Q(A,\epsilon_0)\bar{n}_{\mathrm{tot}}\kappa\tau}|T(\epsilon_0)|e^{A(N-1)}}{\sqrt{1+R^2(\epsilon_0)+T^2(\epsilon_0)e^{4A(N-1)}}}\end{aligned} \tag{2.52}$$

where $\bar{n}_{\mathrm{tot}} = (\bar{n}_{\mathrm{tot}}(0) + \bar{n}_{\mathrm{tot}}(\epsilon_0))/2$.

We see that now, the denominator in Eq. (2.52) also depends on the amplification factor A, which corresponds to the amplification of noise. Because of this, increasing A and/or N indefinitely is no longer optimal. There remains nonetheless an advantage in using a carefully chosen amount of amplification. Ignoring $Q(A,\epsilon_0)$ and maximizing the SNR Eq. (2.52) with respect to the amplification, we see that the optimal choice corresponds to amplification that simply doubles the output noise over pure vacuum noise. In the $\epsilon_0 \ll \kappa$ limit of interest, the condition is:

$$e^{4A^*(N-1)} \equiv \frac{1+R^2(\epsilon_0)}{T^2(\epsilon_0)} \approx \frac{\kappa^2}{8\epsilon_0^2} \tag{2.53}$$

With this optimized choice of A, the SNR written in terms of ϵ_0 is then

$$\mathrm{SNR}_\tau(N,\epsilon_0) = 8^{1/4}\sqrt{Q(A^*,\epsilon_0)\bar{n}_{\mathrm{tot}}\kappa\tau}\sqrt{\frac{\epsilon_0}{\kappa}}. \tag{2.54}$$

We show in Appendix 2.9.7 that $Q(A^*,\epsilon_0) = 1-\mathcal{O}((\frac{8\epsilon_0^2}{\kappa^2})^{\frac{1}{N-1}})$. Comparing against Eq. (2.27),

we see that the optimized amplification has changed the fundamental scaling of the long-time SNR from being linear in the small parameter ϵ_0/κ to a square-root dependence. Thus, by extending our analysis beyond a simple linear-response treatment, we see that the exponential enhancement of the SNR predicted in Eq. (2.27) cannot extend indefinitely: the best one can do is to enhance the SNR (over a conventional dispersive measurement) by a large factor $\sqrt{\kappa/\epsilon_0}$. This behaviour is plotted in Fig. (2.4). We again note that this predicted measurement enhancement does not require a large number of lattice sites; just three is already enough.

The enhanced square-root dependence of the SNR on ϵ_0 is superficially reminiscent of the behaviour found in non-Hermitian exceptional point (EP) sensors [138]. We stress that these phenomena are completely distinct. For EP sensors, it is the frequency of a resonance that exhibits a square root dependence, and not the SNR of a specific measurement (or other metric that also quantifies fluctuations). Further, EP sensing is based on operating near a point where the system's dynamical matrix becomes defective and normal modes coalesce. In contrast, our system is not operating near such a special operating point. As we have stressed, the mechanism for enhanced SNR in our system is based on its directional amplification, and its ability to amplify signals and noise differently.

2.8 Summary and future directions

In this chapter, we have shown how the unique features of non-Hermitian lattice dynamics can be used for highly enhanced Hamiltonian parameter estimation and parametric sensing. We analyzed a concrete setup involving two copies of the Hatano-Nelson model and a symmetry breaking perturbation. The response to the perturbation grows exponentially with system size, even when the total system photon number is kept fixed. Our analysis focused on a specific realization of this idea using a chain of parametrically driven cavities and a standard dispersing coupling to the parameter of interest. Here, even in the presence of quantum noise

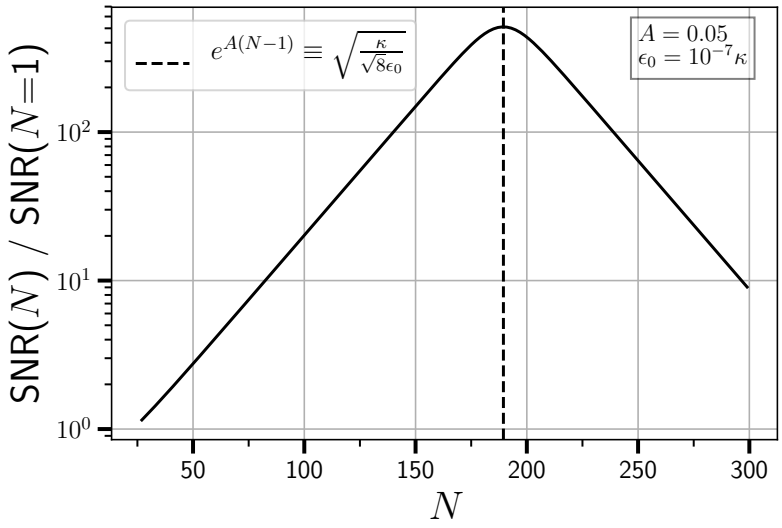

Fig. 2.4: Non-perturbative signal-to-noise ratio in the long time limit $\mathrm{SNR}_\tau(N, \epsilon_0)/\mathrm{SNR}_\tau(1, \epsilon_0)$, as a function of lattice size N. The SNR initially increases exponentially with N, as predicted by our linear-response analysis in Sec. 2.5. For sufficiently large N, linear response breaks down due to the amplification of noise; this causes the SNR to decrease with N for large N. A non-trivial maximum is thus reached for an intermediate value of N given by Eq. (2.53). For this optimal N and a weak perturbation ϵ_0, the SNR scales like $\sqrt{\epsilon_0/\kappa}$ (as opposed to the more standard scaling ϵ_0/κ) . The parameters here are $A = 0.05$, $\epsilon_0 = 10^{-7}\kappa$ and $\bar{n}_{\mathrm{tot}} = 5 \times 10^9$. We only plot the results for odd values of N, which ensures an resonant enhancement of the zero-frequency response (c.f discussion preceding Eq. (2.27))

effects, the SNR and quantum Fisher information both grow exponentially with system size (all the while keeping photon number fixed). The system we described could be achieved in a variety of superconducting circuit and quantum optical platforms, and only requires one to make a homodyne measurement of the output field leaving the sensor. We also analyzed effects that go beyond standard linear-response and Markovian assumptions. Even including higher-order effects, we show that our scheme allows one to dramatically enhance the SNR so that it depends on the square root of the sensing parameter. Our work highlights the usefulness of multi-mode non-Hermitian features that go beyond the mere existence of exceptional points. An open question is whether other unique features attributed to non-Hermiticity, such as exotic topological phases or chiral mode switching, are also advantageous

to quantum sensing problems.

2.9 Appendices

2.9.1 $\mathbb{Z}_2$ symmetry of a non-Hermitian tight-binding model

We discuss in more detail the $\mathbb{Z}_2$ symmetry that we wish to break to order to obtain an exponentially large response. We consider two finite, N site open Hatano-Nelson lattices with opposite chiralities (i.e. oppositely signed imaginary vector potentials A). The time-dependent Schrödinger equation reads

$$\dot{\psi}_n^{\uparrow} = Je^{A}\psi_{n-1}^{\uparrow} - Je^{-A}\psi_{n+1}^{\uparrow} \tag{2.55}$$

$$\dot{\psi}_n^{\downarrow} = Je^{-A}\psi_{n-1}^{\downarrow} - Je^{A}\psi_{n+1}^{\downarrow} \tag{2.56}$$

where σ indexes the two chains. These equations of motion are invariant under a combination of time reversal $\dot{\psi}_n^{\sigma} \to -\dot{\psi}_n^{\sigma}$, spatial inversion $\psi_n^{\sigma} \to \psi_{N+1-n}^{\sigma}$ and pseudospin inversion $\sigma \to \bar{\sigma}$.

While this is a seemingly trivial symmetry, we note that the Heisenberg equations of motion of our dissipation-free realization of the same model

$$\dot{\hat{x}}_n = Je^{A}\hat{x}_{n-1} - Je^{-A}\hat{x}_{n+1}, \tag{2.57}$$

$$\dot{\hat{p}}_n = Je^{-A}\hat{p}_{n-1} - Je^{A}\hat{p}_{n+1}, \tag{2.58}$$

are invariant under the same set of symmetries, where $\hat{x}_n$ and $\hat{p}_n$ play the role of pseudospin. To describe these symmetries requires using operators acting on the bosonic Hilbert space. To this end, we consider the antiunitary time reversal operator $\mathcal{T}$, a unitary rotation operator

$\mathcal{R}$ and the unitary spatial inversion operator $\mathcal{S}$ whose action on the quadratures reads

$$\mathcal{T}\hat{x}_n\mathcal{T}^{-1} = \hat{x}_n,\ \ \mathcal{T}\hat{p}_n\mathcal{T}^{-1} = -\hat{p}_n \tag{2.59}$$

$$\mathcal{R}\hat{x}_n\mathcal{R}^{-1} = \hat{p}_n,\ \ \mathcal{R}\hat{p}_n\mathcal{R}^{-1} = -\hat{x}_n \tag{2.60}$$

$$\mathcal{S}\hat{x}_n\mathcal{S}^{-1} = \hat{x}_{N+1-n},\ \ \mathcal{S}\hat{p}_n\mathcal{S}^{-1} = \hat{p}_{N+1-n}. \tag{2.61}$$

Equivalently, we have

$$\mathcal{T}\hat{a}_n\mathcal{T}^{-1} = \hat{a}_n \tag{2.62}$$

$$\mathcal{R}\hat{a}_n\mathcal{R}^{-1} = -i\hat{a}_n \tag{2.63}$$

$$\mathcal{S}\hat{a}_n\mathcal{S}^{-1} = \hat{a}_{N+1-n} \tag{2.64}$$

With these definitions in hand, it is easy to verify that the Hermitian Hamiltonian which gives the equations of motion Eqs.(2.57) and (2.58)

$$\hat{H}_B = J\sum_{n=1}^{N-1}\left(-e^{-A}\hat{x}_{n+1}\hat{p}_n + e^{A}\hat{p}_{n+1}\hat{x}_n\right). \tag{2.65}$$

is invariant under the combination of time-reversal, rotation, and spatial inversion. Similarly, the non-local perturbation considered in Section 2.5

$$\hat{V}_{\mathrm{NHSE}} = e^{i\varphi}\hat{a}_1^\dagger\hat{a}_N + e^{-i\varphi}\hat{a}_N^\dagger\hat{a}_1 \tag{2.66}$$

is invariant under the same combination of symmetries. Time-reversal changes the phase $\varphi \to -\varphi$, $\hat{V}_{\mathrm{NHSE}}$ commutes with $\mathcal{R}$ and spatial inversion sends $\hat{a}_1^\dagger\hat{a}_N \to \hat{a}_N^\dagger\hat{a}_1$.

2.9.2 Quadrature susceptibility matrices

We first compute the susceptibilities for the $\hat{x}_n$ and $\hat{p}_n$ quadratures, defined as $\hat{a}_n = (\hat{x}_n + i\hat{p}_n)/\sqrt{2}$. The Heisenberg-Langevin equations of motion in this basis are

$$\dot{\hat{x}}_n = -i[\hat{x}_n, \hat{H}_B] - \delta_{n1}\left(\frac{\kappa}{2}\hat{x}_n + \sqrt{\kappa}\left(\sqrt{2}\beta + \hat{X}^{(\mathrm{in})}\right)\right) \tag{2.67}$$

$$\dot{\hat{p}}_n = -i[\hat{p}_n, \hat{H}_B] - \delta_{n1}\left(\frac{\kappa}{2}\hat{p}_n + \sqrt{\kappa}\hat{P}^{(\mathrm{in})}\right), \tag{2.68}$$

where $\hat{X}^{(\mathrm{in})}$ and $\hat{P}^{(\mathrm{in})}$ are the operator equivalent of Gaussian white noise. They average to zero, and their second moment is

$$\langle \hat{X}^{(\mathrm{in})}(t)\hat{X}^{(\mathrm{in})}(t')\rangle = \left(\bar{n}_{\mathrm{th}} + \frac{1}{2}\right)\delta(t-t') \tag{2.69}$$

$$\langle \hat{P}^{(\mathrm{in})}(t)\hat{P}^{(\mathrm{in})}(t')\rangle = \left(\bar{n}_{\mathrm{th}} + \frac{1}{2}\right)\delta(t-t') \tag{2.70}$$

$$\frac{1}{2}\langle\{\hat{X}^{(\mathrm{in})}(t), \hat{P}^{(\mathrm{in})}(t')\}\rangle = 0 \tag{2.71}$$

where $\bar{n}_{\mathrm{th}}$ is the number of thermal quanta in the input field. We now focus on the case where $\bar{n}_{\mathrm{th}} = 0$, with generalizations to finite-temperature inputs being straightforward.

An immense simplification arises by making a local Bogoliubov (squeezing) transformation, such that the Hamiltonian preserves the total number of these new quasiparticles. The dynamical matrix of in this new basis is then explicitly Hermitian. Defining new canonically conjugate quadrature operators $\hat{\tilde{x}}_n$ and $\hat{\tilde{p}}_n$ by

$$\hat{x}_n = e^{A(n-n_0)}\hat{\tilde{x}}_n \tag{2.72}$$

$$\hat{p}_n = e^{-A(n-n_0)}\hat{\tilde{p}}_n \tag{2.73}$$

with n_0 an arbitrary real number, we have

$$\hat{H}_B = J \sum_{n=1}^{N-1} \left(-\hat{\tilde{x}}_{n+1} \hat{\tilde{p}}_j + \hat{\tilde{p}}_{n+1} \hat{\tilde{x}}_j \right) \tag{2.74}$$

$$= iJ \sum_{n=1}^{N-1} \left(\hat{\tilde{a}}^\dagger_{n+1} \hat{\tilde{a}}_n - h.c. \right) \tag{2.75}$$

with $\hat{\tilde{a}}_n = (\hat{\tilde{x}}_n + i\hat{\tilde{p}}_n)/\sqrt{2}$ a transformed canonical annihilation opreator. The parameter n_0 does not enter the Hamiltonian since $\hat{H}_B$ is invariant under a uniform local squeezing operation that doesn't mix quadratures $\hat{x}_n \to e^{-An_0}\hat{x}_n, \hat{p}_n \to e^{An_0}\hat{p}_n$. In this section, it will be convenient to set $n_0 = 1$, so that the annihilation operators on the first stie remain unchanged $\hat{\tilde{a}}_1 = \hat{a}_1$.

The Heisenberg-Langevin equations of motion in this new basis read

$$\dot{\hat{\tilde{x}}}_n = -i[\hat{\tilde{x}}_n, \hat{H}_B] - \delta_{n1} \left(\frac{\kappa}{2} \hat{\tilde{x}}_n + \sqrt{\kappa} \left(\sqrt{2}\beta + \hat{X}^{(\text{in})} \right) \right), \tag{2.76}$$

$$\dot{\hat{\tilde{p}}}_n = -i[\hat{\tilde{p}}_n, \hat{H}_B] - \delta_{n1} \left(\frac{\kappa}{2} \hat{\tilde{p}}_n + \sqrt{\kappa} \hat{P}^{(\text{in})} \right). \tag{2.77}$$

As expected, the response properties of $\hat{\tilde{x}}_n$ and $\hat{\tilde{p}}_n$ are then determined by a completely Hermitian matrix (other than the waveguide-induced decay on the first site).

Using the squeezing transformations Eqs. (2.72)-(2.73) and the fact that the dynamics of the $\hat{x}$ and $\hat{p}$ quadratures are uncoupled, the relevant quadrature-quadrature susceptibilities read

$$\chi^{xx}(n, m; t) = -i\langle[\hat{x}_n(t), \hat{p}_m(0)]\rangle = e^{A(n-m)} \tilde{\chi}^{xx}(n, m; t) \tag{2.78}$$

$$\chi^{pp}(n, m; t) = i\langle[\hat{p}_n(t), \hat{x}_m(0)]\rangle = e^{-A(n-m)} \tilde{\chi}^{pp}(n, m; t) \tag{2.79}$$

$$\chi^{xp}(n, m; t) = i\langle[\hat{x}_n(t), \hat{x}_m(0)]\rangle = 0 \tag{2.80}$$

$$\chi^{px}(n, m; t) = -i\langle[\hat{p}_n(t), \hat{p}_m(0)]\rangle = 0 \tag{2.81}$$

where $\tilde{\chi}^{\alpha\beta}(n,m;t)$ are quadrature response functions of a regular (i.e. reciprocal particle-conserving) tight-binding chain with a waveguide attached to the first site. Note that our convention differs from that used in the condensed matter community, where $\chi^{\alpha\beta}(n,m;t)$ is the response of quadrature α to a force which couples to β in the Hamiltonian. Computing the quadrature-quadrature susceptibilities $\chi^{\alpha\beta}(n,m;t)$ of our non-reciprocal system is then no more complicated than finding the susceptibilities of a reciprocal tight-binding chain $\tilde{\chi}^{xx}(n,m;t)$ and $\tilde{\chi}^{pp}(n,m;t)$.

The susceptibilities of the Hatano-Nelson model Eq. (2.2) are computed in a similar manner. There, instead of a local squeezing transformation, one makes a so called imaginary gauge transformation $|n\rangle \to e^{A(n-j_0)}|n\rangle$ and $\langle n| \to e^{-A(n-j_0)}\langle n|$. In this new gauge, the Hamiltonian is Hermitian and completely independent of A. The factorization of Eq. (2.3) as $\chi(n,m;t) = e^{A(n-m)}\tilde{\chi}(n,m;t)$ immediately follows.

2.9.3 Particle-conserving susceptibilities

Although so far we've only considered quadrature-quadrature response functions, the fact that we can map our Hamiltonian onto a particle conserving one makes it so that it is much simpler to keep track of the dynamics of the single squeezed mode $\hat{\tilde{a}}_n$. Indeed, we have

$$\tilde{\chi}^{xx}(n,m;t) = \tilde{\chi}^{pp}(n,m;t) = \mathrm{Re}\,\tilde{\chi}(n,m;t) \tag{2.82}$$

$$\tilde{\chi}^{px}(n,m;t) = -\tilde{\chi}^{xp}(n,m;t) = \mathrm{Im}\,\tilde{\chi}(n,m;t) \tag{2.83}$$

where

$$\tilde{\chi}(n,m;t) = \langle[\hat{\tilde{a}}_n(t), \hat{\tilde{a}}_m^\dagger(0)]\rangle. \tag{2.84}$$

Because our Hamiltonian is quadratic in boson opeators and conserves total quasiparticle number, we can readily use the single-particle formalism to find the relevant susceptibilities.

If we let $|n\rangle$ denote a position eigenket, we then have

$$\tilde{\chi}(n,m;t) = \langle n| \, e^{-it\left(\tilde{\boldsymbol{H}} - i\frac{\boldsymbol{\kappa}}{2}\right)} \, |m\rangle \tag{2.85}$$

with

$$\tilde{\boldsymbol{H}} = iJ \left(\sum_{n=1}^{N-1} |n+1\rangle \langle n| - h.c. \right) \tag{2.86}$$

$$\boldsymbol{\kappa} = \kappa \, |1\rangle \langle 1| \tag{2.87}$$

It is more convenient to write the susceptibilities in the frequency domain:

$$\tilde{\chi}[n,m;\omega] = \int_0^\infty dt \chi(n,m;t) e^{i\omega t} \tag{2.88}$$

$$= \langle n| \, \frac{i}{\omega \mathbf{1} - \tilde{\boldsymbol{H}} + i\frac{\boldsymbol{\kappa}}{2}} \, |m\rangle \tag{2.89}$$

We'll first compute the susceptibilities without the effects of ϵ or κ, that is

$$\tilde{\chi}_0[n,m;\omega] = \langle n| \, \frac{i}{\omega \mathbf{1} - \tilde{\boldsymbol{H}}} \, |m\rangle \tag{2.90}$$

Written out explicitly, the matrix elements of the susceptibility for a finite open chain then satisfy the difference equation

$$i\tilde{\chi}_0[n-1,m;\omega] - \frac{\omega}{J}\tilde{\chi}_0[n,m;\omega] - i\tilde{\chi}_0[n+1,m;\omega] = -\frac{i\delta_{nm}}{J} \tag{2.91}$$

with boundary conditions $\tilde{\chi}_0[0,m;\omega] = \tilde{\chi}_0[N+1,m;\omega] = 0$. The exact form of the susceptibility matrix is known; here for the sake of completeness we quickly sketch how to obtain it. First, we note that Eq.(2.91) has the form of a translationally invariant Green's function problem in the index space n, with $-i\delta_{nm}/J$ acting as a source term. The general solution

will then consist of a linear combination of the source free solution and a convolution (in the index space n) of the source with the homogeneous solution.

The source free solution, which satisfies

$$i\tilde{\chi}_0^{\mathrm{sf}}[n-1,m;\omega] - \frac{\omega}{J}\tilde{\chi}_0^{\mathrm{sf}}[n,m;\omega] - i\tilde{\chi}_0^{\mathrm{sf}}[n+1,m;\omega] = 0 \tag{2.92}$$

is precisely (up to a factor of i) the recursion relation that defines $T_n(\omega/2J)$ and $U_n(\omega/2J)$, the Chebyshev polynomials of the first and second kind respectively. Since $U_{-1}(\omega/2J) = 0$, and given our boundary condition $\tilde{\chi}_0[0,m;\omega] = 0$, we conclude that the source free solution is

$$\tilde{\chi}_0^{\mathrm{sf}}[n,m;\omega] = c_m i^n U_{n-1}(\frac{\omega}{2J}) \tag{2.93}$$

with c_m a constant that will be used to satisfy the second boundary condition. The full solution to Eq. (2.91) is then

$$\tilde{\chi}_0[n,m\omega] = c_m i^n U_{n-1}(\frac{\omega}{2J}) - \frac{i}{J} i^{n-m} U_{n-m-1}(\frac{\omega}{2J})\Theta(n-m) \tag{2.94}$$

with $\Theta(n-m)$ the Heaviside step function (where $\Theta(0) = 0$). Enforcing the second boundary condition $\tilde{\chi}_0[N+1,m;\omega] = 0$ yields

$$\tilde{\chi}_0[n,m;\omega] = i^{1+n-m}\frac{U_{\min(n,m)-1}(\frac{\omega}{2J})U_{N-\max(n,m)}(\frac{\omega}{2J})}{JU_N(\frac{\omega}{2J})} \tag{2.95}$$

We now turn our attention to computing the response functions in the presence of the waveguide on the first site. Formally, this introduces a local term $-\kappa/2\delta_{n,1}\delta_{m,1}$ to the the dynamical matrix. The full susceptibilities $\tilde{\chi}[n,m;\omega]$ can then readily be solved algebraically

using Dyson's equation

$$\begin{aligned}\tilde{\chi}[n,m;\omega] &= \tilde{\chi}_0[n,m;\omega] - \frac{\kappa}{2}\tilde{\chi}_0[n,1;\omega]\tilde{\chi}[1,m;\omega] \\ &= \tilde{\chi}_0[n,m;\omega] - \frac{\frac{\kappa}{2}\tilde{\chi}_0[n,1;\omega]\tilde{\chi}_0[1,m;\omega]}{1+\frac{\kappa}{2}\tilde{\chi}_0[1,1;\omega]}.\end{aligned} \tag{2.96}$$

Since there is only a driving force on the first site and we are only interested in the response on the first site, we must only compute $\tilde{\chi}[n,1;\omega]$ and $\tilde{\chi}[1,m;\omega]$:

$$\tilde{\chi}[n,1;\omega] = i^n \frac{U_{N-n}(\frac{\omega}{2J})}{JU_N(\frac{\omega}{2J}) + i\frac{\kappa}{2}U_{N-1}(\frac{\omega}{2J})} \tag{2.97}$$

$$\tilde{\chi}[1,m;\omega] = -i^{-m} \frac{U_{N-m}(\frac{\omega}{2J})}{JU_N(\frac{\omega}{2J}) + i\frac{\kappa}{2}U_{N-1}(\frac{\omega}{2J})} \tag{2.98}$$

Because $\tilde{\chi}^{px}(n,m;t) = -\tilde{\chi}^{xp}(n,m;t) = 0$, from Eq. (2.83) we conclude that $\tilde{\chi}[n,m;\omega] = \tilde{\chi}^{xx}[n,m;\omega] = \tilde{\chi}^{pp}[n,m;\omega]$. With this result and Eqs.(2.78)-(2.79), we now have all the relevant quadrature-quadrature susceptibilities.

2.9.4 Total photon number

Let us compute the total steady-state intracavity photon number on each site to zeoreth order in ϵ. To do so, we must solve the Heisenberg-Langevin equations for the cavity annihilation operators $\hat{a}_n$. Recall that we were able to define new squeezed annihilation and creation operators

$$\hat{a}_n = \cosh(A(n-1))\hat{\tilde{a}}_n + \sinh(A(n-1))\hat{\tilde{a}}_n^\dagger \tag{2.99}$$

where the Hamiltonian $\hat{H}_B$ conserved the total number of quasiparticles. Thus, the total number of photons on site n reads

$$\begin{aligned}\langle \hat{a}_n^\dagger \hat{a}_n \rangle &= \cosh(2A(n-1))\langle \hat{\tilde{a}}_n^\dagger \hat{\tilde{a}}_n \rangle \\ &\quad + \sinh(2A(n-1))\,\mathrm{Re}(\langle \hat{\tilde{a}}_n \hat{\tilde{a}}_n \rangle) \\ &\quad + \sinh^2(A(n-1))\end{aligned} \tag{2.100}$$

The last term is due to noise that enter the port on site 1 and is turned into real photons by the parametric amplifier-type interactions. We can readily solve the Heisenberg-Langevin equations for the squeezed modes $\hat{\tilde{a}}_n$:

$$\begin{aligned}\hat{\tilde{a}}_n(t) &= \tilde{\chi}(n,m;t)\hat{\tilde{a}}_m(t) \\ &\quad - \sqrt{\kappa}\beta \int_0^t dt' \tilde{\chi}[n,1;t-t'] \\ &\quad - \sqrt{\kappa} \int_0^t dt' \tilde{\chi}[n,1;t-t']\hat{a}^{(\mathrm{in})}(t')\end{aligned} \tag{2.101}$$

where $\hat{a}^{(\mathrm{in})}(t) = (\hat{X}^{(\mathrm{in})}(t) + i\hat{P}^{(\mathrm{in})}(t))/\sqrt{2}$ is the operator equivalent of Gaussian white noise. Note that we're using Einstein summation notation. Assuming a zero temperature environment we have in the steady-state

$$\langle \hat{\tilde{a}}_n^\dagger \hat{\tilde{a}}_n \rangle = \langle \hat{\tilde{a}}_n \hat{\tilde{a}}_n \rangle = \kappa\beta^2 |\tilde{\chi}[n,1;\omega=0]|^2. \tag{2.102}$$

Using Eq. (2.97). we obtain

$$\begin{aligned}\langle \hat{a}_n^\dagger \hat{a}_n \rangle &= \frac{4\beta^2}{\kappa} e^{2A(n-1)} \sin^2 \frac{\pi}{2} n \\ &\quad + \sinh^2(A(n-1))\end{aligned} \tag{2.103}$$

where we've assumed (and will do so throughout) that N is odd. Summing Eq. (2.103) over all lattice sites gives

$$\begin{aligned}\bar{n}_{\text{tot}} &= \frac{4|\beta|^2}{\kappa}\frac{e^{2A(N+1)}-1}{e^{4A}-1} \\ &+ \frac{1}{4}\left(\frac{\sinh(A(2N-1))}{\sinh(A)} - (2N-1)\right) \\ &= \bar{n}_N \frac{1-e^{-2A(N+1)}}{1-e^{-4A}} + \bar{n}_{\text{vac}}\end{aligned} \tag{2.104}$$

with $\bar{n}_{\text{vac}}$ the photons that are present due to amplified vacuum fluctuations. Thus, the ratio of the average photon number on the last site to the total number of photons $Z(A)$ is

$$Z(A) = \left(\frac{1-e^{-2A(N+1)}}{1-e^{-4A}} + \frac{\bar{n}_{\text{vac}}}{\bar{n}_N}\right)^{-1} \tag{2.105}$$

In the limit where $|\beta|^2/\kappa$ is large, the coherent photons dominate $\bar{n}_{\text{vac}}$, which we can ignore. We then have

$$Z(A) = \frac{1-e^{-4A}}{1-e^{-2A(N+1)}} = 1 - \mathcal{O}(e^{-4A}) \tag{2.106}$$

as in the main text.

2.9.5 QFI for $\hat{V}_{NHSE}$

We are now in a position to compute $\text{QFI}_\tau(N)/\bar{n}_{\text{tot}}$ for any choice of perturbation $\hat{V}$. Recall that that in the large β limit of interest, the QFI coincides with SNR squared, optimizing over the homodyne angle ϕ (see Eqs.2.14). As is written in the main text, see Eq.(2.18), the steady-state signal takes the form

$$\mathcal{S}_\tau(N,\epsilon) = \sqrt{\kappa\tau}|\,\text{Re}[e^{-i\phi}(\delta\langle\hat{x}_1\rangle^{\text{ss}} + i\delta\langle\hat{p}_1\rangle^{\text{ss}})]| \tag{2.107}$$

with $\delta\langle\hat{x}_1\rangle^{\rm ss}$ and $\delta\langle\hat{p}_1\rangle^{\rm ss}$ the steady state linear response of the site-1 average quadrature amplitude to a non-zero ϵ. The signal will depend on the phase of the coherent drive β which we take to be real, as in the main text. Our conclusion that $\hat{V}_{NHSE}$ does not have an exponentially large QFI/$\bar{n}_{\rm tot}$ is independent of the phase of β, as will become evident. This choice of phase is equivalent to driving the $\hat{x}_1$ quadrature with a force $-\sqrt{2\kappa}\beta$, so that the signal is

$$\mathcal{S}_\tau(N,\epsilon) = \kappa\beta\sqrt{2\tau}|\,\mathrm{Re}[e^{-i\phi}(\delta\chi^{xx}[1,1;0] + i\delta\chi^{px}[1,1;\omega])]| \tag{2.108}$$

The form of the responses $\delta\chi^{xx}[1,1;0]$ and $\delta\chi^{px}[1,1;0]$ will depend on $\hat{V}$. For the non-local hopping perturbation

$$\hat{V}_{\rm NHSE} = e^{i\varphi}\hat{a}_1^\dagger\hat{a}_N + e^{-i\varphi}\hat{a}_N^\dagger\hat{a}_1 \tag{2.109}$$

the change to the equations of motion induced by ϵ to the quadratures on the first site read:

$$\delta\dot{\hat{x}}_1 = \epsilon\,(\sin\varphi\,\hat{x}_N + \cos\varphi\,\hat{p}_N) \tag{2.110}$$

$$\delta\dot{\hat{p}}_1 = \epsilon\,(-\cos\varphi\,\hat{x}_N + \sin\varphi\,\hat{p}_N)\,. \tag{2.111}$$

First order perturbation theory then yields

$$\delta\chi^{xx}[1,1;0] = \chi^{xx}[1,1;0](\epsilon\sin\varphi)\chi^{xx}[N,1;0] \tag{2.112}$$

$$\delta\chi^{px}[1,1;0] = \chi^{pp}[1,1;0](-\epsilon\cos\varphi)\chi^{xx}[N,1;0] \tag{2.113}$$

where $\chi^{\alpha\alpha}[n,m;\omega]$ the susceptibilities of the unperturbed system, which we computed in Appendix 2.9.2 and Appendix 2.9.3. The salient feature is that $\chi^{xx}[n,m;\omega] \propto e^{A(n-m)}$ and $\chi^{pp}[n,m;\omega] \propto e^{-A(n-m)}$ due to the phase-dependent chiral propagation. With the factor of

$\chi^{xx}[N,;0]$, it would appear that we have we do in fact have an exponentially large response. Yet it precisely this terms which controls the number of coherent photons on site N, since $\bar{n}_N = \kappa|\beta|^2|\chi^{xx}[N,1,0]|^2$. Expressing the signal in terms of $\bar{n}_N$ gives

$$\mathcal{S}_\tau(N,\epsilon) = \sqrt{8\tau\kappa\bar{n}_N}|\frac{\epsilon}{\kappa}||\sin(\varphi-\phi)| \tag{2.114}$$

where we've used $\chi^{xx}[1,1;0] = \chi^{pp}[1,1;0] = 2/\kappa$ for a chain with a odd number of sites. The form of Eq. (2.114) makes it evident that $\mathrm{SNR}/\sqrt{\bar{n}_{\mathrm{tot}}}$ doesn't scale exponentially with system size, and therefore neither does $\mathrm{QFI}/\bar{n}_{\mathrm{tot}}$.

Despite the perturbation having coupled the two effective Hatano-Nelson chains with an amplitude of $\epsilon\cos\varphi$ (see Eqs. (2.110 and 2.111)), this is not enough to ensure a large $\mathrm{SNR}/\sqrt{\bar{n}_{\mathrm{tot}}}$. The non-local form of $\hat{V}_{\mathrm{NHSE}}$ implies that a wavepacket only experiences unidirectional amplification before exiting the waveguide. In contrast, the perturbation $\hat{V}_N = \hat{a}_N^\dagger\hat{a}_N$ studied throughout the main text allows for amplification before and after interacting with ϵ.

2.9.6 Single-Pole Approximation

As mentioned in the main text, we need to understand finite-time dynamics of our non-Hermitian lattice sensor. While we have the exact frequency-space susceptibilities through Eqs.(2.78-2.81) and Eqs. (2.97)-(2.98) to zeroth-order in ϵ, Fourier transforming to the time-domain becomes an intractable problem. Note that this is only true of the signal: to zeroeth order in ϵ, the noise is always vacuum.

There is however an exact form of the SNR in the limit where the hopping is infinite

$J \to \infty$. In this limit the susceptibilities Eqs. (2.97)-(2.98) take the form

$$\tilde{\chi}[N,1;\omega] = \frac{2i^N}{N+1}\frac{1}{\omega + i\frac{\kappa}{N+1}} \tag{2.115}$$

$$\tilde{\chi}[1,N;\omega] = \frac{-2i^{-N}}{N+1}\frac{1}{\omega + i\frac{\kappa}{N+1}} \tag{2.116}$$

such that the width of the zero mode is $\kappa/(N+1)$. The Fourier transform of each susceptibility (and their product, which is what determines linear response) is then easily computed.

The change to the cavity quadrature amplitude $\hat{p}_1$ at a time t in response to the perturbation ϵ can be found using Eq. (2.101) and first order perturbation theory

$$\begin{aligned}\langle \hat{p}_1(t)\rangle &= -\sqrt{2\kappa}\beta \int_0^t dT \delta\chi^{px}(1,1;T) \\ &= \sqrt{2\kappa}\epsilon\beta \int_0^t dT \int_0^T dT' \chi^{pp}(1,N:T-T')\chi^{xx}(N,1;T')\end{aligned} \tag{2.117}$$

Using $\chi^{xx}(n,m;t) = e^{A(n-m)}\tilde{\chi}(n,m;t)$, $\chi^{pp}(n,m;t) = e^{-A(n-m)}\tilde{\chi}(n,m;t)$, Eqs. (2.115) and (2.116) we get

$$\langle \hat{p}_1(t)\rangle = -\epsilon\sqrt{2\kappa}\beta(\frac{2}{N+1})^2 e^{2A(N-1)} \int_0^t dT T e^{-\frac{\kappa T}{N+1}} \tag{2.118}$$

From which we obtain the signal

$$\begin{aligned}&\mathcal{S}_\tau(N,\epsilon,J\to\infty) = \\ &\frac{\sqrt{2}\kappa|\beta||\epsilon|}{\sqrt{\tau}}(\frac{2}{N+1})^2 e^{2A(N-1)} \int_0^\tau dt \int_0^t dT T e^{-\frac{\kappa T}{N+1}}\end{aligned} \tag{2.119}$$

whereas the noise is always just $\mathcal{N}_\tau(N,\epsilon) = 1/\sqrt{2}$. The SNR for finite τ is then

$$\begin{aligned}&\mathrm{SNR}_\tau(N,\epsilon,J\to\infty) = \\ &\sqrt{\frac{\tau}{\tau_M^*(N)}}\left(1+e^{-\frac{\tau}{t_{esc}(N)}}-\frac{2t_{esc}(N)}{\tau}(1-e^{-\frac{\tau}{t_{esc}(N)}})\right)\end{aligned} \tag{2.120}$$

where recall

$$\tau_M^*(N) = \frac{1}{16Z(A)\bar{n}_{\mathrm{tot}}\kappa}\left(\frac{\kappa}{\epsilon_0}\right)^2 e^{-2A(N-1)} \tag{2.121}$$

is the measurement time when the steady-state expression holds.

We now want to find the measurement time $\tau_M^{J=\infty}(N)$ where in both the weak and strong measurement limit. In the weak measurement limit $\tau_M^*(N) \gg t_{esc}(N)$, we recover the steady state result $\tau_M^{J=\infty}(N) = \tau_M^*(N)$. In the strong measurement limit $\tau_M^*(N) \ll t_{esc}(N)$, we seek the leading order contribution to the measurement time. To that end, let us define

$$\gamma = \frac{\tau_M^{J=\infty}(N)}{\tau_M^*(N)} \tag{2.122}$$

so that

$$\left[\sqrt{\gamma}\left(1+e^{-\gamma\frac{\tau_M^*(N)}{t_{esc}(N)}}\right)-\frac{2t_{esc}(N)}{\tau_M^*(N)\sqrt{\gamma}}\left(1-e^{-\gamma\frac{\tau_M^*(N)}{t_{esc}(N)}}\right)\right]^2 = 1 \tag{2.123}$$

Assuming that $\gamma\tau_M^*(N)/t_{esc}(N)$ is small (which can be verified to be self-consistent after solving for γ), then we can Taylor expand the exponential to third order and obtain

$$\gamma^5 = \left(\frac{\sqrt{6}t_{esc}(N)}{\tau_M^*(N)}\right)^4 \tag{2.124}$$

from which

$$\tau_M^{J=\infty}(N) = \sqrt{6}t_{esc}(N)\sqrt[5]{\frac{\tau_M^*(N)}{\sqrt{6}t_{esc}(N)}} \tag{2.125}$$

as in the main text.

2.9.7 Non-perturbative effects of ϵ_0 to total photon number and output field

We now want to consider the full effect of ϵ_0 on the output field. To do so, we must compute the susceptibilities $\chi_{\epsilon_0}^{\alpha\beta}[1,1;\omega]$ to all orders in ϵ_0. The full Heisenberg-Langevin equations are

$$\dot{\hat{x}}_n = -i[\hat{x}_n, \hat{H}_B + \epsilon_0 \hat{a}_N^\dagger \hat{a}_N] - \delta_{n1}\left(\frac{\kappa}{2}\hat{x}_n + \sqrt{\kappa}\hat{X}^{(\text{in})}\right) \tag{2.126}$$

$$\dot{\hat{p}}_n = -i[\hat{p}_n, \hat{H}_B + \epsilon_0 \hat{a}_N^\dagger \hat{a}_N] - \delta_{n1}\left(\frac{\kappa}{2}\hat{p}_n + \sqrt{\kappa}\hat{P}^{(\text{in})}\right), \tag{2.127}$$

where as in the main text we've incorporated the drive tone amplitude in the definition of the input operators $\langle \hat{X}^{(\text{in})} \rangle = \beta$ and $\langle \hat{P}^{(\text{in})} \rangle = 0$.

Our strategy for solving the Heisenberg-Langevin equations will be nearly identical to that presented in Appendix 2.9.2. The key difference is that our squeezing transformation is now defined as

$$\hat{x}_n = e^{A(n-N)}\hat{\tilde{x}}_n \tag{2.128}$$

$$\hat{p}_n = e^{-A(n-N)}\hat{\tilde{p}}_n. \tag{2.129}$$

In this new frame, the Hamiltonian $\hat{H}_B + \epsilon_0 \hat{\tilde{a}}_N^\dagger \hat{\tilde{a}}_N$ preserves total quasiparticle number $\hat{\tilde{N}}$.

The Heisenberg-Langevin equations are then

$$\dot{\hat{\tilde{x}}}_n = -i[\hat{\tilde{x}}_n, \hat{H}_B + \epsilon_0 \hat{\tilde{a}}_N^\dagger \hat{\tilde{a}}_N] - \delta_{n1}\left(\frac{\kappa}{2}\hat{\tilde{x}}_n + e^{A(N-1)}\sqrt{\kappa}\hat{X}^{(\mathrm{in})}\right) \tag{2.130}$$

$$\dot{\hat{\tilde{p}}}_n = -i[\hat{\tilde{p}}_n, \hat{H}_B + \epsilon_0 \hat{\tilde{a}}_N^\dagger \hat{\tilde{a}}_N] - \delta_{n1}\left(\frac{\kappa}{2}\hat{\tilde{p}}_n + e^{-A(N-1)}\sqrt{\kappa}\hat{P}^{(\mathrm{in})}\right) \tag{2.131}$$

Crucially, we can immediately conclude that our chain is dynamically stable for any value of ϵ_0 and A: the spectrum is determined by the particle conserving Hamiltonian $\hat{H}_B + \epsilon_0 \hat{\tilde{a}}_N^\dagger \hat{\tilde{a}}_N$ and dissipation $\kappa/2$ on the first site.

Using these squeezing transformations in conjunction with Eqs. (2.82) and (2.83), we obtain the full form of the susceptibilities:

$$\chi_{\epsilon_0}^{xx}(n,m;t) = e^{A(n-m)}\,\mathrm{Re}\,\tilde{\chi}_{\epsilon_0}(n,m;t) \tag{2.132}$$

$$\chi_{\epsilon_0}^{pp}(n,m;t) = e^{-A(n-m)}\,\mathrm{Re}\,\tilde{\chi}_{\epsilon_0}(n,m;t) \tag{2.133}$$

$$\chi_{\epsilon_0}^{xp}(n,m;t) = -e^{-A(2N-n-m)}\,\mathrm{Im}\,\tilde{\chi}_{\epsilon_0}(n,m;t) \tag{2.134}$$

$$\chi_{\epsilon_0}^{px}(n,m;t) = e^{A(2N-n-m)}\,\mathrm{Im}\,\tilde{\chi}_{\epsilon_0}(n,m;t) \tag{2.135}$$

where $\tilde{\chi}_{\epsilon_0}(n,m;t)$ is the susceptibility matrix of the complex modes $\hat{\tilde{a}}_n$.

We already have the susceptibilities $\tilde{\chi}[n,m;\omega]$ of our tight-binding chain which incorporate the full effects of the the waveguide via Eq. (2.96). The frequency shift on the last site adds a term $-i\epsilon_0\delta_{n,N}\delta_{m,N}$ to the dynamical matrix. Dyson's equation in frequency space the gives:

$$\tilde{\chi}_{\epsilon_0}[n,m;\omega] = \tilde{\chi}[n,m;\omega] - i\epsilon_0\tilde{\chi}[n,N;\omega]\tilde{\chi}_{\epsilon_0}[N,m;\omega] \tag{2.136}$$

$$= \tilde{\chi}[n,m;\omega] - \frac{i\epsilon_0\tilde{\chi}[n,N;\omega]\tilde{\chi}[N,m;\omega]}{1+i\epsilon_0\tilde{\chi}[N,N;\omega]}. \tag{2.137}$$

Since there is a driving force only on the first site, we just need to find the susceptibilities

to a force on the first site:

$$\tilde{\chi}_{\epsilon_0}[n,1;\omega] = i^n \frac{U_{N-n}(\frac{\omega}{2J}) - \frac{\epsilon_0}{J}U_{N-1-n}(\frac{\omega}{2J})}{JU_N(\frac{\omega}{2J}) + (i\frac{\kappa}{2} - \epsilon_0)U_{N-1}(\frac{\omega}{2J}) - i\frac{\epsilon_0}{J}\frac{\kappa}{2}U_{N-2}(\frac{\omega}{2J})} \tag{2.138}$$

We now compute the steady state total photon number $\bar{n}_{\rm tot}(\epsilon_0)$ when $\epsilon_0 \neq 0$. Recall we are interested in the regime where $\epsilon_0/\kappa \ll 1$ but $e^{A(N-1)}\epsilon_0/\kappa$ is not a priori small. The form of our susceptibilities Eqs.(2.132)-(2.135) implies that A doesn't effect the spectrum, but just the residue of the poles as expected from our previous discussion. A non-zero value of ϵ_0 changes both the coherent drive-induced photon number, in addition to drive-independent photons generated from input vacuum fluctuations. The leading order correction to the total photon number when $\epsilon_0 \neq 0$ is therefore

$$\bar{n}_{\rm tot}(\epsilon_0) = \bar{n}_{\rm tot}(0) + (c\frac{\beta^2}{\kappa} + d)e^{4A(N-1)}(\frac{\epsilon_0}{\kappa})^2 + \mathcal{O}(e^{4A(N-2)}(\frac{\epsilon_0}{\kappa})^2) \tag{2.139}$$

where c and d are constants of order unity. Thus, Eq. (2.52) gives

$$Q(A,\epsilon_0) = \frac{4|\beta|^2 e^{2A(N-1)}/\kappa}{\bar{n}_{\rm tot}(0) + \frac{1}{2}(c\frac{\beta^2}{\kappa} + d)e^{4A(N-1)}(\frac{\epsilon_0}{\kappa})^2 + \mathcal{O}(e^{4A(N-2)}(\frac{\epsilon_0}{\kappa})^2)}. \tag{2.140}$$

With the optimal amplification factor A^*

$$e^{4A^*(N-1)} = \frac{\kappa^2}{8\epsilon_0^2} \tag{2.141}$$

in conjunction with Eq. (2.104), we get

$$Q(A^*,\epsilon_0) = \left(\frac{1 - e^{-2A^*(N+1)}}{1 - e^{-4A^*}} + \mathcal{O}(e^{-2A^*(N-1)})\right)^{-1} \tag{2.142}$$

$$= 1 - \mathcal{O}((\frac{8\epsilon_0^2}{\kappa^2})^{\frac{1}{N-1}}) \tag{2.143}$$

As in the main text. Note that we've taken the relevant limit $\beta^2/\kappa \gg 1$ such that we can ignore the amplified vacuum fluctuations to the total photon number

With the susceptibilities Eqs. (2.132)-2.135, we can also compute the quadrature-quadrature scattering matrix. If we first define

$$s[\omega] = 1 - \kappa\tilde{\chi}_{\epsilon_0}[1,1;\omega] \tag{2.144}$$

$$= \frac{a[\omega] + ib[\omega]}{a[\omega] - ib[\omega]} \tag{2.145}$$

with

$$a[\omega] = JU_N(\frac{\omega}{2J}) - U_{N-1}(\frac{\omega}{2J})\epsilon_0 \tag{2.146}$$

$$b[\omega] = \frac{\kappa}{2}\left(\frac{\epsilon_0}{J}U_{N-2}(\frac{\omega}{2J}) - U_{N-1}(\frac{\omega}{2J})\right) \tag{2.147}$$

then using the input-output boundary conditions Eq. (2.11) we find that the scattering matrix is

$$\boldsymbol{s}[\omega] = \begin{pmatrix} R[\omega] & -T[\omega]e^{-2A(N-1)} \\ T[\omega]e^{2A(N-1)} & R[\omega] \end{pmatrix} \tag{2.148}$$

with

$$R[\omega] = \frac{1}{2}\left(s[\omega] + s^*[-\omega]\right) \tag{2.149}$$

$$T[\omega] = \frac{1}{2i}\left(s[\omega] - s^*[-\omega]\right). \tag{2.150}$$

Note that $|s[\omega]|^2 = 1$, which implies $|R[\omega]|^2 + |T[\omega]|^2 = 1$. The zero-frequency component

of $R(\epsilon_0)$ and $T(\epsilon_0)$ are then:

$$R(\epsilon_0) = -\frac{(\frac{\kappa}{2})^2 - \epsilon_0^2}{(\frac{\kappa}{2})^2 + \epsilon_0^2} \tag{2.151}$$

$$T(\epsilon_0) = \frac{\kappa\epsilon_0}{(\frac{\kappa}{2})^2 + \epsilon_0^2} \tag{2.152}$$

as in the main text.

CHAPTER 3

NONEQUILIBRIUM STATIONARY STATES OF QUANTUM NON-HERMITIAN LATTICE MODELS

3.1 Overview of Results

We show how generic non-Hermitian tight-binding lattice models can be realized in an unconditional, quantum-mechanically consistent manner by constructing an appropriate open quantum system. We focus on the quantum steady states of such models for both fermionic and bosonic systems. Surprisingly, key features and spatial structures in the steady state cannot be simply understood from the non-Hermitian Hamiltonian alone. Using the 1D Hatano-Nelson model as a paradigmatic example, we show that the steady state has a marked sensitivity to boundary conditions. In particular, the open boundary system can exhibit a large macroscopic length scale, despite having no corresponding long timescale. These effects persist in more general models, and are distinct from the localization physics associated with the non-Hermitian skin effect. Further, particle statistics play an unexpected role: the steady-state density profile is dramatically different for fermions versus bosons. Our work highlights the key role of fluctuations in quantum realizations of non-Hermitian dynamics, and provides a starting point for future work on engineered steady states of open quantum systems.

3.2 Introduction

The physics of systems whose dynamics is governed by non-Hermitian Hamiltonians has generated interest in a wide range of fields, from classical optics [54, 26, 138, 35, 63], to topological band theory [73, 69, 43, 61, 70, 12, 8, 133], to soft-matter physics [119, 38, 118, 127, 147, 116, 144, 41]. Introducing non-Hermiticity often means forgoing seemingly

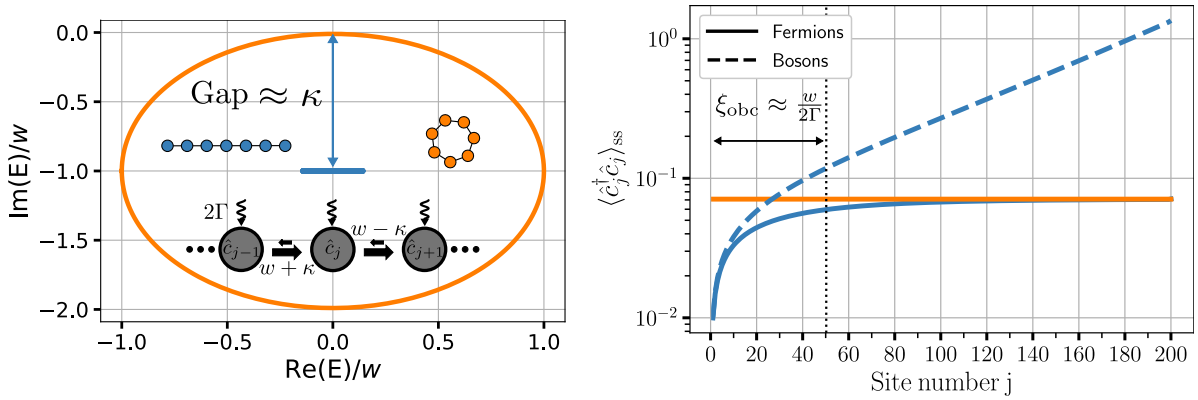

Fig. 3.1: Left: Periodic (orange) and open (blue) chain spectrum of the quantum Hatano-Nelson model with parameters $\kappa = 0.99w$ and $\Gamma = 0.01w$. The spectrum for fermions and bosons only differ by shift of $-i2\Gamma$, and we thus only plot the fermionic spectrum for clarity. Dissipation is used to realize asymmetric hopping amplitudes $w \pm \kappa$, and each site is incoherently pumped at a rate 2Γ. Right: Steady-state occupation $\langle \hat{c}_j^\dagger \hat{c}_j \rangle_{\rm ss}$ of a quantum Hatano-Nelson model under periodic boundary conditions for fermions (orange), and for open boundary conditions (OBC) for both fermions and bosons (blue). Remarkably, despite the existence of a large damping gap, the density is controlled by a large length scale $\xi_{\rm obc} \approx w/(2\Gamma)$. Further, $\xi_{\rm obc}$ is unrelated to $2A = \ln[(w+\kappa)/(w-\kappa)]$, the (inverse) localization length of the non-Hermitian Hamiltonian's OBC left and right eigenvectors. For fermions, $\xi_{\rm obc}$ corresponds to a healing length whereas for bosons it describes the exponentially localized pileup of particles on one edge. Note that we only plot the periodic boundary condition results for fermions, as the bosonic model with the same parameters is dynamically unstable.

basic intuition formed when studying Hermitian models. The extreme sensitivity to small perturbations [87, 20, 68] and having to revisit the bulk-boundary correspondence [141, 64, 52, 41] are a few of many such examples. Understanding these effects often amounts to studying the eigenvalues and corresponding right and left eigenvectors of an effective non-Hermitian Hamiltonian.

In the quantum regime, a fully consistent description of non-Hermitian dynamics requires one to consider an open quantum system, where modes of interest are coupled to dissipative Markovian baths. Conditioned on the absence of a quantum jump, the dynamics are governed by a non-Hermitian Hamiltonian whose anti-Hermitian part is determined by the coupling to the environment [110]. In contrast, the full unconditional dynamics also depends on

fluctuations. Despite numerous works examining non-Hermitian tight-binding models in quantum settings, few studies have fully addressed the unconditioned steady-state properties (for the fermionic case, see e.g. [6, 100]). There thus remain several basic open questions. These include the role of particle statistics, the possible sensitivity of the steady state to boundary conditions (analogous to the non-Hermitian skin effect (NHSE)[145, 146, 82]), and the general connections between the steady state's spatial structure and the underlying non-Hermitian Hamiltonian.

Here we address these questions by studying the steady states of open quantum systems that realize the physics of a target non-Hermitian tight-binding Hamiltonian $\hat{H}_{\text{eff}}$. We begin by discussing the general class of master equations that correspond to the desired $\hat{H}_{\text{eff}}$. We then construct the formal steady-state density matrix $\hat{\rho}_{\text{ss}}$ of such models, emphasizing that this requires specifying both $\hat{H}_{\text{eff}}$ and the unavoidable fluctuations arising from the coupling to dissipation. We find generically that these steady states exhibit features and spatial structures that are not at all obvious if one simply looks at the eigenvectors of $\hat{H}_{\text{eff}}$. Taking the paradigmatic non-reciprocal Hatano-Nelson model [49, 48] as an example, we find that the real-space steady-state occupation $\langle \hat{c}_j^\dagger \hat{c}_j \rangle_{\text{ss}}$ under open boundary conditions is controlled by a new macroscopic length scale ξ_{obc}, which is independent of the localization length of the right and left eigenvectors of $\hat{H}_{\text{eff}}$. Surprisingly, this new long length scale is not associated with or the result of a corresponding long time-scale: the dissipative gap is large under open boundary conditions (see Fig. 3.1). We argue that this feature is not specific to the Hatano-Nelson model by studying two additional models in App. 3.5.7 which feature multiple bands and/or broken time-reversal. Further, we demonstrate that the occupation is strikingly different for fermions and bosons, despite the left and right eigenvectors of $\hat{H}_{\text{eff}}$ being independent of particle statistics. Finally, we demonstrate that the set of orthogonal modes which fully specify the steady state under open boundary conditions are very similar to delocalized standing-wave states, even for extreme non-reciprocity: there is thus no true

analogue of the non-Hermitian skin effect for $\hat{\rho}_{\rm ss}$. Our results provide a framework to understand steady states of general non-Hermitian systems in the quantum regime, and illustrate how fluctuations play a critical role.

3.3 Consistent open-system description of quantum non-Hermitian Hamiltonians

3.3.1 Effective unconditional non-Hermitian Hamiltonians

The motivating question throughout this work is straightforward: if one wants quantum dynamics of a fermionic or bosonic system generated by a target non-Hermitian Hamiltonian

$$\hat{H}_{\rm targ} = \sum_{n,m} (H_{\rm targ})_{nm} \hat{c}_n^\dagger \hat{c}_m, \tag{3.1}$$

what can be said about the steady state? Here $\hat{c}_m$ and $\hat{c}_n^\dagger$ are fermionic or bosonic creation and annihilation operators satisfying canonical anti-commutation and commutation relations respectively. The indices n and m label independent orthogonal modes, and include any and all degrees of freedom such as position, spin or polarization.

Before attempting to formulate an answer, it is imperative to discuss how $\hat{H}_{\rm targ}$ is realized. Implementing an effective non-Hermitian Hamiltonian in a quantum system can be achieved by using parametric-amplifier type interactions [136, 85] or by considering an open quantum system (see e.g. [68]); we focus here on the latter. To ensure that the dynamics are Markovian, as is already implied by Eq. (3.1), the system of interest is coupled to independent Markovian reservoirs which either incoherently add or remove particles, processes described by the jump operators $\hat{L}_\mu = \sum_m l_{\mu m} \hat{c}_m$ and $\hat{G}_\nu = \sum_n g_{\nu n}^* \hat{c}_n^\dagger$ respectively. The coeffecients $l_{\mu n}$ and $g_{\nu n}^*$ specify in what state the particles are removed or added to the system by the environment, with μ and ν indexing the independent loss and pump baths. The equation of motion for

the density matrix has the standard Lindblad form, and can be written as ($\hbar = 1$)

$$\begin{aligned} i\partial_t\hat{\rho} \equiv \mathcal{L}\hat{\rho} = &\left(\hat{\mathcal{H}}_{\text{cond}}\hat{\rho} - \hat{\rho}\hat{\mathcal{H}}_{\text{cond}}^{\dagger}\right) \\ &+ i\sum_{\gamma} L_\gamma \hat{l}_\gamma \hat{\rho}\hat{l}_\gamma^{\dagger} + i\sum_{\delta} G_\delta \hat{g}_\delta^{\dagger}\hat{\rho}\hat{g}_\delta \end{aligned} \tag{3.2}$$

where $\mathcal{L}$ is the Lindbladian superoperator. The conditional Hamiltonian is defined as

$$\begin{aligned} \hat{\mathcal{H}}_{\text{cond}} = &\sum_{n,m} H_{nm}\hat{c}_n^{\dagger}\hat{c}_m \\ &- \frac{i}{2}\sum_{\gamma} L_\gamma \hat{l}_\gamma^{\dagger}\hat{l}_\gamma - \frac{i}{2}\sum_{\delta} G_\delta \left(1 \mp \hat{g}_\delta^{\dagger}\hat{g}_\delta\right) \end{aligned} \tag{3.3}$$

with $-$ and $+$ corresponding to fermionic and bosonic creation and annihilation operators respectively. We have defined $\hat{l}_\gamma = \sum_m \langle l_\gamma | m\rangle\, \hat{c}_m$ and $\hat{g}_\delta^{\dagger} = \sum_n \langle n|g_\delta\rangle\, \hat{c}_n^{\dagger}$, where $|l_\gamma\rangle$ and $|g_\delta\rangle$ are eigenvectors of the Hermitian positive semi-definite matrices $L_{nm} = (\boldsymbol{l}^{\dagger}\boldsymbol{l})_{nm}$ and $G_{nm} = (\boldsymbol{g}^{\dagger}\boldsymbol{g})_{nm}$ with corresponding eigenvalues L_γ and G_δ. Thus, the Hermitian matrix $\boldsymbol{H}$ describes the coherent Hamiltonian of the isolated system, whereas the matrices $\boldsymbol{L}$ and $\boldsymbol{G}$ completely capture the effects of the dissipative baths. Note that the choice of coherent Hamiltonian and dissipators leads to a master equation with a $U(1)$ symmetry $\hat{c}_n^{\dagger} \to e^{i\varphi}\hat{c}_n^{\dagger}$, $\hat{c}_m \to e^{-i\varphi}\hat{c}_m$. Our results and the phenomena we discuss do not fundamentally rely on this symmetry. They can readily be extended to quadratic Hamiltonians $\hat{H}$ which do not preserve particle number and arbitrary dissipiators which are linear in creation and annihilation operators.

By unraveling the master equation to a stochastic Schrödinger equation, one can show that $\hat{\mathcal{H}}_{\text{cond}}$ generates time evolution of the system conditioned on the absence of a quantum jump [21, 39]. The conditional Hamiltonian is thus only directly accessible by post-selecting measurement outcomes. While this is feasible in some platforms [97], it is generally challenging and involves discarding a large volume of data. More conventional experiments do

not post-select, and thus probe the full unconditioned dynamics of $\hat{\rho}$. Yet in this setting, it is not obvious that it is even possible to attribute the evolution of the density matrix to a single-particle Hamiltonian as we did for the post-selected evolution. How then should we think about the unconditioned evolution of $\hat{\rho}$?

The answer lies in the unconditional equations of motion of the normal-ordered covariance matrix $\langle \hat{c}_n^\dagger \hat{c}_m \rangle$ which reads (see App. 3.5.2)

$$\begin{aligned} i\partial_t \langle \hat{c}_n^\dagger \hat{c}_m \rangle = &\sum_a \Big((H_{\text{eff}})_{ma} \langle \hat{c}_n^\dagger \hat{c}_a \rangle - (H_{\text{eff}}^\dagger)_{an} \langle \hat{c}_a^\dagger \hat{c}_m \rangle \Big) \\ &+ iG_{mn} \end{aligned} \tag{3.4}$$

where

$$\boldsymbol{H}_{\text{eff}} \equiv \boldsymbol{H} - \frac{i}{2} (\boldsymbol{L} \pm \boldsymbol{G}) . \tag{3.5}$$

The $+$ and $-$ is for fermions and bosons respectively. This effective Hamiltonian $\boldsymbol{H}_{\text{eff}}$, which fully incorporates the effects of the jumps, is in general distinct from the effective Hamiltonian relevant to no-jump conditional evolution. From Eq. (3.3), this conditional Hamiltonian is

$$\boldsymbol{H}_{\text{cond}} = \boldsymbol{H} - \frac{i}{2} (\boldsymbol{L} \mp \boldsymbol{G}) . \tag{3.6}$$

Note that $\boldsymbol{H}_{\text{eff}}$ and $\boldsymbol{H}_{\text{cond}}$ only coincide in the absence of incoherent pumping (i.e. $\boldsymbol{G} = 0$). We stress that the identification of $\boldsymbol{H}_{\text{eff}}$ from the covariance matrix dynamics is independent of how correlators are ordered. Other ordering prescriptions lead to the same dynamical matrix $\boldsymbol{H}_{\text{eff}}$ (only the inhomogeneous term in the equations is modified, see App. 3.5.2). As shown in Refs. [112, 113], solving Eq. (3.4) is tantamount to knowing the full structure of the Lindbladian $\mathcal{L}$. In particular, the steady state density matrix is Gaussian, and hence

fully characterized by two-point averages. Eq. (3.4) thus lets us unambiguously identify the non-Hermitian dynamical matrix relevant to the unconditional steady state as $\boldsymbol{H}_{\text{eff}}$.

Eq. (3.4) is particularly easy to interpret when our particles are bosons. In this case, our system could also be described using the Heisenberg-Langevin equations

$$i\partial_t \hat{c}_m = \sum_a (H_{\text{eff}})_{ma} \hat{c}_l - \sum_\mu l_{\mu m} \hat{\eta}_\mu - \sum_\nu g^*_{\nu m} \hat{\zeta}^\dagger_\nu \tag{3.7}$$

which are equivalent to the master equation. The inhomogeneous terms $\hat{\eta}_\mu$ and $\hat{\zeta}^\dagger_\nu$ are the operator equivalent of independent Gaussian white noise with zero mean and unit variance (see Ref. [27] for a pedagogical introduction). The upshot is that Eq. (3.4) affords a similar interpretation for *either* particle type: $\hat{c}_m$ evolves under $\boldsymbol{H}_{\text{eff}}$ while being driven by white noise, and particle statistics only play a role in determining the anti-Hermitian part of $\boldsymbol{H}_{\text{eff}}$, the difference being a simple change of sign. For bosons, pump baths tend to generate amplification and exponential growth of amplitude and particle number. In contrast, for fermions, the Pauli principle makes this impossible and precludes exponential growth. This is enforced by the simple sign change in Eq. (3.5).

3.3.2 Constructing valid quantum descriptions of a target non-Hermitian Hamiltonian

Eq. (3.4) shows how a non-Hermitian Hamiltonian $\boldsymbol{H}_{\text{eff}}$ naturally arises in the description of unconditional dissipative quantum dynamics. We now ask a reverse engineering question: if one *starts* with a given, non-Hermitian Hamiltonian of interest $\boldsymbol{H}_{\text{targ}}$, how does one construct a valid corresponding quantum open system? This amounts to making consistent choices of both $\boldsymbol{H}_{\text{eff}}$ and the pumping matrix $\boldsymbol{G}$ appearing in Eq. (3.4) to match the desired dynamics. This construction is a crucial first step in understanding how any interesting features of $\boldsymbol{H}_{\text{targ}}$ might manifest themselves in a quantum setting (including the steady state).

Naively, one might start by simply picking $\boldsymbol{H}_{\text{eff}}$ in Eq. (3.4) to be identical to the desired Hamiltonian $\boldsymbol{H}_{\text{targ}}$. The validity of this procedure surprisingly depends on particle statistics. For fermions, we need to mindful of a constraint arising from the exclusion principle: $\boldsymbol{H}_{\text{eff}}$ for fermions cannot give rise to exponential growth, implying that the anti-Hermitian part of $\boldsymbol{H}_{\text{eff}}$ must be negative semi-definite. This follows directly from Eq. (3.5). Thus, for fermions, we will in general have to add loss to $\boldsymbol{H}_{\text{targ}}$ to satisfy this constraint. In contrast, choosing $\boldsymbol{H}_{\text{eff}} = \boldsymbol{H}_{\text{targ}}$ for bosons is always permissible.

We in general however will require more than a valid master equation, but will also want to ensure the existence of a unique steady-state. For this, the eigenvalues of the dynamical matrix $\boldsymbol{H}_{\text{eff}}$ must have negative-definite imaginary parts. To achieve this, we will generically have to add extra loss to bosonic Hamiltonians as well. To that end, let λ denote the largest positive eigenvalue of $-i(\boldsymbol{H}_{\text{targ}} - \boldsymbol{H}_{\text{targ}}^{\dagger})/2$. We will then choose $\boldsymbol{H}_{\text{eff}}$ according to:

$$\boldsymbol{H}_{\text{eff}} \equiv \lim_{\nu \to 0^+} \left(\boldsymbol{H}_{\text{targ}} - i(\lambda + \nu)\mathbf{1} \right). \tag{3.8}$$

This is a minimal prescription for satisfying the constraint for fermions and bosons: we simply add enough uniform loss to each mode to ensure the no-gain condition is satisfied. It implies that the eigenvectors of $\boldsymbol{H}_{\text{eff}}$ coincide that of $\boldsymbol{H}_{\text{targ}}$, and their spectra differ at most by a trivial global shift. This ensures that any interesting and desirable novel non-Hermitian phenomena exhibited by $\boldsymbol{H}_{\text{targ}}$ will also be present in $\boldsymbol{H}_{\text{eff}}$. Note that having $\nu = 0^+$ ensures a unique steady state.

We stress that the no-gain condition on the anti-Hermitian part of $\boldsymbol{H}_{\text{eff}}$ is strictly speaking distinct from requiring that the eigenvalues of $\boldsymbol{H}_{\text{eff}}$ have negative-definite imaginary part. The former, for fermions, ensures consistency with a valid master equation while the later, for both types of particles, is required for the existence of the steady-state.

Having $\boldsymbol{H}_{\text{eff}}$ match $\boldsymbol{H}_{\text{targ}}$ means that the drift terms in Eq. (3.4) directly mirror the desired non-Hermitian dynamics. This does not however specify our open quantum system:

we also need to specify $\boldsymbol{G}$ (i.e. the noise) in a manner that is consistent with $\boldsymbol{H}_{\text{eff}}$. There are of course many different ways to achieve this. In what follows, we present two simple and physically motivated approaches.

Method 1 - Minimal Prescription

Recall that the anti-Hermitian part of $\boldsymbol{H}_{\text{eff}}$ is determined by Eq. (3.5). The simplest way to fully specify our open quantum system is to have both the loss matrix $\boldsymbol{L}$ and pumping matrix $\boldsymbol{G}$ be proportional to the anti-Hermitian part of $\boldsymbol{H}_{\text{eff}}$. This leads to:

$$\boldsymbol{L} \equiv \begin{cases} i(1-\epsilon)(\boldsymbol{H}_{\text{eff}} - \boldsymbol{H}_{\text{eff}}^{\dagger}) & \text{fermions} \\ i\epsilon(\boldsymbol{H}_{\text{eff}} - \boldsymbol{H}_{\text{eff}}^{\dagger}) & \text{bosons} \end{cases} \tag{3.9}$$

$$\boldsymbol{G} \equiv \begin{cases} i\epsilon(\boldsymbol{H}_{\text{eff}} - \boldsymbol{H}_{\text{eff}}^{\dagger}) & \text{fermions} \\ i(\epsilon-1)(\boldsymbol{H}_{\text{eff}} - \boldsymbol{H}_{\text{eff}}^{\dagger}) & \text{bosons} \end{cases} \tag{3.10}$$

where the parameter ϵ ($0 \leq \epsilon \leq 1$ for fermions and $\epsilon > 1$ for bosons) determines the balance between pumping and loss. Diagonalizing $\boldsymbol{L}$ or $\boldsymbol{G}$ and specifying ϵ then directly determines one possible set of loss and pumping jump operators $\hat{L}_\mu$ and $\hat{G}_\nu$. This method gives us a simple way of generating a valid open system (for either fermions or bosons) with a minimal number of extra assumptions. The only additional parameter introduced (beyond the desired target Hamiltonian $\boldsymbol{H}_{\text{targ}}$) is ϵ. It controls the average particle number in the system, and hence plays the rough role of a chemical potential.

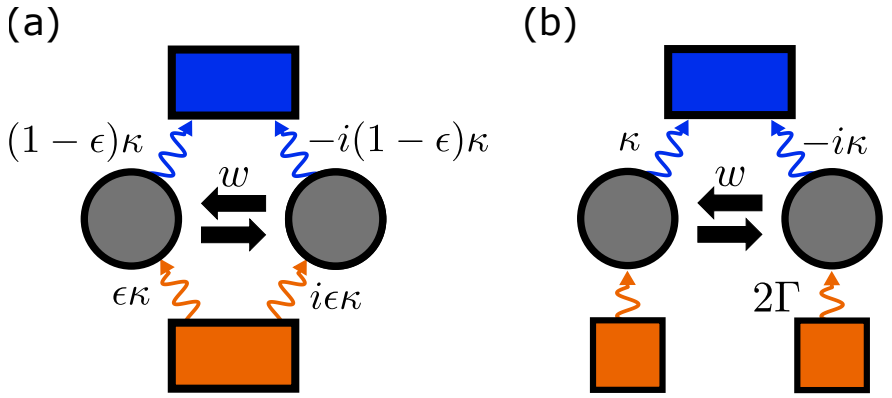

Fig. 3.2: Two different ways to realize the dissipative version of the fermionic quantum Hatano-Nelson model. Although both methods lead to an effective Hatano-Nelson Hamiltonian, they do not have the same steady state, since the noise $\boldsymbol{G}$ is not equivalent. (a) In the first method, each loss bath (blue) has an equivalent pumping bath (orange). The parameter ϵ controls the strength of the fluctuations $\boldsymbol{G}$. (b) In method two, the non-reciprocal hopping is realized using loss dissapators only. Each mode is also subject to uniform pumping, which leads to a non-trivial steady state.

Method 2 - Featureless Pumping

An alternate approach that in many cases is more experimentally tractable is to only use structured loss to realize the anti-Hermitian part of $\boldsymbol{H}_{\text{eff}}$, i.e. $\boldsymbol{L} = i(\boldsymbol{H}_{\text{eff}} - \boldsymbol{H}_{\text{eff}}^{\dagger})$. Of course, one still needs some pumping to have a steady state with non-zero particle number. This can be achieved by also introducing spatially uniform, featureless pumping to the system: $\boldsymbol{G} = 2\Gamma\mathbf{1}$, where Γ is an overall pumping rate. This pumping only changes $\boldsymbol{H}_{\text{eff}}$ by a constant diagonal term, implying that it still faithfully reflects the dynamics of the desired non-Hermitian Hamiltonian $\boldsymbol{H}_{\text{targ}}$. This is the method we employ throughout the main text. A visual comparison of the two methods for fermions is shown in Fig 3.2. Note that for bosons, pumping always decreases decay rates and care must be take to ensure dynamical stability (by, e.g. adding additional background loss).

3.3.3 *Steady state* $\hat{\rho}_{\rm ss}$

Having constructed a consistent master equation corresponding to the target dynamics $\hat{H}_{\rm targ}$, we now characterize the steady state of Eq. (3.2). With a quadratic coherent Hamiltonian and linear jump operators, the stationary-state is Gaussian and completely determined by the steady-state covariance matrix

$$F_{mn} \equiv \langle \hat{c}_n^\dagger \hat{c}_m \rangle_{\rm ss}. \tag{3.11}$$

If we assume that all eigenvalues of $\boldsymbol{H}_{\rm eff}$ have a non-zero negative imaginary part (as ensured by our construction in the previous subsection) then the steady state is unique, with $\boldsymbol{F}$ satisfying the so-called Lyaponov equation

$$\boldsymbol{H}_{\rm eff}\boldsymbol{F} - \boldsymbol{F}\boldsymbol{H}_{\rm eff}^\dagger = -i\boldsymbol{G}, \tag{3.12}$$

which follows from Eq. (3.4). The formal solution to $\boldsymbol{F}$ reads

$$\begin{aligned} F_{mn} &= \int_{-\infty}^{\infty} \frac{d\omega}{2\pi} \langle m| \frac{1}{\omega \mathbf{1} - \boldsymbol{H}_{\rm eff}} \boldsymbol{G} \frac{1}{\omega \mathbf{1} - \boldsymbol{H}_{\rm eff}^\dagger} |n\rangle \\ &= \sum_\delta G_\delta \int_{-\infty}^{\infty} \frac{d\omega}{2\pi} \langle m| \frac{1}{\omega \mathbf{1} - \boldsymbol{H}_{\rm eff}} |g_\delta\rangle \langle g_\delta| \frac{1}{\omega \mathbf{1} - \boldsymbol{H}_{\rm eff}^\dagger} |n\rangle . \end{aligned} \tag{3.13}$$

The last expression provides a simple intuitive interpreitation. At each frequency, the pump baths populates the state $|g_\delta\rangle$ at a rate G_δ which then evolves under the propagator $(\omega \mathbf{1} - \boldsymbol{H}_{\rm eff})^{-1}$ to different sites $|m\rangle$ in the lattice.

We stress that $\hat{\rho}_{ss}$ is thus controlled both by the non-Hermitian Hamiltonian *and* the fluctuations from the loss and pumping baths. This exact solution F_{mn} should be contrasted with previously suggested prescriptions on how to associate steady states with a given non-Hermitian Hamiltonian. These methods, such as exponentiating the non-Hermitian Hamil-

tonian [53, 83] or occupying the right or left eigenstates [142] are either ad-hoc or assume conditional dynamics. They are thus not relevant to the generic (unconditional) situation we consider.

If $\boldsymbol{H}_{\text{eff}}$ can be diagonalized, then the steady state correlation matrix can also be written as:

$$\boldsymbol{F} = -i \sum_{\alpha,\beta} \left|\psi_\alpha^R\right\rangle \left(\frac{\langle \psi_\alpha^L | \boldsymbol{G} | \psi_\beta^L \rangle}{E_\alpha - E_\beta^*} \right) \left\langle \psi_\beta^R \right| \tag{3.14}$$

where $\left|\psi_\alpha^R\right\rangle$ and $\left|\psi_\alpha^L\right\rangle$ are the right and left biorthonormal $\langle \psi_\alpha^L | \psi_\beta^R \rangle = \delta_{\alpha\beta}$ eigenvectors of $\boldsymbol{H}_{\text{eff}}$ with eigenvalue E_α. The form of $\boldsymbol{F}$ reminds us how we should interpret the eigenvectors of a non-Hermitian matrix. A right eigenvector $\left|\psi_\alpha^R\right\rangle$ is a mode whose temporal evolution is trivial and determined by the eigenvalue E_α, akin to how one normally thinks of eigenstates of a Hermitian matrix. The meaning of the left eigenstate $\left|\psi_\alpha^L\right\rangle$ is more subtle: it describes the susceptibility of the corresponding right eigenvector to a spatially varying perturbation. More concretely, the overlap $\left\langle \psi_\alpha^L \middle| g_l \right\rangle$ quantifies how the gain bath l "populates" the state $\left|\psi_\alpha^R\right\rangle$ [120].

Note that if we choose to implement our non-Hermitian dynamics using structured loss and uniform pumping (i.e. $\boldsymbol{G} = 2\Gamma \mathbf{1}$. c.f. Sec. 3.3.2), then Eq. (3.14) reduces to:

$$\boldsymbol{F} = -2i\Gamma \sum_{\alpha,\beta} \left|\psi_\alpha^R\right\rangle \left(\frac{\langle \psi_\alpha^L | \psi_\beta^L \rangle}{E_\alpha - E_\beta^*} \right) \left\langle \psi_\beta^R \right|. \tag{3.15}$$

Even in this seemingly simple case, we see that the steady state does correspond to a simple statistical mixture of right eigenvectors.

We have thus in principle achieved our goal of identifying the steady state: it is completely determined by the non-Hermitian Hamiltonian $\boldsymbol{H}_{\text{eff}}$ and the noise matrix $\boldsymbol{G}$ through Eqs. (3.13) and (3.14). As we will now show, these formal expressions do not immediately

provide useful intuition. In particular, the non-trivial interplay between the dynamics and the noise can lead to a steady state which cannot be understood by considering either independently. Further, there exist subtle new length scales in the steady state that are not associated with any one eigenvector, and which are not obvious from the general expression in Eq. (3.13).

3.3.4 Relevance to other work

We pause to note connections and differences between our work and previous studies connecting non-Hermitian physics, open quantum systems and steady states. While most works focus on conditional dynamics and the conditional Hamiltonian $\hat{\mathcal{H}}_{\text{cond}}$, several papers have addressed aspects of unconditional evolution and the role played by $\boldsymbol{H}_{\text{eff}}$. We stress that our work is markedly distinct from these previous studies. Refs. [75, 100, 6] discuss $\hat{\rho}_{\text{ss}}$ in the context of topological classification, which is not the focus here. The steady states of continuum interacting systems exhibiting non-Hermitian structures has also been studied in certain cases (see e.g. [46, 45]); this is also distinct from our non-Hermitian band-structure setting. Other works such as Refs. [79, 128, 96] explore the relaxation dynamics towards the stationary state, as determined solely by $\boldsymbol{H}_{\text{eff}}$. In contrast, our focus is the steady state itself, which manifestly depends on *both* the dynamics $\boldsymbol{H}_{\text{eff}}$ and the noise $\boldsymbol{G}$. The analysis in Ref. [33] does include the effect of fluctuations but focuses solely on infinite translationally invariant systems. Here, we show that the steady state is drastically different with boundaries present, in a manner that is not a trivial consequence of the NHSE.

Further, we analyze non-Hermitian Hamiltonian of both fermions and bosons, whereas previous works have mostly focused exclusively on the fermionic case.

We also note that quantum non-reciprocal models have been previously studied, motivated by applications to quantum engineering. Most works focus on few-mode systems, but lattices have also been considered recently [93, 87]. Unlike our work, the motivation in

these previous studies is different, and the focus is primarily on the output state of radiation emitted from the lattice.

3.4 Quantum Hatano-Nelson Model

We now focus on determining the steady state of an N-site Hatano-Nelson model, which describes particles asymmetrically hopping on a 1D lattice [49, 48]. In addition to being among the simplest of non-Hermitian tight-binding models, it also displays rich features such as the non-Hermitian skin effect [145, 64, 85] and non-Hermitian topology [8]. It thus serves as the ideal candidate to study how the non-Hermitian Hamiltonian imprints itself on the steady state.

The target Hamiltonian of interest reads

$$\hat{H}^{\mathrm{HN}}_{\mathrm{targ}} = \sum_j \left[\frac{w+\kappa}{2} \hat{c}^\dagger_{j+1} \hat{c}_j + \frac{w-\kappa}{2} \hat{c}^\dagger_j \hat{c}_{j+1} \right] \tag{3.16}$$

where without loss of generality we take $w, \kappa > 0$. Note the anti-Hermitian part of this Hamiltonian (proportional to κ) is not negative semi-definite, regardless of boundary conditions. To permit a quantum treatment valid for both fermions and bosons, we thus modify the Hamiltonian by adding minimal uniform loss, resulting in a valid $\boldsymbol{H}_{\mathrm{eff}}$ whose anti-Hermitian part is now negative semi-definite as required (c.f. Eq. (3.8)). Further, we will use method 2 (c.f. Sec. 3.3.2) to realize this non-Hermitian, non-reciprocal Hamiltonian using a set of structured, non-local loss baths and uniform incoherent pumping.

Following the above prescription, we obtain a Lindblad master equation (c.f. Eq. (3.2)) corresponding to the target Hatano-Nelson Hamiltonian. The coherent Hamiltonian $\hat{H}$ and

jump operators $\hat{L}_j$ and $\hat{G}_j$ are given by (see App. 3.5.3)

$$\hat{H} = \frac{w}{2} \sum_j \left(\hat{c}_{j+1}^\dagger \hat{c}_j + h.c. \right) \tag{3.17}$$

$$\hat{L}_j = \sqrt{\kappa} \left(\hat{c}_j - i\hat{c}_{j+1} \right) \tag{3.18}$$

$$\hat{G}_j = \sqrt{2\Gamma} \hat{c}_j^\dagger \tag{3.19}$$

where w is the coherent nearest-neighbour hopping, κ is the decay rate, Γ is the pumping rate. The resulting non-Hermitian Hamiltonian is (up to a constant) that of the Hatano-Nelson model: $\boldsymbol{H}_{\text{eff}} = \boldsymbol{H}_{\text{targ}}^{\text{HN}} - i(\kappa \pm \Gamma)\mathbf{1}$. Note that similar structured loss dissipators have been used to study non-reciprocal hopping in previous works, albeit with very different motivations (see e.g. [90, 81, 93, 62]).

While our mapping is general, we focus in what follows on the interesting case of strong non-reciprocity ($\kappa \lesssim w$) and weak pumping ($\Gamma \ll w, \kappa$). In this limit, the natural expectation is that the pumping serves only as a weak probe of the underlying non-Hermitian dynamics: its only purpose is to populate the system without disrupting the dynamics. As we will show, this is surprisingly not the case: the weak pumping rate Γ determines a new, extremely long system length scale. Further, for open boundary conditions, this long length scale is not related to a corresponding long relaxation time scale (i.e. the dissipative gap remains constant as $\Gamma \to 0$).

3.4.1 Periodic boundary conditions

We first work with periodic boundary conditions. With the effective Hamiltonian $\boldsymbol{H}_{\text{eff}}$ and pumping matrix $\boldsymbol{G}$, we can readily use the formalism described in the previous section to determine the steady-state correlation matrix $\boldsymbol{F}$. It is perhaps however more instructive to write the master equation in momentum-space. Letting N denote the number of sites in our

lattice and $\hat{c}_k = \sum_n e^{-ikn}\hat{c}_n/\sqrt{N}$, we have:

$$i\partial_t\hat{\rho} = \sum_k w\cos k[\hat{c}_k^\dagger\hat{c}_k, \hat{\rho}\ ] + i\sum_k \kappa(k)\mathcal{D}[\hat{c}_k]\hat{\rho} + i2\Gamma\sum_k \mathcal{D}[\hat{c}_k^\dagger]\hat{\rho} \tag{3.20}$$

where $\kappa(k) = 2\kappa(1+\sin k)$ and the allowed momenta are $k = 2\pi q/N$ with q an integer running from 1 to N. This form of the master equation serves as a useful reminder that non-Hermitian hopping can also be interpreted as momentum-depending damping $\kappa(k)$. This is also apparent by considering the spectrum of $\boldsymbol{H}_{\text{eff}}$ which reads $E(k) = w\cos k - i\kappa(1+\sin k)\mp i\Gamma$. To ensure stability in the bosonic case $\text{Im}(E(k)) < 0$, we always work in the limit of weak pumping and where the quantization of k leads to $\Gamma < \kappa(1+\sin k)$ for all allowed k.

It is clear from Eq. (3.20) that there will be no steady-state coherences between different momentum states. The independent baths add and remove particles from these orthogonal modes, and the coherent dynamics can not cause any transition between such states. The only non-vanishing steady-state component in this basis are the diagonal elements

$$\langle\hat{c}_k^\dagger\hat{c}_k\rangle_{\text{ss}} = \frac{1}{e^{\beta\epsilon(k)}\pm 1} \tag{3.21}$$

where we have defined the effective Boltzman factor

$$e^{-\beta\epsilon(k)} \equiv \frac{2\Gamma}{\kappa(k)}. \tag{3.22}$$

The steady state of the periodic-boundary condition Hatano-Nelson model is thus completely determined by these effective momentum-dependent Boltzmann factors. The non-reciprocity of our system reflects itself in an asymmetry of the momentum-space occupancy of mode at k versus $2\pi - k$. The real-space steady-state density is of course uniform, as required by translational invariance. We also stress that only the product of β and $\epsilon(k)$ is physically meaningful.

A simple but crucial point is that our steady state is insensitive to the coherent Hamiltonian $\hat{H}$; the steady state would not change even if we added additional (translationally-invariant) terms to $\hat{H}$. This is a general feature of master equations where the Hamiltonian $\boldsymbol{H}$, loss $\boldsymbol{L}$ and pumping matrices $\boldsymbol{G}$ commute with one another. In this instance, it is always possible to write the master equation in a compact form by using the basis which diagonalizes all three matrices, in analogy with Eq. (3.20). The physics underling the steady states of these models are then readily understood in terms of a orthogonal set of modes, the same as the effective Hamiltonian $\boldsymbol{H}_{\text{eff}}$.

For instance, in this translationally-invariant model, the real-space correlation functions for fermions can be easily obtained using Eq. (3.21):

$$\langle \hat{c}_j^\dagger \hat{c}_p \rangle_{\text{ss}} = \frac{1}{N} \sum_k \frac{\Gamma e^{-i(j-p)k}}{\Gamma + \kappa(1+\sin k)} \sim e^{-|j-p|/\xi_{\text{pbc}}} \tag{3.23}$$

where the difference $j-p$ is understood to be modulo N. Note that bosons are generically unstable in this model due to the additional pumping Γ, and there is thus no steady state. Here ξ_{pbc} is length scale determined by the dissipation, and is defined by $\kappa \cosh \xi_{\text{pbc}}^{-1} \equiv \kappa + \Gamma$. For small pumping it behaves as $\xi_{\text{pbc}} = \sqrt{\kappa/(2\Gamma)}$ (see App. 3.5.4 for details). This (inverse) length scale can be readily extracted by considering the spectrum of our periodic chain $E(k) = w\cos k - i\kappa(1+\sin k) - i\Gamma$. The smallest decay rate of any mode is Γ. It is thus not surprising that this quantity gives rise to a large length scale. In fact, it was shown in Ref. [33] that for a transitionally- invariant non-Hermitian tight-binding model with periodic boundary conditions, this is *always* the case: a divergent correlation length must be accompanied by a critical slowing down, i.e. a vanisingly small decay rate. Surprisingly, we will see that this intuitive connection between large length and times scales will be violated by introducing boundaries.

3.4.2 Open boundary conditions

We now examine the properties of our quantum Hatano-Nelson chain under open (rather than periodic) boundary conditions. It is well known that this change of boundary conditions dramatically alters the spectrum and eigenvectors of $\boldsymbol{H}_{\text{eff}}$ [49, 48]. At a formal level, this can be understood as arising from an incompatibility between the Hermitian and anti-Hermitian parts of $\boldsymbol{H}_{\text{eff}}$. For periodic boundary conditions, both are diagonalized by plane waves, whereas with open boundary conditions these matrices no longer commute. This incompatibility has a direct consequence on our quantum master equation (specified by Eqs. (3.17)-(3.19)): the jump operators associated with our structured loss can now cause transitions between different eigenstates of the coherent Hamiltonian $\hat{H}$. As we will see, this directly leads to a far more interesting steady state than in the periodic boundary condition case.

The most immediate consequence of having boundaries is that the steady-state average density $\langle \hat{c}_j^\dagger \hat{c}_j \rangle_{\text{ss}}$ will not be spatially uniform, as shown in Fig. 3.3. It is tempting to assume that this will simply reflect the NHSE; however, we show in the following that this is due to a distinct mechanism.

In the conventional scenario, the NHSE causes right eigenvectors to localize at one edge: $\left\langle j \middle| \psi_\alpha^R \right\rangle \propto e^{Aj}$ with the inverse localization length A given by

$$A = \frac{1}{2} \ln \left(\frac{w+\kappa}{w-\kappa} \right). \tag{3.24}$$

The appearance of this short lengthscale A^{-1} is accompanied by an opening of the dissipative gap: the decay rate of all eigenmodes of $\boldsymbol{H}_{\text{eff}}$ become large, unlike its periodic counterpart which has nearly undamped modes, see Fig. (3.1). Conventional wisdom would then suggest that any length scale in the open boundary case is much smaller than the periodic boundary lengthscale $\xi_{\text{pbc}} \gg \xi_{\text{obc}}$; particles are so heavily damped that they can

not propagate very far. However, surprisingly, the opposite is true: not only is the characteristic length for the steady state in open boundary condition $\xi_{\mathrm{obc}} = w/(2\Gamma)$ completely unrelated to the localization length A of right and left eigenvectors, but it is also parametrically larger than the lengthscale of the equivalent system with periodic boundary conditions $\xi_{\mathrm{pbc}} = \sqrt{\kappa/(2\Gamma)}$ at small Γ. Hence, simply knowing about the NHSE and its impact on the eigenvectors or eigenvalues does not immediately let one understand the spatial dependence of the steady-state density. We expect this to be a generic feature of open quantum systems exhibiting NHSE: we have provided two more examples in App. 3.5.7.

Instead of thinking about eigenvectors of eigenvalues of $\boldsymbol{H}_{\mathrm{eff}}$, a more fruitful starting point is to use the alternate formal solution for the steady-state correlation matrix given in Eq. (3.13). This yields

$$\langle \hat{c}_j^\dagger \hat{c}_j \rangle_{\mathrm{ss}} = 2\Gamma \sum_{p=1}^{N} \int_{-\infty}^{\infty} \frac{d\omega}{2\pi} |G^R_{\mathrm{obc}}[j,p;\omega]|^2 \tag{3.25}$$

with $G^R_{\mathrm{obc}}[j,p;\omega] \equiv \langle j| \left(\omega \mathbf{1} - \boldsymbol{H}_{\mathrm{eff}}\right)^{-1} |p\rangle$ the real-space retarded Green's function with open boundaries. Equation (3.25) reminds us how the incoherent pumping populates each site. A pump bath attached to site p injects a particle with frequency ω which then propagates to site j with an amplitude given by $G^R_{\mathrm{obc}}[j,p;\omega]$. The total particle number is thus this amplitude squared summed over all baths and frequencies.

The physical picture provided to us by Eq. (3.25) implies that we should attempt to understand the real-space propagation dynamics of $\boldsymbol{H}_{\mathrm{eff}}$ as encoded by the Green's function. Although the NHSE forces both the eigenvectors and eigenvalues of $\boldsymbol{H}_{\mathrm{eff}}$ to change drastically when there are edges, on physical grounds the same should not be true of the Green's function. For the short-ranged Hamiltonian under consideration, we expect for large enough system size N that the response for open boundary conditions is well approximated by the infinite-system Green's function $G^R_{\mathrm{obc}}[j,p;\omega] \approx G^R_{\infty}[j-p;\omega]$, at least within the bulk

$1 \ll j, p \ll N$. The length scale which controls the steady-state occupation $\langle \hat{c}_j^\dagger \hat{c}_j \rangle_{\rm ss}$ is therefore essentially determined by how far a particle injected into the boundary-free chain can propagate before it loses an appreciable amount of its amplitude.

The dispersion of the Hatano-Nelson model $E(k) = w \cos k - i\kappa(1+\sin k) \mp i\Gamma$ can be readily used to extract this length scale. Indeed, ignoring the boundaries affords us the possibility to think about propagation in terms of plane waves. We first note that the least damped momentum mode at $k = -\pi/2$ also has the largest group velocity $w(\partial_k \cos k)|_{k=-\pi/2} = w > 0$ which implies a right-moving mode. We can thus estimate the relevant decay length as this maximal group velocity w divided by the residual decay rate Γ of that mode. We thus have $G^R_{\rm obc}[j, p; 0] \sim e^{\mp |j-p|/(w/\Gamma)}$ when $p < j$. Note the sign difference for fermions versus bosons: Γ induces additional damping for fermions yet bosons experience spatial amplification as a consequence of the additional pumping.

The above heuristic estimate is confirmed by a more careful analysis of the open-boundary Green's function provided in App. 3.5.5.

It is demonstrated that $G^R_{\rm obc}[j, p; \omega] \approx G^R_\infty[j-p; \omega]$ and $G^R_{\rm obc}[j, p; 0] \sim e^{\mp |j-p|/(w/\Gamma)}$ are excellent approximations in the strong non-reciprocity $\kappa \approx w$ and weak pumping $\Gamma \ll w, \kappa$ limit. Generically, one can also associate a (direction-dependent) decay length to $G^R[j, p; w]$ for arbitrary ω: for $j > p$ it is roughly w/Γ near zero-frequency and drops quickly to zero outside the band $\omega \approx w$. However in the limit of interest where the spacing of the modes is much smaller than their width, the occupation is dominated by low frequencies and we find

(see App. 3.5.5 for details)

$$\begin{aligned}\langle \hat{c}_j^\dagger \hat{c}_j \rangle_{\rm ss} &\overset{\kappa \to w}{\approx} \frac{\Gamma}{\kappa \pm \Gamma} \left(1 + C_1 \sum_{p<j} \frac{e^{\mp 2|j-p|/(w/\Gamma)}}{\sqrt{|p-j|}} \right) \\ &\approx \begin{cases} \frac{\Gamma}{\kappa+\Gamma} \left(\frac{\mathrm{erf}(\sqrt{\frac{j}{\xi_{\rm obc}}})}{\sqrt{\xi_{\rm obc}^{-1}}} + C_2 \right), & \text{fermions} \\ \frac{\Gamma}{\kappa-\Gamma} \left(\frac{\mathrm{erfi}(\sqrt{\frac{j}{\xi_{\rm obc}}})}{\sqrt{\xi_{\rm obc}^{-1}}} + C_3 \right), & \text{bosons.} \end{cases} \end{aligned} \tag{3.26}$$

In the first line, we immediately consider the limit of extreme non-reciprocity where only pump baths attached to sites on the left of a given site j contribute to the occupation. In this limit, the localization length $1/A$ associated with the NHSE goes to zero yet, in contrast, we see the emergence of a new length scale $\xi_{\rm obc} = w/(2\Gamma)$ which controls the quantum steady state of the open boundary condition system. Here, erf and erfi are the error and imaginary error function respectively, and C_1, C_2, C_3 are constants (see App. 3.5.5).

Equation (3.26) is a central result of our work. It demonstrates that the spatial distribution of the steady-state occupation is controlled by a new macroscopic length scale $\xi_{\rm obc} = w/(2\Gamma)$, despite the absence of a long time scale. In addition, $\xi_{\rm obc}$ does not resemble any right or left eigenvector of $\boldsymbol{H}_{\rm eff}$. Colloquially, the open-boundary steady state has "remembered" the long propagation length of the periodic chain but not the associated long time scale that came with it. Further, it shows that this new emergent lengthscale has a dramatically different interpretation depending on particle statistics. For fermions it corresponds to a *decay length*, whereas for bosons it represents an *amplification length*.

In Fig. 3.1 we plot the steady-state occupation $\langle \hat{c}_j^\dagger \hat{c}_j \rangle_{\rm ss}$ and find behaviour consistent with the above interpretation. The density of fermions in the steady state is suppressed over a length scale $\xi_{\rm obc}$ on the left edge of the system, and saturates as we move to the right at a value coinciding with the expected constant PBC occupancy. In contrast, the number of bosons increases exponentially as one moves to the right edge of the system, with $\xi_{\rm obc}$ now

serving as the associated localization length. The numerically-computed results in Fig. 3.1 do not differ from the analytical prediction of Eq. (3.26) on the presented scale.

In Fig. 3.3 we plot the scaled steady-state occupation $\langle \hat{c}_j^\dagger \hat{c}_j \rangle_{\rm ss} / \langle \hat{c}_N^\dagger \hat{c}_N \rangle_{\rm ss}$ over a range of Γ. The behaviour here has a simple origin. Vanishingly small pumping $\Gamma \approx 0$ implies a large length scale $\xi_{\rm obc} \gg N$ and we expect the density of particles in the steady-state to be essentially independent of statistics: the particles must propagate a large distance before the effects of Γ are noticeable. This is verified by taking the $\xi_{\rm obc} \gg j$ limit of Eq. (3.26), which gives

$$\langle \hat{c}_j^\dagger \hat{c}_j \rangle_{\rm ss} \sim \frac{\Gamma}{\kappa \pm \Gamma} \left(1 + \frac{2}{\sqrt{\pi}} \left(\sqrt{j} - 1 \right) \right) \tag{3.27}$$

where the $+$ $(-)$ sign is for fermions (bosons).

As we increase the pumping, fermions will experience additional damping. Particles injected by the baths into the chain can therefore not propagate as far before decaying. The length scale $\xi_{\rm obc}$ thus becomes smaller, and the particle density will saturate more rapidly as we move from left to right. In contrast, bosons are less damped as we increase Γ, but this simply means particles can propagate further, and we expect that the accumulation of particles on the right edge becomes more pronounced. Both these predictions are in agreement with Fig. 3.3, and with the analytical result obtained for $\xi_{\rm obc}$ in the limit of larger pumping (see Eq. (3.63)).

The analysis presented in this section shows conclusively that in a quantum realization of the Hatano-Nelson model, a large dissipative gap in the spectrum of $\boldsymbol{H}_{\rm eff}$ does not preclude the existence of a long length scale. Further, neither the spatial structure of left or right eigenvectors can be used to infer the steady-state occupation $\langle \hat{c}_j^\dagger \hat{c}_j \rangle_{\rm ss}$ under open boundary conditions. Do these two features holds generically? Referring back to Eq. (3.25) and the accompanying discussion, we expect this to be the case. The steady-state occupation is controlled by the real-space Green's function and unlike the spectrum and eigenvectors,

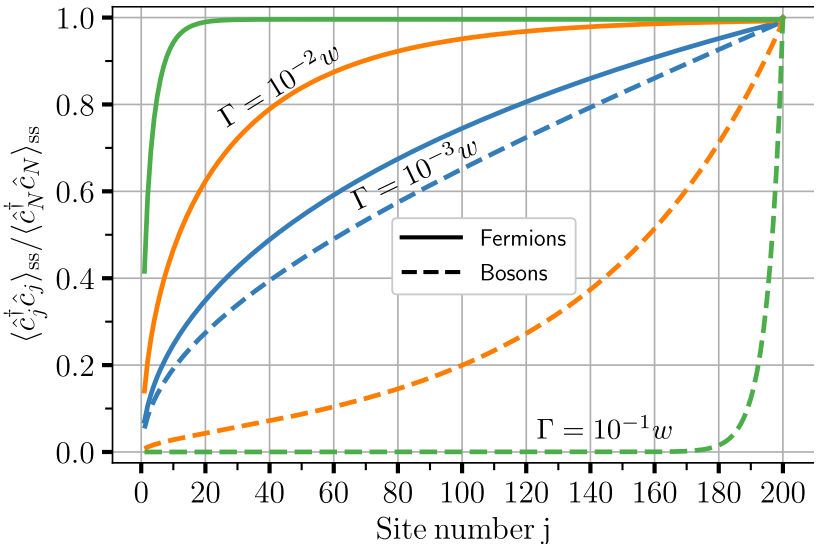

Fig. 3.3: Scaled steady-state occupation $\langle \hat{c}_j^\dagger \hat{c}_j \rangle_{\rm ss} / \langle \hat{c}_N^\dagger \hat{c}_N \rangle_{\rm ss}$ under open boundary conditions of the Hatano-Nelson model realized with a coherent Hamiltonian and dissipators Eqs. (3.17)-(3.19) for $N = 200$ sites and $\kappa = 0.99w$. For small enough pumping, the occupation for bosons and fermions are essentially identical. As we increase the pumping, the length scale $\xi_{\rm obc}$ decreases. In the fermionic case this leads to a depletion of particles on the left-hand side of the chain. For bosons, this leads to exponential localization of particles on the right hand side of the system. Note that unlike the periodic boundary condition case, the bosonic model is dynamically stable for these parameters ($\kappa \leq w$ and $\Gamma < \kappa$). These numeric plots are indinguishable from the analytical forms predicted by Eqs. (3.26) on this scale.

the former is largely unaffected by the NHSE when changing boundary conditions. The long attenuation length in the infinite-sized model can therefore show up in the finite open-boundary case, despite having a large damping gap. To verify this prediction, we briefly analyze two additional non-Hermitian models in App. 3.5.7. Both models exhibit, a large dissipative gap, yet there stills exists a large length scale in both models which can be extracted from the Green's function of the infinite-sized model.

The validity of $G^R_{\rm obc}[j, p; \omega] \approx G^R_\infty[j - p; \omega]$ also makes it clear that the sensitivity to boundary conditions is not caused by the NHSE. Once this approximation has been made, the only remaining information regarding boundary conditions is the trivial one: particles can not tunnel directly between the first and last site. Given the propensity for particles to propagate to the right, this implies that a pump bath attached to the first site can contribute

to to the total particle number on site N, but not vice-versa. Thus, the asymmetry we see in the occupation is categorically not due to a change in the spectrum or eigenvectors of $\boldsymbol{H}_{\text{eff}}$ and therefore not due to the NHSE. Rather, the built-in non-reciprocity of the effective Hamiltonian is the sole reason we see just a drastic change under different geometries.

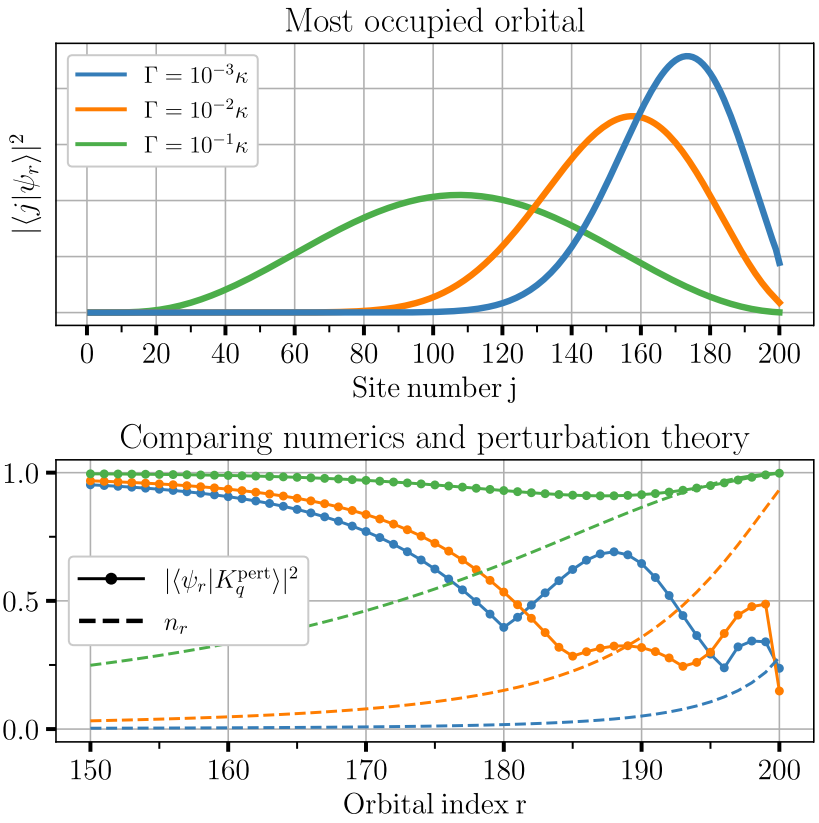

Fig. 3.4: Top: real-space wavefunction squared $|\langle j|\psi_r\rangle|^2$ of the most occupied steady state orbital for our quantum Hatano-Nelson model with open boundary conditions, $N = 200$ and $w = 0.9\kappa$. The model is realized using a coherent Hamiltonian and dissipators Eqs. (3.17)-(3.19). Despite the strong non-reciprocity for our chosen parameters, this dominant orbital wavefunction does not exhibit the exponential localization associated with the NHSE. Bottom: same parameters, steady state orbital occupation n_r (dashed lines) and the overlap squared $|\langle\psi_r|K_q^{\text{pert}}\rangle|^2$ between the exact orbitals $|\psi_r\rangle$ and the ones obtained from second order perturbation theory in w, $\left|K_q^{\text{pert}}\right\rangle$ (dotted lines). Despite the large value of w, the perturbative expression for the orbitals still provides a reasonable approximation for most orbitals. This implies that the majority of orbitals are spatially extended over the whole chain, and have no resemblance to the right and left eigenvectors of $\boldsymbol{H}_{\text{eff}}$.

3.4.3 Orbitals

The steady-state real-space average occupation only gives us partial information about $\hat{\rho}_{\text{ss}}$. In general, one would need knowledge of all possible steady-state correlations to recreate $\hat{\rho}_{\text{ss}}$. The Gaussian nature of our steady state greatly simplifies this task: all higher-order correlations are completely determined by the two-point correlation matrix $\boldsymbol{F}$ (i.e. Wick's theorem holds). Indeed, if we let $|\psi_r\rangle$ denote the eigenvectors of $\boldsymbol{F}$ with eigenvalue n_r then the Gaussian nature of the steady state implies

$$\hat{\rho}_{\text{ss}} = \frac{\exp\left(\sum_r \ln\left(\frac{n_r}{1\mp n_r}\right)\hat{c}_r^\dagger \hat{c}_r\right)}{\mathcal{Z}} \tag{3.28}$$

where $\mathcal{Z}$ is a normalization constant, $-$ $(+)$ is for fermions (bosons) and $\hat{c}_r$ and $\hat{c}_r^\dagger$ are the (orthogonal) annihilation and creation operators associated with $|\psi_r\rangle$. We thus see that the eigenvectors $|\psi_r\rangle$ represent real-space wavefunctions of orbitals that are independently occupied in the steady state.

Identifying this structure leads to an obvious question: does the spatial structure of these occupied-orbital wavefunctions change drastically in going from periodic to open boundary conditions? Note that these wavefunctions $|\psi_r\rangle$ are eigenvectors of a Hermitian matrix, and hence form a complete orthonormal basis. They thus cannot coincide with either the right or left eigenvectors of $\boldsymbol{H}_{\text{eff}}$. In what follows, we show something even stronger: these occupied orbital wavefunctions do not exhibit any singular behaviour remotely analogous to the non-Hermitian skin effect.

It is tempting to argue that this is to be expected, given that $\boldsymbol{F}$ is a Hermitian matrix. One might argue that these objects, unlike their non-Hermitian counterparts, are more robust to perturbations (such as varying boundary conditions) and that singular behavior of their eigenstates is ruled out by construction. This intuition is however incorrect. Perhaps the

best way to demonstrate why this reasoning is incorrect is to express $\boldsymbol{F}$ as

$$\boldsymbol{F} = \int_0^\infty dt e^{-i\boldsymbol{H}_{\text{eff}}t}\boldsymbol{G}e^{i\boldsymbol{H}_{\text{eff}}^\dagger t}. \tag{3.29}$$

Perturbations to $\boldsymbol{H}_{\text{eff}}$ which are naively thought to be small therefore have an infinite amount of time to influence the steady state. This can already be seen by considering the steady-state occupation $\langle \hat{c}_j^\dagger \hat{c}_j \rangle_{\text{ss}}$ of fermions versus bosons as see in Fig. (3.1). The only difference between their effective Hamiltonians is the small uniform rate Γ. Nevertheless, this leads to an exponentially large difference in average particle number on the last site $\langle \hat{c}_N^\dagger \hat{c}_N \rangle_{\text{ss}} \sim e^{\mp 2\Gamma/wN}$. It it thus not immediately obvious that changing boundary conditions does not drastically alter the orbitals $|\psi_r\rangle$ in analogy with the NHSE.

We focus on the most interesting regime of strong non-reciprocity where w is just slightly smaller than κ. Obtaining the desired occupied-orbital wavefunctions $|\psi_r\rangle$ analytically by diagonalizing $\boldsymbol{F}$ is unfortunately infeasible. Instead, we use a perturbative argument that has three steps. We first find the steady-state correlation matrix $\boldsymbol{F}_0$ for the case where the coherent hopping vanishes $w \to 0$. We next calculate the leading order corrections for small w. Finally, we argue that (somewhat surprisingly) this perturbative-in-w expression remains approximately valid even for modestly large values of hopping.

Consider then the case $w = 0$, where we have a fully reciprocal system but with only dissipative hopping processes mediate by the loss baths. One finds that in this case, the steady state covariance matrix has the form

$$\boldsymbol{F}_0 = \sum_{K_q} n_{K_q} \left|K_q\right\rangle \left\langle K_q\right|. \tag{3.30}$$

Here $\left|K_q\right\rangle$ are standing-wave states with a center of mass momentum $\pi/2$

$$\left\langle j\middle|K_q\right\rangle = \sqrt{\frac{2}{N+1}} e^{i\frac{\pi}{2}j} \sin K_q j. \tag{3.31}$$

n_{K_q} is the corresponding occupation, completely determined by the eigenvalues of $\boldsymbol{G}$ and $\boldsymbol{L}$

$$n_{K_q} = \frac{G_{K_q}}{L_{K_q} + G_{K_q}} = \frac{\Gamma}{\kappa(1 + \cos K_q) + \Gamma} \tag{3.32}$$

with $K_q = q\pi/(N+1)$ and q an integer that runs from 1 to N. The orbitals and occupation numbers strongly resemble what we would find with periodic boundaries. This should not be a surprise, as there is no non-reciprocity and all the dynamics can be understood in terms of the Hermitian matrix $\boldsymbol{L}$.

Now we wish to consider the effect of a finite but small coherent hopping matrix element w. Writing the steady-state correlation matrix as $\boldsymbol{F} = \boldsymbol{F}_0 + w\boldsymbol{F}_1 + \mathcal{O}(w^2)$ and using Eq. (3.12) we obtain

$$\langle K_q|\boldsymbol{F}_1|K_{q'}\rangle = \frac{i}{w}\frac{n_{K_q} - n_{K'_q}}{G_{K_q} + L_{K_q} + G_{K_{q'}} + L_{K_{q'}}}\langle K_q|\boldsymbol{H}|K'_q.\rangle \tag{3.33}$$

The overlap $\langle K_q|\boldsymbol{H}|K_{q'}\rangle$ is zero if K_q and $K_{q'}$ have the same parity and

$$\langle K_q|\boldsymbol{H}|K'_q\rangle = \frac{wi}{N+1}\frac{\sin K_q \sin K'_q}{\sin\left(\frac{K'_q - K_q}{2}\right)\sin\left(\frac{K'_q + K_q}{2}\right)} \tag{3.34}$$

$$\approx \begin{cases} \frac{wi}{N+1}, & K_q \approx K_{q'} \approx 0 \text{ or } \pi \\ \frac{w2i}{\pi}, & K_q \approx K_{q'} \approx \frac{\pi}{2} \end{cases} \tag{3.35}$$

otherwise. In addition to the expected overlap $\langle K_q|\boldsymbol{H}|K_{q'}\rangle$ there are two factors that contribute to the first order correction. The numerator of Eq. (3.33) implies that states which have nearly identical occupations $n_{K_q} \approx n_{K_{q'}} \implies K_q \approx K_{q'}$ are not strongly mixed. States which are weakly damped $G_{K_q} + L_{K_q} \approx \Gamma \implies K_q \approx \pi$ are more sensitive to the perturbation than states which are heavily damped, which occurs when $K_q \approx 0$. We stress that Eq. (3.33) implies that the smallest dimensionless parameter in our problem is w/Γ (i.e.

when $K_q \approx K_{q'} \approx -\pi$).

The higher-order perturbative corrections to $\boldsymbol{F}$ have a similar structure to Eq. (3.33) in that they also depend on the ratio of population differences to decay rates of the unperturbed orbitals (see App. 3.5.6). Taking all three terms into account, we thus expect orbitals near $K_q \approx 0$ to be nearly unchanged by the perturbation $\boldsymbol{H}$ even when $w \approx \kappa$, both because their damping rate is large, and the overlap $\langle K_q|\boldsymbol{H}|K_{q'}\rangle$ with other modes is small. Conversely, we expect orbitals near $K_q \approx \pi$ to mix strongly since they are weakly damped.

The above expectation is borne out by comparing the numerically computed orbitals $|\psi_r\rangle$ and the second-order correction $\left|K_q^{\text{pert}}\right\rangle$ to $\boldsymbol{F}$, as shown in Fig. 3.4. Despite being in a regime with strong non-reciprocity and hence large w ($w = 0.9\kappa$), perturbation theory still describes the 150 least-occupied orbitals (which we do not plot) extremely well: they are nearly standing-wave states. The most-occupied orbitals are the ones which perturbation theory describes less accurately. Nonetheless, these orbitals are still relatively delocalized, and have no resemblance to the right or left eigenvectors of $\boldsymbol{H}_{\text{eff}}$. Finally as we increase Γ, and thus the decay rate of all modes, our perturbation theory is more accurate, as predicted by Eq. (3.33).

These results verify the central claim of this section: the occupied orbitals which characterize our quantum steady state do not exhibit any analogue of the NHSE. These occupied orbitals have a form similar to the reciprocal case $w = 0$, and do not exhibit any exponential localization.

3.5 Conclusion

We have presented a systematic method for constructing open quantum systems whose unconditional physics reflects that of a desired non-Hermitian tight-binding lattice Hamiltonian. We identify generic features of the steady states of such quantum lattice models, focusing on the case where the target Hamiltonian is non-reciprocal. A crucial conclusion is that the

steady state cannot in general be understood solely using the effective Hamiltonian $\hat{H}_{\text{eff}}$. First, fluctuations play a crucial role in determining $\hat{\rho}_{\text{ss}}$, and their form is not uniquely determined by $\hat{H}_{\text{eff}}$ (though is constrained by it). Further, taking the Hatano-Nelson model as an example, we have demonstrated that even when fluctuations are spatially featureless (i.e. uniform incoherent pumping), the spectrum, left and right eigenvectors of $\hat{H}_{\text{eff}}$ cannot be simply used to infer even the most basic features of the steady state. For weak pumping, we find that our system under open boundary conditions exhibits a new long length scale ξ_{obc}. This scale has no relation to the localization length of the left and right eigenvectors, nor to the existence of an extremely small relaxation rate (dissipative gap). Particle statistics also play a surprising role in the form of the steady state. Finally, we have shown that the orbital states (the eigenstates of $\hat{\rho}_{\text{ss}}$) do not exhibit any analogue of the non-Hermitian skin effect. Unlike the left and right eigenvectors of $\hat{H}_{\text{eff}}$, they do not become exponentially localized under a change of boundary conditions; in fact, a majority of them are very nearly standing-wave states.

Our work naturally leads to several interesting questions regarding the interplay of dynamics, noise, and the steady state. For instance, one could ask to what extent non-trivial correlated fluctuations (i.e. when the incoherent pumping has a non-trivial spatial structure) can lead to an interesting steady state. To that end, we briefly analyze such a model in App. 3.6, where we find a steady-state occupation which might naively be interpreted as a consequence of the NHSE, despite the lack of non-reciprocity. Taking the opposite approach presented in this paper, by starting with a target steady state and attempting to classify the allowable $\boldsymbol{H}_{\text{eff}}$ and $\boldsymbol{G}$, would also be extremely interesting.

3.5.1 Appendices

3.5.2 Equations of motion - correlation functions

In this appendix, we derive the equations of motion for the normal ordered correlation function $\langle \hat{c}_n^\dagger \hat{c}_m \rangle$. The jump operators are $\hat{L}_\mu = \sum_n l_{\mu m} \hat{c}_m$ and $\hat{G}_\nu = \sum_n g^*_{\nu n} \hat{c}_n^\dagger$, from which we obtain

$$i\partial_t \hat{\rho} = \sum_{a,b} H_{ab}[\hat{c}_a^\dagger \hat{c}_b, \hat{\rho}] + i \sum_{a,b} L_{ab} \left(\hat{c}_b \hat{\rho} \hat{c}_a^\dagger - \frac{1}{2}\{\hat{c}_a^\dagger \hat{c}_b, \hat{\rho}\} \right) + i \sum_{a,b} G_{ab} \left(\hat{c}_a^\dagger \hat{\rho} \hat{c}_b - \frac{1}{2}\{\hat{c}_b \hat{c}_a^\dagger, \hat{\rho}\} \right) \tag{3.36}$$

where $\{\cdot, \cdot\}$ is the anti-commutator and, as in the main text, $L_{ab} = (\boldsymbol{l}^\dagger \boldsymbol{l})_{ab}$ and $G_{ab} = (\boldsymbol{g}^\dagger \boldsymbol{g})_{ab}$. Thus, the equations of motion for the normal ordered correlation function are

$$\begin{aligned} i\partial_t \langle \hat{c}_n^\dagger \hat{c}_m \rangle = &\sum_{a,b} H_{a,b} \langle [\hat{c}_n^\dagger \hat{c}_m, \hat{c}_a^\dagger \hat{c}_b] \rangle + \frac{i}{2} \sum_{a,b} L_{ab} \langle \hat{c}_a^\dagger [\hat{c}_n^\dagger \hat{c}_m, \hat{c}_b] + [\hat{c}_a^\dagger, \hat{c}_n^\dagger \hat{c}_m] \hat{c}_b \rangle \\ &+ \frac{i}{2} \sum_{a,b} G_{ab} \langle \hat{c}_b [\hat{c}_n^\dagger \hat{c}_m, \hat{c}_a^\dagger] + [\hat{c}_b, \hat{c}_n^\dagger \hat{c}_m] \hat{c}_a^\dagger \rangle \end{aligned} \tag{3.37}$$

Using fermionic anti-commutation and bosonic commutation relations, we get

$$\begin{aligned} i\partial_t \langle \hat{c}_n^\dagger \hat{c}_m \rangle = &\sum_a \left(H_{ma} \langle \hat{c}_n^\dagger \hat{c}_a \rangle - H_{an} \langle \hat{c}_a^\dagger \hat{c}_m \rangle \right) - \frac{i}{2} \sum_a \left(L_{ma} \langle \hat{c}_n^\dagger \hat{c}_a \rangle + L_{an} \langle \hat{c}_a^\dagger \hat{c}_m \rangle \right) \\ &\mp \frac{i}{2} \sum_a \left(G_{ma} \langle \hat{c}_a \hat{c}_n^\dagger \rangle + G_{an} \langle \hat{c}_m \hat{c}_a^\dagger \rangle \right) \end{aligned} \tag{3.38}$$

where $\mp$ is for fermions and bosons respectively. Using the anti-commutation and commutation relation once more, along with $\boldsymbol{L}^\dagger = \boldsymbol{L}$ and $\boldsymbol{G}^\dagger = \boldsymbol{G}$, we recover Eq. (3.4) in the main text. The anti-normal-ordered correlation function has the same dynamical matrix $\boldsymbol{H}_{\text{eff}}$, but

with a different inhomogeneous term:

$$i\partial_t\langle\hat{c}_m\hat{c}_n^\dagger\rangle = \sum_a \Big((H_{\rm eff})_{ma}\langle\hat{c}_a\hat{c}_n^\dagger\rangle - (H_{\rm eff}^\dagger)_{an}\langle\hat{c}_m\hat{c}_a^\dagger\rangle\Big) + iL_{mn}, \tag{3.39}$$

which follows from the preservation of equal time anti-commutation or commutation relations.

3.5.3 Hatano-Nelson Hamiltonian using Method 2

Here we construct a quantum effective non-Hermitian Hamiltonian and noise matrix whose dynamics are equivalent to a Lindblad master equation for the Hatano-Nelson model using Method 2 in the main text. Writing the target Hamiltonian Eq. (3.16) in momentum space, we have

$$\hat{H}_{\rm targ}^{\rm HN} = \sum_k \left(w\cos k - i\kappa\sin k\right)\hat{c}_k^\dagger\hat{c}_k \tag{3.40}$$

The largest positive eigenvalue of the anti-Hermitian part is clearly κ. Thus, the effective Hamiltonian reads

$$\hat{H}_{\rm eff} = \sum_k \left(w\cos k - i\kappa(1+\sin k) \mp i\Gamma\right)\hat{c}_k^\dagger\hat{c}_k \tag{3.41}$$

where, as always, $\mp$ is for fermions and bosons respectively so that $\boldsymbol{H}_{\rm eff} = \boldsymbol{H}_{\rm targ}^{\rm HN} - i(\kappa\pm\Gamma)\mathbf{1}$. To obtain a set of real-space dissipators, it is convenient to write the master equation in momentum space as in Eq. (3.20) then Fourier transform back to position space. We obtain

$$\begin{aligned} i\partial_t\hat{\rho} = {} & \frac{w}{2}\sum_j[\hat{c}_{j+1}^\dagger\hat{c}_j + h.c., \hat{\rho}] \\ & + i\sum_j \mathcal{D}[\sqrt{\kappa}(\hat{c}_j - i\hat{c}_{j+1})]\hat{\rho} + i\sum_j \mathcal{D}[\sqrt{2\Gamma}\hat{c}_j^\dagger]\hat{\rho} \end{aligned} \tag{3.42}$$

i.e. the coherent Hamiltonian and dissipators in Eqs. (3.17)-(3.19). Note that there is a small but important detail when dealing with different boundary conditions. For periodic boundary conditions $\hat{c}_j = \hat{c}_{j+N}$, Eq. (3.20) and Eq. (3.42) are equivalent whereas for open boundary conditions $\hat{c}_0 = \hat{c}_{N+1} = 0$ they are not. For this choice of geometry, there are independent loss baths attached to site 1 and N in addition to the one on each bond that lead to non-reciprocal hopping. The lack of translational invariance then precludes the possibility of writing the master equation where the jump operators are independent momentum creation and annihilation operators.

3.5.4 Steady state correlation function - PBC

Using the definition of the periodic system lengthscale $\kappa \cosh \xi_{\text{pbc}}^{-1} = \kappa + \Gamma$, we have

$$\begin{aligned}\langle \hat{c}_j^\dagger \hat{c}_p \rangle_{\text{ss}} &= \frac{\Gamma}{\kappa N} \sum_k \frac{e^{-i(j-p)k}}{\cosh \xi_{\text{pbc}}^{-1} + \sin k} \\ &= \frac{\Gamma}{\kappa N \sinh \xi_{\text{pbc}}^{-1}} \sum_k \left(\frac{e^{-i(j-p)k}}{1 + ie^{-ik} e^{-\xi_{\text{pbc}}^{-1}}} - \frac{e^{-i(j-p)k}}{1 + ie^{-ik} e^{\xi_{\text{pbc}}^{-1}}} \right)\end{aligned} \tag{3.43}$$

Since the k are integer multiples of $2\pi/N$, we can perform a simple geometric sum to obtain

$$\sum_{l=0}^{N-1} \frac{i^{-l} e^{-ikl} e^{\pm \xi_{\text{pbc}}^{-1} l}}{1 - i^{-N} e^{\pm \xi_{\text{pbc}}^{-1} N}} = \frac{1}{1 + ie^{-ik} e^{\pm \xi_{\text{pbc}}^{-1}}} \tag{3.44}$$

Inserting Eq. (3.44) into Eq. (3.43), only the $l = p - j$ term survives, again due to the quantization of k (where $p - j$) is understood modulo N. After some simplification we are left with

$$\langle \hat{c}_j^\dagger \hat{c}_p \rangle_{\text{ss}} = \frac{\Gamma i^{-(p-j)}}{\kappa \sinh \xi_{\text{pbc}}^{-1}} \left(\frac{e^{-(p-j)/\xi_{\text{pbc}}}}{1 - i^{-N} e^{-N/\xi_{\text{pbc}}}} - \frac{e^{(p-j)/\xi_{\text{pbc}}}}{1 - i^{-N} e^{N/\xi_{\text{pbc}}}} \right) \tag{3.45}$$

which recovers the scaling of Eq. (3.23) in the main text.

3.5.5 Steady-state occupation under open boundary conditions

In this appendix, we find approximate expressions for the steady-state occupation $\langle \hat{c}_j^\dagger \hat{c}_j \rangle_{\rm ss}$ under open boundary conditions. It is worth pointing out immediately that since the eigenvectors and eigenvalues of the Hatano-Nelson model are known [49], we can use the formal expression Eq. (3.14) and solve for $\langle \hat{c}_j^\dagger \hat{c}_j \rangle_{\rm ss}$ without approximations. Assuming $w > \kappa$ throughout, we have

$$\langle \hat{c}_j^\dagger \hat{c}_j \rangle_{\rm ss} = \sum_{K_q, K_{q'}, p} \frac{e^{2A(j-p)}}{\mathcal{N}} \frac{\sin K_q j \sin K_q p \sin K_{q'} p \sin K_{q'} j}{J(\cos\big(K_q\big) - \cos\Big(K_{q'}\Big)) - i2(\kappa \pm \Gamma)} \tag{3.46}$$

where $\mathcal{N}^{-1} = -i8\Gamma/(N+1)^2$, $2A = \ln((w+\kappa)/(w-\kappa))$, and $J = \sqrt{w^2 - \kappa^2}$. The standing-wave momenta are quantized by $K_q = \pi q/(N+1)$ where q is an integer that runs from 1 to N. Although exact, Eq. (3.46) is practically useless, and does not immediately tell us qualitative features of the steady-state occupation. For instance, it is not evident that the small difference in uniform dissipation for fermions and bosons $\kappa \pm \Gamma$ can lead to a drastic change in $\langle \hat{c}_j^\dagger \hat{c}_j \rangle_{\rm ss}$ as seen in Fig. 3.1.

We will instead work with the other formal solution to the steady-state occupation, given by Eq. (3.25). We must therefore first find the retarded frequency-space Green's function of the open chain. This has been done in previous work [85, 87], but we present here a different approach that will allow us to simultaneously find the response of the periodic chain and compare in what manner the two differ. To that end, we first find the time-domain Green's function $G^R_\infty(j,p;t)$ for an infinite lattice, whose equations of motion are

$$\begin{aligned} &i\partial_t G^R_\infty(j,p;t) - \frac{(w+\kappa)}{2} G^R_\infty(j-1,p;t) \\ &- \frac{(w-\kappa)}{2} G^R_\infty(j+1,p;t) + i s_\pm G^R_\infty(j,l;t) = \delta(t)\delta_{j,p}. \end{aligned} \tag{3.47}$$

along with the initial condition $G^R_\infty(j,p,0) = -i\delta_{j,p}$ with $\delta(t)$ the Dirac delta function and

$\delta_{j,p}$ the Kronecker delta function. For notational convenience, we have set $s_\pm = \kappa \pm \Gamma$. These can readily be solved by using the plane wave solutions, and with an infinite-sized system there is no quantization condition on the momentum. Thus

$$\begin{aligned} G^R_\infty(j,p;t) &= -i\Theta(t)e^{-s_\pm t}\int_{-\pi}^{\pi}\frac{dk}{2\pi}e^{ik(j-p)}e^{-i(w\cos k - i\kappa\sin k)t} \\ &= -i\Theta(t)e^{-s_\pm t}e^{A(j-l)}\int_{-\pi}^{\pi}\frac{dk}{2\pi}e^{ik(j-p)}e^{-iJ\cos kt} \end{aligned} \tag{3.48}$$

where in the last line we have made an imaginary gauge transformation $k \to k - iA$ using the definition of Eq. (3.24). Although seemingly ad-hoc, this transformation can be justified using complex analysis. Viewed as a complex variable, the integrand is a holomorphic function of k, and one then constructs a rectangle in the complex plane over which the integral is zero. Two sides of the rectangle cancel, after which one equates the two functions above.

The frequency-space response is obtained by taking the Fourier transform of Eq. (3.48), after which we have

$$\begin{aligned} G^R_\infty[j,p;\omega] &= e^{A(j-p)}\int_{-\pi}^{\pi}\frac{dk}{2\pi}\frac{e^{ik(j-p)}}{w + is_\pm - J\cos k} \\ &= -i\frac{e^{A(j-p)}e^{-iQ[\omega]|j-p|}}{J\sin Q[\omega]} \end{aligned} \tag{3.49}$$

where we have used the residue theorem to compute the integral. The complex wavevector $Q[\omega]$ is defined by

$$w + is_\pm = J\cos Q[\omega] \tag{3.50}$$

and we always chose the imaginary part of $Q[\omega]$ to be negative such that $e^{-iQ[\omega]}$ lies in the unit circle. One can also readily verify that this satisfies the Fourier-transformed version of Eq. (3.47).

To obtain the retarted response of a chain with periodic boundary conditions, we note that the equations of motion Eq. (3.47) remain unchaged, except the boundary conditions are now $G^R_{\text{pbc}}[j+N,p;\omega] = G^R_{\text{pbc}}[j,p+N;\omega] = G^R_{\text{pbc}}[j,p;\omega]$. By linearity of the equations, the solution is then

$$\begin{aligned} G^R_{\text{pbc}}[j,p;\omega] &= \sum_{r=-\infty}^{\infty} G^R_{\infty}[j-p+Nr;\omega] \\ &= \frac{-ie^{A(j-p)}}{J\sin Q[\omega]}\left(\frac{e^{-iQ[\omega](j-p)}}{1-e^{AN-iQ[\omega]N}} - \frac{e^{iQ[\omega](j-p)}}{1-e^{AN+iQ[\omega]N}}\right) \end{aligned} \tag{3.51}$$

where $j-p$ is understood to be modulo N. Each term $r \neq 0$ in Eq. (3.51) should be interpreted as an additional round trip by the particle. That is, in going from site p to j, the particle can propagate clockwise or counter-clockwise any number of times. The total Green's function is then the sum of each of these processes.

Next we compute the Green's function of a finite-sized open chain. The particle will propagate in the bulk as it would in the infinite-sized system, without knowledge of the boundaries. Instead of round trips as in the periodic system, however, when it reaches the edge the particle can now "bounce" off on an open boundary, acquiring a phase shift of π in the process. Summing over all possible bounces, we have

$$\begin{aligned} G^R_{\text{obc}}[j,p;\omega] &= \frac{-ie^{A(j-p)}}{J\sin Q[\omega]}\sum_{r=-\infty}^{\infty}\left(e^{-iQ[\omega](|2(N+1)r+|n-p||)} - e^{-iQ[\omega](|2(N+1)r+|n+p|)|}\right) \\ &= e^{A(j-p)}\frac{2\sin Q[\omega]\min(j,p)\sin Q[\omega](N+1-\max(j,p))}{J\sin Q[\omega]\sin Q[\omega](N+1)} \end{aligned} \tag{3.52}$$

in agreement with previously obtained results [85]. We stress once again that each term in the sum above should be interpreted as scattering off either boundary.

Our remaining task is to compute the integral over all frequency

$$\langle \hat{c}_j^\dagger \hat{c}_j \rangle_{\rm ss} = 2\Gamma \sum_{p=1}^{N} \int_{-\infty}^{\infty} \frac{d\omega}{2\pi} |G^R_{\rm obc}[j,p;\omega]|^2. \tag{3.53}$$

We stress again that this can in principle be computed exactly, see Eq. (3.46). The first step in finding a more enlightening approximate expression is to note that the dominating contribution to the integral occurs when the imaginary part of the complex wavevector $Q[\omega]$ is smallest. Since the real and imaginary part of $Q[\omega]$

$$Q[\omega] = k[\omega] + iR[\omega] \tag{3.54}$$

are not independent, it will be convenient to first make a change of variables $\omega \to k$ in the integral. Comparing the dispersion Eq. (3.50) and the definition of Eq. (3.54), while also requiring that $R[k]$ is negative, we obtain

$$\frac{d\omega}{|\sin Q[\omega]|^2} = \frac{J^2 dk}{\sqrt{s_\pm^2 + (J\sin k)^2}} \tag{3.55}$$

$$e^{R[k]} = \frac{\sqrt{s_\pm^2 + (J\sin k)^2} - s_\pm}{J\sin k} \tag{3.56}$$

where the integration variable k goes from 0 to π. We can interpret $-R[k]$ as a sort of momentum-dependent inverse decay length (even though we have open boundary conditions and momentum is not a good quantum number). That is, $-R[k]$ corresponds to how far can a particle with momentum k can propagate in the lattice before decaying. This damping is minimal when the magnitude of the group velocity $|J\sin k|$ is maximal, i.e. at $k = \pi/2$. Conversely, when the group velocity vanishes at $k = 0, \pi$, there is no propagation $-R[k] \to \infty$.

The formal expression for the steady-state occupation then reads

$$\langle \hat{c}_j^\dagger \hat{c}_j \rangle_{\rm ss} = 8\Gamma \sum_{p=1}^{N} e^{2A(j-l)} \int_0^\pi \frac{dk}{2\pi} \frac{|\sin Q[k] \min(j,p)|^2 |\sin Q[k](N+1-\max(j,p))|^2}{\sqrt{s_\pm^2 + (J\sin k)^2} |\sin Q[k](N+1)|^2}. \tag{3.57}$$

where $Q[k] = k + iR[k]$. We now make our first approximation and assume that the time it takes for a particle to traverse the chain, i.e. the length N divided by the group velocity J, is much larger than its lifetime $1/s_\pm$. This is equivalent to the requirement in the main text that the spacing of the modes are much smaller than their widths $J/N \ll s_\pm$. Expanding $Q[k]$ to lowest order in $s_\pm/J$, it follows that this condition implies $|e^{-iQ[k]N}| \ll 1$ for all k. Consequently, we approximate the response by keeping only the leading order term in $e^{-iQ[k]}$. From Eq. (3.52), this is exactly equivalent to taking the no-bounce limit $G^R_{\rm obc}[j,p;\omega] \approx G^R_\infty[j,p;\omega]$. We thus expect this approximation to worsen when j or p are near a boundary. Note that the condition $J/N \ll s_\pm$ is easily satisfied in the limit of strong non-reciprocity $\kappa \approx w$ since $J = \sqrt{w^2 - \kappa^2}$.

Within the no-bounce approximation, we obtain

$$\langle \hat{c}_j^\dagger \hat{c}_j \rangle_{\rm ss} \approx 2\Gamma \sum_{p=1}^{N} e^{2A(j-p)} \int_0^\pi \frac{dk}{2\pi} \frac{e^{2R[k]|j-p|}}{\sqrt{s_\pm^2 + (J\sin k)^2}} \tag{3.58}$$

In the limit of strong non-reciprocity $J \ll s_\pm$, the $p = j$ term can be approximated as $\Gamma/s_\pm$. For $p \neq j$ we use Laplace's method to compute the integral. We approximate $R[k]$ by expanding to second order near its maximum at $k = \pi/2$ and compute the Gaussian integral by extending the bounds of integration to infinity. We are left with

$$\langle \hat{c}_j^\dagger \hat{c}_j \rangle_{\rm ss} \approx \frac{\Gamma}{s_\pm} \left(1 + \sqrt{\frac{s_\pm}{\pi\sqrt{s_\pm^2 + J^2}}} \sum_{p\neq j} \frac{e^{2A(j-p) - 2A'|j-p|}}{\sqrt{|j-p|}} \right) \tag{3.59}$$

where

$$A' \equiv -R\Big[\frac{\pi}{2}\Big] = \ln\left(\frac{\sqrt{s_\pm^2 + J^2} + s_\pm}{J}\right)$$
$$= A + \ln\left(1 \pm \frac{\Gamma}{w}\right) + \mathcal{O}\left(\frac{(w-\kappa)\Gamma^2}{w^3}\right) \tag{3.60}$$

Comparing with Eq. (3.26), we have

$$C_1 = \sqrt{\frac{s_\pm}{\pi\sqrt{s_\pm^2 + J^2}}} \tag{3.61}$$

In the limit of perfect non-reciprocity $\kappa \to w$ we have $A \to \infty$ and $J \to 0$. Only pump baths to the left of a given site contribute to its population and thus

$$\langle \hat{c}_j^\dagger \hat{c}_j \rangle_{\rm ss} \approx \frac{\Gamma}{s_\pm}\left(1 + \frac{1}{\sqrt{\pi}}\sum_{p<j} \frac{e^{\mp\frac{|j-p|}{\xi_{\rm obc}}}}{\sqrt{|j-p|}}\right) \tag{3.62}$$

where

$$\xi_{\rm obc} = \left|\left(2\ln\left(1 \pm \frac{\Gamma}{w}\right)\right)^{-1}\right| \tag{3.63}$$

Approximating the sum as an integral, we obtain

$$\langle \hat{c}_j^\dagger \hat{c}_j \rangle_{\rm ss} \approx \begin{cases} \frac{\Gamma}{\kappa+\Gamma}\left(1 + \frac{\mathrm{erf}(\sqrt{\frac{j}{\xi_{\rm obc}}}) - \mathrm{erf}(\frac{1}{\sqrt{\xi_{\rm obc}}})}{\sqrt{\xi_{\rm obc}^{-1}}}\right), & \text{fermions} \\ \frac{\Gamma}{\kappa-\Gamma}\left(1 + \frac{\mathrm{erfi}(\sqrt{\frac{j}{\xi_{\rm obc}}}) - \mathrm{erfi}(\frac{1}{\sqrt{\xi_{\rm obc}}})}{\sqrt{\xi_{\rm obc}^{-1}}}\right), & \text{bosons} \end{cases} \tag{3.64}$$

$$\overset{j \ll \xi_{\rm obc}}{=} \frac{\Gamma}{\kappa \pm \Gamma}\left(1 + \frac{2}{\sqrt{\pi}}\left(\sqrt{j} - 1\right)\right). \tag{3.65}$$

where we recover the results in the main text by setting

$$C_2 = 1 - \frac{\mathrm{erf}(\frac{1}{\sqrt{\xi_{\mathrm{obc}}}})}{\xi_{\mathrm{obc}}^{-1}} \tag{3.66}$$

$$C_3 = 1 - \frac{\mathrm{erfi}(\frac{1}{\sqrt{\xi_{\mathrm{obc}}}})}{\xi_{\mathrm{obc}}^{-1}} \tag{3.67}$$

We emphasize that the exact solution of Eq. (3.46) could not have easily predicted these analytic results. Further we have shown that bulk dynamics alone, by making the no-bounce approximation $G^R_{\mathrm{obc}}[j,l;\omega] \approx G^R_{\infty}[j,l;\omega]$, was sufficient to correctly capture the steady-state occupation.

3.5.6 Perturbation theory for orbitals

We now use perturbation theory to find the second-order correction in w to the standing-wave orbitals. This is unlike standard perturbation theory in that the steady-state correlation matrix $\boldsymbol{F}$ depends on w to all orders

$$\boldsymbol{F} = \sum_{r=0}^{\infty} w^r \boldsymbol{F}_r. \tag{3.68}$$

Finding the orbitals to the correct order is then a two step process: we must first find $\boldsymbol{F}_r$ to the requisite order and only then solve for the corrected eigenstates. As discussed in the main text, the zeroeth order term is

$$\boldsymbol{F}_0 = \sum_{K_q} n_{K_q} \left|K_q\right\rangle \left\langle K_q\right|. \tag{3.69}$$

To find $\boldsymbol{F}_r$ to any other order $r \geq 1$, we insert $\boldsymbol{F}$ into Eq. (3.12) and equate terms at each order in w on both sides. We are left with a recursive relation between $\boldsymbol{F}_r$ and $\boldsymbol{F}_{r+1}$ whose

solution is

$$\boldsymbol{F}_r = \frac{i}{w} \sum_{K_q, K_{q'}} \left(\frac{\left\langle K_q \right| \left(\boldsymbol{F}_{r-1} \boldsymbol{H} - \boldsymbol{H} \boldsymbol{F}_{r-1} \right) \left| K_{q'} \right\rangle}{L_{K_q} + G_{K_q} + L_{K_{q'}} + L_{K_{q'}}} \right) \left| K_q \right\rangle \left\langle K_{q'} \right| \tag{3.70}$$

For instance, using Eq. (3.69) we recover Eq. (3.33) in the main text.

Once we have computed these corrections to the steady-state correlation matrix to the desired order, we can then compute the orbitals to that same order. This proceedds more like standard perturbation theory. For instance, the unormalized corrected orbital is given by

$$\begin{aligned} \left| K_q^{\text{pert}} \right\rangle = \left| K_q \right\rangle &+ w \sum_{K_{q'} \neq K_q} \frac{\left\langle K_{q'} \right| \boldsymbol{F}_1 \left| K_q \right\rangle}{n_{K_q} - n_{K_{q'}}} \left| K_{q'} \right\rangle \\ &+ w^2 \sum_{K_{q'} \neq K_q} \frac{\left\langle K_{q'} \right| \boldsymbol{F}_2 \left| K_q \right\rangle}{n_{K_q} - n_{K_{q'}}} \left| K_{q'} \right\rangle \\ &+ w^2 \sum_{\substack{K_{q'} \neq K_q \\ K_{q''} \neq K_q}} \frac{\left\langle K_{q'} \right| \boldsymbol{F}_1 \left| K_{q''} \right\rangle \left\langle K_{q''} \right| \boldsymbol{F}_1 \left| K_{q'} \right\rangle}{(n_{K_q} - n_{K_{q'}})(n_{K_q} - n_{K_{q''}})} \left| K_{q'} \right\rangle . \end{aligned} \tag{3.71}$$

which are the states we use when comparing the numerically computed orbitals $|\psi_r\rangle$ in Fig. 3.4.

We also note that, with these corrected orbitals, one can also compute the correction to perturbative corrections to the occupation n_r.Suppose we were able to find the exact orbital states $|\psi_r\rangle$, which are by definition eigevectors of $\boldsymbol{F}$. Then taking the expectation value of both sides of Eq. (3.12), we obtain

$$n_r = \frac{\langle \psi_r | \boldsymbol{G} | \psi_r \rangle}{\langle \psi_r | \boldsymbol{G} | \psi_r \rangle + \langle \psi_r | \boldsymbol{L} | \psi_r \rangle} \tag{3.72}$$

Replacing $|\psi_r\rangle$ with its perturbative correction gives the occupation to the desired order.

3.5.7 Two additional non-Hermitian tight-binding models

Non-Hermitian SSH model

In this appendix, we will briefly study one version of the non-Hermitian SSH model initially considered in Ref. [73]. We will restrict ourselves to the fermionic case, since the analysis for the bosonic case essentially follows the same logic. To obtain a quantum-mechanically consistent effective Hamiltonian, we will follow Method 2 and add a minimal amount of loss. The effective non-Hermitian Hamiltonian reads

$$\begin{aligned}\hat{H}_{\text{eff}}^{\text{SSH}} =& \sum_j \left(\frac{w-\kappa}{2}\hat{c}_{A,j}^\dagger \hat{c}_{B,j} + \frac{w+\kappa}{2}\hat{c}_{B,j}^\dagger \hat{c}_{A,j}\right) \\ &+ \sum_j \left(\frac{u+\gamma}{2}\hat{c}_{A,j+1}^\dagger \hat{c}_{B,j} + \frac{u-\gamma}{2}\hat{c}_{B,j}^\dagger \hat{c}_{A,j+1}\right) \\ &- i\sum_j \left(\Gamma + \frac{\kappa+\gamma}{2}\right)\left(\hat{c}_{A,j}^\dagger \hat{c}_{A,j} + \hat{c}_{B,j}^\dagger \hat{c}_{B,j}\right)\end{aligned} \tag{3.73}$$

where A and B label the two sites in a unit cell, $w \pm \kappa$ are the intra cell hopping and $u \pm \gamma$ the inter cell hopping. This model is known to exhibit the NHSE for any value of non-reciprocal hopping (in the sense that the spectrum collapses to a line in the complex plane). Note that if $u = w$ and $\gamma = \kappa$, we recover the Hatano-Nelson model.

We first wish to describe this model for an infinitely large lattice. Fourier transforming to momentum space we obtain

$$\hat{H}_{\text{eff}}^{\text{SSH}} = \sum_k \hat{\boldsymbol{C}}_k^\dagger \boldsymbol{H}_{\text{eff}}(k) \hat{\boldsymbol{C}}_k \tag{3.74}$$

where $\hat{\boldsymbol{C}}_k^\dagger = (\hat{c}_{A,k}^\dagger, \hat{c}_{B,k}^\dagger)$ and

$$\boldsymbol{H}_{\text{eff}}(k) = \begin{pmatrix} -i(\Gamma + \frac{\kappa+\gamma}{2}) & \frac{w-\kappa}{2} + \frac{u+\gamma}{2}e^{-ik} \\ \frac{w+\kappa}{2} + \frac{u-\gamma}{2}e^{ik} & -i(\Gamma + \frac{\kappa+\gamma}{2}) \end{pmatrix} \tag{3.75}$$

is the effective Hamiltonian. There are two bands, and the complex energies are

$$\begin{aligned} E_\pm(k) = \pm\frac{1}{2}\sqrt{J^2 + \tilde{J}^2 + 2J\tilde{J}\cos\Big(k + i(A + \tilde{A})\Big)} \\ - i(\Gamma + \frac{\kappa+\gamma}{2}) \end{aligned} \tag{3.76}$$

where $J = \sqrt{w^2 - \kappa^2}, 2A = \ln(w+\kappa)/(w-\kappa)$ as before and we have introduced $\tilde{J} = \sqrt{u^2 - \gamma^2}, 2\tilde{A} = \ln(u+\gamma)/(u-\gamma)$. Despite the potentially interesting band structure, the steady state is completely determined by the anti-Hermitian part of the effective Hamiltonian. As discussed in the main text, the baths can not cause transitions between momentum eigenstates. In the infinite time limit the only structure that remains in the incoherent pumping and decay. As before, the most interesting feature of this model is the open-boundary steady-state occupation.

We would like to argue that the most interesting feature we see in the Hatano-Nelson model, namely the existence of a large length scale that is directly tied to real-space propagation dynamics, is still present in this generalized model. To this end, we will compare two different methods for computing $\langle \hat{c}_{A/B,j}^\dagger \hat{c}_{A/B,j} \rangle_{\text{ss}}$ under open boundary conditions. We first numerically solve the Lyaponov equation Eq. (3.12), which is straightforward. For the second method, we will use the formal solution Eq. (3.13) except we will approximate the open-boundary Green's function by that of an infinite chain (just as we did in App. 3.5.5).

We therefore first need to find the real-space Green's funciton for an infinite-sized lattice.

The momentum- space retarded Green's function is simply

$$\begin{aligned}
&\begin{pmatrix} G^R_{\infty,AA}[k;\omega] & G^R_{\infty,AB}[k;\omega] \\ G^R_{\infty,BA}[k;\omega] & G^R_{\infty,BB}[k;\omega] \end{pmatrix} = \frac{1}{\omega \mathbf{1} - \boldsymbol{H}_{\text{eff}}(k)} \\
&= \frac{1}{[(\omega+is)^2 - \frac{1}{4}(J^2+\tilde{J}^2) - \frac{1}{2}J\tilde{J}\cos\Big(k + i(A+\tilde{A})\Big)]} \\
&\times \begin{pmatrix} \omega + is & \frac{1}{2}(Je^{-A} + e^{-ik}\tilde{J}e^{\tilde{A}}) \\ \frac{1}{2}(Je^{A} + e^{ik}\tilde{J}e^{-\tilde{A}}) & \omega + is \end{pmatrix}
\end{aligned} \tag{3.77}$$

where $s = \Gamma + (\kappa+\gamma)/2$. Taking the Fourier transform to real space, we obtain

$$\begin{pmatrix} G^R_{\infty,AA}[j,p;\omega] & G^R_{\infty,AB}[j,p;\omega] \\ G^R_{\infty,BA}[j,p;\omega] & G^R_{\infty,BB}[j,p;\omega] \end{pmatrix} = \int_{-\pi}^{\pi} \frac{dk}{2\pi} \frac{e^{ik(j-p)}}{\omega \mathbf{1} - \boldsymbol{H}_{\text{eff}}(k)}$$

The integral can be computed analytically using the residue theorem. We have

$$G^R_{\infty,AA}[j,p;\omega] = \frac{-2ie^{(j-p)(A+\tilde{A})}}{J\tilde{J}\sin\tilde{Q}[\omega]}(\omega+is)e^{-i\tilde{Q}[\omega]|j-p|} \tag{3.78}$$

$$G^R_{\infty,BB}[j,p;\omega] = \frac{-2ie^{(j-p)(A+\tilde{A})}}{J\tilde{J}\sin\tilde{Q}[\omega]}(\omega+is)e^{-i\tilde{Q}[\omega]|j-p|} \tag{3.79}$$

$$\begin{aligned}
G^R_{\infty,AB}[j,p;\omega] = \frac{-ie^{(j-p)(A+\tilde{A})-A}}{J\tilde{J}\sin\tilde{Q}[\omega]}(&Je^{-i\tilde{Q}[\omega]|j-p|} \\
&+\tilde{J}e^{-i\tilde{Q}[\omega]|j-p-1|})
\end{aligned} \tag{3.80}$$

$$G^R_{\infty,BA}[j,p;\omega] = \frac{-ie^{(j-p)(A+\tilde{A})+A}}{J\tilde{J}\sin\tilde{Q}[\omega]}(Je^{-i\tilde{Q}[\omega]|j-p|} + \tilde{J}e^{-i\tilde{Q}[\omega]|j-p+1|}) \tag{3.81}$$

Using these expressions, we can then approximate the real-space steady-state occupation of this non-Hermitian SSH model as

$$\langle \hat{c}^\dagger_{A,j}\hat{c}_{A,j}\rangle_{\text{ss}} \approx 2\Gamma\sum_p \int_{-\infty}^{\infty}\frac{d\omega}{2\pi}(|G^R_{\infty,AA}[j,p;\omega]|^2 + |G^R_{\infty,AB}[j,p;\omega]|^2). \tag{3.82}$$

$$\langle \hat{c}^\dagger_{B,j}\hat{c}_{B,j}\rangle_{\text{ss}} \approx 2\Gamma\sum_p \int_{-\infty}^{\infty}\frac{d\omega}{2\pi}(|G^R_{\infty,BA}[j,p;\omega]|^2 + |G^R_{\infty,BB}[j,p;\omega]|^2). \tag{3.83}$$

by numerically computing the integrals over frequency.

In Fig. 3.5 we plot the numerically exact result (which comes from directly solving Eq. (3.12)), the approximate solution Eqs. (3.82)-(3.83) in addition to the open and periodic spectrum for a given choice of parameters. There are two salient features. First note that there is still a large length scale which describes the steady-state occupation, despite the existence of a dissipative gap of order $(\kappa+\gamma)/2$. The length scale associated with this gap would only be on the order of a few lattice sites, which is evidently not how $\langle \hat{c}^\dagger_j\hat{c}_j\rangle_{\text{ss}}$ behaves. Further, seeing as the approximate and exact solutions are nearly identical, it follows that this length scale is encoded in the the Green's function for an infinite system, and has nothing to do with the open-boundary geometry. This once again justifies the approximation that, in the bulk, the retarded Green's function is largely unaffected by the NHSE, even though

the eigenvalues and eigenvectors change dramatically depending on boundary conditions.

Hatano-Nelson with next-nearest neighbour hopping

We now analyze another non-Hermitian tight-binding model: the Hatano-Nelson model with an additional next- nearest-neighbour (NNN) Hermitian hopping term. Since the anti-Hermitian part of the effective Hamiltonian is the same as the Hatano-Nelson model we can use the same set of dissipators. The effective Hamiltonian reads

$$\begin{aligned}\hat{H}_{\text{eff}}^{NNN} = &\sum_j \left(\frac{w+\kappa}{2} \hat{c}_{j+1}^\dagger \hat{c}_j + \frac{w-\kappa}{2} \hat{c}_j^\dagger \hat{c}_{j+1} \right) \\ &+ \frac{T}{2} \sum_j \left(e^{i\phi} \hat{c}_{j+2} \hat{c}_j + e^{-i\phi} \hat{c}_j \hat{c}_{j+2} \right) \\ &- i(\Gamma + \kappa) \sum_j \hat{c}_j^\dagger \hat{c}_j \end{aligned} \tag{3.84}$$

where T is the real hopping amplitude and ϕ an arbitrary real phase. Note that if $\phi \neq 0, \pi$ we have broken time-reversal symmetry, as the phase ϕ cannot be gauged away. We once again stress that for periodic boundary conditions, only the dissipation determines the steady state which is characterized by the momentum-space occupation, see Eq. (3.21). We therefore only consider the open boundary case.

We know that if the next-nearest-neighbour hopping is zero, the propagation dynamics favors rightward propagation. The naive assumption is that this still holds for arbitrary T and ϕ, since the added next-nearest-neighbour hopping does not *a priori* favor left or right propagation as it is Hermitian. Using this line of thinking, we would expect particles to pile up on the right side, just like the original Hatano-Nelson model. In Fig. 3.6 we show that there exists a set of parameters for which the opposite is true: in the steady state particles pile up on the left side, but with the same long length scale $\xi_{\text{obc}} \approx w/(2\Gamma)$ as in

the Hatano-Nelson model. There is still a dissipative gap, and thus the naive expectation is that the associated length scale is very small. Further, the periodic and open boudnary spectrum looks nothing like the original Hatnao-Nelson model. How are we to understand this behavior?

The answer is to consider the dispersion of an infinite-sized chain, which can be readily found from Eq. (3.84) and gives $E(k) = w\cos(k) + T\cos(2k-\phi) - i\kappa(1+\sin k) - i\Gamma$. The least-damped mode is at $k = -\pi/2$, and the corresponding group velocity for the chosen parameters $T = w$ and $\phi = \pi/2$ is $w\partial_k(\cos k)|_{k=-\pi/2} + w\partial_k \cos(2k-\pi/2)|_{k=-\pi/2} = -w < 0$. Thus, with the inclusion of the next-nearest neighbour hopping, the least-damped mode now propagates to the left instead of the right. Further, we can once again estimate the relevant decay length as the group velocity divided by the residual decay rate Γ and recover $\xi_{\text{obc}} \approx w/(2\Gamma)$. Note that the right and left eigenvectors of the open chain also resemble nothing like the steady-state occupation $\langle \hat{c}_j^\dagger \hat{c}_j \rangle_{\text{ss}}$. With the chosen parameters, about 60% are localized to the right of the chain, and nearly 40% are localized to the left.

3.6 Steady state for noise with real-space correlations

Here we briefly study a model whose noise matrix $\boldsymbol{G}$ has a non-trivial spatial correlations. As we have shown in the main text, non-reciprocal dynamics can lead to an interesting steady state even when the noise is uniform. To disentangle the effects of non-reciprocity and the possibly interesting consequences of real-space fluctuation correlations, we seek a set of dissipators and coherent Hamiltonian which give rise to an effective reciprocal Hamiltonian.

Working with fermionic particles, this can be achieved by choosing

$$\hat{H} = \frac{w}{2} \sum_j \left(\hat{c}_{j+1}^\dagger \hat{c}_j + h.c. \right) \tag{3.85}$$

$$\hat{L}_j = \sqrt{\kappa} \left(\hat{c}_j - i\hat{c}_{j+1} \right) \tag{3.86}$$

$$\hat{G}_j = \sqrt{\Gamma} \left(\hat{c}_j^\dagger - i\hat{c}_{j+1}^\dagger \right) \tag{3.87}$$

and setting the decay and pumping rate to be the same $\kappa = \Gamma$. The effective Hamiltonian and noise matrix are

$$\boldsymbol{H}_{\text{eff}} = \boldsymbol{H} - i2\Gamma\mathbf{1} \tag{3.88}$$

$$\boldsymbol{G} = -i\Gamma \sum_j \left(|j+1\rangle \langle j| - |j\rangle \langle j+1| \right) + 2\Gamma\mathbf{1} \tag{3.89}$$

The effective Hamiltonian corresponds to a reciprocal tight-binding model with a uniform decay rate Γ. The noise matrix also has a similar structure, except the hopping matrix element is purely imaginary. This leads to an incompatibility between the dynamics and the noise, which can formally be written as $[\boldsymbol{H}, \boldsymbol{G}] \neq 0$: $\boldsymbol{H}$ and $\boldsymbol{G}$ can not be diagonalized by a common set of eigenvectors. Consequently, the dynamics can cause transitions between particles added by the gain baths to any eigenstate of $\boldsymbol{G}$ as is made clear by the formal solution to the steady-state correlation matrix $\boldsymbol{F}$ in Eq. (3.14).

The discord between the noise and the dynamics leads to a non-trivial steady-state occupation $\langle \hat{c}_j^\dagger \hat{c}_j \rangle_{\text{ss}}$ as we show in Fig. 3.7. In the bulk, we recover the expected occupation of half-filling, seeing as we have set $\kappa = \Gamma$. The occupation at the boundaries however is non-trivial, with an excess of particles at one edge and an equivalently depleted number at the opposite edge. We stress that this effect can not be attributed to non-reciprocity, as there is none. In a similar vain, it can not be explained by any novel non-Hermitian phenomena such as the NHSE: the dynamical matrix $\boldsymbol{H}$ is only trivially non-Hermitian in that it has a

uniform decay.

The goal of this appendix is not to fully characterize the steady state of this model, but rather to point out how structured fluctuations can lead to interesting behavior even when the dynamics are reciprocal. That being said, we can provide a simple intuitive reason as to why there is an accumulation of particles on one edge and a lack of them on the other. We first note that the eigenvectors of $\boldsymbol{G}$ are standing-wave states with a center of mass momentum $\pi/2$

$$\langle j | K_q \rangle = \sqrt{\frac{2}{N+1}} e^{i\frac{\pi}{2}j} \sin K_q j \tag{3.90}$$

with corresponding eigenvalues

$$G_{K_q} = 2\Gamma(1 - \cos K_q). \tag{3.91}$$

Using the dispersion our system, Eq. (3.90) tells us that the group velocity of a standing wave with momentum K_q is $\partial_k (w \cos k)|_{k=\frac{\pi}{2}\pm K_q} = -w \cos K_q$. Further, recall that the eigenvalues of $\boldsymbol{G}$ correspond to the rate at which the baths add particles to the corresponding eigenstate. Together with Eq. (3.91), we thus see that the baths adds right-moving particles $-w \cos K_q > 0$ at a higher than than left moving particles $-w \cos K_q < 0$. This succinctly explains why, at least qualitatively, there is an population imbalance in the steady state. The only dimensionless parameter in the problem, w/Γ, also controls a length scale which determines how the boundary occupation deviates from half-filling. As we increase Γ particles decay more quickly out of the system, and the number disparity between left-movers and right-movers because immaterial.

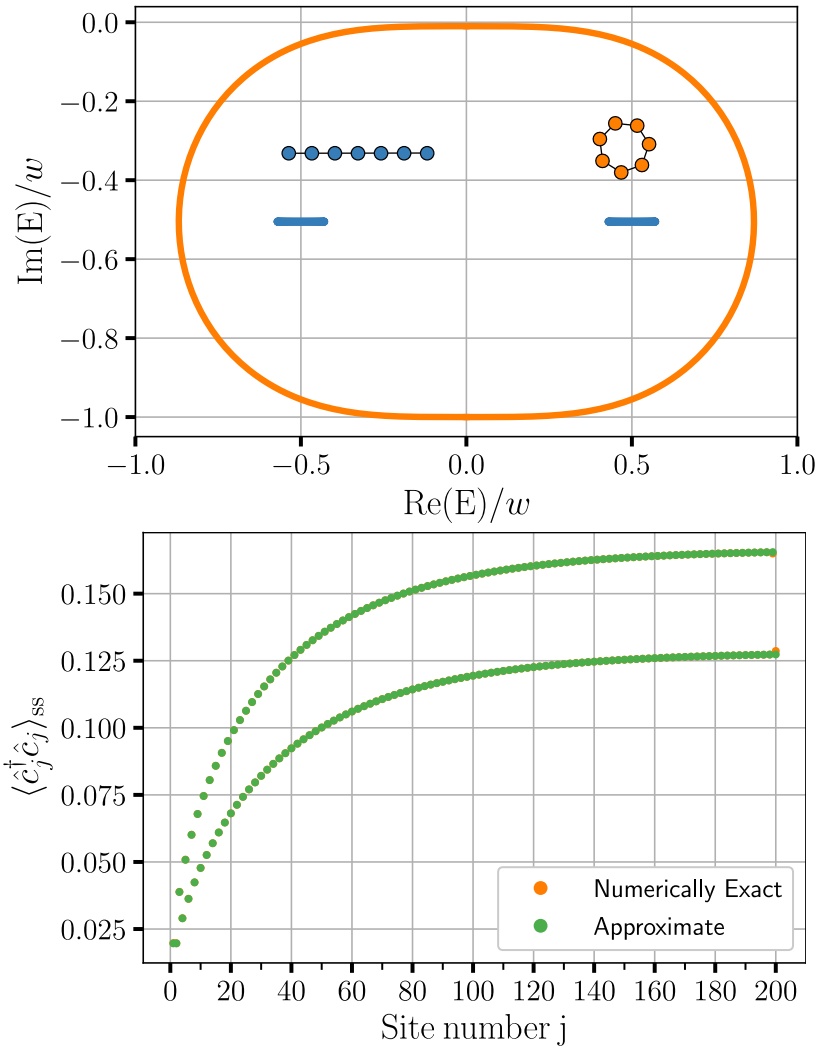

Fig. 3.5: Top: Periodic (orange) and open (blue) boundary spectrum of the SSH model described in Eq. (3.73) for $w = u = 1, \kappa = 0, \gamma = 0.99$ and $\Gamma = 0.01$ (i.e. only non-reciprocal hopping on every second bond). The model is known to exhibit the NHSE: all the energies to collapse to the real line and all right eigenvectors are localized to one side of the chain. The periodic boundary system has a gap of order Γ, whereas the open chain has a gap of order $(\kappa+\gamma)/2$. Bottom: Plot of the real-space steady-state occupation $\langle \hat{c}_j^\dagger \hat{c}_j \rangle_{\text{ss}}$ for the parameters above with $N = 200$ total sites (100 unit cells). Even and odd sites correspond to the A and B sublattice degrees of freedom respectively. Despite the large damping gap, there is still a large length scale which characterizes the steady-state occupation. The numerically exact method, which we obtain by directly solving the matrix equation Eq. (3.12) is essentially identical to the solution obtained by approximating the open-boundary Green's function by its infinite-system counterpart (see Eqs. (3.82)-(3.83)).

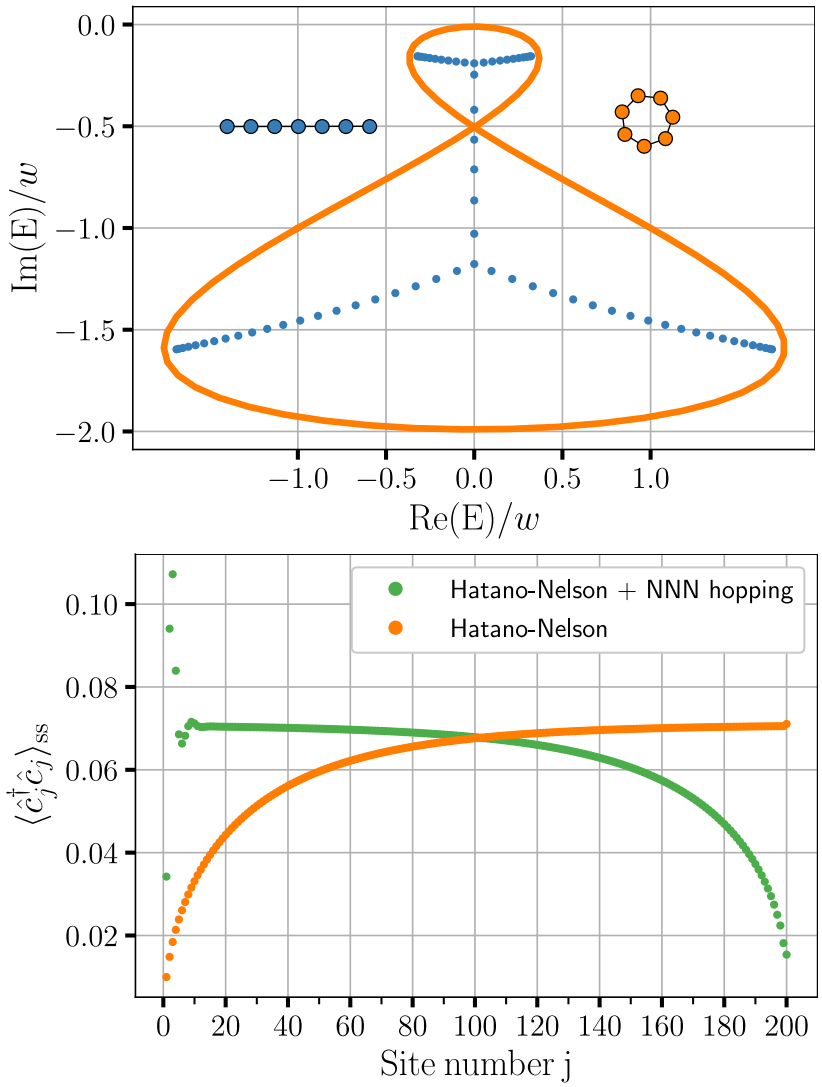

Fig. 3.6: Top: Periodic (orange) and open (blue) boundary spectrum of the Hatano-Nelson model with NNN hopping described in Eq. (3.84) for $w = T = 1$, $\kappa = 0.99$, $\phi = \pi/2$ and $\Gamma = 0.01$. Note that the open chain spectrum is only using $N = 70$ sites, due to numerical stability issues in computing the eigenvalues. The periodic boundary system has a gap of order Γ, whereas the open chain gap is of order of magnitude smaller than κ. The system exhibits the NHSE, with nearly 60% of all right eigenvectors localized to the right, and 40% localized to the left of the chain under open boundary conditions. Bottom: Plot of the real-space steady-state occupation $\langle \hat{c}_j^\dagger \hat{c}_j \rangle_{\text{ss}}$ for the Hatano-Nelson model and the Hatano-Nelson model with NNN hopping with the parameters above for a chain with $N = 200$ sites. The two models share the same large length scale $\xi_{\text{obc}} \approx w/(2\Gamma)$ despite having very different eigenvalues and eigenvectors.

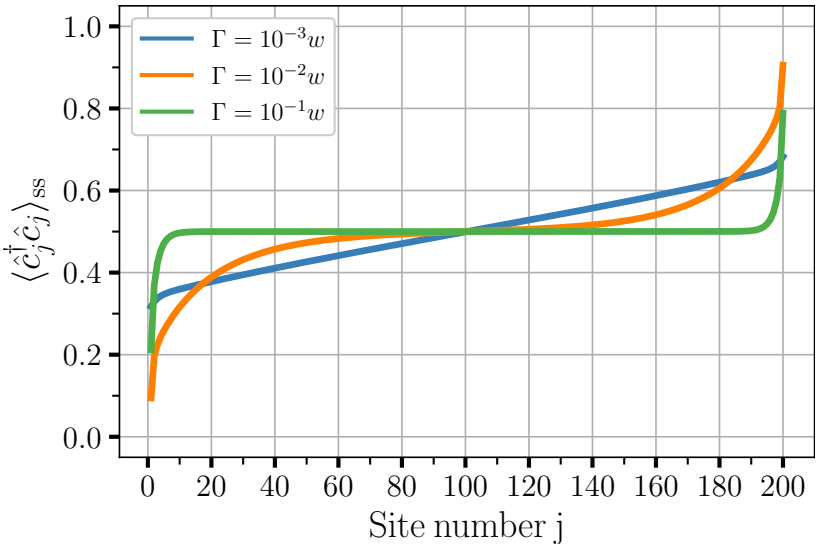

Fig. 3.7: Steady-state occupation $\langle \hat{c}_j^\dagger \hat{c}_j \rangle_{\rm ss}$ of a reciprocal tight-binding model with a non-trivial noise correlation matrix. The effective Hamiltonian and noise are realized with the coherent Hamiltonian and dissipators Eqs. (3.85-3.87). Despite the lack of non-reciprocity, there is an accumulation and depletion of particles on opposite ends of the chain. This can be attributed to non-uniform pumping, which adds right-movers to the chain at a higher rate than left-movers.

CHAPTER 4

EXACT SOLUTIONS OF INTERACTING DISSIPATIVE SYSTEMS VIA WEAK SYMMETRIES

This chapter contains previously-published material found in Ref. ([84]). Reuse is permitted according to the copyright agreement used by *Physical Review Letters*.

4.1 Overview of Results

We demonstrate how the presence of continuous weak symmetry can be used to *analytically* diagonalize the Liouvillian of a class of Markovian dissipative systems with strong interactions or nonlinearity. This enables an exact description of the full dynamics and dissipative spectrum. Our method can be viewed as implementing an exact, sector-dependent mean-field decoupling, or alternatively, as a kind of quantum-to-classical mapping. We focus on two canonical examples: a nonlinear bosonic mode subject to incoherent loss and pumping, and an inhomogeneous quantum Ising model with arbitrary connectivity and local dissipation. In both cases, we calculate and analyze the full dissipation spectrum. Our method is applicable to a variety of other systems, and could provide a powerful new tool for the study of complex driven-dissipative quantum systems.

4.2 Introduction

Identifying symmetries provides powerful insights into non-dissipative quantum systems, often providing a route towards finding exact descriptions of dynamics and thermal states. The key ingredient is usually the direct connection between the existence of symmetry and dynamically-conserved quantities. Turning to dissipative (open) quantum systems, the situation becomes more subtle, as the non-unitary nature of the evolution makes the link between symmetry and conservation laws less direct (see, e.g. [74, 3, 18, 22, 149, 76]). In

the typical case of a Markovian system described by a Lindblad master equation, one often has only a so-called "weak symmetry" [18]. A weak symmetry leaves the full Lindbladian invariant under a given transformation while changing the system operators which couple to dissipation (i.e. the jump operators). While this symmetry ensures that the generator of the dynamics (i.e. the Liouvillian) has a block-diagonal structure, it does not guarantee the existence of a true conserved quantity. Hence, while such weak symmetries can simplify numerical calculations [117, 121], they are not *a priori* a useful tool for obtaining analytic solutions.

Here, we show that in many cases, the existence of a continuous weak symmetry is in fact a far more powerful tool that one might initially suspect. We show how a weak symmetry can be exploited to fully and *analytically* diagonalize a set of non-trivial Lindblad superoperators that describe interacting, dissipative quantum systems. As explained below, this is possible because the weak symmetry makes an unusual kind of mean-field decoupling exact in each symmetry-constrained block, reducing it to an effective (but unusual) non-interacting problem (see Fig. 4.1). Alternatively, the solution method can be viewed as a kind of quantum-to-classical mapping. The underlying mechanism arises in a wide class of models, but for concreteness, we analyze in detail both a bosonic example (a nonlinear bosonic mode subject to thermal dissipation), and a dissipative spin model (a quantum Ising model subject to single-spin dephasing and relaxation). Both these examples are directly relevant to a variety of systems under active experimental study. Our approach yields closed form expressions for all eigenvalues and eigenvectors of the Liouvillian, enabling one to clearly identify structures that would not be apparent otherwise. This diagonalization provides a full picture of the dissipative dynamics, and also allows the calculation of a variety of observable quantities (e.g. correlation functions).

We stress that our general method is distinct from approaches used in previous work to obtain exact descriptions of specific quantum dissipative models, e.g. [1, 30, 31, 103, 23, 24,

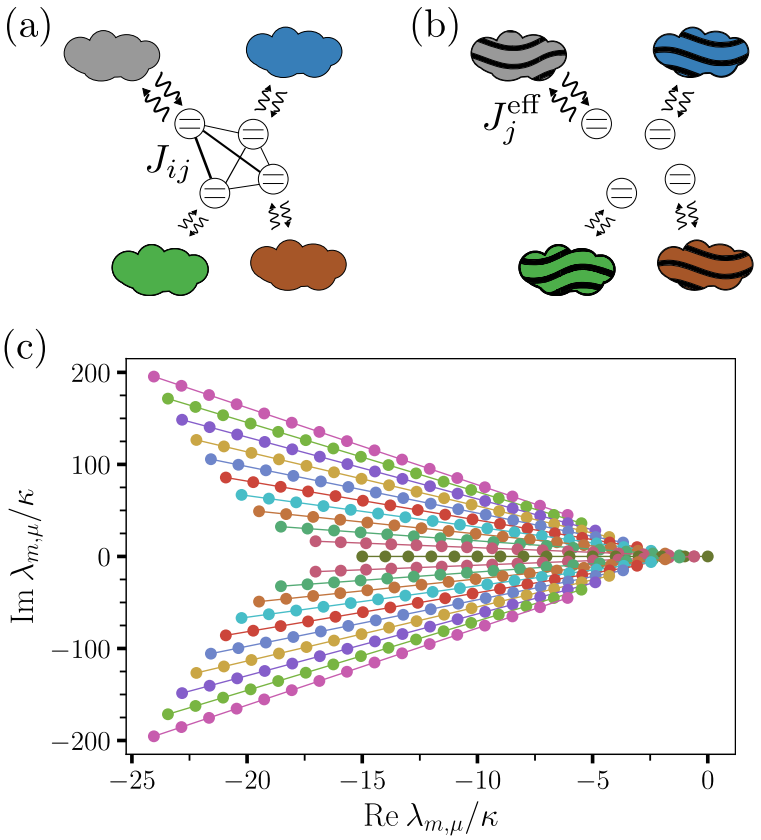

Fig. 4.1: (a) Schematic of the second model analyzed in this work: N two-level systems interact via arbitrary Ising interactions J_{ij}, and are also subject to local dissipation, c.f. Eq. (4.10). (b) Using weak symmetry, one can make an *exact* mean-field decoupling for each symmetry-constrained dynamical sector, leaving one with an easily-solved but unusual independent, dissipative spin problem. (c) A similar solution method can be used for an incoherently-driven non-linear bosonic mode (c.f. Eq. (4.1)), enabling an exact calculation of the Liouvillian eigenvalues $\lambda_{m,\mu}$. We plot these here for $|m| \leq 10$ and $\mu \leq 15$. Each color corresponds to a different value of $|m|$. By fixing m, the level spacing $\lambda_{m,\mu+1} - \lambda_{m,\mu} = -\tilde{\kappa}_m - i\tilde{U}_m$ is constant, reflecting the non-interacting nature of the problem in each symmetry-constrained block. We work in a rotating frame where ω_0 is shifted to 0, and set $U = \kappa, \bar{n}_{\text{th}} = 0.1$.

129, 132, 88, 10, 37, 98, 124, 123, 114, 19, 99, 115]. Our method provides the exact dissipative spectrum and eigenvectors, and moreover, presents them in a simple and intuitive form which is tailor-made to perform analytic computations. This is crucial, as it provides the necessary starting point if one wants to make use of the burgeoning tool of Lindblad perturbation theory [71, 72, 47, 4] to more complicated systems.

4.3 Dissipative Kerr Oscillator

Consider a bosonic mode with a Kerr (or Hubbard) type nonlinearity, subject to Markovian thermal dissipation. The evolution of the system density matrix $\hat{\rho}$ is (setting $\hbar = 1$):

$$\begin{aligned}\partial_t \hat{\rho} = &-i[\omega_0 \hat{a}^\dagger \hat{a} + \frac{U}{2}\hat{a}^\dagger \hat{a}^\dagger \hat{a}\hat{a}, \hat{\rho}] + \kappa(\bar{n}_{\text{th}} + 1)\mathcal{D}[\hat{a}]\hat{\rho} \\ &+ \kappa \bar{n}_{\text{th}} \mathcal{D}[\hat{a}^\dagger]\hat{\rho} \equiv \mathcal{L}\hat{\rho}. \end{aligned} \tag{4.1}$$

Here $\hat{a}$ is the mode annihilation operator, ω_0 (U) is the mode natural frequency (nonlinearity), κ the energy decay rate, and $\bar{n}_{\text{th}}$ the bath's thermal occupation. We define $\mathcal{D}[\hat{X}]\hat{\rho} \equiv \hat{X}\hat{\rho}\hat{X}^\dagger - \{\hat{X}^\dagger \hat{X}, \hat{\rho}\}/2$. Eq. (4.1) has an obvious weak $U(1)$ symmetry, as it is invariant under $\hat{a} \to e^{-i\theta}\hat{a}$. This gives $\mathcal{L}$ a block-diagonal structure [22, 3, 18, 121, 94], which has been used previously to simplify numerical calculations [117, 121]. We show below that something more powerful is possible: despite the nonlinearity, the weak symmetry can also be used to analytically diagonalize *each block* and thus all of $\mathcal{L}$. Our analysis complements and extends previous studies that derive exact results for this model without explicit use of weak symmetry [103, 31, 23, 24]. In particular, our approach provides simple analytic expressions for *all* eigenvalues and eigenvectors of $\mathcal{L}$.

To diagonalize $\mathcal{L}$, we use the formalism of third-quantization [112, 113, 2]; relevant details can be found in the SM 4.6. One first introduces four new superoperators $\hat{\boldsymbol{a}}_{\text{L}} |\hat{\rho}\rangle \equiv |\hat{a}\hat{\rho}\rangle$, $\hat{\boldsymbol{a}}_{\text{R}} |\hat{\rho}\rangle \equiv |\hat{\rho}\hat{a}\rangle$, $\hat{\boldsymbol{a}}^\dagger_{\text{L}} |\hat{\rho}\rangle \equiv |\hat{a}^\dagger\hat{\rho}\rangle$, and $\hat{\boldsymbol{a}}^\dagger_{\text{R}} |\hat{\rho}\rangle \equiv |\hat{\rho}\hat{a}^\dagger\rangle$ which we will refer to as annihilation and creation superoperators. We will also reserve the bold typeface to indicate a third-quantized superoperator $\mathcal{L} \to \hat{\boldsymbol{\mathcal{L}}}$. We can now express our Liouvillian as $\hat{\boldsymbol{\mathcal{L}}} = (-i\omega_0 + \kappa/2)\hat{\mathbf{1}} + \hat{\boldsymbol{\mathcal{L}}}_0 + \hat{\boldsymbol{\mathcal{L}}}_{\text{int}}$

where

$$\hat{\boldsymbol{\mathcal{L}}}_0 = \underline{\hat{\boldsymbol{a}}}^\dagger \begin{pmatrix} -i\omega_0 - \frac{\kappa}{2}(2\bar{n}_{\rm th}+1) & \kappa\bar{n}_{\rm th} \\ \kappa(\bar{n}_{\rm th}+1) & i\omega_0 - \frac{\kappa}{2}(2\bar{n}_{\rm th}+1) \end{pmatrix} \underline{\hat{\boldsymbol{a}}} \tag{4.2}$$

$$\hat{\boldsymbol{\mathcal{L}}}_{\rm int} = -i\frac{U}{2}\left(\hat{\boldsymbol{a}}_{\rm L}^\dagger\hat{\boldsymbol{a}}_{\rm L} - \hat{\boldsymbol{a}}_{\rm R}\hat{\boldsymbol{a}}_{\rm R}^\dagger\right)\left(\hat{\boldsymbol{a}}_{\rm L}^\dagger\hat{\boldsymbol{a}}_{\rm L} + \hat{\boldsymbol{a}}_{\rm R}\hat{\boldsymbol{a}}_{\rm R}^\dagger - \hat{\mathbf{1}}\right) \tag{4.3}$$

correspond to the quadratic and interacting parts of the Linbladian respectively. Here $\underline{\hat{\boldsymbol{a}}}^\dagger = \begin{pmatrix} \hat{\boldsymbol{a}}_{\rm L}^\dagger & \hat{\boldsymbol{a}}_{\rm R}^\dagger \end{pmatrix}$. The quadratic part of the superoperator $\hat{\boldsymbol{\mathcal{L}}}_0$ is easily diagonalized via standard third-quantization techniques [112, 113]. The nonlinear quartic terms however represent a true interaction of third-quantized bosons, and seemingly destroys exact solvability.

We now exploit the weak symmetry of our system. At the superoperator level, the weak symmetry corresponds to the invariance of Eq. (4.3) under $\hat{\boldsymbol{a}}_{\rm L/R} \to \hat{\boldsymbol{a}}_{\rm L/R}e^{-i\theta}$. The superoperator generating this effective unitary transformation is $\hat{\boldsymbol{a}}_{\rm L}^\dagger\hat{\boldsymbol{a}}_{\rm L} - \hat{\boldsymbol{a}}_{\rm R}\hat{\boldsymbol{a}}_{\rm R}^\dagger$, which immediately implies $[\hat{\boldsymbol{\mathcal{L}}}, \hat{\boldsymbol{a}}_{\rm L}^\dagger\hat{\boldsymbol{a}}_{\rm L} - \hat{\boldsymbol{a}}_{\rm R}\hat{\boldsymbol{a}}_{\rm R}^\dagger] = 0$. Standard linear algebra then dictates that $\hat{\boldsymbol{\mathcal{L}}}$ is block-diagonal in the eigenbasis of $\hat{\boldsymbol{a}}_{\rm L}^\dagger\hat{\boldsymbol{a}}_{\rm L} - \hat{\boldsymbol{a}}_{\rm R}\hat{\boldsymbol{a}}_{\rm R}^\dagger$. We can thus write $\hat{\boldsymbol{\mathcal{L}}} = \bigoplus_m \hat{\boldsymbol{\mathcal{L}}}_m$, where each block $\hat{\boldsymbol{\mathcal{L}}}_m$ is indexed by m, an eigenvalue of $\hat{\boldsymbol{m}} \equiv \hat{\boldsymbol{a}}_{\rm L}^\dagger\hat{\boldsymbol{a}}_{\rm L} - \hat{\boldsymbol{a}}_{\rm R}\hat{\boldsymbol{a}}_{\rm R}^\dagger$. A simple calculation reveals that any outer-product of Fock states $|p\rangle\langle q|$ is an eigenvector of the generator $\hat{\boldsymbol{m}}|p\rangle\langle q| = [\hat{a}^\dagger\hat{a}, |p\rangle\langle q|] = m|p\rangle\langle q|$ and the corresponding eigenvalue $m = p - q \in \mathbb{Z}$ characterizes the degree of coherence or off-diagonalness in Fock space. Further, since any outer product of Fock states of the form $|p+n\rangle\langle q+n|$ has the same eigenvalue as $|p\rangle\langle q|$, each block $\hat{\boldsymbol{\mathcal{L}}}_m$ is infinite in extent.

While weak symmetry provides a block-diagonal structure, we are still left with the seemingly formidable task of diagonalizing the infinite-dimensional matrix corresponding to each block; further, apart from $m = 0$, each block's form depends on the non-trivial interaction U. As we now show, surprisingly these remaining tasks can be done exactly. By definition $\hat{\boldsymbol{\mathcal{L}}}_m$, is the full Lindbladian projected onto the subspace spanned by eigenvectors of $\hat{\boldsymbol{m}}$ with eigenvalue m. We may thus, in each block $\hat{\boldsymbol{\mathcal{L}}}_m$, make the substitution $\hat{\boldsymbol{m}} \to m$.

Next, note that the non-linear part of $\mathcal{L}$ can be written as

$$\hat{\boldsymbol{\mathcal{L}}}_{\text{int}} = -i\frac{U}{2}\hat{\boldsymbol{m}} \times \hat{\boldsymbol{\mathcal{L}}}_0' \tag{4.4}$$

where $\hat{\boldsymbol{\mathcal{L}}}_0' = \left(\hat{\boldsymbol{a}}_{\text{L}}^\dagger \hat{\boldsymbol{a}}_{\text{L}} + \hat{\boldsymbol{a}}_{\text{R}} \hat{\boldsymbol{a}}_{\text{R}}^\dagger - \hat{\mathbf{1}}\right)$ is quadratic in creation an annihilation superoperators. Projecting onto the subspace indexed by m, when have $\hat{\boldsymbol{\mathcal{L}}}_{\text{int}} \to -iUm/2\hat{\boldsymbol{\mathcal{L}}}_0'$. We finally obtain

$$\begin{aligned}\hat{\boldsymbol{\mathcal{L}}}_m = \underline{\hat{\boldsymbol{a}}}^\dagger &\begin{pmatrix} -i\frac{Um}{2} - \frac{\kappa}{2}(2\bar{n}_{\text{th}} + 1) & \kappa\bar{n}_{\text{th}} \\ \kappa(\bar{n}_{\text{th}} + 1) & -i\frac{Um}{2} - \frac{\kappa}{2}(2\bar{n}_{\text{th}} + 1) \end{pmatrix} \underline{\hat{\boldsymbol{a}}} \\ &+ (-i(\omega_0 - U)m + \frac{\kappa}{2})\hat{\mathbf{1}}. \end{aligned} \tag{4.5}$$

We thus have a crucial first result: in each symmetry-constrained sector, $\hat{\boldsymbol{\mathcal{L}}}$ becomes quadratic in creation and annihilation superoperators, and can thus be diagonalized exactly. It is as though a mean-field ansatz has become exact in each block (though note the mean-field decoupling is block dependent, and results in a Liouvillian that is not in Lindblad form). We stress that the mere existence of a weak symmetry was not enough for solvability, as this by itself only guarantees the existence of the block-diagonal structure. Instead, we also needed the interacting part of the Lindbladian to factor as in Eq. (4.4). Identifying this general structure is a main result of this work.

As it is quadratic in creation and annihilation superoperators, Eq. (4.5) can be diagonalized using conventional third-quantization. One ultimately needs to diagonalize a 2×2 matrix in each sector to obtain both the eigenvalues and eigenvectors. We denote the Liouvillian eigenvalues $\lambda_{m,\mu}$ where m labels the different symmetry-constrained blocks (i.e. the degree of off-diagonalness), and the non-negative integer μ labels eigenmodes in a given block. It roughly characterizes the average number of particles in the eigenmode. Using the

above structure (see SM 4.6), we find:

$$\lambda_{m,\mu} = -i\left[\omega_0 - U + \frac{\tilde{U}_m}{2}(|m| + 1 + 2\mu)\right] m \\ - \frac{1}{2}\Big[\tilde{\kappa}_m(|m| + 1 + 2\mu) - \kappa\Big] \tag{4.6}$$

where

$$\tilde{U}_m = |U|\,\mathrm{Im}\sqrt{(\frac{\kappa}{Um})^2 - 1 + 2i\frac{\kappa}{Um}(2\bar{n}_{\mathrm{th}} + 1)} \tag{4.7}$$

$$\tilde{\kappa}_m = \kappa\,\mathrm{Re}\sqrt{1 - (\frac{Um}{\kappa})^2 + 2i\frac{Um}{\kappa}(2\bar{n}_{\mathrm{th}} + 1)} \tag{4.8}$$

are renormalized sector-dependent non-linearities and decay rates respectively. Note these are bounded by $\kappa \leq \tilde{\kappa}_m \leq \kappa(2\bar{n}_{\mathrm{th}} + 1)$ and $|U| \leq |\tilde{U}_m| \leq |U|(2\bar{n}_{\mathrm{th}} + 1)$. If $\kappa \to 0$, $\tilde{U}_m \to U$, whereas for non-zero κ it is temperature dependent. We also see that the effective damping rate in each sector generically depends on temperature when $U \neq 0$. In Fig. 4.1 we plot the spectrum for $|m| \leq 10$ and $\mu \leq 15$. Expressions for eigenvectors are provided in the SM 4.6.

The ability to analytically describe the eiegenvectors and eigenvalues evidently constitutes a full solution of our system: any quantity we wish to calculate or initial state we wish to time-evolve can be readily computed using the spectral decomposition of $\hat{\boldsymbol{\mathcal{L}}}$. This spectral information in and of itself carries a wealth of physically and experimentally relevant information. We will focus on one such example, the retarded Green's function $G^R(t) \equiv -i\Theta(t)\langle[\hat{a}(t), \hat{a}^\dagger(0)]\rangle$ which controls how the average value $\langle\hat{a}(t)\rangle$ changes in response to a weak coherent drive applied at time $t = 0$. Since $\hat{\rho}_{\mathrm{ss}}$ is an incoherent mixture of Fock states, it is an element of the $m = 0$ block. Applying $\hat{a}^\dagger$ to either side of the density matrix raises the coherence by one, and thus excites all $m = 1$ right eigenvectors. Using the spectral decomposition of $e^{\hat{\boldsymbol{\mathcal{L}}}t}$, we show in the SM 4.6 that

$$G^R(t) = -i\Theta(t)\frac{e^{-i(\omega_0-U)t+\frac{\kappa}{2}t}}{\left(\cosh\left(\frac{\tilde{\kappa}_1+i\tilde{U}_1}{2}t\right)+R_1\sinh\left(\frac{\tilde{\kappa}_1+i\tilde{U}_1}{2}t\right)\right)^2}. \tag{4.9}$$

where $R_1 = (\kappa + iU(2\bar{n}_{\rm th}+1))/(\tilde{\kappa}_1 + i\tilde{U}_1)$ in agreement with Ref. [31]. Fourier-transforming Eq. (4.9) gives us the frequency-resolved Green's function $G^R[\omega]$, which can easily be accesssed in several experimental platforms. In a similar manner, higher-order response functions can be directly tied to eigenvalues and eigenvectors for higher m modes.

While for clarity we have focused here on a single-mode problem, a completely analogous approach allows one to analytically diagonalize a truly many-body model, where we now have a set of bosonic modes, each with Kerr nonlinearities and thermal dissipation, coupled to one another via cross-Kerr interaction of the form $U_{ab}\hat{a}^\dagger\hat{a}\hat{b}^\dagger\hat{b}$. As we show in the SM 4.6, our method applies directly here: in each symmetry-constrained block, the non-trivial interaction terms become effectively quadratic. We also show this setup remains solvable if we were to add dephasing to each mode (as described by the dissipators $2\kappa_{\phi,j}\mathcal{D}[\hat{a}_j^\dagger\hat{a}_j]\hat{\rho}$).

4.4 Dissipative Ising Model

We next show that our symmetry-based approach can be used for a completely different kind of system, namely a dissipative Ising model of N spins. The Lindblad master equation reads

$$\begin{aligned}\partial_t\hat{\rho} = &-i\Big[\sum_{j<k}J_{jk}\hat{\sigma}_j^z\hat{\sigma}_k^z + \sum_j h_j\hat{\sigma}_j^z, \hat{\rho}\Big] + \sum_j \gamma_{-,j}\mathcal{D}[\hat{\sigma}_j^-]\hat{\rho} \\ &+ \sum_j \gamma_{+,j}\mathcal{D}[\hat{\sigma}_j^+]\hat{\rho} + \sum_j \gamma_{\phi,j}\mathcal{D}[\hat{\sigma}_j^z]\hat{\rho} \equiv \mathcal{L}\hat{\rho}.\end{aligned} \tag{4.10}$$

It describes N interacting two-level systems with arbitrary Ising couplings J_{jk}, each with its own local magnetic field h_j. Each spin is also subject to local spin relaxation, pumping, and

dephasing characterized by the rates $\gamma_{-,j}$, $\gamma_{+,j}$ and $\gamma_{\phi,j}$ respectively.

Note that $\mathcal{L}$ is invariant under arbitrary, independent local rotations around the z axis of each spin, i.e. $\hat{\sigma}_j^{\pm} \to e^{\pm i\theta_j}\hat{\sigma}_j^{\pm}$. There are thus N weak $U(1)$ symmetries, one for each spin, generated by the superoperators $[\hat{\sigma}_j^z, \cdot]/2$. Each of these generators has two non-degenerate eigenvalues $m_j = \pm 1$ whose eigenvectors are coherences $|\uparrow_j\rangle\langle\downarrow_j| = \hat{\sigma}_j^+$ and $|\downarrow_j\rangle\langle\uparrow_j| = \hat{\sigma}_j^-$. There is also a two-fold degenerate eigenvalue $m_j = 0$ with associated population eigenvectors $|\uparrow_j\rangle\langle\uparrow_j|$ and $|\downarrow_j\rangle\langle\downarrow_j|$. The Lindbladian necessarily commutes with each generator and thus takes on a block diagonal form, where each block is indexed by $\vec{M} = \{m_1, \ldots, m_N\}$, i.e. the vector formed by the eigenvalues of the generators. Given that the $m_j = \pm 1$ eigenvalues are non-degenerate whereas the $m_j = 0$ eigenvalues are two-fold degenerate, for a specific block indexed by $\vec{M}$, we can parition our spins into a a set of "frozen" spins (i.e. spins j with $m_j = \pm 1$) and "active" spins (i.e. spins j with $m_j = 0$). Within the specific block described by a given $\vec{M}$, the populations of the active spins can fluctuate. Formally, if we let $\hat{\rho}_{\vec{M}}$ denote the density matrix projected onto the subspace indexed by $\vec{M}$, then we have

$$\begin{aligned}\hat{\rho}_{\vec{M}} &= \hat{\rho}_{\text{froz}} \times \hat{\rho}_{\text{act}} \\ &= \left(\prod_{j \text{ frozen}} \hat{\sigma}_j^{m_j}\right)\left(\sum_{\vec{s}_{\text{act}}} P(\vec{s}_{\text{act}})\,|\vec{s}_{\text{act}}\rangle\langle\vec{s}_{\text{act}}|\right)\end{aligned} \tag{4.11}$$

where $\vec{s}_{\text{act}} = \{s_j \mid j \text{ active}\}$ and $s_j \in \{\uparrow_j, \downarrow_j\}$. In each block $\hat{\rho}_{\vec{M}}$ factorizes as a product over coherences $\hat{\rho}_{\text{froz}}$ and a *classical* density matrix $\hat{\rho}_{\text{act}}$ described entirely by a probability distribution $P(\vec{s}_{\text{act}})$ for a ensemble of two-level systems. If we let $z(\vec{M})$ denote the number of zero eigenvalues of $\vec{M}$, which is by definition the number of active spins, then the size of the Lindblad block indexed by $\vec{M}$ is $2^{z(\vec{M})}$.

Just as in the dissipative non-linear oscillator model, the existence of weak symmetry is not enough to make the system analytically solvable, as it only guarantees the block diagonal structure of Eq. (4.11). There are still many blocks whose dimension is exponentially large in

the number of spins, encoding what would seem to be a complicated dissipative many-body problem. Instead, further simplification emerges from the form of the interaction and the fact that a mean-field decoupling becomes exact in each symmetry sector. We show in the SM 4.6 that, upon projecting into the subspace indexed by $\vec{M}$, this amounts to making the replacement

$$\Big[\sum_{j<k} J_{jk}\hat{\sigma}_j^z\hat{\sigma}_k^z, \hat{\rho}\Big] \to \{\sum_j J_j^{\text{eff}}(\vec{M})\hat{\sigma}_j^z, \hat{\rho}_{\vec{M}}\} \tag{4.12}$$

where we have defined $J_j^{\text{eff}}(\vec{M}) = \sum_{k\neq j} J_{jk}m_k$. Using Eq. (4.12), we therefore see that within each block, mean-field theory becomes exact: the spin-spin interaction has been replaced by a (sector-dependent) static z magnetic field on each spin, $J_j^{\text{eff}}(\vec{M})$. Combined with the local nature of the dissipation, it follows that the classical probability describing the active spin factorizes $\hat{\rho}_{\text{act}} = \prod_{j\,\text{act}} \left(p_{\uparrow,j}\left|\uparrow_j\right\rangle\left\langle\uparrow_j\right| + p_{\downarrow,j}\left|\downarrow_j\right\rangle\left\langle\downarrow_j\right|\right)$ and the equations of motion for the coefficients read

$$\partial_t \begin{pmatrix} p_{\uparrow,j} \\ p_{\downarrow,j} \end{pmatrix} = \begin{pmatrix} -2iJ_j^{\text{eff}} - \gamma_{-,j} & \gamma_{+,j} \\ \gamma_{-,j} & 2iJ_j^{\text{eff}} - \gamma_{+,j} \end{pmatrix} \begin{pmatrix} p_{\uparrow,j} \\ p_{\downarrow,j} \end{pmatrix} \tag{4.13}$$

where, for the sake of compactness, we have dropped the $\vec{M}$ dependence of J_j^{eff}.

The above exact decoupling has thus allowed us to map a many-body quantum problem onto an effective classical model of non-interacting spins. To see this explicitly, note that Eq. (4.13) would correspond precisely to a classical master equation for a two-state system if not for the strange imaginary terms $\propto J_j^{\text{eff}}$ on the diagonals. These terms also admit a simple classical interpretation. Consider the random variable $\hat{s}_j = \int_0^t dt'\hat{\sigma}_j^z(t')$, i.e. the integral of the classical telegraph fluctuations of spin j. We can now interpret $2J_j^{\text{eff}}$ as a conjugate variable to this stochastic quantity (i.e. a so-called "counting field"). Viewed as a function of $2J_j^{\text{eff}}$, the solution to Eq. (4.13) allows us to obtain the time-dependent moment-

generating function of $\hat{s}_j$, i.e. $\Lambda[2J_j^{\text{eff}}] = \int ds_j P(s_j) e^{-2iJ_j^{\text{eff}} s_j}$. In a concrete sense, one concludes that the frozen spins are measuring the classical fluctuations of the active spins at a rate determined by J_{ij}. The upshot is that our solution method can be viewed as having made a quantum-to-classical mapping in each symmetry-constrained block.

The above exact decoupling of spins in each symmetry block immediately implies that all Liouvillian eigenvalues can be written as a sum over single-spin eigenvalues $\lambda_j(\vec{M})$. A simple calculation yields

$$\lambda_j(\vec{M}) = \begin{cases} \mp i2h_j - \Gamma_j - 2\gamma_{\phi,j}, & j \text{ frozen} \\ -\Gamma_j \pm \sqrt{\Gamma_j^2 - 4J_j^{\text{eff}}(J_j^{\text{eff}} + i\eta_j)}, & j \text{ active} \end{cases} \tag{4.14}$$

with $\Gamma_j = (\gamma_{+,j} + \gamma_{-,j})/2$ and $\eta_j = (\gamma_{+,j} - \gamma_{-,j})/2$. Equation (4.14) tells us that coherences $|{\downarrow_j}\rangle\langle{\uparrow_j}|$ and $|{\uparrow_j}\rangle\langle{\downarrow_j}|$ behave as expected: they oscillate with a frequency controlled by the local magnetic field and decay at a rate set by the local dephasing and relaxation processes, independently of all other spins. Populations however both decay and oscillate depending on the strength of the counting field $2J^{\text{eff}}$ relative to the strength of the relaxation processes. The right and left eigenvectors factorize in a similar way, and one only needs to solve a 2×2 matrix eigenvalue problem to determine their form. As such, we leave those details to the SM 4.6.

With both the eigenvectors and eigenvalues, we can again compute any physical quantity of interest for this model. In the SM 4.6, we provide an example of this, for the case where all spins are initially all pointing along the x direction. Analogous quantities were calculated in Ref. [36] using an alternative method. Our approach greatly simplifies the calculation, and also allows insights not possible using the trajectory method of Ref. [36], as we have access to the full dissipation spectrum. For example, we find that our many-body Liouvillian can exhibit an exceptional point (EP) structure (see SM 4.6), wherein the dynamics are exceptionally sensitive to small parameter changes. Such Lindblad EPs have

been the subject of considerable recent interest [56, 95, 7], though there are few truly many-body examples. Our approach can also be used to analytically find the full time-evolved many-body density matrix $\hat{\rho}(t)$ for an arbitrary initial condition (which would be difficult if not impossible to do using trajectories). Finally, as shown in the SM 4.6, our method is also applicable to the situation where there the magnetic fields and Ising couplings are time-dependent; the symmetry and effective mean-field decoupling structure of the interaction remain intact. This greatly reduces the numerical cost of time-evolving the density matrix and could be used to address problems where the couplings and magnetic fields are random.

Similar to our discussion of the dissipative nonlinear bosonic model earlier, we have for clarity sketched the simplest non-trivial dissipative spin model where our symmetry-based solution method holds. The effective quantum-to-classical mapping we have established is in fact valid for a large class of dissipative spin models. For example, there are still N weak $U(1)$ symmetries if we add to our model correlated spin-loss or flips for an arbitrarily large number of spins such as, e.g. $\mathcal{D}[\hat{\sigma}_j^- \hat{\sigma}_k^+]$. The block-diagonal decomposition Eq. (4.11) thus follows, as does the mean-field replacement Eq. (4.12). The only difference is that classical probability distribution describing the active spins does not factorize; nevertheless the equations of motion in each block is exactly equivalent to a classical master equation of correlated spins with a counting field for each spin J_j^{eff}. This suggests that our approach could be a powerful means to attack a range of dissipative spin models.

4.5 Summary and future directions

Our work shows how continuous weak symmetries can enable the analytic solution of a wide class of interacting dissipative quantum models. While we analyzed to specific examples (one bosonic, the other spin-based), we stress that the method could be applied to a variety of other systems. It also provides a powerful starting point for systematic approximation methods for systems with additional terms that break the relevant weak symmetry. For example,

as our approach provides simple analytic expressions for all eigenvalues and eigenvectors, it could be directly combined with Lindblad perturbation theory [71, 72, 47]. In future work, it would be interesting to reformulate the general structure we have exploited here in terms of a dissipative Keldysh action [126, 58]; this could enable an extension of our method to non-Markovian dissipative systems.

4.6 Supplementary Material

4.6.1 Eigenvectors and eigenvalues of incoherently-driven non-linear oscillator Lindbladian

In this section, we find the eigenvectors and eigenvalues of the incoherently-driven non-linear oscillator, whose third quantized form is given by Eqs (1)-(2) in the main text. As we then explain in the subsequent discussion following this equation, one can make use of the $U(1)$ symmetry to reduce the problem to a quadratic one in each block $\hat{\boldsymbol{\mathcal{L}}}_m$ by making the substitution $\hat{\boldsymbol{a}}_{\mathrm{L}}^\dagger \hat{\boldsymbol{a}}_{\mathrm{L}} - \hat{\boldsymbol{a}}_{\mathrm{R}} \hat{\boldsymbol{a}}_{\mathrm{R}}^\dagger \to m$. Using commutation relations $[\hat{\boldsymbol{a}}_{\mathrm{L}}, \hat{\boldsymbol{a}}_{\mathrm{L}}^\dagger] = -[\hat{\boldsymbol{a}}_{\mathrm{R}}, \hat{\boldsymbol{a}}_{\mathrm{R}}^\dagger] = \hat{\mathbf{1}}$ along with the fact that any superoperator which acts on the left commutes with those acting on the right, we get

$$\begin{aligned}\hat{\boldsymbol{\mathcal{L}}}_m = &\left(-i(\omega_0 - U)m + \frac{\kappa}{2}\right)\hat{\mathbf{1}} + \kappa(\bar{n}_{\mathrm{th}} + 1)\hat{\boldsymbol{a}}_{\mathrm{R}}^\dagger \hat{\boldsymbol{a}}_{\mathrm{L}} + \kappa \bar{n}_{\mathrm{th}} \hat{\boldsymbol{a}}_{\mathrm{L}}^\dagger \hat{\boldsymbol{a}}_{\mathrm{R}} \\ &+ \left(-i\frac{U}{2}m - \frac{\kappa}{2}(2\bar{n}_{\mathrm{th}} + 1)\right)\left(\hat{\boldsymbol{a}}_{\mathrm{L}}^\dagger \hat{\boldsymbol{a}}_{\mathrm{L}} + \hat{\boldsymbol{a}}_{\mathrm{R}}^\dagger \hat{\boldsymbol{a}}_{\mathrm{R}}\right). \end{aligned} \tag{4.15}$$

Following standard third-quantization, we first want to find a set of superoperators which satisfy

$$[\hat{\boldsymbol{\mathcal{L}}}_m, \hat{\boldsymbol{c}}_{+,m}^\dagger] = -\frac{\Gamma_m}{2}\hat{\boldsymbol{c}}_{+,m}^\dagger, \quad [\hat{\boldsymbol{\mathcal{L}}}_m, \hat{\boldsymbol{d}}_{+,m}] = \frac{\Gamma_m}{2}\hat{\boldsymbol{d}}_{+,m} \tag{4.16}$$

$$[\hat{\boldsymbol{\mathcal{L}}}_m, \hat{\boldsymbol{c}}_{-,m}] = -\frac{\Gamma_m}{2}\hat{\boldsymbol{c}}_{-,m}, \quad [\hat{\boldsymbol{\mathcal{L}}}_m, \hat{\boldsymbol{d}}_{-,m}^\dagger] = \frac{\Gamma_m}{2}\hat{\boldsymbol{d}}_{-,m}^\dagger. \tag{4.17}$$

In addition, the only non-vanishing commutation relation between these superoperators should be

$$[\hat{\boldsymbol{d}}_{+,m}, \hat{\boldsymbol{c}}^{\dagger}_{+,m}] = [\hat{\boldsymbol{c}}_{-,m}, \hat{\boldsymbol{d}}^{\dagger}_{-,m}] = \hat{\mathbf{1}}. \tag{4.18}$$

Making an ansatz that $\hat{\boldsymbol{c}}_{-,m}$ and $\hat{\boldsymbol{d}}_{+,m}$ are linear combinations of $\hat{\boldsymbol{a}}_{\mathrm{L}}$ and $\hat{\boldsymbol{a}}_{\mathrm{R}}$ whereas $\hat{\boldsymbol{c}}^{\dagger}_{+,m}$ and $\hat{\boldsymbol{d}}^{\dagger}_{-,m}$ are linear combinations of $\hat{\boldsymbol{a}}^{\dagger}_{\mathrm{L}}$ and $\hat{\boldsymbol{a}}^{\dagger}_{\mathrm{R}}$, we can use the superoperator commutation relation to turn Eqs. (4.16)-(4.17) into a 2×2 matrix eigenvalue problem. These can be readily solved and gives

$$\Gamma_m = \sqrt{\kappa^2 - U^2 m^2 + 2i\kappa U m(2\bar{n}_{\mathrm{th}} + 1)} \tag{4.19}$$

Note that we always choose the branch cut of the square root such that $\mathrm{Re}\,\Gamma_m > 0$. We can then define

$$\begin{pmatrix} \hat{\boldsymbol{d}}_{+,m} \\ \hat{\boldsymbol{c}}_{-,m} \end{pmatrix} = \frac{1}{\sqrt{2}} \begin{pmatrix} A_{+,m} & -A_{-,m} \\ B_{-,m} & -B_{+,m} \end{pmatrix} \begin{pmatrix} \hat{\boldsymbol{a}}_{\mathrm{L}} \\ \hat{\boldsymbol{a}}_{\mathrm{R}} \end{pmatrix} \tag{4.20}$$

$$\begin{pmatrix} \hat{\boldsymbol{d}}^{\dagger}_{-,m} \\ \hat{\boldsymbol{c}}^{\dagger}_{+,m} \end{pmatrix} = \frac{1}{\sqrt{2}} \begin{pmatrix} -A_{-,m} & A_{+,m} \\ B_{+,m} & -B_{-,m} \end{pmatrix} \begin{pmatrix} \hat{\boldsymbol{a}}^{\dagger}_{\mathrm{L}} \\ \hat{\boldsymbol{a}}^{\dagger}_{\mathrm{R}} \end{pmatrix} \tag{4.21}$$

where

$$A_{m,\pm} = \frac{1}{2\Gamma_m}(iUm \pm (\Gamma_m + \kappa) + 2\kappa(2\bar{n}_{\mathrm{th}} + 1)) \quad B_{m,\pm} = \frac{1}{\Gamma_m + \kappa}(\Gamma_m + \kappa \pm iUm) \tag{4.22}$$

as the superoperators which satisfy Eqs. (4.16-4.18). Expressing $\hat{\boldsymbol{\mathcal{L}}}_m$ in this new basis, we obtain

$$\hat{\boldsymbol{\mathcal{L}}}_m = \left(-i(\omega_0 - U)m - \frac{(\Gamma_m - \kappa)}{2}\right)\hat{\mathbf{1}} - \frac{\Gamma_m}{2}\left(\hat{\boldsymbol{c}}^{\dagger}_{+,m}\hat{\boldsymbol{d}}_{+,m} - \hat{\boldsymbol{c}}_{-,m}\hat{\boldsymbol{d}}^{\dagger}_{-,m}\right). \tag{4.23}$$

We now want to find the right and left "vacuum" of each sector, that is to say operators which satisfy

$$\hat{\boldsymbol{d}}_{+,m} \left|\hat{0}^r_m\right\rangle = \hat{\boldsymbol{d}}^\dagger_{-,m} \left|\hat{0}^r_m\right\rangle = 0, \tag{4.24}$$

$$\left\langle \hat{0}^l_m \right| \hat{\boldsymbol{c}}^\dagger_{+,m} = \left\langle \hat{0}^l_m \right| \hat{\boldsymbol{c}}_{-,m} = 0. \tag{4.25}$$

Using the definitions Eqs. (4.20)-(4.21), one can easily demonstrate that these states are Gaussian

$$\hat{0}^r_m = (1 - e^{-\beta^r_m}(e^{-\beta^l_m})^*) \sum_{n=0}^{\infty} e^{-\beta^r_m n} \left|n\right\rangle \left\langle n\right| \tag{4.26}$$

$$(\hat{0}^l_m)^\dagger = \sum_{n=0}^{\infty} (e^{-\beta^l_m n})^* \left|n\right\rangle \left\langle n\right| \tag{4.27}$$

with complex Boltzmann factors defined as

$$e^{-\beta^r_m} = \frac{iUm - (\Gamma_m + \kappa) + 2\kappa(2\bar{n}_{\text{th}} + 1)}{iUm + (\Gamma_m + \kappa) + 2\kappa(2\bar{n}_{\text{th}} + 1)}, \tag{4.28}$$

$$(e^{-\beta^l_m})^* = \frac{\Gamma_m + \kappa - iUm}{\Gamma_m + \kappa + iUm}. \tag{4.29}$$

The normalization is chosen such that $\langle \hat{0}^l_m | \hat{0}^r_m \rangle = \text{Tr}\left(\hat{0}^l_m\right)^\dagger \hat{0}^r_m = 1$. Further, note that in the limit $U \to 0$ (or in the $m = 0$ sector) we recover $\hat{0}^r_m \to \hat{\rho}_{\text{ss}}, \hat{0}^l_m \to \hat{1}$ where $\hat{\rho}_{\text{ss}}$ is the steady state, i.e. the Gaussian state with zero mean an average occupation $\bar{n}_{\text{th}}$.

With these "vacuum" states and the compact form of $\hat{\boldsymbol{\mathcal{L}}}_m$ provided in Eq. (4.23), we are

now in a position to describe the eigenvectors and eigenvalues of $\hat{\boldsymbol{\mathcal{L}}}$. They are given by

$$\left|\hat{r}_{m,\mu}\right\rangle = \frac{1}{\sqrt{\mu!(\mu+|m|)!}} \begin{cases} (\hat{\boldsymbol{c}}^\dagger_{+,m}\hat{\boldsymbol{c}}_{-,m})^\mu (\hat{\boldsymbol{c}}^\dagger_{+,m})^m \left|\hat{0}^r_m\right\rangle, & m \geq 0 \\ (\hat{\boldsymbol{c}}^\dagger_{+,m}\hat{\boldsymbol{c}}_{-,m})^\mu (-\hat{\boldsymbol{c}}_{-,m})^{-m} \left|\hat{0}^r_m\right\rangle, & m < 0 \end{cases} \tag{4.30}$$

$$\langle\hat{l}_{m,\mu}| = \frac{1}{\sqrt{\mu!(\mu+|m|)!}} \begin{cases} \left\langle\hat{0}^l_m\right| (\hat{\boldsymbol{d}}_{+,m})^m (-\hat{\boldsymbol{d}}^\dagger_{-,m}\hat{\boldsymbol{d}}_{+,m})^\mu, & m \geq 0 \\ \left\langle\hat{0}^l_m\right| (\hat{\boldsymbol{d}}^\dagger_{-,m})^{-m} (-\hat{\boldsymbol{d}}^\dagger_{-,m}\hat{\boldsymbol{d}}_{+,m})^\mu, & m < 0 \end{cases} \tag{4.31}$$

and have the corresponding eigenvalues are

$$\lambda_{m,\mu} = -i(\omega_0 - U)m - \frac{(\Gamma_m - \kappa)}{2} - \frac{\Gamma_m}{2}(|m| + 2\mu). \tag{4.32}$$

which is identical to the result in the main text once we correctly identify the renormalized decay rate and non-linearity as $\tilde{\kappa}_m = \mathrm{Re}\,\Gamma_m$ and $\tilde{U}_m = \mathrm{Im}\,\Gamma_m$. To arrive at this result, we must first remember that by definition $\hat{\boldsymbol{\mathcal{L}}}_m$ is the full Lindbladian projected onto the subspace spanned by eigenvectors of $\hat{\boldsymbol{a}}^\dagger_{\mathrm{L}}\hat{\boldsymbol{a}}_{\mathrm{L}} - \hat{\boldsymbol{a}}_{\mathrm{R}}\hat{\boldsymbol{a}}^\dagger_{\mathrm{R}}$ with an eigenvalue of m. Using the commutation relations

$$[\hat{\boldsymbol{a}}^\dagger_{\mathrm{L}}\hat{\boldsymbol{a}}_{\mathrm{L}} - \hat{\boldsymbol{a}}_{\mathrm{R}}\hat{\boldsymbol{a}}^\dagger_{\mathrm{R}}, \hat{\boldsymbol{a}}_{\mathrm{L/R}}] = -\hat{\boldsymbol{a}}_{\mathrm{L/R}} \tag{4.33}$$

$$[\hat{\boldsymbol{a}}^\dagger_{\mathrm{L}}\hat{\boldsymbol{a}}_{\mathrm{L}} - \hat{\boldsymbol{a}}_{\mathrm{R}}\hat{\boldsymbol{a}}^\dagger_{\mathrm{R}}, \hat{\boldsymbol{a}}^\dagger_{\mathrm{L/R}}] = \hat{\boldsymbol{a}}^\dagger_{\mathrm{L/R}} \tag{4.34}$$

we see that $\hat{\boldsymbol{a}}_{\mathrm{L/R}}$ and $\hat{\boldsymbol{a}}^\dagger_{\mathrm{L/R}}$ lowers or raises the eigenvalue m by one respectively. The same is then true of $\hat{\boldsymbol{c}}_{-,m}, \hat{\boldsymbol{d}}_{+,m}$ and $\hat{\boldsymbol{c}}^\dagger_{+,m}, \hat{\boldsymbol{d}}^\dagger_{-,m}$ respectively. Both $\left|\hat{0}^r_m\right\rangle$ and $\langle\hat{0}^l_m|$ are a linear combination of Fock state projectors, and they are therefore elements of the $m = 0$ subspace. By construction, the left and right eigenvectors thus satisfy $(\hat{\boldsymbol{a}}^\dagger_{\mathrm{L}}\hat{\boldsymbol{a}}_{\mathrm{L}} - \hat{\boldsymbol{a}}_{\mathrm{R}}\hat{\boldsymbol{a}}^\dagger_{\mathrm{R}})\left|\hat{r}_{m,\mu}\right\rangle = m\left|\hat{r}_{m,\mu}\right\rangle$

and $\langle \hat{l}_{m,\mu}|(\hat{\boldsymbol{a}}_{\mathrm{L}}^{\dagger}\hat{\boldsymbol{a}}_{\mathrm{L}} - \hat{\boldsymbol{a}}_{\mathrm{R}}\hat{\boldsymbol{a}}_{\mathrm{R}}^{\dagger}) = m\langle \hat{l}_{m,\mu}|$. It then follows that

$$\hat{\boldsymbol{\mathcal{L}}}\left|\hat{r}_{m,\mu}\right\rangle = \hat{\boldsymbol{\mathcal{L}}}_m\left|\hat{r}_{m,\mu}\right\rangle \tag{4.35}$$

$$\langle \hat{l}_{m,\mu}|\hat{\boldsymbol{\mathcal{L}}} = \langle \hat{l}_{m,\mu}|\hat{\boldsymbol{\mathcal{L}}}_m. \tag{4.36}$$

We can then use Eq. (4.23), the commutation relations Eq. (4.18) and the defining property of $\left|\hat{0}_m^r\right\rangle$ and $\langle \hat{0}_m^l|$ in Eqs. (4.24)-(4.25) to show that $\left|\hat{r}_{m,\mu}\right\rangle$ and $\langle \hat{l}_{m,\mu}|$ are the eigenvectors of $\hat{\boldsymbol{\mathcal{L}}}$ with eigenvalues $\lambda_{m,\mu}$. Further, using the same commutation relations in Eq. (4.18) and the normalization $\langle \hat{0}_m^l|\hat{0}_m^r\rangle = 1$ one can show the normalization convention we have chosen is such that the biorthogonality condition

$$\langle \hat{l}_{m',\mu'}|\hat{r}_{m,\mu}\rangle = \delta_{m,m'}\delta_{\mu,\mu'} \tag{4.37}$$

is satisfied.

Note that we readily obtain a simple intuituve result rule by Taylor expanding the eigenvalues and eigenvectors to first order in κ and $\bar{n}_{\mathrm{th}}$. We first note that when $\bar{n}_{\mathrm{th}} \to 0$ and $\bar{n}_{\mathrm{th}}$, the "vacuum" states in each sector coincide with the vacuum state projector

$$\lim_{\bar{n}_{\mathrm{th}}\to 0,\kappa\to 0} \hat{0}_m^r = \lim_{\bar{n}_{\mathrm{th}}\to 0,\kappa\to 0} (\hat{0}_m^l)^{\dagger} = |0\rangle\langle 0|. \tag{4.38}$$

Another simple calculation yields, in the same limit,

$$\lim_{\bar{n}_{\mathrm{th}}\to 0,\kappa\to 0} \begin{pmatrix} \hat{\boldsymbol{d}}_{+,m} \\ \hat{\boldsymbol{c}}_{-,m} \end{pmatrix} = \begin{pmatrix} \frac{1}{\sqrt{2}} & 0 \\ 0 & -\sqrt{2} \end{pmatrix} \begin{pmatrix} \hat{\boldsymbol{a}}_{\mathrm{L}} \\ \hat{\boldsymbol{a}}_{\mathrm{R}} \end{pmatrix} \tag{4.39}$$

$$\lim_{\bar{n}_{\mathrm{th}}\to 0,\kappa\to 0} \begin{pmatrix} \hat{\boldsymbol{d}}_{-,m}^{\dagger} \\ \hat{\boldsymbol{c}}_{+,m}^{\dagger} \end{pmatrix} = \begin{pmatrix} 0 & \frac{1}{\sqrt{2}} \\ \sqrt{2} & 0 \end{pmatrix} \begin{pmatrix} \hat{\boldsymbol{a}}_{\mathrm{L}}^{\dagger} \\ \hat{\boldsymbol{a}}_{\mathrm{R}}^{\dagger} \end{pmatrix}. \tag{4.40}$$

Using the definition of the right and left eigenvectors Eqs. (4.30)-(4.31), we recover the fact

that the right and left eigenvectors are Fock state projectors (up to an irrelevant normalization factor):

$$\lim_{\bar{n}_{\rm th}\to 0,\kappa\to 0} \hat{r}_{m,\mu} = (-1)^{\mu}(\sqrt{2})^{2\mu+|m|} \begin{cases} |\mu+|m|\rangle \langle \mu|\,, & m \geq 0 \\ |\mu\rangle \langle \mu+|m||\,, & m < 0 \end{cases} \tag{4.41}$$

$$\lim_{\bar{n}_{\rm th}\to 0,\kappa\to 0} \hat{l}^{\dagger}_{m,\mu} = (-1)^{\mu}(\sqrt{2})^{-2\mu-|m|} \begin{cases} |\mu\rangle \langle \mu+|m||\,, & m \geq 0 \\ |\mu+|m|\rangle \langle \mu|\,, & m < 0 \end{cases} \tag{4.42}$$

We can then use Lindblad perturbation theory [71, 72] to compute the decay rate $-\mathrm{Re}\lambda_{m,\mu}$ to first order in κ. If we let $\hat{\boldsymbol{\mathcal{V}}}$ denote the part of the full Lindblad superoperator which describes dissipation, then can write the first order correction to the eigenvalues in complete analogy to standard first-order perturbation theory

$$\begin{aligned} \mathrm{Re}\lambda_{m,\mu} &= \langle \hat{l}_{m,\mu}|\hat{\boldsymbol{\mathcal{V}}}\,|\hat{r}_{m,\mu}\rangle + \mathcal{O}(\kappa^2) \\ &= -\kappa(\bar{n}_{\rm th}+1)\frac{2\mu+|m|}{2} - \kappa\bar{n}_{\rm th}(\frac{2\mu+|m|}{2}+1) + \mathcal{O}(\kappa^2) \end{aligned} \tag{4.43}$$

which agrees with Eq. (4.32) upon expanding Γ_m to first order. The first term is simply the average of the Fermi's Golden rule decay rate of the Fock states $|\mu+|m|\rangle$ and $|\mu\rangle$ with the appropriate stimulated emission factor. The second term is the average decay rate of $|\mu+|m|+1\rangle$ and $|\mu+1\rangle$ with the stimulated absorption term $\bar{n}_{\rm th}$. We also note, as we do in the main text, that this provides an upper bound to the renormalized sector-dependent decay rates $\tilde{\kappa}_m$ as show in Fig. 4.2

4.6.2 Retarded response function

Here we analytically find the retarded Green's function of the thermal Kerr oscillator. If we recall the definition of the third-quantized inner product $\langle \hat{B}|\hat{A}\rangle \equiv \mathrm{Tr}\,\hat{B}^{\dagger}\hat{A}$ and the an-

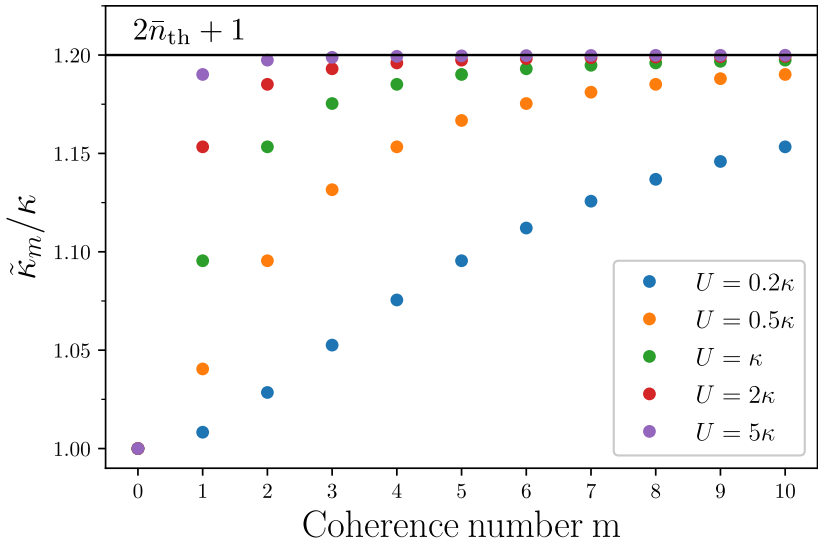

Fig. 4.2: Renormalized decay rate $\tilde{\kappa}_m$ as a function of m for various values of U and $\bar{n}_{\rm th}=0.1$. For $\kappa \ll Um$, one reaches the upper bound of the renormalized decay rate $\tilde{\kappa}_m \lesssim \kappa(2\bar{n}_{\rm th}+1)$ (see Sec. I of the SM for details).

nihilation and creation superoperators $\hat{\boldsymbol{a}}_{\rm L}\,|\hat{\rho}\rangle \equiv |\hat{a}\hat{\rho}\rangle$, $\hat{\boldsymbol{a}}_{\rm R}\,|\hat{\rho}\rangle \equiv |\hat{\rho}\hat{a}\rangle$, $\hat{\boldsymbol{a}}^{\dagger}_{\rm L}\,|\hat{\rho}\rangle \equiv |\hat{a}^{\dagger}\hat{\rho}\rangle$, and $\hat{\boldsymbol{a}}^{\dagger}_{\rm R}\,|\hat{\rho}\rangle \equiv |\hat{\rho}\hat{a}^{\dagger}\rangle$ then with the help of the quantum regression theorem we can write

$$G^{R}(t) = -i\Theta(t)\langle[\hat{a}(t),\hat{a}^{\dagger}(0)]\rangle \tag{4.44}$$

$$= -i\Theta(t)\left(\langle\hat{1}|\hat{\boldsymbol{a}}_{\rm L}e^{\hat{\boldsymbol{\mathcal{L}}}t}\hat{\boldsymbol{a}}^{\dagger}_{\rm L}|\hat{\rho}_{\rm ss}\rangle - \langle\hat{1}|\hat{\boldsymbol{a}}_{\rm R}e^{\hat{\boldsymbol{\mathcal{L}}}t}\hat{\boldsymbol{a}}^{\dagger}_{\rm R}|\hat{\rho}_{\rm ss}\rangle)\right) \tag{4.45}$$

Using the spectral decomposition of $\hat{\boldsymbol{\mathcal{L}}}$, we can write the propegator as

$$e^{\hat{\boldsymbol{\mathcal{L}}}t} = \sum_{m=-\infty}^{\infty}\sum_{\mu=0}^{\infty} e^{\lambda_{m,\mu}t}|\hat{r}_{m,\mu}\rangle\langle\hat{l}_{m,\mu}| \tag{4.46}$$

Recall the both $|\hat{\rho}_{\rm ss}\rangle$ and $\langle\hat{1}|$, being a sum of Fock state projectors, are elements of the $m=0$ subspace. From Eqs. (4.34)-(4.33), it follows that $\hat{\boldsymbol{a}}^{\dagger}_{\rm L/R}|\hat{\rho}_{\rm ss}\rangle$ and $\langle\hat{1}|\hat{\boldsymbol{a}}_{\rm L/R}$ belong in the $m=1$ subspace and are thus orthogonal to all right and left eigenvectors for which $m\neq 1$. Using

Eqs. (4.30)-(4.31) we have

$$G^R(t) = -i\Theta(t)\sum_{\mu=0}^{\infty} e^{\lambda_{1,\mu}t}\left(\langle\hat{1}|\hat{\boldsymbol{a}}_{\rm L}|\hat{r}_{1,\mu}\rangle\langle\hat{l}_{1,\mu}|\hat{\boldsymbol{a}}_{\rm L}^{\dagger}|\hat{\rho}_{\rm ss}\rangle - (\hat{\boldsymbol{a}}_{\rm L}\rightarrow\hat{\boldsymbol{a}}_{\rm R})\right)$$
$$= -i\Theta(t)\sum_{\mu=0}^{\infty}\frac{e^{\lambda_{1,\mu}t}(-1)^{\mu}}{\mu!(\mu+1)!}\Bigg(\langle\hat{1}|\hat{\boldsymbol{a}}_{\rm L}(\hat{\boldsymbol{c}}_{+,1}^{\dagger})^{\mu+1}(\hat{\boldsymbol{c}}_{-,1})^{\mu}|\hat{0}_1^r\rangle\langle\hat{0}_1^l|(\hat{\boldsymbol{d}}_{+,1})^{\mu+1}(\hat{\boldsymbol{d}}_{-,1}^{\dagger})^{\mu}\hat{\boldsymbol{a}}_{\rm L}^{\dagger}|\hat{\rho}_{\rm ss}\rangle$$
$$-(\hat{\boldsymbol{a}}_{\rm L}\rightarrow\hat{\boldsymbol{a}}_{\rm R})\Bigg). \tag{4.47}$$

To evaluate these matrix elements, we must use the fact that $\hat{0}_m^r$ and $\hat{0}_m^l$ are generalized Gaussian operators. Thus, one can use the Baker-Campbell-Hausdorff formula (or via direct computation) to write

$$\hat{\boldsymbol{a}}_{\rm R}^{\dagger}|\hat{0}_m^r\rangle = |\hat{0}_m^r\hat{a}^{\dagger}\rangle = e^{-\beta_m^r}|\hat{a}^{\dagger}\hat{0}_m^r\rangle = e^{-\beta_m^r}\hat{\boldsymbol{a}}_{\rm L}^{\dagger}|\hat{0}_m^r\rangle \tag{4.48}$$
$$\langle\hat{0}_m^l|\hat{\boldsymbol{a}}_{\rm R} = \langle\hat{0}_m^l\hat{a}^{\dagger}| = \langle\hat{a}\hat{0}_m^l|(e^{-\beta_m^l})^* = \langle\hat{0}_m^l|\hat{\boldsymbol{a}}_{\rm L}(e^{-\beta_m^l})^* \tag{4.49}$$

where the complex Boltzmann factors are defined in Eqs. (4.28)-(4.29). From the definition of $\hat{\boldsymbol{c}}_{-,m}, \hat{\boldsymbol{c}}_{+,m}^{\dagger}, \hat{\boldsymbol{d}}_{+,m}$ and $\hat{\boldsymbol{d}}_{-,m}^{\dagger}$ we then have

$$\langle\hat{1}|\hat{\boldsymbol{a}}_{\rm L}(\hat{\boldsymbol{c}}_{+,1}^{\dagger})^{\mu+1}(\hat{\boldsymbol{c}}_{-,1})^{\mu}|\hat{0}_1^r\rangle = \left(\frac{-i\sqrt{2}U}{\Gamma_1+\kappa}\right)^{\mu}\left(\frac{\Gamma_1+\kappa+iU}{\sqrt{2}(\Gamma_1+\kappa)}\left[1-e^{-\beta_1^r}(e^{-\beta_1^l})^*\right]\right)^{\mu+1}$$
$$\times\langle(\hat{a}^{\dagger})^{\mu+1}|(\hat{a}^{\dagger})^{\mu+1}\hat{0}_1^r\rangle \tag{4.50}$$

$$\langle\hat{0}_1^l|(\hat{\boldsymbol{d}}_{+,1})^{\mu+1}(\hat{\boldsymbol{d}}_{-,1}^{\dagger})^{\mu}\hat{\boldsymbol{a}}_{\rm L}^{\dagger}|\hat{\rho}_{\rm ss}\rangle = \left(\frac{1}{\sqrt{8}\Gamma_1}\left[iU+\Gamma_1+\kappa+2\kappa(2\bar{n}_{\rm th}+1)\right](1-e^{-\beta_1^r}(e^{-\beta_1^l})^*)\right)^{\mu+1}$$
$$\times\left(\frac{-1}{\sqrt{8}\Gamma_1}\left[iU-\Gamma_1-\kappa+2\kappa(2\bar{n}_{\rm th}+1)\right](1-e^{\beta_1^r}e^{\beta})\right)^{\mu}\langle(\hat{a}^{\dagger})^{\mu+1}\hat{0}_1^l|(\hat{a}^{\dagger})^{\mu+1}\hat{\rho}_{\rm ss}\rangle \tag{4.51}$$

We can also readily compute the remaining overlaps as

$$\begin{aligned}\langle(\hat{a}^\dagger)^{\mu+1}|(\hat{a}^\dagger)^{\mu+1}\hat{0}_1^r\rangle &= \mathrm{Tr}\left(\hat{a}^{\mu+1}(\hat{a}^\dagger)^{\mu+1}\hat{0}_1^r\right) = \sum_{n=0}^{\infty}\frac{(n+1)\cdots(n+\mu+1)e^{-\beta_1^r n}}{(1-e^{-\beta_1^r}(e^{-\beta_1^l})^*)^{-1}} \\ &= (\mu+1)!\frac{(1-e^{-\beta_1^r}(e^{-\beta_1^l})^*)}{(1-e^{-\beta_1^r})^{\mu+2}} \end{aligned} \tag{4.52}$$

$$\begin{aligned}\langle(\hat{a}^\dagger)^{\mu+1}\hat{0}_1^l|(\hat{a}^\dagger)^{\mu+1}\hat{\rho}_{\mathrm{ss}}\rangle &= \mathrm{Tr}\left((\hat{0}_1^l)^\dagger\hat{a}^{\mu+1}(\hat{a}^\dagger)^{\mu+1}\hat{\rho}_{\mathrm{ss}}\right) \\ &= (\mu+1)!\frac{1-e^{-\beta}}{(1-e^{-\beta}(e^{-\beta_1^l})^*)^{\mu+2}} \end{aligned} \tag{4.53}$$

Putting all of this together after some straightforward but algebra, we obtain

$$\langle\hat{1}|\hat{\boldsymbol{a}}_{\mathrm{L}}(\hat{\boldsymbol{c}}_{+,1}^\dagger)^{\mu+1}(\hat{\boldsymbol{c}}_{-,1})^\mu|\hat{0}_1^r\rangle\langle\hat{0}_1^l|(\hat{\boldsymbol{d}}_{+,1})^{\mu+1}(\hat{\boldsymbol{d}}_{-,1}^\dagger)^\mu\hat{\boldsymbol{a}}_{\mathrm{L}}^\dagger|\hat{\rho}_{\mathrm{ss}}\rangle = ((\mu+1)!)^2\frac{4(\bar{n}_{\mathrm{th}}+1)}{(1+R_1)^2}\left(\frac{1-R_1}{1+R_1}\right)^\mu \tag{4.54}$$

where, as in the main text,

$$R_1 = \frac{\kappa + iU(2\bar{n}_{\mathrm{th}}+1)}{\tilde{\kappa}_1 + i\tilde{U}_1} \tag{4.55}$$

with $\kappa_1 = \mathrm{Re}\,\Gamma_1$ and $\tilde{\Gamma}_1 = \mathrm{Im}\,\Gamma_1$. Using $\langle\hat{1}|\hat{\boldsymbol{a}}_{\mathrm{L}} = \langle\hat{1}|\hat{\boldsymbol{a}}_{\mathrm{R}}$ and $\hat{\boldsymbol{a}}_{\mathrm{R}}^\dagger|\hat{\rho}_{\mathrm{ss}}\rangle = \bar{n}_{\mathrm{th}}/(\bar{n}_{\mathrm{th}}+1)\hat{\boldsymbol{a}}_{\mathrm{L}}^\dagger|\hat{\rho}_{\mathrm{ss}}\rangle$ we also immediately obtain

$$\langle\hat{0}_1^l|(\hat{\boldsymbol{d}}_{+,1})^{\mu+1}(\hat{\boldsymbol{d}}_{-,1}^\dagger)^\mu\hat{\boldsymbol{a}}_{\mathrm{L}}^\dagger|\hat{\rho}_{\mathrm{ss}}\rangle = ((\mu+1)!)^2\frac{4\bar{n}_{\mathrm{th}}}{(1+R_1)^2}\left(\frac{1-R_1}{1+R_1}\right)^\mu. \tag{4.56}$$

Thus, the retarted Green's function takes the form

$$G^R(t) = -i\Theta(t)e^{-i(\omega_0-U)t+\frac{\kappa}{2}t}\frac{4}{(R_1+1)^2}\sum_{\mu=0}^{\infty}(\mu+1)e^{-(\tilde{\kappa}_1+i\tilde{U}_1)(\mu+1)t}\left(\frac{R_1-1}{R_1+1}\right)^{\mu}$$
$$= -i\Theta(t)\frac{e^{-i(\omega_0-U)t+\frac{\kappa}{2}t}}{\left(\cosh\left(\frac{\tilde{\kappa}_1+i\tilde{U}_1}{2}t\right)+R_1\sinh\left(\frac{\tilde{\kappa}_1+i\tilde{U}_1}{2}t\right)\right)^2} \tag{4.57}$$

which is identical with Eq. (9) in the main text, and matches the result in Ref. [31].

4.6.3 Extending the method to interacting oscillators and dephasing

Here, we will briefly explain how our solution technique is also applicable to the case where several oscillators are subject to a density-density interaction. For the sake of clarity, we will focus on the case where there are only two oscillators with mode annihilation operators $\hat{a}$ and $\hat{b}$; the generalization to an arbitrary number of oscillators readily follows. The master equation reads

$$\partial_t\hat{\rho} = (\mathcal{L}_a+\mathcal{L}_b)\hat{\rho} - iU_{ab}[\hat{a}^\dagger\hat{a}\hat{b}^\dagger\hat{b},\hat{\rho}] \tag{4.58}$$

where $\mathcal{L}_a$ and $\mathcal{L}_b$ are the superoperators which describe the uncoupled non-linear oscillators as in Eqs (1)-(2) of the main text, which we already know how to diagonalize. Crucially the weak symmetries that allowed us to solve the $U_{ab}=0$ case are still present. The eigenstates are thus labelled by m_a and m_b, which are the integer eigenvalues of the superoperators $[\hat{a}^\dagger\hat{a},\cdot]$ and $[\hat{b}^\dagger\hat{b},\cdot]$ respectively. To see why this proves useful, note that we can use standard commutator rules to write the density-density interaction as

$$U_{ab}[\hat{a}^\dagger\hat{a}\hat{b}^\dagger\hat{b},\hat{\rho}] = \frac{U_{ab}}{2}\left(\{\hat{a}^\dagger\hat{a},[\hat{b}^\dagger\hat{b},\hat{\rho}]\}+\{\hat{b}^\dagger\hat{b},[\hat{a}^\dagger\hat{a},\hat{\rho}]\}\right) \tag{4.59}$$

Projecting Eq. (4.59) onto the fixed m_a, m_b subspace $\hat{\rho}_{m_a,m_b}$ we then obtain

$$U_{ab}[\hat{a}^\dagger\hat{a}\hat{b}^\dagger\hat{b},\hat{\rho}] \to \frac{U_{ab}m_b}{2}\{\hat{a}^\dagger\hat{a},\hat{\rho}_{m_a,m_b}\} + \frac{U_{ab}m_a}{2}\{\hat{b}^\dagger\hat{b},\hat{\rho}_{m_a,m_b}\} \tag{4.60}$$

There are thus two salient features that emerge once we coupled several oscillators via a density-density interaction. The first is that once we project onto the blocks indexed by the coherence numbers, the problem reduces to an effectively quadratic one. Further, we also see that mean field theory becomes exact within each block: the a oscillator only affects the b oscillator through the number m_a and vice-versa. The eigenvectors and eigenvalues can readily be found via the using third-quantization and the procedure presented in Sec. 4.6.1. This reasoning applies to an arbitrary number of oscillators, as long as they each coupled to their own independent Markovian environment.

Introducing dephasing still makes this problem solvable, and in fact proves to be trivial using our method. Indeed, not only is the weak $U(1)$ symmetry still present, but upon projecting onto the fixed m_a subspace, it is found that the dephasing superoperator can be replaced by a number:

$$2\kappa_\phi\mathcal{D}[\hat{a}^\dagger\hat{a}]\hat{\rho} = -\kappa_{\phi,a}[\hat{a}^\dagger\hat{a},[\hat{a}^\dagger\hat{a},\hat{\rho}]] \to -\kappa_\phi m^2\hat{\rho}_m. \tag{4.61}$$

Thus, dephasing only shifts the eigenvalues by $-\kappa_\phi m^2$, whereas the eigenvectors do not change.

4.6.4 Eigenvectors and eigenvalues of the dissipative Ising model

We now analytically find the eigenvalues and eigenvectors of the dissipative Ising model as written in Eq. (12) in the main text. Introducing the superoperators

$$\hat{\boldsymbol{\sigma}}^-_{L,j}\,|\hat{\rho}\rangle \equiv |\hat{\sigma}^-_j\hat{\rho}\rangle, \quad \hat{\boldsymbol{\sigma}}^-_{R,j}\,|\hat{\rho}\rangle \equiv |\hat{\rho}\hat{\sigma}^-_j\rangle \tag{4.62}$$

$$\hat{\boldsymbol{\sigma}}^+_{L,j}\,|\hat{\rho}\rangle \equiv |\hat{\sigma}^+_j\hat{\rho}\rangle, \quad \hat{\boldsymbol{\sigma}}^+_{R,j}\,|\hat{\rho}\rangle \equiv |\hat{\rho}\hat{\sigma}^+_j\rangle \tag{4.63}$$

$$\hat{\boldsymbol{\sigma}}^z_{L,j}\,|\hat{\rho}\rangle \equiv |\hat{\sigma}^z_j\hat{\rho}\rangle, \quad \hat{\boldsymbol{\sigma}}^z_{R,j}\,|\hat{\rho}\rangle \equiv |\hat{\rho}\hat{\sigma}^z_j\rangle \tag{4.64}$$

one can write the third-quantized form of the Lindbladian as

$$\begin{aligned}\hat{\boldsymbol{\mathcal{L}}} = &-i\sum_{j<k} J_{jk}\left(\hat{\boldsymbol{\sigma}}^z_{L,j}\hat{\boldsymbol{\sigma}}^z_{L,k} - \hat{\boldsymbol{\sigma}}^z_{R,j}\hat{\boldsymbol{\sigma}}^z_{R,k}\right) - i\sum_j h_j\left(\hat{\boldsymbol{\sigma}}^z_{L,j} - \hat{\boldsymbol{\sigma}}^z_{R,j}\right)\\
&+\sum_j \gamma_{-,j}\left(\hat{\boldsymbol{\sigma}}^-_{L,j}\hat{\boldsymbol{\sigma}}^+_{R,j} - \frac{1}{2}(\hat{\boldsymbol{\sigma}}^+_{L,j}\hat{\boldsymbol{\sigma}}^-_{L,j} + \hat{\boldsymbol{\sigma}}^-_{R,j}\hat{\boldsymbol{\sigma}}^+_{R,j})\right)\\
&+\sum_j \gamma_{+,j}\left(\hat{\boldsymbol{\sigma}}^+_{L,j}\hat{\boldsymbol{\sigma}}^-_{R,j} - \frac{1}{2}(\hat{\boldsymbol{\sigma}}^-_{L,j}\hat{\boldsymbol{\sigma}}^+_{L,j} + \hat{\boldsymbol{\sigma}}^+_{R,j}\hat{\boldsymbol{\sigma}}^-_{R,j})\right) + \sum_j \gamma_{\phi,j}\left(\hat{\boldsymbol{\sigma}}^z_{L,j}\hat{\boldsymbol{\sigma}}^z_{R,j} - \hat{\mathbf{1}}\right).\end{aligned} \tag{4.65}$$

Note that our conventions imply $[\hat{\boldsymbol{\sigma}}^-_{L,j}, \hat{\boldsymbol{\sigma}}^+_{L,j}] = \hat{\boldsymbol{\sigma}}^z_{L,j}$ and $[\hat{\boldsymbol{\sigma}}^-_{R,j}, \hat{\boldsymbol{\sigma}}^+_{R,j}] = -\hat{\boldsymbol{\sigma}}^z_{R,j}$. Further, these superoperators inherent some of the properties of spin raising and lowering operators, such as $(\hat{\boldsymbol{\sigma}}^-_{\mathrm{L/R},j})^2 = (\hat{\boldsymbol{\sigma}}^+_{\mathrm{L/R},j})^2 = 0$ and $\{\hat{\boldsymbol{\sigma}}^-_{\mathrm{L/R},j}, \hat{\boldsymbol{\sigma}}^+_{\mathrm{L/R},j}\} = (\hat{\boldsymbol{\sigma}}^z_{\mathrm{L/R}})^2 = \hat{\mathbf{1}}$. In this model there are N weak $U(1)$ symmetries, one for each spin. Since the master equation is invariant under $\hat{\sigma}^-_j \to e^{-i\theta_j}\hat{\sigma}^-_j$, the third-quantized version of the Lindbladian is unchanged when making the transformation $\hat{\boldsymbol{\sigma}}^-_{L/R,j} \to e^{-i\theta_j}\hat{\boldsymbol{\sigma}}^-_{L/R,j}$. Using the superoperator commutation relations, one can show that the corresponding unitary operator is $e^{i\theta_j/2(\hat{\boldsymbol{\sigma}}^z_{L,j} - \hat{\boldsymbol{\sigma}}^z_{R,j})}\hat{\boldsymbol{\sigma}}^-_{L/R,j}e^{-i\theta_j/2(\hat{\boldsymbol{\sigma}}^z_{L,j} - \hat{\boldsymbol{\sigma}}^z_{R,j})} = e^{-i\theta_j}\hat{\boldsymbol{\sigma}}^-_{L/R,j}$. The Lindbladian therefore commutes with each generator, and thus can be written in block-diagonal form $\hat{\boldsymbol{\mathcal{L}}} = \bigoplus_{\vec{M}} \hat{\boldsymbol{\mathcal{L}}}_{\vec{M}}$ where $\vec{M} = \{m_1, \ldots, m_N\}$ is a list indexing each block whose elements m_j are eigenavlues of $(\hat{\boldsymbol{\sigma}}^z_{L,j} - \hat{\boldsymbol{\sigma}}^z_{R,j})/2$. The generators have two non-degenerate eigenvalues $m_j = 1$ and $m_j = -1$

with associated eigenoperator $\left|\uparrow_j\right\rangle\left\langle\downarrow_j\right|$ and $\left|\downarrow_j\right\rangle\left\langle\uparrow_j\right|$ respectively, in addition to a two-fold degenerate eigenvalue $m_j = 0$ with eigenoperators $\left|\uparrow_j\right\rangle\left\langle\uparrow_j\right|$ and $\left|\downarrow_j\right\rangle\left\langle\downarrow_j\right|$. The size of the block $\hat{\boldsymbol{\mathcal{L}}}_{\vec{M}}$ is thus $2^{z(\vec{M})}$ where $z(\vec{M})$ is the number of zero eigenvalues in the list $\vec{M}$.

Now we wish to use the main idea of this work presented in the main text: once we replace the generators by their eigenvalues in a given subspace, mean-field theory becomes exact. To that end, using the property $(\hat{\boldsymbol{\sigma}}^z_{\mathrm{L/R}})^2 = \hat{\mathbf{1}}$, we can write

$$\begin{aligned}\hat{\boldsymbol{\sigma}}^z_{L,j}\hat{\boldsymbol{\sigma}}^z_{L,k} - \hat{\boldsymbol{\sigma}}^z_{R,j}\hat{\boldsymbol{\sigma}}^z_{R,k} &= \frac{1}{2}\left((\hat{\boldsymbol{\sigma}}^z_{L,j} + \hat{\boldsymbol{\sigma}}^z_{L,k})^2 - (\hat{\boldsymbol{\sigma}}^z_{R,j} + \hat{\boldsymbol{\sigma}}^z_{R,k})^2\right) \\ &= \frac{1}{2}\left(\hat{\boldsymbol{\sigma}}^z_{L,j} - \hat{\boldsymbol{\sigma}}^z_{R,j} + \hat{\boldsymbol{\sigma}}^z_{L,k} - \hat{\boldsymbol{\sigma}}^z_{R,k}\right)\left(\hat{\boldsymbol{\sigma}}^z_{L,j} + \hat{\boldsymbol{\sigma}}^z_{R,j} + \hat{\boldsymbol{\sigma}}^z_{L,k} + \hat{\boldsymbol{\sigma}}^z_{R,k}\right).\end{aligned} \tag{4.66}$$

Projecting $\hat{\boldsymbol{\mathcal{L}}}$ onto the subspace indexed by $\vec{M} = \{m_1, \ldots, m_N\}$, we can then replace the generators by their eigenvalue $(\hat{\boldsymbol{\sigma}}^z_{L,j} - \hat{\boldsymbol{\sigma}}^z_{R,j})/2 \to m_j$. Within this subspace, the interaction then takes the form

$$\sum_{j<k} J_{jk}(m_j + m_k)\left(\hat{\boldsymbol{\sigma}}^z_{L,j} + \hat{\boldsymbol{\sigma}}^z_{R,j} + \hat{\boldsymbol{\sigma}}^z_{L,k} + \hat{\boldsymbol{\sigma}}^z_{R,k}\right) = \sum_j J^{\mathrm{eff}}_j(\vec{M})\left(\hat{\boldsymbol{\sigma}}^z_{L,j} + \hat{\boldsymbol{\sigma}}^z_{R,j}\right) \tag{4.67}$$

where as in the main text we have defined

$$J^{\mathrm{eff}}_j = \sum_{k\neq j} J_{jk} m_k. \tag{4.68}$$

The exactness of mean-field theory in each block thus implies that we are now tasked with finding the eigenvalues of N pseudo-Liouvillians which act independently on each spin:

$$\hat{\boldsymbol{\mathcal{L}}}_{\vec{M}} = \sum_j \hat{\boldsymbol{\mathcal{L}}}_j(\vec{M}). \tag{4.69}$$

The form of $\hat{\boldsymbol{\mathcal{L}}}_j(\vec{M})$ follows immediately from Eq. (4.65) and Eq. (4.67). As discussed in the main text, the fact that the $m_j = \pm 1$ eigenvalues are non-degenerate whereas the $m_j = 0$ are immediately implies that there are a set of frozen and active spins described by populations and coherence's respectively. Since the $m_j = 0$ eigenvalues are two-fold degenerate, we need another list $\vec{\chi} = \{\chi_j \,|\, j \,\text{frozen}\}$ of size $z(\vec{M})$ to label the eigenvectors and eigenvalues in each block where $\chi_j = \pm$. The right and left eigenvectors can thus be written as

$$|\hat{r}_{\vec{M},\vec{\chi}}\rangle = |\hat{r}_{\text{froz}} \times \hat{r}_{\text{act}}\rangle = | \left(\prod_{j \text{ frozen}} \hat{\sigma}_j^{m_j} \right) \left(\prod_{j \text{ active}} \left(r_{\uparrow,\chi_j} |\uparrow_j\rangle \langle\uparrow_j| + r_{\downarrow,\chi_j} |\downarrow_j\rangle \langle\downarrow_j| \right) \right) \rangle \tag{4.70}$$

$$\langle \hat{l}_{\vec{M},\vec{\chi}}| = \langle \hat{l}_{\text{froz}} \times \hat{l}_{\text{act}}| = \langle \left(\prod_{j \text{ frozen}} \hat{\sigma}_j^{m_j} \right) \left(\prod_{j \text{ active}} \left(l_{\uparrow,\chi_j} |\uparrow_j\rangle \langle\uparrow_j| + l_{\downarrow,\chi_j} |\downarrow_j\rangle \langle\downarrow_j| \right) \right) | \tag{4.71}$$

where, for the sake of compactness, we have dropped the explicit $\vec{M}$ dependence of $r_{\uparrow/\downarrow,\chi_j}$ and $l_{\uparrow/\downarrow,\chi_j}$. The eigenvalues can then be written as

$$\lambda_{\vec{M},\vec{\chi}} = \sum_j \lambda_j(\vec{M}, \chi_j) \tag{4.72}$$

For frozen spins, one does not need to solve an eigenvalue problem: to obtain $\lambda_j(\vec{M}, \chi_j)$ one must simply apply $\hat{\boldsymbol{\mathcal{L}}}_j(\vec{M})$ to the coherences and obtain the eigenvalue Eq. (16) in the main text. A simple calculation reveals that the eigenvectors and eigenvalues of the active spins satisfy:

$$\begin{pmatrix} -2iJ_j^{\text{eff}}(\vec{M}) - \gamma_{-,j} & \gamma_{+,j} \\ \gamma_{-,j} & 2iJ_j^{\text{eff}}(\vec{M}) - \gamma_{+,j} \end{pmatrix} \begin{pmatrix} r_{\uparrow,\chi_j} \\ r_{\downarrow,\chi_j} \end{pmatrix} = \lambda_j(\vec{M}, \chi_j) \begin{pmatrix} r_{\uparrow,\chi_j}(\vec{M}) \\ r_{\downarrow,\chi_j}(\vec{M}) \end{pmatrix}, \tag{4.73}$$

$$\begin{pmatrix} -2iJ_j^{\text{eff}}(\vec{M}) - \gamma_{-,j} & \gamma_{-,j} \\ \gamma_{+,j} & 2iJ_j^{\text{eff}}(\vec{M}) - \gamma_{+,j} \end{pmatrix} \begin{pmatrix} l^*_{\uparrow,\chi_j} \\ l^*_{\downarrow,\chi_j} \end{pmatrix} = \lambda_j(\vec{M},\chi_j) \begin{pmatrix} l^*_{\uparrow,\chi_j} \\ l^*_{\downarrow,\chi_j} \end{pmatrix}. \tag{4.74}$$

The above equations are readily solved, and we obtain

$$r_{\uparrow,\pm} = \frac{\eta_j(\Gamma_j + \eta_j)}{\Gamma_j \left(2(\eta_j - iJ_j^{\text{eff}})) + \Gamma_j \mp \sqrt{\Gamma_j^2 - 4J_j^{\text{eff}}(J_j^{\text{eff}} + i\eta_j)}\right)} \tag{4.75}$$

$$r_{\downarrow,\pm} = \frac{\eta_j(\Gamma_j - \eta_j)}{\Gamma_j \left(2(\eta_j - iJ_j^{\text{eff}})) - \Gamma_j \pm \sqrt{\Gamma_j^2 - 4J_j^{\text{eff}}(J_j^{\text{eff}} + i\eta_j)}\right)} \tag{4.76}$$

$$l^*_{\uparrow,\pm} = \pm\frac{\Gamma_j}{2\eta_j} \frac{2(\eta_j - iJ_j^{\text{eff}}) - \Gamma_j \pm \sqrt{\Gamma_j^2 - 4J_j^{\text{eff}}(J_j^{\text{eff}} + i\eta_j)}}{\sqrt{\Gamma_j^2 - 4J_j^{\text{eff}}(J_j^{\text{eff}} + i\eta_j)}} \tag{4.77}$$

$$l^*_{\downarrow,\pm} = \pm\frac{\Gamma_j}{2\eta_i} \frac{2(\eta_j - iJ_j^{\text{eff}}) + \Gamma_j \mp \sqrt{\Gamma_j^2 - 4J_j^{\text{eff}}(J_j^{\text{eff}} + i\eta_j)}}{\sqrt{\Gamma_j^2 - 4J_j^{\text{eff}}(J_j^{\text{eff}} + i\eta_j)}} \tag{4.78}$$

where as in the main text $\Gamma_j = (\gamma_{+,j} + \gamma_{-,j})/2$, $\eta_j = (\gamma_{+,j} - \gamma_{-,j})/2$ The normalization has been chosen such that the biorthogonality condition

$$\langle \hat{l}_{\vec{M}',\vec{S}'} | \hat{r}_{\vec{M},\vec{S}} \rangle = \delta_{\vec{M},\vec{M}'} \delta_{\vec{S},\vec{S}'} \tag{4.79}$$

is satisfied. Further, we have also chosen the normalization such that the steady state has unit trace. The corresponding eigenvalues are then found to match those found in Eq. (16) in the main text.

We end this section by pointing out the existence of several exceptional points (EP) in this model. An EP occurs when both the eigenvalues and eigenvectors of a non-Hermitian matrix coalesce, thus rendering it undiagonalizable [50]. The order of the degeneracy is know as the order of the EP, and it is well-know that at an EP, the spectrum is exceptionally sensitive to

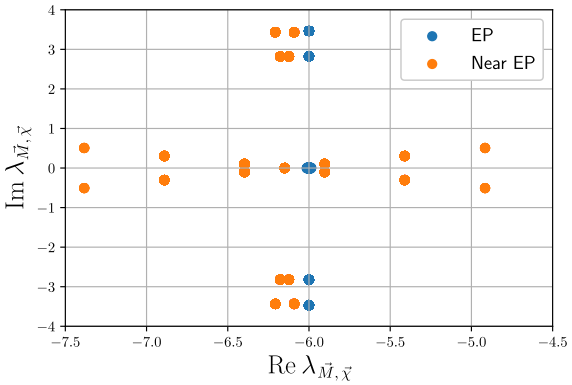

Fig. 4.3: Select eigenvalues of the dissipative Ising Lindbladian as written in Eq. (4.65) at an EP ($\gamma_{+,j} = \gamma_{-,j} = 1$ and $J = 0.5$) and near an EP ($\gamma_{+,j} = 1.05, \gamma_{-,j} = 1$ and $J = 0.5$). The perturbation $\delta\gamma_+ = 0.05$ causes a much larger shift of the eigenvalues on the order of $\sqrt{\delta\gamma_+} = 0.22$.

perturbations ϵ of certain parameters, where the change of the eigenvalues scale like $(\epsilon)^{1/n}$ [50]. Since our problem reduces to a solving a set of 2×2 matrices, it is clear that we can have at most second-order EPs. It is easy to see that these necessarily occur when

$$\sqrt{\Gamma_j^2 - 4J_j^{\text{eff}}(J_j^{\text{eff}} + i\eta_j)} = 0 \implies \eta_j = (\gamma_{+,j} - \gamma_{-,j})/2 = 0 \quad \text{and} \quad \Gamma_j = \pm 2J_j^{\text{eff}}. \tag{4.80}$$

To obtain an EP, the incoherent pumping and decay rate must therefore be the same. One way to obtain a large number of second-order EP's is then to make both the incoherent pumping and decay uniform $\gamma_{+,j} = \gamma_{-,j} = \Gamma_j = \gamma$ and set all the coherent interaction terms to be uniform as well $J_{jk} = J = \gamma/2$. Then $J_j^{\text{eff}} = J\sum_{m\neq k} m_k$ and we obtain a set of EPs when $\sum_{m\neq k} m_k = \pm 1$. In Fig. (4.3) we plot the spectrum near and at an EP. We see that the small perturbation induces a large change in the eigenvalues.

4.6.5 Decay of single-spin coherence in the dissipative Ising model

In this section we compute the single-spin coherence $\langle \hat{\sigma}_j^+(t) \rangle$ using the eigenvalue and eigenvector decomposition of the Lindbladian discussed in the previous section, assuming that all

spins at time $t = 0$ are initially in the x direction. Using third-quantized notation, we have

$$\begin{aligned}\langle\hat{\sigma}_j^+(t)\rangle &= \langle\hat{1}|\hat{\boldsymbol{\sigma}}_{L,j}^+ e^{\hat{\boldsymbol{\mathcal{L}}}t}|\hat{\rho}(0)\rangle = \langle\hat{1}|\hat{\boldsymbol{\sigma}}_{L,j}^+ \sum_{\vec{M},\vec{\chi}} e^{\lambda_{\vec{M},\vec{\chi}}t}|\hat{r}_{\vec{M},\vec{\chi}}\rangle\langle\hat{l}_{\vec{M},\vec{\chi}}|\hat{\rho}(0)\rangle \\ &= \sum_{\vec{M},\vec{\chi}} e^{\lambda_{\vec{M},\vec{\chi}}t}\,\mathrm{Tr}\Big(\hat{\sigma}_j^+\hat{r}_{\vec{M},\vec{\chi}}\Big)\,\mathrm{Tr}\Big(\hat{l}^\dagger_{\vec{M},\vec{\chi}}\hat{\rho}(0)\Big) \end{aligned} \tag{4.81}$$

Note that the block-diagonal structure greatly simplifies the summation above, as we are only probing a specific set of eigenmodes. More concretely, the only modes that contribute are those for which the only frozen spins is spin j, whereas all others are active:

$$\mathrm{Tr}\Big(\hat{\sigma}_j^+\hat{r}_{\vec{M},\vec{\chi}}\Big) = \begin{cases} \prod_{k\neq j}(r_{\uparrow,\chi_k} + r_{\downarrow,\chi_k}), & m_j = -1,\ m_k = 0\ \forall\ k \neq j \\ 0, & \text{otherwise.} \end{cases} \tag{4.82}$$

There are thus only 2^{N-1} out of the 4^N terms in Eq. (4.81) that do not vanish. The fact that the eigenvectors and initial state factorize over a product of single spins, in addition to the fact that the eigenvalues can be written as $\lambda_{\vec{M},\vec{\chi}} = \sum_j \lambda_j(\vec{M},\chi_j)$ directly leads the factorization of the end result

$$\begin{aligned}\langle\hat{\sigma}_j^+(t)\rangle &= \frac{e^{(2ih_j-\Gamma_j-2\gamma_{\phi,j})t}}{2}\prod_{k\neq j}\left(\sum_{\chi_k=\pm}\frac{e^{\lambda_k(\vec{M},\chi_k)t}}{2}\Big[(r_{\uparrow,\chi_k}+r_{\downarrow,\chi_k})(l^*_{\uparrow,\chi_k}+l^*_{\downarrow,\chi_k})\Big]\right) \\ &= \frac{e^{(2ih_j-\Gamma_j-2\gamma_{\phi,j})t}}{2}\prod_{k\neq j}\left(e^{-\Gamma_k t}\left[\cosh(S_k t)+\frac{\Gamma_k}{S_k}\sinh(S_k t)\right]\right) \end{aligned} \tag{4.83}$$

where $S_k = \sqrt{\Gamma_k^2 - 4J_k^{\mathrm{eff}}(J_k^{\mathrm{eff}} + i\eta_k)}$ and $J_k^{\mathrm{eff}} = -J_{kj}$. This matches the result in Ref. [36], yet Eq. (4.83) was obtained with only a few lines of algebra. Further, we note that in principle have access to the full many-body density matrix of the time-evolved initial state.

4.6.6 Including dynamical disorder in the dissipative Ising model

In the main text and in this Supplementary Materials, we have demonstrated that the existence of weak-symmetires in the dissipative Ising model allows one to diagonalize the Liouvillian. One can find the spectrum in addition to the right and left eigenvectors, which implies that one can time-evolve an arbitrary initial density matrix. In this section, we demonstrate that our method is still applicable to the situation where one has dynamical disorder in the magnetic field or Ising couplings (i.e. such terms are now allowed to be time-dependent). To be more precise, we now show that if one has a master equation

$$\begin{aligned}\partial_t\hat{\rho} = -i[\sum_{j<k} J_{jk}(t)\hat{\sigma}_j^z\hat{\sigma}_k^z + \sum_j h_j(t)\hat{\sigma}_j^z, \hat{\rho}] + \sum_j \gamma_{-,j}\mathcal{D}[\hat{\sigma}_j^-]\hat{\rho} \\ + \sum_j \gamma_{+,j}\mathcal{D}[\hat{\sigma}_j^+]\hat{\rho} + \sum_j \gamma_{\phi,j}\mathcal{D}[\hat{\sigma}_j^z]\hat{\rho} \equiv \mathcal{L}(t)\hat{\rho}.\end{aligned} \tag{4.84}$$

then time-evolving an initial density matrix is no more complicated than solving a set of coupled linear differential equations in two variables.

We first note that one can readily eliminate the magnetic fields by moving to a rotating frame:

$$\hat{\rho} \to e^{-i\sum_j \int_0^t dT h_j(T)\hat{\sigma}_j^z}\hat{\rho}e^{i\sum_j \int_0^t dT h_j(T)\hat{\sigma}_j^z}, \tag{4.85}$$

such that the only difficulty when compared to the static model now lies in the time-dependent Ising couplings. Crucially, the time-dependence does not ruin the weak symmetries nor the mean-field-like decoupling of the interaction in each block present in the static case. Consequently, the Lindbladian is still invariant under an arbitrary local rotation

about the z axis and, upon projecting onto a fixed $\vec{M}$ subspace, we have the replacement

$$[\sum_{j<k} J_{jk}(t)\hat{\sigma}_j^z\hat{\sigma}_k^z, \hat{\rho}] \to \sum_j \{J_j^{\text{eff}}(t,\vec{M})\hat{\sigma}_j^z, \hat{\rho}_{\vec{M}}\} \tag{4.86}$$

where we have defined $J_j^{\text{eff}}(t,\vec{M}) = \sum_{k\neq j} J_{jk}(t)m_k$. We now, as before, drop the explicit $\vec{M}$ dependence of $J_j^{\text{eff}}(t,\vec{M})$. After fixing a specific symmetry-constrained sector $\vec{M}$, which is equivalent to fixing a set of active and frozen spins we can write the density matrix projected onto the subspace $\vec{M}$ as

$$\hat{\rho}_{\vec{M}} = \hat{\rho}_{\text{froz}} \times \hat{\rho}_{\text{act}} = \left(\prod_{j \text{ frozen}} \hat{\sigma}_j^{m_j}\right)\left(\sum_{\vec{s}_{\text{act}}} P(\vec{s}_{\text{act}}) \left|\vec{s}_{\text{act}}\right\rangle \left\langle\vec{s}_{\text{act}}\right|\right) \tag{4.87}$$

where $\vec{s}_{\text{act}} = \{s_j \,|\, j \text{ active}\}$, $s_j \in \{\uparrow_j, \downarrow_j\}$, and $m_j = \pm 1$. Just as in the time-translationally invariant situation, the factorization of the interaction Eq. (4.86) further implies that the classical probability distribution $P(\vec{s}_{\text{act}})$ factorizes over the individual spins

$$\hat{\rho}_{\text{act}} = \prod_{j \text{ act}} \left(p_{\uparrow,j}\left|\uparrow_j\right\rangle\left\langle\uparrow_j\right| + p_{\downarrow,j}\left|\downarrow_j\right\rangle\left\langle\downarrow_j\right|\right), \tag{4.88}$$

where the equations of motion for the coefficients reads

$$\partial_t \begin{pmatrix} p_{\uparrow,j} \\ p_{\downarrow,j} \end{pmatrix} = \begin{pmatrix} -2iJ_j^{\text{eff}}(t) - \gamma_{-,j} & \gamma_{+,j} \\ \gamma_{-,j} & 2iJ_j^{\text{eff}}(t) - \gamma_{+,j} \end{pmatrix} \begin{pmatrix} p_{\uparrow,j} \\ p_{\downarrow,j} \end{pmatrix} \tag{4.89}$$

For an arbitrary time-dependent field $J^{\text{eff}}(t)$, we are not aware of a closed-form solution to Eq. (4.89). Nevertheless, the upshot is that one has greatly simplified the problem: one now only has to solve a set of linear differential equations in 2 variables which can readily be done numerically. Further, if one were to consider the case where $J_{ij}(t)$ and $h_j(t)$ were random, our method could then readily be used to numerically average over these random variables.

CHAPTER 5

REFORMULATING THIRD QUANTIZATION: IDENTIFYING DISSIPATION AND FLUCTUATIONS, EQUIVALENCE TO PHASE-SPACE REPRESENTATIONS, AND CONNECTIONS TO KELDYSH FIELD THEORY

5.1 Introduction

Open quantum systems are generically much more difficult to characterize than their closed-system counterparts. One typically has to consider density matrices instead of pure states, and the system can be driven out of equilibrium through its coupling to the environment. This increase in complexity has lead to the development of new theoretical techniques or extensions of well-established ones that can account for the open nature of the problem at hand. Unsurprisingly, different fields have their own set of tools that are tailored-made to address specific questions of interest. In a many-body problem for example, one can not possibly hope to keep track of the full density matrix of the system, nor is such information necessary to any experimentally-relevant quantities. The workhorse in this instance is Keldysh field theory [58], which allows one to compute pertinent steady-state correlations functions in a manner that is analogous to standard thermal-equilibrium many-body theory. In contrast, in a quantum information setting we are often interested in the state itself rather than expectation values of a few observables. The starting point is thus generally an equation of motion for the density matrix which, for a large number of experimental and theoretical works, is a Markovian Lindblad master equation [77]. Phase-space representations of a quantum state such as the Wigner quasiprobability distribution [39] is yet another tool often used in quantum optics, which allows one to both readily compare and differentiate classical and quantum theories.

Quadratic systems of bosons or fermions coupled to Markovian baths are arguably the simplest examples of open quantum systems. Computing average values and correlation functions is straightforward using either the master equation, Keldysh field theory or the Heisenberg-Langevin equations. However, it is often useful to understand the full dissipative eigenvectors and eigenvalues of the Lindbladian. This information, in principle, allows one to determine the full time evolution of an arbitrary initial state which is needed if one wants to e.g. understand the Fock state structure. Recently, Prosen [112] and Prosen and Seligman [113] introduced third quantization, which allows one to obtain the spectral decomposition of these Liouvillians in a manner that is analogous to diagonalizing a second-quantized quadratic Hamiltonian. The method however does not make it intuitively evident to what extent the open nature of the problem changes the standard closed-system diagonalization procedure. Further, it is not clear how it is related to other standard open quantum system methods. A more physically-transparent formulation of third quantization which also makes a clear connection to other well-known approaches would thus make it an overall more useful tool.

In this work we present an alternate reformulation of third quantization which satisfies both criteria simultaneously. This is achieved by introducing a new set of canonical superoperators, defined in Eqs. (5.29-(5.30). In this basis, one directly identifies the two pieces of data that determine any quadratic Lindbladian: a non-Hermitian Hamiltonian which effectively controls the dynamics and a matrix which encodes the noise. This separation of dissipation and fluctuations further reveals a fundamental symmetry of these models. We show that this symmetry can be used to effectively gauge away the fluctuations using a novel similarity transformation implemented at the superoperator level. This provides a simple quantum-oriented way to demonstrate that the eigenvalues of the Lindbladian are independent of noise in linear systems.

The superoperators we introduce also already makes the connection between the Lindbla-

dian and the Keldysh formalism evident. We make this notion exact by formulating a path integral representation of third quantization over a finite time contour. Further, we demonstrate that third quantization is clearly linked to phase space representations of the density matrix. Namely, we show that the Wigner function and the characteristic function [39] can be thought of as “wavefunctions" in the basis of what is essentially the third-quantized equivalent of coherent states.

5.2 Diagonalization using classical and quantum superoperators

While the method we discuss can be applied to arbitrary multi-mode bosonic quadratic Lindbladians, for clarity we discuss these ideas in the simplest possible setting: a harmonic oscillator coupled to a thermal Markovian bath. Our starting point is the equation of motion for the density matrix (with $\hbar = 1$ throughout)

$$i\partial_t \hat{\rho} = \omega_0[\hat{a}^\dagger \hat{a}, \hat{\rho}] + i\kappa(\bar{n}_{\text{th}} + 1)\mathcal{D}[\hat{a}]\hat{\rho} + i\kappa\bar{n}_{\text{th}}\mathcal{D}[\hat{a}^\dagger]\hat{\rho} \equiv \mathcal{L}\hat{\rho} \tag{5.1}$$

where $\hat{a}$ is the bosonic annihilation operator of the oscillator, ω_0 is its frequency, κ its decay rate and $\bar{n}_{\text{th}}$ is the thermal occupation of the bath. Here, we have defined the usual dissipator as $\mathcal{D}[\hat{X}]\hat{\rho} = \hat{X}\hat{\rho}\hat{X}^\dagger - \{\hat{X}^\dagger\hat{X}, \hat{\rho}\}/2$ and $\mathcal{L}$ as the Liouvillian superoperator. Our goal is to diagonalize $\mathcal{L}$. It is convenient to think of operators as being elements of a Hilbert space $\hat{\rho} \to |\hat{\rho}\rangle\rangle$ with the usual Hilbert-Schmidt inner product

$$\langle\langle \hat{X}|\hat{Y}\rangle\rangle \equiv \text{Tr}\left(\hat{X}^\dagger \hat{Y}\right) \tag{5.2}$$

for arbitrary operators $\hat{X}$ and $\hat{Y}$.[1] Using this notation, superoperators become operators acting on this new space and we therefor write them with hats. Further, to differentiate them from operators acting on the Hilbert space of wavefunctions, we write all superoperators using a bold typeface $\mathcal{L} \to \hat{\boldsymbol{\mathcal{L}}}$. The inner product Eq. (5.2) then allows us to define the Hermitian adjoint of any superoperator. For instance the adjoint Liouvillian, which controls the time evolution of observables, is in standard second quantized form given by

$$\mathcal{L}^\dagger \hat{Y} = \omega_0[\hat{a}^\dagger \hat{a}, \hat{Y}] - i\kappa(\bar{n}_{\text{th}} + 1)\mathcal{D}^\dagger[\hat{a}]\hat{Y} - i\kappa\bar{n}_{\text{th}}\mathcal{D}^\dagger[\hat{a}^\dagger]\hat{Y} \tag{5.3}$$

with $\mathcal{D}^\dagger[\hat{X}]\hat{Y} = \hat{X}^\dagger \hat{Y}\hat{X} - \{\hat{X}^\dagger\hat{X}, \hat{Y}\}/2$ the adjoint dissipator. As the Linbladian is non-Hermitian $\hat{\boldsymbol{\mathcal{L}}} \neq \hat{\boldsymbol{\mathcal{L}}}^\dagger$, to diagonalize it we must find both its right and left eigenvectors. That is, we seek operators and complex numbers which satisfy

$$\hat{\boldsymbol{\mathcal{L}}}|\hat{r}_{\mu,\nu}\rangle\rangle = |\mathcal{L}\hat{r}_{\mu,\nu}\rangle\rangle = E_{\mu,\nu}|\hat{r}_{\mu,\nu}\rangle\rangle \tag{5.4}$$

$$\langle\langle \hat{l}_{\mu,\nu}|\hat{\boldsymbol{\mathcal{L}}} = \langle\langle \mathcal{L}^\dagger \hat{l}_{\mu,\nu}| = E_{\mu,\nu}\langle\langle \hat{l}_{\mu,\nu}| \tag{5.5}$$

where, with some foresight, we have labelled the eigenstates by two non-negative integers $\mu, \nu \geq 0$.

Although the physical interpretation of the right and left eigenvectors may not be straightforward, the eigenvalues have a simple intuitive meaning. The real part of $E_{\mu,\nu}$ corresponds to the energy difference of eigenstates, whereas the imaginary component dictates the rate of decay. We can thus immediate conclude that the spectrum of $\hat{\boldsymbol{\mathcal{L}}}$ must not depend on $\bar{n}_{\text{th}}$; for no observable oscillates or decays in a temperature-dependent manner. This simply reflects the fact that a linear system's response to fluctuations is independenf of its state. This is

1. Technically, for the infinite-dimensional spaces under consideration, both $\hat{X}$ and $\hat{Y}$ must be trace class to be part of this Hilbert space of operators. This is cumbersome, since operators of interest such as $\hat{a}$ and $\hat{a}^\dagger$ do not satisfy this property. Nevertheless, we will use the language and notation that one uses for a normal Hilbert space.

not immediately obvious from Eq. (5.1), yet is almost trivial if one considers the equivalent Heisenberg-Langevin equation of Keldysh action of this model. How then can we identify these fluctuations and reach this conclusion working directly from the master equation?

We argue that this can be straightforwardly done by introducing appropriate third-quantized superoperators defined by

$$\hat{\boldsymbol{a}}_{\rm cl}|\hat{\rho}\rangle\rangle \equiv \frac{1}{\sqrt{2}}|\{\hat{a},\hat{\rho}\}\rangle\rangle, \qquad \hat{\boldsymbol{a}}_{\rm q}|\hat{\rho}\rangle\rangle \equiv \frac{1}{\sqrt{2}}|[\hat{a},\hat{\rho}]\rangle\rangle \tag{5.6}$$

$$\hat{\boldsymbol{a}}^\dagger_{\rm cl}|\hat{\rho}\rangle\rangle \equiv \frac{1}{\sqrt{2}}|\{\hat{a}^\dagger,\hat{\rho}\}\rangle\rangle, \qquad \hat{\boldsymbol{a}}^\dagger_{\rm q}|\hat{\rho}\rangle\rangle \equiv \frac{1}{\sqrt{2}}|[\hat{a}^\dagger,\hat{\rho}]\rangle\rangle. \tag{5.7}$$

which we refer to as classical and quantum superoperators. The naming convention is in analogy with Keldysh field theory, which is justified by writing the Lindblbadian in this basis of superoperators

$$\hat{\boldsymbol{\mathcal{L}}} = (\omega_0 - i\frac{\kappa}{2})\hat{\boldsymbol{a}}^\dagger_{\rm q}\hat{\boldsymbol{a}}_{\rm cl} + (\omega_0 + i\frac{\kappa}{2})\hat{\boldsymbol{a}}_{\rm q}\hat{\boldsymbol{a}}^\dagger_{\rm cl} - i\kappa(2\bar{n}_{\rm th}+1)\hat{\boldsymbol{a}}^\dagger_{\rm q}\hat{\boldsymbol{a}}_{\rm q}. \tag{5.8}$$

This is evidently reminiscent of the Keldysh action for this same model [58], and we make this connection more explicit in Sec. 5.4. Just as in the field theory description, the coefficients of $\hat{\boldsymbol{a}}^\dagger_{\rm q}\hat{\boldsymbol{a}}_{\rm cl}$ and $\hat{\boldsymbol{a}}_{\rm q}\hat{\boldsymbol{a}}^\dagger_{\rm cl}$ serve as an effective non-Hermitian Hamiltonian, whereas the term $\hat{\boldsymbol{a}}^\dagger_{\rm q}\hat{\boldsymbol{a}}_{\rm q}$ should be thought of as the fluctuations that must accompany the dissipation. Indeed, although $\hat{\boldsymbol{a}}^\dagger_{\rm cl}$ and $\hat{\boldsymbol{a}}^\dagger_{\rm q}$ are the conjugate of $\hat{\boldsymbol{a}}_{\rm cl}$ and $\hat{\boldsymbol{a}}_{\rm q}$, they are not the creation operators of true bosonic modes since $[\hat{\boldsymbol{a}}_{\rm cl},\hat{\boldsymbol{a}}^\dagger_{\rm cl}] = [\hat{\boldsymbol{a}}_{\rm q},\hat{\boldsymbol{a}}^\dagger_{\rm q}] = 0$. Thus, we can not interpret $\hat{\boldsymbol{a}}^\dagger_{\rm cl}\hat{\boldsymbol{a}}_{\rm cl}$ and $\hat{\boldsymbol{a}}^\dagger_{\rm q}\hat{\boldsymbol{a}}_{\rm q}$ as number operators. Rather, despite being non-Hermitian, we should think of $\hat{\boldsymbol{a}}^\dagger_{\rm q}\hat{\boldsymbol{a}}_{\rm cl}$ and $-\hat{\boldsymbol{a}}_{\rm q}\hat{\boldsymbol{a}}^\dagger_{\rm cl}$ as operators whose eigenvalues correspond to a number of quanta in a mode. This follows since the only non-vanishing commutation relation amongst the superoperators are

$$[\hat{\boldsymbol{a}}_{\rm cl},\hat{\boldsymbol{a}}^\dagger_{\rm q}] = [\hat{\boldsymbol{a}}_{\rm q},\hat{\boldsymbol{a}}^\dagger_{\rm cl}] = \hat{\mathbf{1}}, \tag{5.9}$$

with $\hat{\mathbf{1}}$ the identity superoperator. Given their status as number operators, to determine their eigenvectors we must first find the "vacuums" of $\hat{\boldsymbol{a}}_{\rm cl}, \hat{\boldsymbol{a}}_{\rm cl}^\dagger$ and $\hat{\boldsymbol{a}}_{\rm q}, \hat{\boldsymbol{a}}_{\rm q}^\dagger$. These are simply the parity and identity operator

$$\hat{0}_{\rm cl} \equiv 2e^{i\pi\hat{a}^\dagger\hat{a}} \rightarrow \hat{\boldsymbol{a}}_{\rm cl}|\hat{0}_{\rm cl}\rangle\rangle = \hat{\boldsymbol{a}}_{\rm cl}^\dagger|\hat{0}_{\rm cl}\rangle\rangle = 0 \tag{5.10}$$

$$\hat{0}_{\rm q} \equiv \hat{1} \rightarrow \hat{\boldsymbol{a}}_{\rm q}|\hat{0}_{\rm q}|\rangle\rangle = \hat{\boldsymbol{a}}_{\rm q}^\dagger|\hat{0}_{\rm q}\rangle\rangle = 0 \tag{5.11}$$

which follows since $e^{i\pi\hat{a}^\dagger\hat{a}}$ and $\hat{1}$ respectively anti-commute and commute with both $\hat{a}$ and $\hat{a}^\dagger$. In complete analogy with a simple harmonic oscillator, we can obtain the eigenvectors by repeatedly applying the appropriate creation operators on the vacuums. Thus, we find that $\frac{1}{\sqrt{\mu!\nu!}}(\hat{\boldsymbol{a}}_{\rm q}^\dagger)^\mu(-\hat{\boldsymbol{a}}_{\rm q})^\nu|\hat{0}_{\rm cl}\rangle\rangle$ and $\frac{1}{\sqrt{\mu!\nu!}}\langle\langle\hat{0}_{\rm q}|(\hat{\boldsymbol{a}}_{\rm cl})^\mu(\hat{\boldsymbol{a}}_{\rm cl}^\dagger)^\nu$ are the right and left eigenvectors of $\hat{\boldsymbol{a}}_{\rm q}^\dagger\hat{\boldsymbol{a}}_{\rm cl}$ and $\hat{\boldsymbol{a}}_{\rm q}\hat{\boldsymbol{a}}_{\rm cl}^\dagger$ with eigenvalue μ and $-\nu$ respectively.

Although this conclusion may give credence to the idea that $\hat{\boldsymbol{a}}_{\rm q}^\dagger\hat{\boldsymbol{a}}_{\rm cl}$ and $\hat{\boldsymbol{a}}_{\rm q}^\dagger\hat{\boldsymbol{a}}_{\rm cl}$ serve as effective non-Hermitian Hamiltonians, at first glance it may appear to be useless. The Lindbladian also contains the temperature-dependent $\hat{\boldsymbol{a}}_{\rm q}^\dagger\hat{\boldsymbol{a}}_{\rm q}$ noise term, which necessarily couples these eigenvectors. Yet we have already reasoned that the spectrum of $\hat{\boldsymbol{\mathcal{L}}}$ must be independent of $\bar{n}_{\rm th}$; the temperature only affects the eigenvectors. There must therefore exist a similarity transformation which eliminates this dependence entirely from the Linbladian. Defining

$$\hat{\boldsymbol{\mathcal{V}}} \equiv e^{-(2\bar{n}_{\rm th}+1)\hat{\boldsymbol{a}}_{\rm q}^\dagger\hat{\boldsymbol{a}}_{\rm q}} \tag{5.12}$$

and using the commutation relations Eq. (5.9) along with the Baker-Campbell-Hausdorff identity, one verifies that

$$\hat{\boldsymbol{\mathcal{V}}}^{-1}\hat{\boldsymbol{\mathcal{L}}}\hat{\boldsymbol{\mathcal{V}}} = (\omega_0 - i\frac{\kappa}{2})\hat{\boldsymbol{a}}_{\rm q}^\dagger\hat{\boldsymbol{a}}_{\rm cl} + (\omega_0 + i\frac{\kappa}{2})\hat{\boldsymbol{a}}_{\rm q}\hat{\boldsymbol{a}}_{\rm cl}^\dagger. \tag{5.13}$$

In this new frame the superoperator is not in Lindblad form due to the presence of a negative rate

$$\mathcal{V}^{-1}\mathcal{L}\mathcal{V}\hat{\rho} = \omega_0[\hat{a}^\dagger\hat{a},\hat{\rho}] + i\frac{\kappa}{2}\left(\mathcal{D}[\hat{a}]\hat{\rho} - \mathcal{D}[\hat{a}^\dagger]\hat{\rho}\right), \tag{5.14}$$

yet this is irrelevant for diagaonlization purposes. We have thus made a non-trivial mapping from a noisy damped harmonic oscillator to its fluctuation-free equivalent which , being in diagonal form, immediately indicates that only the eigenvectors of $\hat{\boldsymbol{\mathcal{L}}}$ are temperature-dependent whereas its spectrum is not. This is a consequence of the usual separation of dynamics and noise in linear systems, yet here there are quantum consequences, seeing as how the eigenmodes of the Liouvillian have a Fock state structure.

One might think that this separation can be destroyed by introducing a $\hat{\boldsymbol{a}}^\dagger_{\rm cl}\hat{\boldsymbol{a}}_{\rm cl}$ term in the third-quantized Lindbladian; the similarity transformation $e^{-(2\bar{n}_{\rm th}+1)\hat{\boldsymbol{a}}^\dagger_{\rm q}\hat{\boldsymbol{a}}_{\rm q}}$ would no longer bring $\hat{\boldsymbol{\mathcal{L}}}$ to a diagonal form, since it commutes with the quantum superoperators but not the classical ones. Such a term is however forbidden by the trace-preserving nature of the dynamics $\mathrm{Tr}(\mathcal{L}\hat{\rho}) = \langle\langle\hat{0}_q|\hat{\boldsymbol{\mathcal{L}}}|\hat{\rho}\rangle\rangle = 0$, which a classical-classical term would violate . Our ability to eliminate the fluctuations in problem can, at a quantum level, be understood as a special kind of symmetry; linearity and conservation of probability. In non-linear quantum systems, which are of course also probability-conserving, fluctuations can impact the dynamics, thus destroying this symmetry.

With Eq. (5.13) already in diagonal form, the similarity transformation allows us to simply relate the eigenvectors $\hat{r}_{\mu,\nu}, \hat{l}_{\mu,\nu}$ of $\hat{\boldsymbol{\mathcal{L}}}$ to those of $\hat{\boldsymbol{a}}^\dagger_{\rm q}\hat{\boldsymbol{a}}_{\rm cl}$ and $\hat{\boldsymbol{a}}_{\rm q}\hat{\boldsymbol{a}}^\dagger_{\rm cl}$. They are given by

$$|\hat{r}_{\mu,\nu}\rangle\rangle = \frac{1}{\sqrt{\mu!\nu!}}e^{-(2\bar{n}_{\rm th}+1)\hat{\boldsymbol{a}}^\dagger_{\rm q}\hat{\boldsymbol{a}}_{\rm q}}(\hat{\boldsymbol{a}}^\dagger_{\rm q})^\mu(-\hat{\boldsymbol{a}}_{\rm q})^\nu|\hat{0}_{\rm cl}\rangle\rangle = \frac{1}{\sqrt{\mu!\nu!}}(\hat{\boldsymbol{a}}^\dagger_{\rm q})^\mu(-\hat{\boldsymbol{a}}_{\rm q})^\nu|\hat{\rho}_{\rm ss}\rangle\rangle, \tag{5.15}$$

$$\langle\langle\hat{l}_{\mu,\nu}| = \frac{1}{\sqrt{\mu!\nu!}}\langle\langle\hat{0}_{\rm q}|(\hat{\boldsymbol{a}}_{\rm cl})^\mu(\hat{\boldsymbol{a}}^\dagger_{\rm cl})^\nu e^{(2\bar{n}_{\rm th}+1)\hat{\boldsymbol{a}}^\dagger_{\rm q}\hat{\boldsymbol{a}}_{\rm q}}\frac{1}{\sqrt{\mu!\nu!}}\langle\langle\hat{0}_{\rm q}|(\hat{\boldsymbol{a}}_{\rm cl}(\bar{n}_{\rm th}))^\mu(\hat{\boldsymbol{a}}^\dagger_{\rm cl}(\bar{n}_{\rm th}))^\nu \tag{5.16}$$

with corresponding eigenvalues

$$E_{\mu,\nu} = (\omega_0 - i\frac{\kappa}{2})\mu - (\omega_0 + i\frac{\kappa}{2})\nu. \tag{5.17}$$

Here we have defined

$$\hat{\boldsymbol{a}}_{\rm cl}(\bar{n}_{\rm th}) \equiv \hat{\boldsymbol{\mathcal{V}}}\hat{\boldsymbol{a}}_{\rm cl}\hat{\boldsymbol{\mathcal{V}}}^{-1} = \hat{\boldsymbol{a}}_{\rm cl} + (2\bar{n}_{\rm th}+1)\hat{\boldsymbol{a}}_{\rm q} \tag{5.18}$$

$$\hat{\boldsymbol{a}}^\dagger_{\rm cl}(\bar{n}_{\rm th}) \equiv \hat{\boldsymbol{\mathcal{V}}}\hat{\boldsymbol{a}}^\dagger_{\rm cl}\hat{\boldsymbol{\mathcal{V}}}^{-1} = \hat{\boldsymbol{a}}^\dagger_{\rm cl} - (2\bar{n}_{\rm th}+1)\hat{\boldsymbol{a}}^\dagger_{\rm q} \tag{5.19}$$

where note that since $\hat{\boldsymbol{\mathcal{V}}}$ is not unitary, $\hat{\boldsymbol{a}}^\dagger_{\rm cl}(\bar{n}_{\rm th})$ is not the conjugate of $\hat{\boldsymbol{a}}_{\rm cl}(\bar{n}_{\rm th})$ despite the notation. This is however of no concern, seeing as the similarity transformations preserve all commutation relations

$$[\hat{\boldsymbol{a}}_{\rm cl}(\bar{n}_{\rm th}), \hat{\boldsymbol{a}}^\dagger_{\rm q}] = [\hat{\boldsymbol{a}}_{\rm q}, \hat{\boldsymbol{a}}^\dagger_{\rm cl}(\bar{n}_{\rm th})] = \hat{\mathbf{1}}. \tag{5.20}$$

We can thus identify $\hat{\boldsymbol{a}}_{\rm cl}(\bar{n}_{\rm th}), \hat{\boldsymbol{a}}_{\rm q}$ and $\hat{\boldsymbol{a}}^\dagger_{\rm cl}(\bar{n}_{\rm th}), \hat{\boldsymbol{a}}_{\rm q}$ as the correct independent "quasiparticle" superoperators which create excitation with a definite energy and decay rate. Although the vacuum of the quantum superoperators is the identity, the right vacuum of these new classical superoperators is the steady state

$$\hat{\boldsymbol{a}}_{\rm cl}(\bar{n}_{\rm th})|\hat{\rho}_{\rm ss}\rangle\rangle = \hat{\boldsymbol{a}}^\dagger_{\rm cl}(\bar{n}_{\rm th})|\hat{\rho}_{\rm ss}\rangle\rangle = 0, \tag{5.21}$$

where we have identified $\hat{\rho}_{\rm ss}$ from Eq. (5.15) as the unique zero-eigenvalue eigenvector of the Lindbladian.

The form of these eigenvectors is still somewhat unsatisfactory. For instance, using Eq. (5.15), the right eigenvectors are given by nested commutators of $\hat{a}^\dagger, \hat{a}$ and the steady state. For large μ and ν, the representation of these operators is difficult to obtain explicitly in the Fock basis and are largely uninformative. Further, it is well-known that the steady

state of this model is a Gaussian thermal state.

$$\hat{\rho}_{\rm ss} = \frac{1}{\bar{n}_{\rm th}+1}\sum_{n=0}^{\infty}\left(\frac{\bar{n}_{\rm th}}{\bar{n}_{\rm th}+1}\right)^n |n\rangle\langle n| \tag{5.22}$$

with $|n\rangle$ a Fock state. Although one can show that this state does satisfy Eq. (5.21), our diagonalization procedure simply asserts that this is equivalent to the similarity transformation applied to the classical vacuum $e^{-(2\bar{n}_{\rm th}+1)\hat{\boldsymbol{a}}_{\rm q}^\dagger\hat{\boldsymbol{a}}_{\rm q}}|\hat{0}_{\rm cl}\rangle\rangle$. The later is by definition an infinite sum of an increasing number of nested commutators between $\hat{a}$, $\hat{a}^\dagger$ and the parity operator

$$\hat{\rho}_{\rm ss} \stackrel{?}{=} 2e^{-(\bar{n}_{\rm th}+\frac{1}{2})[\hat{a}^\dagger,[\hat{a},\cdot]]}e^{i\pi\hat{a}^\dagger\hat{a}}. \tag{5.23}$$

While seemingly devoid of physical content, we shall now demonstrate that these eigenvectors and similarity transformation become physically transparent in phase space.

5.3 Third Quantization and the Wigner function

There are several, ultimately equivalent phase-space quasi-probability distributions of the density matrix; we chose the Wigner function for reasons that will soon become obvious. Up to a normalization constant and scaling of the phase-space variable α, it is defined as [39]

$$W_{\hat{\rho}}(\alpha) \equiv 2\,{\rm Tr}\left(e^{i\pi\hat{a}^\dagger\hat{a}}\hat{D}^\dagger(\sqrt{2}\alpha)\hat{\rho}\right) \tag{5.24}$$

with $\hat{D}(\alpha) \equiv e^{\alpha\hat{a}^\dagger-\alpha^*\hat{a}}$ the displacement operator. For the model under consideration, a textbook calculation gives its equation of motion as

$$i\partial_t W_{\hat{\rho}}(\alpha) = \Big[-(\omega_0 - i\frac{\kappa}{2})\partial_\alpha\alpha + (\omega_0+i\frac{\kappa}{2})\partial_{\alpha^*}\alpha^* + i\kappa(2\bar{n}_{\rm th}+1)\partial_\alpha\partial_{\alpha^*}\Big]W_{\hat{\rho}}(\alpha). \tag{5.25}$$

The form of the Fokker-Planck equation is reminiscent of the third-quantized form of $\hat{\boldsymbol{\mathcal{L}}}$, see Eq. (5.8). In particular, it is tempting to make the formal identification between the noise and the diffusion terms $\hat{\boldsymbol{a}}_{\mathrm{q}}^{\dagger}\hat{\boldsymbol{a}}_{\mathrm{q}} \leftrightarrow -\partial_{\alpha}\partial_{\alpha^*}$. Taking this line of reasoning further, we would thus conclude that $\hat{\boldsymbol{\mathcal{V}}} = e^{(2\bar{n}_{\mathrm{th}}+1)\partial_{\alpha}\partial_{\alpha^*}}$. Going to Fourier space, where differentiation becomes multiplication, and then back to phase space using the convolution theorem we would thus tentatively write

$$W_{\mathcal{V}\hat{\rho}}(\alpha) \stackrel{?}{=} \int \frac{d^2\beta}{(2\bar{n}_{\mathrm{th}}+1)\pi} e^{-\frac{|\alpha-\beta|^2}{2\bar{n}_{\mathrm{th}}+1}} W_{\hat{\rho}}(\beta) \tag{5.26}$$

where $d^2\gamma \equiv d\mathrm{Re}(\gamma)d\mathrm{Im}(\gamma)$ for any complex γ. One of the main results of this section is that our formalism will be able to make Eq. (5.26) precise: the similarity transformation used to remove the noise is equivalent to a convolution by a Gaussian of width $2\bar{n}_{\mathrm{th}}+1$ in phase space.

The second main result of this section is a physical insight into the structure of the eigenmodes when compared to Fock states. Focusing on population eigenmodes $\mu = \nu$ and Fock state projectors $|\mu\rangle\langle\mu|$ for simplicity we have

$$W_{\hat{r}_{\mu,\mu}}(\alpha) = \frac{2(-1)^{\mu} e^{-\frac{|\alpha|^2}{2\bar{n}_{\mathrm{th}}+1}}}{(2\bar{n}_{\mathrm{th}}+1)^{\mu+1}} L_{\mu}\left(\frac{|\alpha|^2}{2\bar{n}_{\mathrm{th}}+1}\right), \tag{5.27}$$

$$W_{|\mu\rangle\langle\mu|}(\alpha) = 2(-1)^{\mu} e^{-|\alpha|^2} L_{\mu}(2|\alpha|^2) \tag{5.28}$$

where L_{μ} is the μ-th Laguerre polynomial. Unlike the explicit construction in standard third-quantized form Eq. (5.15) which requires computing nested commuators of $\hat{a}, \hat{a}^{\dagger}$ and $\hat{\rho}_{\mathrm{ss}}$, in this representation $\hat{r}_{\mu,\nu}$ bear a striking similarity to Fock states. In fact, they are almost equivalent once one re-scales the phase-space variable $\alpha_{\mathrm{cl}} \to \alpha_{\mathrm{cl}}/(2\bar{n}_{\mathrm{th}}+1)$. This property also holds when comparing arbitrary right eigenmodes $\hat{r}_{\mu,\nu}$ and outer products of Fock states $|\mu\rangle\langle\nu|$ which we show in Appendix 5.6.1. There we also give the phase-space

representations of the left eigenvectors.

The final main result of this section is in fact the method we develop which we used to arrive at Eqs. (5.26)-(5.27). As we now show, the starting point of this approach is to ask and answer a simple natural question: what are the eigenvectors of the classical and quantum superoperators? Thankfully such operators are already familiar from quantum optics. For any complex number α and η let us define corresponding displaced parity and displacement operators respectively

$$\hat{\alpha}_{\rm cl} \equiv 2\hat{D}(\sqrt{2}\alpha)e^{i\pi\hat{a}^\dagger\hat{a}}, \tag{5.29}$$

$$\hat{\eta}_{\rm q} \equiv \hat{D}(\sqrt{2}\eta). \tag{5.30}$$

Using the defining property of the displacement operator and parity operators, a simple calculation yields

$$\hat{\boldsymbol{a}}_{\rm cl}|\hat{\alpha}_{\rm cl}\rangle\rangle = \alpha|\hat{\alpha}_{\rm cl}\rangle\rangle, \;\; \hat{\boldsymbol{a}}^\dagger_{\rm cl}|\hat{\alpha}_{\rm cl}\rangle\rangle = \alpha^*|\hat{\alpha}_{\rm cl}\rangle\rangle, \tag{5.31}$$

$$\hat{\boldsymbol{a}}_{\rm q}|\hat{\eta}_{\rm q}\rangle\rangle = \eta|\hat{\eta}_{\rm q}\rangle\rangle, \quad \hat{\boldsymbol{a}}^\dagger_{\rm q}|\hat{\eta}_{\rm q}\rangle\rangle = \eta^*|\hat{\eta}_{\rm q}\rangle\rangle. \tag{5.32}$$

The spectrum of each superoperator is thus the whole complex plane. These eigenvectors are evidently reminiscent of the familiar coherent states, an analogy we can make even stronger by writing

$$|\hat{\alpha}_{\rm cl}\rangle\rangle = e^{\alpha\hat{\boldsymbol{a}}^\dagger_{\rm q}-\alpha^*\hat{\boldsymbol{a}}_{\rm q}}|\hat{0}_{\rm cl}\rangle\rangle, \tag{5.33}$$

$$|\hat{\eta}_{\rm q}\rangle\rangle = e^{\eta\hat{\boldsymbol{a}}^\dagger_{\rm cl}-\eta^*\hat{\boldsymbol{a}}_{\rm cl}}|\hat{0}_{\rm q}\rangle\rangle \tag{5.34}$$

just as coherent states are displaced vacuum. Unlike coherent states however, which are not eigenvectors of $\hat{a}^\dagger$, $\hat{\boldsymbol{a}}_{\rm cl}, \hat{\boldsymbol{a}}^\dagger_{\rm cl}$ and $\hat{\boldsymbol{a}}_{\rm q}, \hat{\boldsymbol{a}}^\dagger_{\rm q}$ have the same eigenvectors, a consequence of $[\hat{\boldsymbol{a}}_{\rm cl}, \hat{\boldsymbol{a}}^\dagger_{\rm cl}] = [\hat{\boldsymbol{a}}_{\rm q}, \hat{\boldsymbol{a}}^\dagger_{\rm q}] = 0$. For the same reason, the $\hat{\alpha}_{\rm cl}$ and $\hat{\eta}_{\rm q}$ are orthogonal to other

eigenstates of the same kind:

$$\langle\langle\hat{\alpha}_{\rm cl}|\hat{\beta}_{\rm cl}\rangle\rangle = {\rm Tr}\left(\hat{\alpha}_{\rm cl}^{\dagger}\hat{\beta}_{\rm cl}\right) = 2\pi\delta(\alpha-\beta), \tag{5.35}$$

$$\langle\langle\hat{\alpha}_{\rm q}|\hat{\beta}_{\rm q}\rangle\rangle = {\rm Tr}\left(\hat{\eta}_{\rm q}^{\dagger}\hat{\lambda}_{\rm q}\right) = \frac{\pi}{2}\delta(\eta-\lambda) \tag{5.36}$$

where the trace was computed using the basis of coherent states. These operators can then be used to form a resolution of the identity

$$\hat{\mathbf{1}} = \int\frac{d^2\alpha}{2\pi}|\hat{\alpha}_{\rm cl}\rangle\rangle\langle\langle\hat{\alpha}_{\rm cl}| = \int\frac{2d^2\eta}{\pi}|\hat{\eta}_{\rm q}\rangle\rangle\langle\langle\hat{\eta}_{\rm q}| \tag{5.37}$$

from which it follows that we can write the density matrix as

$$|\hat{\rho}\rangle\rangle = \int\frac{d^2\alpha_{\rm cl}}{2\pi}W_{\hat{\rho}}(\alpha)|\hat{\alpha}_{\rm cl}\rangle\rangle = \int\frac{2d^2\alpha_{\rm q}}{\pi}\Lambda_{\hat{\rho}}(\eta)|\hat{\eta}_{\rm q}\rangle\rangle \tag{5.38}$$

with

$$W_{\hat{\rho}}(\alpha) \equiv \langle\langle\hat{\alpha}_{\rm cl}|\hat{\rho}\rangle\rangle = 2\,{\rm Tr}\left(e^{i\pi\hat{a}^{\dagger}\hat{a}}\hat{D}^{\dagger}(\sqrt{2}\alpha)\hat{\rho}\right), \tag{5.39}$$

$$\Lambda_{\hat{\rho}}(\eta) \equiv \langle\langle\hat{\eta}_{\rm q}|\hat{\rho}\rangle\rangle = {\rm Tr}\left(\hat{D}^{\dagger}(\sqrt{2}\eta)\hat{\rho}\right). \tag{5.40}$$

Third quantization is thus naturally related to the continuous-variable phase formulations of open quantum systems; $W_{\hat{\rho}}(\alpha)$ and $\Lambda_{\hat{\rho}}(\eta)$ are precisely the Wigner function and its characteristic function respectively, which serve as "wavefunctions" of the density matrix.

It is well-know that $W_{\hat{\rho}}(\alpha)$ and $\Lambda_{\hat{\rho}}(\eta)$ are Fourier transforms of each other [39], which we can recover by computing the overlap

$$\langle\langle\hat{\alpha}_{\rm cl}|\hat{\eta}_{\rm q}\rangle\rangle = {\rm Tr}\left(\hat{\alpha}_{\rm cl}^{\dagger}\hat{\eta}_{\rm q}\right) = e^{\eta\alpha^{*}-\eta^{*}\alpha}, \tag{5.41}$$

and using the definitions Eqs. (5.39)-(5.40) with the resolution of the identify Eq. (5.37) to

obtain

$$W_{\hat{\rho}}(\alpha) = \int \frac{2d^2\eta}{\pi} e^{\eta\alpha^* - \eta^*\alpha} \Lambda_{\hat{\rho}}(\eta) \tag{5.42}$$

$$\Lambda_{\hat{\rho}}(\eta) = \int \frac{d^2\alpha}{2\pi} e^{\eta^*\alpha - \eta\alpha^*} W_{\hat{\rho}}(\alpha). \tag{5.43}$$

Just as position and momentum eigenkets corresponds to a perfectly spatially-localized or delocalized particle in standard quantum mechanics, the eigenkets $|\hat{\alpha}_{\rm cl}\rangle\rangle$ and $|\hat{\eta}_{\rm q}\rangle\rangle$ can be thought of as states in phase space which are perfectly localized at α or delocalized with wavevector η. That α and η are Fourier transform pairs is also consistent with $\hat{\boldsymbol{a}}_{\rm cl}, \hat{\boldsymbol{a}}_{\rm q}^\dagger$ and $\hat{\boldsymbol{a}}_{\rm q}, \hat{\boldsymbol{a}}_{\rm cl}^\dagger$ being conjugate to one another. This can be further demonstrated by using Eqs. (5.33)-(5.34) to write

$$\langle\langle\hat{\eta}_{\rm q}|\hat{\boldsymbol{a}}_{\rm cl} = \partial_{\eta^*}\langle\langle\hat{\eta}_{\rm q}|, \quad \langle\langle\hat{\alpha}_{\rm cl}|\hat{\boldsymbol{a}}_{\rm q}^\dagger = -\partial_\alpha\langle\langle\hat{\alpha}_{\rm cl}| \tag{5.44}$$

$$\langle\langle\hat{\alpha}_{\rm cl}|\hat{\boldsymbol{a}}_{\rm q} = \partial_{\alpha^*}\langle\langle\hat{\alpha}_{\rm q}|, \quad \langle\langle\hat{\eta}_{\rm q}|\hat{\boldsymbol{a}}_{\rm cl}^\dagger = -\partial_\eta\langle\langle\hat{\eta}_{\rm q}|. \tag{5.45}$$

Given any third-quantized Lindbladian, we can then use Eqs. (5.39)-(5.40) and Eqs. (5.44)-(5.45) to readily find the equation of motion for either the Wigner or the characteristic function. For the model under consideration for instance, we have

$$i\partial_t|\hat{\rho}\rangle\rangle = \left[(\omega_0 - i\frac{\kappa}{2})\hat{\boldsymbol{a}}_{\rm q}^\dagger\hat{\boldsymbol{a}}_{\rm cl} + (\omega_0 + i\frac{\kappa}{2})\hat{\boldsymbol{a}}_{\rm q}\hat{\boldsymbol{a}}_{\rm cl}^\dagger - i\kappa(2\bar{n}_{\rm th}+1)\hat{\boldsymbol{a}}_{\rm q}^\dagger\hat{\boldsymbol{a}}_{\rm q}\right]|\hat{\rho}\rangle\rangle \tag{5.46}$$

$$\updownarrow$$

$$i\partial_t W_{\hat{\rho}}(\alpha) = \left[-(\omega_0 - i\frac{\kappa}{2})\partial_\alpha\alpha + (\omega_0 + i\frac{\kappa}{2})\partial_{\alpha^*}\alpha^* + i\kappa(2\bar{n}_{\rm th}+1)\partial_\alpha\partial_{\alpha^*}\right]W_{\hat{\rho}}(\alpha) \tag{5.47}$$

$$\updownarrow$$

$$i\partial_t\Lambda_{\hat{\rho}}(\eta) = \left[(\omega_0 - i\frac{\kappa}{2})\eta^*\partial_{\eta^*} - (\omega_0 + i\frac{\kappa}{2})\eta\partial_\eta - i\kappa(2\bar{n}_{\rm th}+1)\eta^*\eta\right]\Lambda_{\hat{\rho}}(\eta). \tag{5.48}$$

From now on, we will write the classical and quantum superoperators and their action on

these eigenvectors as equivalent, e.g. $\hat{\boldsymbol{a}}_{\rm cl} = \alpha = \partial_{\eta^*}$.

It is worth stressing that by using the resolution of the identity Eq. (5.37), one can obtain a phase-space representation of of an arbitrary operator $W_{\hat{X}}(\alpha) \equiv \langle\langle\hat{\alpha}_{\rm cl}|\hat{X}\rangle\rangle = 2\,\mathrm{Tr}\Big(e^{i\pi\hat{a}^\dagger\hat{a}}\hat{D}(\sqrt{2}\alpha)\hat{X}\Big)$. This is nothing but the Weyl quantization rule [28]. Our approach however does more than simply recover this standard formalism, as we can now formally identify the similarity transformation as being equivalent to convolution with a Gaussian of width $2\bar{n}_{\rm th}+1$. Being diagonal in the quantum basis, $\hat{\boldsymbol{\mathcal{V}}} = e^{-(2\bar{n}_{\rm th}+1)\hat{\boldsymbol{a}}_{\rm q}^\dagger\hat{\boldsymbol{a}}_{\rm q}}$ simply acts by multiplication on the characteristic function $\Lambda_{\mathcal{V}\hat{\rho}}(\eta) = e^{-(2\bar{n}_{\rm th}+1)|\eta|^2}\Lambda_{\hat{\rho}}(\eta)$. Going back to the Wigner function using Eq. (5.42) then gives Eq. (5.26). This is also consistent with our intuition; convolving with a Gaussian tends to spread to and delocalize any distribution, which explains why the similarity transformation $e^{-(2\bar{n}_{\rm th}+1)\hat{\boldsymbol{a}}_{\rm q}^\dagger\hat{\boldsymbol{a}}_{\rm q}}$ was able to remove the noise or, equivalently, the diffusion term in the Fokker-Planck equation.

The right eigenvectors of $\hat{\boldsymbol{\mathcal{L}}}$ also have a very simply form in phase space:

$$W_{\hat{r}_{\mu,\nu}}(\alpha) \equiv \frac{1}{\sqrt{\mu!\nu!}}\langle\langle\hat{\alpha}_{\rm cl}|(\hat{\boldsymbol{a}}_{\rm q}^\dagger)^\mu(-\hat{\boldsymbol{a}}_{\rm q})^\nu|\hat{\rho}_{\rm ss}\rangle\rangle = \frac{(-1)^{\mu+\nu}}{\sqrt{\mu!\nu!}}\partial_\alpha^\mu\partial_{\alpha^*}^\nu W_{\hat{\rho}_{\rm ss}}(\alpha) \tag{5.49}$$

and we show explicitly in Appendix 5.6.1 that we obtain Eq. (5.27). Finally, note that the diagonalization procedure is still valid even when there is no dissipation $\bar{n}_{\rm th} \to 0, \kappa \to 0$ despite $W_{|\mu\rangle\langle\mu|}(\alpha) \neq W_{\hat{r}_{\mu,\mu}}(\alpha)$ in this limit. This is because without decay, each eigenvalue $E_{\mu,\nu} = \omega_0(\mu-\nu)$ is infinitely degenerate and thus there is no unique way to diagnoalize $\hat{\boldsymbol{\mathcal{L}}}$; our approach picks out one linearly-independent set of eigenvectors out of the infinitely-many available ones. This is most obvious by writing $\hat{\boldsymbol{\mathcal{L}}} = \omega_0(\hat{\boldsymbol{a}}_{\rm q}^\dagger\hat{\boldsymbol{a}}_{\rm cl} + \hat{\boldsymbol{a}}_{\rm q}\hat{\boldsymbol{a}}_{\rm cl}^\dagger) = \omega_0(-\partial_\alpha\alpha + \partial_{\alpha^*}\alpha^*) = \omega_0 i\partial_\phi$ where ϕ is the phase of α.

5.4 Propagator via the Keldysh path integral

With the spectral decomposition of $\hat{\boldsymbol{\mathcal{L}}}$ in hand, we can in principle determine the full time-dependent density matrix via

$$|\hat{\rho}(t)\rangle\rangle = e^{-i\hat{\boldsymbol{\mathcal{L}}}t}|\hat{\rho}(0)\rangle\rangle = \sum_{\mu,\nu} e^{-iE_{\mu,\nu}t} c_{\mu,\nu}|\hat{r}_{\mu,\nu}\rangle\rangle \tag{5.50}$$

with $c_{\mu,\nu} \equiv \langle\langle \hat{l}_{\mu,\nu}|\hat{\rho}(0)\rangle\rangle$. This representation leaves a lot to be desired. Even though one could technically obtain a Wigner function for $\hat{\rho}(t)$ from Eq. (5.50), the discrete nature of the eigenmodes still remains; the continuous nature of phase space is seemingly lost. To reinstate and highlight this feature, a more natural description of time evolution is given by the matrix element

$$K(\eta, \alpha; t) \equiv \langle\langle \hat{\eta}_{\rm q}|e^{-i\hat{\boldsymbol{\mathcal{L}}}t}|\hat{\alpha}_{\rm cl}\rangle\rangle \tag{5.51}$$

which in principle contains the same information as the spectral decomposition of $\hat{\boldsymbol{\mathcal{L}}}$. Physically, the kernel $K(\eta, \alpha; t)$ is the transition amplitude of having started at the phase-space point α and ending up in a plane wave with wavevector η at a time t later, see Eq. (5.41) and accompanying discussion. Using the resolution of the identity

$$\hat{\mathbf{1}} = \int \frac{d^2a_{{\rm cl},j} d^2a_{{\rm q},j}}{\pi^2} e^{a_{{\rm q},j}a^*_{{\rm cl},j} - a^*_{{\rm q},j}a_{{\rm cl},j}} |\hat{a}_{{\rm cl},j}\rangle\rangle\langle\langle \hat{a}_{{\rm q},j}| \tag{5.52}$$

we can obtain a path-integral description of Eq. (5.51) using the familiar prescription [5]. The central object will be a functional very similar to the standard Keldysh action of a thermally-damped harmonic oscillator. There are however important differences that emerge when computing the propagator. We emphasize these here, leaving the technical and mostly-familiar details in Appendix 5.6.2.

Once these details have been taken into account, we are left with a path integral repre-

sentation of the kernel

$$K(\eta,\alpha;t) =, \int \mathcal{D}[a_{\rm cl},a_{\rm q}] e^{iS[a_{\rm cl},a_{\rm q}]+i\int_0^t dt' \left(\underline{a}^\dagger(t')\cdot\underline{J}(t')+\underline{J}^\dagger(t')\cdot\underline{a}(t')\right)} \tag{5.53}$$

where $\mathcal{D}[a_{\rm cl},a_{\rm q}]$ is the usual functional integration measure, the action takes the form

$$S[a_{\rm cl},a_{\rm q}] = \int_0^t\int_0^t dt'dt'' \begin{pmatrix} a^*_{\rm cl}(t') & a^*_{\rm q}(t') \end{pmatrix} \mathbb{G}^{-1}(t',t'') \begin{pmatrix} a_{\rm cl}(t'') \\ a_{\rm q}(t'') \end{pmatrix}, \tag{5.54}$$

and the inverse of the matrix Green's function reads

$$\mathbb{G}^{-1}(t',t'') = \delta(t'-t'') \begin{pmatrix} 0 & i\partial_{t'} - (\omega_0 + i\frac{\kappa}{2}) \\ i\partial_{t'} - (\omega_0 - i\frac{\kappa}{2}) & i\kappa(2\bar{n}_{\rm th}+1) \end{pmatrix}. \tag{5.55}$$

Throughout this work, we will denote matrices with a blackboard bold font to distinguish them from operators and superoperators. Vectors like $\underline{a}^\dagger(t') \equiv \left(a^*_{\rm cl}(t'), a^*_{\rm q}(t')\right)$ and the source term

$$\underline{J}^\dagger(t') \equiv i\left(-\eta^*\delta(t), \alpha\delta(0)\right) \tag{5.56}$$

will be underlined.

The first departure from the usual Keldysh path integral is already evident from Eq. (5.54), where we work with a finite time contour of length t. Although $\mathbb{G}^{-1}$ is symbolically the same regardless of the length of the time contour, the matrix Green's function

$$\mathbb{G}(t',t'') \equiv \begin{pmatrix} G^K(t',t'') & G^R(t',t'') \\ G^A(t',t'') & 0 \end{pmatrix} \tag{5.57}$$

is sensitive to such changes. In particular, the retarded $G^R(t',t'')$ and advanced $G^A(t',t'')$

Green's function remains the same regardless of the contour, whereas the Keldysh Green's $G^K(t',t'')$ function does not

$$G^R(t',t'') = -i\Theta(t'-t'')e^{-i(\omega_0 - i\frac{\kappa}{2})(t'-t'')} \tag{5.58}$$

$$G^A(t',t'') = (G^R(t'',t'))^* \tag{5.59}$$

$$\begin{aligned} G^K(t',t'') &= -i\kappa(2\bar{n}_{\rm th}+1)\int_0^t dT G^R(t',T)G^A(T,t'') \\ &= -i(2\bar{n}_{\rm th}+1)e^{-i\omega_0(t'-t'')}[e^{-\frac{\kappa}{2}|t'-t''|} - e^{-\frac{\kappa}{2}(t'+t'')}] \end{aligned} \tag{5.60}$$

with $\Theta(t)$ the Heaviside step function. Crucially, the discrete-time path integral makes it clear that the correct choice of the Heaviside step function at zero is $\Theta(0) = 1$. We also note that source Eq. (5.56) is not usually present in the usual Keldysh formalism; within our version of the path integral however it is the only term which keeps track of the boundary terms α and η.

The path integral can be computed in the usual manner when we have a quadratic action and a source term. Making the displacement

$$\underline{a}(t') \to \underline{a}(t') - \int_0^t dt'' \mathbb{G}(t',t'')\underline{J}(t'') \tag{5.61}$$

and, using $\int \mathcal{D}[a_{\rm cl},a_{\rm q}]e^{iS[a_{\rm cl},a_{\rm q}]} = \det(i\mathbb{G}) = 1$ just as in the usual Keldysh formalism, we obtain

$$\begin{aligned} K(\eta,\alpha;t) &= e^{-i\int_0^t dt'dt''\underline{J}^\dagger(t')\mathbb{G}(t',t'')\underline{J}(t'')} \\ &= e^{-(2\bar{n}_{\rm th}+1)(1-e^{-\kappa t})|\eta|^2 + e^{-\frac{\kappa}{2}t}[\eta^*\alpha e^{-i\omega_0 t} - \text{c.c.}]}. \end{aligned} \tag{5.62}$$

As expected due to the quadratic nature of the Lindbladian, the propagator is a Gaussian function of α and η. Equation (5.62) can independently be verified to be correct by noting that it must satisfy Eq. (5.48) along with the initial condition $K(\eta,\alpha;0) = e^{\eta^*\alpha - \eta\alpha^*}$.

Although here $\hat{\boldsymbol{\mathcal{L}}}$ was quadratic in creation and annihilation superoperators, it is evident that a path integral representation of the propagator can be obtained for arbitrary Lindbladians. The replacement rule $\hat{\boldsymbol{\mathcal{L}}}(\hat{\boldsymbol{a}}_{\rm q}, \hat{\boldsymbol{a}}_{\rm cl}) \to \mathcal{L}(a_{\rm q}(t'), a_{\rm cl}(t'))$ within the action however is only valid once all $\hat{\boldsymbol{a}}_{\rm q}$ and $\hat{\boldsymbol{a}}_{\rm q}^{\dagger}$ are to the left of all $\hat{\boldsymbol{a}}_{\rm cl}$ and $\hat{\boldsymbol{a}}_{\rm cl}^{\dagger}$. This is due to the form of the resolution of the identity Eq. (5.37). This convention is different than the one used in the standard coherent-state path integral, where one must ensure that the Lindlabidan is normal-ordered [126]. No differences emerge in this linear setting, but the two different prescriptions will produce two different Keldysh actions for an interacting problem.

5.5 Summary and future directions

By introducing a new set of canonical third-quantized superoperators, we have bee able to identity a fundamental symmetry of the Lindbladian of a thermally-damped harmonic oscillator. Further, this symmetry was shown to be useful; we could formally eliminate fluctuations through the use of a novel similarity transformation. This then allowed to show how third quantization was related to more standard open quantum-sytems approaches such as phase-space representations of the density matrix and the Keldysh path integral. Future work will extend the formalism developed here to both multi-mode bosonic and fermionic quadratic masters equations; the linearity and symmetry should once again enable one to formally eliminate the fluctuations from the Lindbladian.

We end this work by highlighting the differences between our approach and the standard formulation of third quantization for bosons introduced by Prosen and Seligman's [113]. Their starting point is a different set of superoperators than Eqs (5.6)-(5.7), which nevertheless satisfy almost canonical commutation relations. Although they necessarily obtain the same eigenvalues as eigenvectors for $\hat{\boldsymbol{\mathcal{L}}}$ as those presented here, they do not do so by first performing a similarity transformation which allows one to gauge away the fluctuations. Further, they do not make the connection between third quantization, the Wigner function,

and Keldysh field theory that we do. Although it may seem as though the main difference between the two approaches is a mere change of basis — which should never change the physics — the classical and quantum superoperators we introduce is precisely what allowed us to make the connection between these three formulations clear.

5.6 Appendices

5.6.1 Phase-space representations of right and left eigenvectors of a single thermally-damped harmonic oscillator

We can easily derive the phase-space representations of the right and left eigenvectors using the rule discussed in the main text $\hat{\boldsymbol{a}}_{\rm cl} = \alpha = \partial_{\eta^*}, \hat{\boldsymbol{a}}^\dagger_{\rm cl} = \alpha^* = -\partial_\eta, \hat{\boldsymbol{a}}_{\rm q} = \eta = \partial_{\alpha^*}, \hat{\boldsymbol{a}}^\dagger_{\rm q} = \eta^* = -\partial_\alpha$. Starting with the right eigenvectors

$$
\begin{aligned}
W_{\hat{r}_{\mu,\nu}}(\alpha) &\equiv \langle\langle \hat{\alpha}_{\rm cl}|\hat{r}_{\mu,\nu}\rangle\rangle = \frac{1}{\sqrt{\mu!\nu!}}\langle\langle \hat{\alpha}_{\rm cl}|(\hat{\boldsymbol{a}}^\dagger_{\rm q})^\mu(-\hat{\boldsymbol{a}}_{\rm q})^\nu|\hat{\rho}_{\rm ss}\rangle\rangle = \frac{(-1)^{\mu+\nu}}{\sqrt{\mu!\nu!}}\partial^\mu_\alpha\partial^\nu_{\alpha^*}W_{\hat{\rho}_{\rm ss}}(\alpha) \\
&= \frac{2(-1)^\mu}{\sqrt{\mu!\nu!}}\sum_{j=0}^{\mu}\binom{\mu}{j}\partial^j_\alpha\left(\frac{\alpha}{2\bar{n}_{\rm th}+1}\right)^\nu\partial^{\mu-j}_\alpha\left(\frac{e^{-\frac{|\alpha|^2}{2\bar{n}_{\rm th}+1}}}{2\bar{n}_{\rm th}+1}\right) \\
&= \frac{2e^{-\frac{|\alpha|^2}{2\bar{n}_{\rm th}+1}}}{\sqrt{\mu!\nu!}}\sum_{j=0}^{\min(\mu,\nu)}\frac{\mu!\nu!}{j!(\mu-j)!(\nu-j)!}\frac{(-1)^j(\alpha^*)^{\mu-j}\alpha^{\nu-j}}{(2\bar{n}_{\rm th}+1)^{\mu+\nu-j+1}} \\
&= \sqrt{\frac{\min(\mu,\nu)!}{\max(\mu,\nu)!}}\frac{2(-1)^{\min(\mu,\nu)}e^{-\frac{|\alpha|^2}{2\bar{n}_{\rm th}+1}}}{(2\bar{n}_{\rm th}+1)^{\max(\mu,\nu)+1}}e^{-i\phi_{\rm cl}(\mu-\nu)}|\alpha|^{|\mu-\nu|}L^{|\mu-\nu|}_{\min(\mu,\nu)}\left(\frac{|\alpha|^2}{2\bar{n}_{\rm th}+1}\right) \qquad (5.63)
\end{aligned}
$$

where $\phi_{\rm cl}$ is the phase of α and $L^{|\mu-\nu|}_{\min(\mu,\nu)}$ is an associated Laguerre polynomial. Using $[\hat{\boldsymbol{a}}_{\rm cl}, \hat{\boldsymbol{a}}^\dagger_{\rm cl}] = 0$, the left eigenvectors can be written as

$$\begin{aligned} W^*_{\hat{l}_{\mu,\nu}}(\alpha) &\equiv \frac{1}{\sqrt{\mu!\nu!}} \langle\langle \hat{0}_{\rm q}| \hat{\boldsymbol{a}}^\mu_{\rm cl} (\hat{\boldsymbol{a}}^\dagger_{\rm cl})^\nu e^{(2\bar{n}_{\rm th}+1)\hat{\boldsymbol{a}}^\dagger_{\rm q}\hat{\boldsymbol{a}}_{\rm q}} |\hat{\alpha}_{\rm cl}\rangle\rangle \\ &= \frac{1}{\sqrt{\mu!\nu!}} \partial^\mu_{\eta^*}\partial^\nu_\eta \langle\langle \hat{0}_{\rm q}| e^{\eta^*\hat{\boldsymbol{a}}_{\rm cl} + \eta\hat{\boldsymbol{a}}^\dagger_{\rm cl}} e^{(2\bar{n}_{\rm th}+1)\hat{\boldsymbol{a}}^\dagger_{\rm q}\hat{\boldsymbol{a}}_{\rm q}} |\hat{\alpha}_{\rm cl}\rangle\rangle \Big|_{\eta=\eta^*=0}. \end{aligned} \tag{5.64}$$

Using the Baker-Campbell-Hausdorff identity, we can move $e^{\eta^*\hat{\boldsymbol{a}}_{\rm cl} + \eta\hat{\boldsymbol{a}}^\dagger_{\rm cl}}$ past the factor of $e^{(2\bar{n}_{\rm th}+1)\hat{\boldsymbol{a}}^\dagger_{\rm q}\hat{\boldsymbol{a}}_{\rm q}}$ and use the defining property of the classical and quantum eigenvectors to obtain

$$\begin{aligned} W^*_{\hat{l}_{\mu,\nu}}(\alpha) &= \frac{1}{\sqrt{\mu!\nu!}} \partial^\mu_{\eta^*}\partial^\nu_\eta e^{-(2\bar{n}_{\rm th}+1)|\eta|^2 + \eta^*\alpha + \eta\alpha^*}\Big|_{\eta=\eta^*=0} \\ &= \frac{1}{\sqrt{\mu!\nu!}} \sum_{j=0}^{\min(\mu,\nu)} \frac{\mu!\nu!(-(2\bar{n}_{\rm th}+1))^j}{j!(\mu-j)!(\nu-j)!} \alpha^{\mu-j}(\alpha^*)^{\nu-j} \\ &= \sqrt{\frac{\min(\mu,\nu)!}{\max(\mu,\nu)!}} \frac{(-1)^{\min(\mu,\nu)}}{(2\bar{n}_{\rm th}+1)^{-\min(\mu,\nu)}} e^{i\phi_{\rm cl}(\mu-\nu)} |\alpha|^{|\mu-\nu|} L^{|\mu-\nu|}_{\min(\mu,\nu)}\left(\frac{|\alpha|^2}{2\bar{n}_{\rm th}+1}\right). \end{aligned} \tag{5.65}$$

5.6.2 Propagator of a thermally-damped harmonic oscillator - Details

In this Appendix, we provide the explicit computations which led us to the continuous-time representation of the propagator $K(\eta, \alpha_{\rm cl}; t) = \langle\langle \hat{\alpha}_{\rm q}| e^{-i\hat{\boldsymbol{\mathcal{L}}}t} |\hat{\alpha}_{\rm cl}\rangle\rangle$ in Eq. ([5]) and divide the propagator in N parts $e^{-i\hat{\boldsymbol{\mathcal{L}}}t} = e^{-i\hat{\boldsymbol{\mathcal{L}}}\Delta t}\cdots e^{-i\hat{\boldsymbol{\mathcal{L}}}\Delta t}$ with $\Delta t = t/N$. We then insert the resolution of the identity Eq. (5.52) between each element $e^{-i\hat{\boldsymbol{\mathcal{L}}}\Delta t}$. Expanding to linear order in Δt and re-exponentiating gives

$$\langle\langle \hat{a}_{{\rm q},j}| e^{-i\hat{\boldsymbol{\mathcal{L}}}\Delta t} |\hat{a}_{{\rm cl},j-1}\rangle\rangle = \quad e^{a^*_{{\rm q},j}a_{{\rm cl},j-1} - a_{{\rm q},j}a^*_{{\rm cl},j-1} - i\mathcal{L}(a_{{\rm q},j}, a_{{\rm cl},j-1})\Delta t} + \mathcal{O}([\Delta t]^2) \tag{5.66}$$

where $\mathcal{L}(a_{{\rm q},j}, a_{{\rm cl},j-1}) \equiv \langle\langle \hat{a}_{{\rm q},j}| \hat{\boldsymbol{\mathcal{L}}} |\hat{a}_{{\rm cl},j-1}\rangle\rangle$. Using the defining property of the classical and quantum eigenvectors Eqs. (5.31)-(5.32), $\mathcal{L}(a_{{\rm q},j}, a_{{\rm cl},j-1})$ is obtained by simply replacing the

classical and quantum superoperators that appear in $\hat{\boldsymbol{\mathcal{L}}}$ by $a_{\mathrm{cl},j-1}$ and $a_{\mathrm{q},j}$ respectively. We thus have

$$K(\eta, \alpha_{\mathrm{cl}}; t) = \int \prod_{j=1}^{N} \frac{da_{\mathrm{cl},j} a_{\mathrm{q},j}}{\pi^2} e^{i\left(\tilde{\underline{a}}^\dagger \tilde{\mathbb{G}}^{-1} \tilde{\underline{a}} + \tilde{\underline{a}}^\dagger \cdot \underline{\tilde{J}} + \underline{\tilde{J}}^\dagger \cdot \tilde{\underline{a}}\right)} + \mathcal{O}([\Delta t]^2) \tag{5.67}$$

where the tilde indicates that we are working with discrete-time objects. We have defined the two $2N$ column vectors

$$\tilde{\underline{a}} = \begin{pmatrix} a_{\mathrm{cl},1} \\ \vdots \\ a_{\mathrm{cl},N} \\ a_{\mathrm{q},1} \\ \vdots \\ a_{\mathrm{q},N} \end{pmatrix} \tag{5.68}$$

and

$$\underline{\tilde{J}} = -i \begin{pmatrix} 0 \\ \vdots \\ -\eta \\ \alpha_{\mathrm{cl}} \\ \vdots \\ 0 \end{pmatrix}, \tag{5.69}$$

the latter only having 2 non-zero entries at position N and $N+1$. The discrete inverse matrix Green's function is given by

$$\tilde{\mathbb{G}}^{-1} \equiv \begin{pmatrix} 0 & [\tilde{\mathbb{G}}^{-1}]^A \\ [\tilde{\mathbb{G}}^{-1}]^R & [\tilde{\mathbb{G}}^{-1}]^K \end{pmatrix} \tag{5.70}$$

where $[\tilde{\mathbb{G}}^{-1}]^R$ and $[\tilde{\mathbb{G}}^{-1}]^A$ are Hermitian conjugate $N \times N$ lower and upper-triangular matrices respectively, whose only non-vanishing elements are on the main off-diagonal

$$[\tilde{\mathbb{G}}^{-1}]^R = \begin{pmatrix} i & & & & \\ -ih & i & & & \\ & -ih & \ddots & & \\ & & \ddots & \ddots & \\ & & & -ih & i \end{pmatrix} \tag{5.71}$$

$$[\tilde{\mathbb{G}}^{-1}]^A = \begin{pmatrix} -i & ih^* & & & \\ & -i & ih^* & & \\ & & \ddots & \ddots & \\ & & & \ddots & ih^* \\ & & & & -i \end{pmatrix}, \tag{5.72}$$

where $h \equiv 1 - i(\omega_0 - i\kappa/2)\Delta t$. The Keldysh component is simply proportional to the identity

$$\left[\tilde{\mathbb{G}}^{-1}\right]^K = i\kappa(2\bar{n}_{\text{th}} + 1)\mathbb{1}. \tag{5.73}$$

We can readily obtain the matrix Green's function since its inverse has a vanishing upper-left block

$$\tilde{\mathbb{G}} = \begin{pmatrix} \tilde{\mathbb{G}}^K & \tilde{\mathbb{G}}^R \\ \tilde{\mathbb{G}}^A & 0 \end{pmatrix} \tag{5.74}$$

where

$$\left(\tilde{\mathbb{G}}^R\right)_{jj'} = \begin{cases} 0, & j' > j \\ -ih^{j-j'} & j \geq j' \end{cases} \tag{5.75}$$

$$\left(\tilde{\mathbb{G}}^A\right)_{jj'} = \begin{cases} i(h^*)^{j'-j}, & j' \geq j \\ 0, & j > j' \end{cases} \tag{5.76}$$

$$\begin{aligned} \left(\tilde{\mathbb{G}}^K\right)_{jj'} &= -i\kappa(2\bar{n}_{\text{th}}+1)\sum_{k=1}^{N}\Delta t\left(\tilde{\mathbb{G}}^R\right)_{jk}\left(\tilde{\mathbb{G}}^A\right)_{kj'} \\ &= \frac{-i(2\bar{n}_{\text{th}}+1)}{1-\frac{\Delta t}{\kappa}(\omega_0^2+(\frac{\kappa}{2})^2)}h^j(h^*)^{j'}\left(h^{-\min(j,j')}(h^*)^{-\min(j,j')}-1\right). \end{aligned} \tag{5.77}$$

In Eq. (5.67), we can then make the displacement

$$\underline{\tilde{a}} \to \underline{\tilde{a}} - \tilde{\mathbb{G}}\underline{\tilde{J}} \tag{5.78}$$

and perform the integral over the various $a_{\text{cl},j}$ and $a_{\text{q},j}$ using the well-known result for Gaussian integrals $\int\prod_{j=1}^{N}\frac{da_{\text{cl},j}a_{\text{q},j}}{\pi^2}e^{i\underline{\tilde{a}}^\dagger\tilde{\mathbb{G}}^{-1}\underline{\tilde{a}}} = \det\left(i\tilde{\mathbb{G}}\right)$ [5]. Since the lower-right block of $\tilde{\mathbb{G}}$ vanishes and because the retarded and advanced Green's functions are lower and upper

triangular respectively, we have $\det\left(i\tilde{\mathbb{G}}\right) = \det\left(\tilde{\mathbb{G}}^R\right)\det\left(\tilde{\mathbb{G}}^A\right) = 1$. We are then left with

$$\begin{aligned} K(\eta, \alpha_{\rm cl}; t) &= \exp\left(-i\underline{\tilde{J}}^\dagger \tilde{\mathbb{G}}\underline{\tilde{J}}\right) + \mathcal{O}([\Delta t]^2) \\ &= \exp\left(-i\left[|\eta|^2(\tilde{\mathbb{G}}^K)_{NN} - \eta^*\alpha_{\rm cl}(\tilde{\mathbb{G}}^R)_{N1} - \eta\alpha^*_{\rm cl}(\tilde{\mathbb{G}}^A)_{1N}\right]\right) + \mathcal{O}([\Delta t]^2) \end{aligned}$$

Using Eqs. (5.75)-(5.77) and taking the $N \to \infty$ limit while keeping the length of the contour fixed $\Delta t N = t$, we recover Eq. (5.62). As we have emphasized in the main text, Eqs. (5.75)-(5.76) indicate that the correct normalization of the Heaviside step function at time $t = 0$ as they appear in the retarded and advanced Green's function is $\Theta(0) = 1$.

BIBLIOGRAPHY

[1] G. S. Agarwal. Master-equation approach to spontaneous emission. *Phys. Rev. A*, 2: 2038–2046, Nov 1970. doi:10.1103/PhysRevA.2.2038. URL https://link.aps.org/doi/10.1103/PhysRevA.2.2038.

[2] Victor V. Albert. Lindbladians with multiple steady states: theory and applications, 2018.

[3] Victor V. Albert and Liang Jiang. Symmetries and conserved quantities in lindblad master equations. *Phys. Rev. A*, 89:022118, Feb 2014. doi:10.1103/PhysRevA.89.022118. URL https://link.aps.org/doi/10.1103/PhysRevA.89.022118.

[4] Victor V. Albert, Barry Bradlyn, Martin Fraas, and Liang Jiang. Geometry and response of lindbladians. *Phys. Rev. X*, 6:041031, Nov 2016. doi:10.1103/PhysRevX.6.041031. URL https://link.aps.org/doi/10.1103/PhysRevX.6.041031.

[5] Alexander Altland and Ben D Simons. *Condensed Matter Field Theory*. Cambridge University Press, 2010.

[6] Alexander Altland, Michael Fleischhauer, and Sebastian Diehl. Symmetry classes of open fermionic quantum matter. *Phys. Rev. X*, 11:021037, May 2021. doi:10.1103/PhysRevX.11.021037. URL https://link.aps.org/doi/10.1103/PhysRevX.11.021037.

[7] Ievgen I. Arkhipov, Adam Miranowicz, Fabrizio Minganti, and Franco Nori. Liouvillian exceptional points of any order in dissipative linear bosonic systems: Coherence functions and switching between $\mathcal{PT}$ and anti-$\mathcal{PT}$ symmetries. *Phys. Rev. A*, 102: 033715, Sep 2020. doi:10.1103/PhysRevA.102.033715. URL https://link.aps.org/doi/10.1103/PhysRevA.102.033715.

[8] Yuto Ashida, Zongping Gong, and Masahito Ueda. Non-hermitian physics. *Advances in Physics*, 69:249–435, 2021. doi:10.1080/00018732.2021.1876991. URL https://www.tandfonline.com/doi/full/10.1080/00018732.2021.1876991.

[9] Leonardo Banchi, Samuel L. Braunstein, and Stefano Pirandola. Quantum fidelity for arbitrary gaussian states. *Phys. Rev. Lett.*, 115:260501, Dec 2015. doi:10.1103/PhysRevLett.115.260501. URL https://link.aps.org/doi/10.1103/PhysRevLett.115.260501.

[10] Nicola Bartolo, Fabrizio Minganti, Wim Casteels, and Cristiano Ciuti. Exact steady state of a kerr resonator with one- and two-photon driving and dissipation: Controllable wigner-function multimodality and dissipative phase transitions. *Phys. Rev. A*, 94: 033841, Sep 2016. doi:10.1103/PhysRevA.94.033841. URL https://link.aps.org/doi/10.1103/PhysRevA.94.033841.

[11] Sh. Barzanjeh, D. P. DiVincenzo, and B. M. Terhal. Dispersive qubit measurement by interferometry with parametric amplifiers. *Phys. Rev. B*, 90:134515, Oct 2014. doi:10.1103/PhysRevB.90.134515. URL https://link.aps.org/doi/10.1103/PhysRevB.90.134515.

[12] Emil J. Bergholtz, Jan Carl Budich, and Flore K. Kunst. Exceptional topology of non-hermitian systems. *Rev. Mod. Phys.*, 93:015005, 2021. doi:10.1103/RevModPhys.93.015005. URL https://journals.aps.org/rmp/abstract/10.1103/RevModPhys.93.015005.

[13] B Andrei Bernevig and Taylor L Hughes. *Topological Insulators and Topological Superconductors*. Princeton University Press, stu - student edition edition, 2013.

[14] Alexandre Blais, Ren-Shou Huang, Andreas Wallraff, S. M. Girvin, and R. J. Schoelkopf. Cavity quantum electrodynamics for superconducting electrical circuits: An architecture for quantum computation. *Phys. Rev. A*, 69:062320, Jun 2004. doi:10.1103/PhysRevA.69.062320. URL https://link.aps.org/doi/10.1103/PhysRevA.69.062320.

[15] Alexandre Blais, Arne L. Grimsmo, S. M. Girvin, and Andreas Wallraff. Circuit quantum electrodynamics. *Rev. Mod. Phys.*, 93:025005, May 2021. doi:10.1103/RevModPhys.93.025005. URL https://link.aps.org/doi/10.1103/RevModPhys.93.025005.

[16] Martin Brandenbourger, Xander Locsin, Edan Lerner, and Corentin Coulais. Non-reciprocal robotic metamaterials. *Nature Communications*, 10(1):4608, 2019.

[17] Samuel L. Braunstein and Carlton M. Caves. Statistical distance and the geometry of quantum states. *Phys. Rev. Lett.*, 72:3439–3443, May 1994. doi:10.1103/PhysRevLett.72.3439. URL https://link.aps.org/doi/10.1103/PhysRevLett.72.3439.

[18] Berislav Buča and Tomaž Prosen. A note on symmetry reductions of the lindblad equation: transport in constrained open spin chains. *New J. Phys.*, 14(7):073007, July 2012.

[19] Berislav Buča, Cameron Booker, Marko Medenjak, and Dieter Jaksch. Bethe ansatz approach for dissipation: exact solutions of quantum many-body dynamics under loss. *New J. Phys.*, 22(12):123040, December 2020.

[20] Jan Carl Budich and Emil J. Bergholtz. Non-hermitian topological sensors. *Phys. Rev. Lett.*, 125:180403, Oct 2020. doi:10.1103/PhysRevLett.125.180403. URL https://link.aps.org/doi/10.1103/PhysRevLett.125.180403.

[21] Howard Carmichael. *An open systems approach to quantum optics*, volume 18. Springer Science & Business Media, 2009.

[22] Marco Cattaneo, Gian Luca Giorgi, Sabrina Maniscalco, and Roberta Zambrini. Symmetry and block structure of the liouvillian superoperator in partial secular approximation. *Phys. Rev. A*, 101:042108, Apr 2020. doi:10.1103/PhysRevA.101.042108. URL https://link.aps.org/doi/10.1103/PhysRevA.101.042108.

[23] S Chaturvedi and V Srinivasan. Solution of the master equation for an attenuated or amplified nonlinear oscillator with an arbitrary initial condition. *J. Mod. Opt.*, 38(4): 777–783, April 1991.

[24] S Chaturvedi and V Srinivasan, V. Class of exactly solvable master equations describing coupled nonlinear oscillators. *Phys. Rev. A*, 43(7):4054–4057, April 1991.

[25] Chong Chen, Liang Jin, and Ren-Bao Liu. Sensitivity of parameter estimation near the exceptional point of a non-hermitian system. *New Journal of Physics*, 21(8):083002, aug 2019.

[26] Weijian Chen, Şahin Kaya Özdemir, Guangming Zhao, Jan Wiersig, and Lan Yang. Exceptional points enhance sensing in an optical microcavity. *Nature*, 548(7666):192–196, 2017.

[27] A. A. Clerk, M. H. Devoret, S. M. Girvin, Florian Marquardt, and R. J. Schoelkopf. Introduction to quantum noise, measurement, and amplification. *Rev. Mod. Phys.*, 82: 1155–1208, Apr 2010. doi:10.1103/RevModPhys.82.1155. URL https://link.aps.org/doi/10.1103/RevModPhys.82.1155.

[28] T.L. Curtright, D.B. Fairlie, and C.K. Zachos. *A Concise Treatise On Quantum Mechanics In Phase Space*. World Scientific Publishing Company, 2013. ISBN 9789814520461. URL https://books.google.com/books?id=WSs8DQAAQBAJ.

[29] C. L. Degen, F. Reinhard, and P. Cappellaro. Quantum sensing. *Rev. Mod. Phys.*, 89: 035002, Jul 2017. doi:10.1103/RevModPhys.89.035002. URL https://link.aps.org/doi/10.1103/RevModPhys.89.035002.

[30] P D Drummond and D F Walls. Quantum theory of optical bistability. i. nonlinear polarisability model. *Journal of Physics A: Mathematical and General*, 13(2):725–741, feb 1980. doi:10.1088/0305-4470/13/2/034. URL https://doi.org/10.1088/0305-4470/13/2/034.

[31] M I Dykman and M A Krivoglaz. Theory of nonlinear oscillations interacting with a medium. *Soviet Physics Reviews(vol 5)*, page pp 265–441, 1984.

[32] A. Eddins, J. M. Kreikebaum, D. M. Toyli, E. M. Levenson-Falk, A. Dove, W. P. Livingston, B. A. Levitan, L. C. G. Govia, A. A. Clerk, and I. Siddiqi. High-efficiency measurement of an artificial atom embedded in a parametric amplifier. *Phys. Rev. X*, 9:011004, Jan 2019. doi:10.1103/PhysRevX.9.011004. URL https://link.aps.org/doi/10.1103/PhysRevX.9.011004.

[33] J. Eisert and T. Prosen. Noise-driven quantum criticality, 2010.

[34] Ramy El-Ganainy, Konstantinos G Makris, Mercedeh Khajavikhan, Ziad H Musslimani, Stefan Rotter, and Demetrios N Christodoulides. Non-hermitian physics and pt symmetry. *Nature Physics*, 14(1):11–19, 2018.

[35] Ramy El-Ganainy, Mercedeh Khajavikhan, Demetrios N Christodoulides, and Sahin K Ozdemir. The dawn of non-hermitian optics. *Commun Phys*, 2(1):1–5, 2019.

[36] Michael Foss-Feig, Kaden R A Hazzard, John J Bollinger, and Ana Maria Rey. Nonequilibrium dynamics of arbitrary-range ising models with decoherence: An exact analytic solution. *Phys. Rev. A*, 87(4):042101, April 2013.

[37] Michael Foss-Feig, Jeremy T Young, Victor V Albert, Alexey V Gorshkov, and Mohammad F Maghrebi. Solvable family of driven-dissipative many-body systems. *Phys. Rev. Lett.*, 119(19):190402, November 2017.

[38] Michel Fruchart, Ryo Hanai, Peter B. Littlewood, and Vincenzo Vitelli. Non-reciprocal phase transitions. *Nature*, 592:363, 2021. doi:10.1038/s41586-021-03375-9. URL `https://www.nature.com/articles/s41586-021-03375-9`.

[39] Crispin Gardiner and Peter Zoller. *Quantum noise: a handbook of Markovian and non-Markovian quantum stochastic methods with applications to quantum optics*. Springer Science & Business Media, 2004.

[40] Mario F. Gely, Adrián Sanz Mora, Shun Yanai, Rik van der Spek, Daniel Bothner, and Gary A. Steele. Emergence of nonlinear friction from quantum fluctuations, 2021.

[41] Ananya Ghatak, Martin Brandenbourger, Jasper van Wezel, and Corentin Coulais. Observation of non-hermitian topology and its bulk–edge correspondence in an active mechanical metamaterial. *Proceedings of the National Academy of Sciences*, 117(47): 29561–29568, 2020. ISSN 0027-8424. doi:10.1073/pnas.2010580117. URL `https://www.pnas.org/content/117/47/29561`.

[42] Vittorio Giovannetti, Seth Lloyd, and Lorenzo Maccone. Advances in quantum metrology. *Nature photonics*, 5(4):222, 2011.

[43] Zongping Gong, Yuto Ashida, Kohei Kawabata, Kazuaki Takasan, Sho Higashikawa, and Masahito Ueda. Topological phases of non-hermitian systems. *Phys. Rev. X*, 8 (3):031079, 2018. ISSN 2160-3308. doi:10.1103/PhysRevX.8.031079. URL `https://link.aps.org/doi/10.1103/PhysRevX.8.031079`.

[44] Ph Grangier and J-Ph Poizat. A simple quantum picture for the petermann excess noise factor. *The European Physical Journal D-Atomic, Molecular, Optical and Plasma Physics*, 1(1):97–104, 1998.

[45] Ryo Hanai and Peter B. Littlewood. Critical fluctuations at a many-body exceptional point. *Physical Review Research*, 2(3):033018, July 2020. doi:10.1103/physrevresearch.2.033018.

[46] Ryo Hanai, Alexander Edelman, Yoji Ohashi, and Peter B. Littlewood. Non-hermitian phase transition from a polariton bose-einstein condensate to a photon laser. *Physical Review Letters*, 122(18):185301, May 2019. doi:10.1103/physrevlett.122.185301.

[47] Ryo Hanai, Alexander McDonald, and Aashish Clerk. Intrinsic mechanisms for drive-dependent purcell decay in superconducting quantum circuits, 2021.

[48] Naomichi Hatano and David R. Nelson. Localization transitions in non-hermitian quantum mechanics. *Phys. Rev. Lett.*, 77:570–573, Jul 1996. doi:10.1103/PhysRevLett.77.570. URL `https://link.aps.org/doi/10.1103/PhysRevLett.77.570`.

[49] Naomichi Hatano and David R. Nelson. Vortex pinning and non-hermitian quantum mechanics. *Phys. Rev. B*, 56:8651–8673, Oct 1997. doi:10.1103/PhysRevB.56.8651. URL `https://link.aps.org/doi/10.1103/PhysRevB.56.8651`.

[50] W D Heiss. The physics of exceptional points. *J. Phys. A: Math. Theor.*, 45(44): 444016, October 2012.

[51] W D Heiss. The physics of exceptional points. *Journal of Physics A: Mathematical and Theoretical*, 45(44):444016, oct 2012. doi:10.1088/1751-8113/45/44/444016. URL `https://doi.org/10.1088%2F1751-8113%2F45%2F44%2F444016`.

[52] Loïc Herviou, Jens H. Bardarson, and Nicolas Regnault. Defining a bulk-edge correspondence for non-hermitian hamiltonians via singular-value decomposition. *Phys. Rev. A*, 99:052118, May 2019. doi:10.1103/PhysRevA.99.052118. URL `https://link.aps.org/doi/10.1103/PhysRevA.99.052118`.

[53] Loïc Herviou, Nicolas Regnault, and Jens H. Bardarson. Entanglement spectrum and symmetries in non-Hermitian fermionic non-interacting models. *SciPost Phys.*, 7:69, 2019. doi:10.21468/SciPostPhys.7.5.069. URL `https://scipost.org/10.21468/SciPostPhys.7.5.069`.

[54] Hossein Hodaei, Absar U. Hassan, Steffen Wittek, Hipolito Garcia-Gracia, Ramy El-Ganainy, Demetrios N. Christodoulides, and Mercedeh Khajavikhan. Enhanced sensitivity at higher-order exceptional points. *Nature*, 548(7666):187–191, 2017. ISSN 0028-0836, 1476-4687. doi:10.1038/nature23280. URL `http://www.nature.com/articles/nature23280`.

[55] G Y Hu and R F O'Connell. Analytical inversion of symmetric tridiagonal matrices. *Journal of Physics A: Mathematical and General*, 29(7):1511–1513, apr 1996. doi:10.1088/0305-4470/29/7/020.

[56] Andrea Insinga, Bjarne Andresen, Peter Salamon, and Ronnie Kosloff. Quantum heat engines: Limit cycles and exceptional points. *Phys. Rev. E*, 97:062153, Jun 2018. doi:10.1103/PhysRevE.97.062153. URL https://link.aps.org/doi/10.1103/PhysRevE.97.062153.

[57] Zhang Jiang. Quantum fisher information for states in exponential form. *Phys. Rev. A*, 89:032128, Mar 2014. doi:10.1103/PhysRevA.89.032128. URL https://link.aps.org/doi/10.1103/PhysRevA.89.032128.

[58] Alex Kamenev. *Field Theory of Non-Equilibrium Systems*. Cambridge University Press, 2011. doi:10.1017/CBO9781139003667.

[59] C. L. Kane and E. J. Mele. Quantum spin hall effect in graphene. *Phys. Rev. Lett.*, 95:226801, Nov 2005. doi:10.1103/PhysRevLett.95.226801. URL https://link.aps.org/doi/10.1103/PhysRevLett.95.226801.

[60] C. L. Kane and E. J. Mele. Z_2 topological order and the quantum spin hall effect. *Phys. Rev. Lett.*, 95:146802, Sep 2005. doi:10.1103/PhysRevLett.95.146802. URL https://link.aps.org/doi/10.1103/PhysRevLett.95.146802.

[61] Kohei Kawabata, Ken Shiozaki, Masahito Ueda, and Masatoshi Sato. Symmetry and topology in non-hermitian physics. *Phys. Rev. X*, 9:041015, Oct 2019. doi:10.1103/PhysRevX.9.041015. URL https://link.aps.org/doi/10.1103/PhysRevX.9.041015.

[62] Maximilian Keck, Davide Rossini, and Rosario Fazio. Persistent currents by reservoir engineering. *Phys. Rev. A*, 98:053812, Nov 2018. doi:10.1103/PhysRevA.98.053812. URL https://link.aps.org/doi/10.1103/PhysRevA.98.053812.

[63] Vladimir V. Konotop, Jianke Yang, and Dmitry A. Zezyulin. Nonlinear waves in $\mathcal{PT}$-symmetric systems. *Rev. Mod. Phys.*, 88:035002, Jul 2016. doi:10.1103/RevModPhys.88.035002. URL https://link.aps.org/doi/10.1103/RevModPhys.88.035002.

[64] Flore K. Kunst, Elisabet Edvardsson, Jan Carl Budich, and Emil J. Bergholtz. Biorthogonal bulk-boundary correspondence in non-hermitian systems. *Phys. Rev. Lett.*, 121:026808, Jul 2018. doi:10.1103/PhysRevLett.121.026808. URL https://link.aps.org/doi/10.1103/PhysRevLett.121.026808.

[65] C. Laflamme and A. A. Clerk. Weak qubit measurement with a nonlinear cavity: Beyond perturbation theory. *Phys. Rev. Lett.*, 109:123602, Sep 2012. doi:10.1103/PhysRevLett.109.123602. URL https://link.aps.org/doi/10.1103/PhysRevLett.109.123602.

[66] Yu-Hung Lai, Yu-Kun Lu, Myoung-Gyun Suh, Zhiquan Yuan, and Kerry Vahala. Observation of the exceptional-point-enhanced sagnac effect. *Nature*, 576(7785):65–69, 2019.

[67] W. Langbein. No exceptional precision of exceptional-point sensors. *Phys. Rev. A*, 98: 023805, Aug 2018. doi:10.1103/PhysRevA.98.023805. URL https://link.aps.org/doi/10.1103/PhysRevA.98.023805.

[68] Hoi-Kwan Lau and Aashish A Clerk. Fundamental limits and non-reciprocal approaches in non-hermitian quantum sensing. *Nature communications*, 9(1):1–13, 2018.

[69] Ching Hua Lee and Ronny Thomale. Anatomy of skin modes and topology in non-hermitian systems. *Phys. Rev. B*, 99:201103, May 2019. doi:10.1103/PhysRevB.99.201103. URL https://link.aps.org/doi/10.1103/PhysRevB.99.201103.

[70] Tony E. Lee. Anomalous edge state in a non-hermitian lattice. *Phys. Rev. Lett.*, 116 (13):133903, 2016. ISSN 0031-9007, 1079-7114. doi:10.1103/PhysRevLett.116.133903. URL https://link.aps.org/doi/10.1103/PhysRevLett.116.133903.

[71] Andy C. Y. Li, F. Petruccione, and Jens Koch. Perturbative approach to markovian open quantum systems. *Scientific Reports*, 4:48879, May 2014. doi:10.1038/srep04887. URL http://www.nature.com/articles/srep04887.

[72] Andy C. Y. Li, F. Petruccione, and Jens Koch. Resummation for nonequilibrium perturbation theory and application to open quantum lattices. *Phys. Rev. X*, 6:021037, Jun 2016. doi:10.1103/PhysRevX.6.021037. URL https://link.aps.org/doi/10.1103/PhysRevX.6.021037.

[73] Simon Lieu. Topological phases in the non-hermitian su-schrieffer-heeger model. *Phys. Rev. B*, 97:045106, Jan 2018. doi:10.1103/PhysRevB.97.045106. URL https://link.aps.org/doi/10.1103/PhysRevB.97.045106.

[74] Simon Lieu, Ron Belyansky, Jeremy T. Young, Rex Lundgren, Victor V. Albert, and Alexey V. Gorshkov. Symmetry breaking and error correction in open quantum systems. *Phys. Rev. Lett.*, 125:240405, Dec 2020. doi:10.1103/PhysRevLett.125.240405. URL https://link.aps.org/doi/10.1103/PhysRevLett.125.240405.

[75] Simon Lieu, Max McGinley, and Nigel R. Cooper. Tenfold way for quadratic lindbladians. *Phys. Rev. Lett.*, 124:040401, Jan 2020. doi:10.1103/PhysRevLett.124.040401. URL https://link.aps.org/doi/10.1103/PhysRevLett.124.040401.

[76] Simon Lieu, Max McGinley, Oles Shtanko, Nigel R. Cooper, and Alexey V. Gorshkov. Kramers' degeneracy for open systems in thermal equilibrium, 2021.

[77] G. Lindblad. On the generators of quantum dynamical semigroups. *Communications in Mathematical Physics*, 48(2), 1976.

[78] Seth Lloyd. Enhanced sensitivity of photodetection via quantum illumination. *Science*, 321(5895):1463–1465, 2008.

[79] Stefano Longhi. Unraveling the non-hermitian skin effect in dissipative systems. *Phys. Rev. B*, 102:201103, Nov 2020. doi:10.1103/PhysRevB.102.201103. URL https://link.aps.org/doi/10.1103/PhysRevB.102.201103.

[80] Joseph Maciejko, Taylor L. Hughes, and Shou-Cheng Zhang. The quantum spin hall effect. *Annual Review of Condensed Matter Physics*, 2(1):31–53, 2011. doi:10.1146/annurev-conmatphys-062910-140538. URL https://doi.org/10.1146/annurev-conmatphys-062910-140538.

[81] Daniel Malz and Andreas Nunnenkamp. Current rectification in a double quantum dot through fermionic reservoir engineering. *Phys. Rev. B*, 97:165308, Apr 2018. doi:10.1103/PhysRevB.97.165308. URL https://link.aps.org/doi/10.1103/PhysRevB.97.165308.

[82] V M Martinez Alvarez, J E Barrios Vargas, and L E F Foa Torres. Non-Hermitian robust edge states in one dimension: Anomalous localization and eigenspace condensation at exceptional points. *Phys. Rev. B.*, 97(12):121401, March 2018.

[83] Norifumi Matsumoto, Masaya Nakagawa, and Masahito Ueda. Embedding the yang-lee quantum criticality in open quantum systems. *arXiv:2012.13144*, 2020.

[84] A. McDonald and A. A. Clerk. Exact solutions of interacting dissipative systems via weak symmetries. *Phys. Rev. Lett.*, 128:033602, Jan 2022. doi:10.1103/PhysRevLett.128.033602. URL https://link.aps.org/doi/10.1103/PhysRevLett.128.033602.

[85] A. McDonald, T. Pereg-Barnea, and A. A. Clerk. Phase-dependent chiral transport and effective non-hermitian dynamics in a bosonic kitaev-majorana chain. *Phys. Rev. X*, 8:041031, Nov 2018. doi:10.1103/PhysRevX.8.041031. URL https://link.aps.org/doi/10.1103/PhysRevX.8.041031.

[86] A. McDonald, R. Hanai, and A. A. Clerk. Nonequilibrium stationary states of quantum non-hermitian lattice models. *Phys. Rev. B*, 105:064302, Feb 2022. doi:10.1103/PhysRevB.105.064302. URL https://link.aps.org/doi/10.1103/PhysRevB.105.064302.

[87] Alexander McDonald and Aashish A. Clerk. Exponentially-enhanced quantum sensing with non-hermitian lattice dynamics. *Nat. Commun.*, 11:5382, 2020. doi:10.1038/s41467-020-19090-4. URL https://www.nature.com/articles/s41467-020-19090-4.

[88] Mariya V. Medvedyeva, Fabian H. L. Essler, and Toma ž Prosen. Exact bethe ansatz spectrum of a tight-binding chain with dephasing noise. *Phys. Rev. Lett.*, 117:137202, Sep 2016. doi:10.1103/PhysRevLett.117.137202. URL https://link.aps.org/doi/10.1103/PhysRevLett.117.137202.

[89] A. Metelmann and A. A. Clerk. Nonreciprocal photon transmission and amplification via reservoir engineering. *Phys. Rev. X*, 5:021025, Jun 2015. doi:10.1103/PhysRevX.5.021025. URL https://link.aps.org/doi/10.1103/PhysRevX.5.021025.

[90] A. Metelmann and A. A. Clerk. Nonreciprocal photon transmission and amplification via reservoir engineering. *Phys. Rev. X*, 5:021025, Jun 2015. doi:10.1103/PhysRevX.5.021025. URL https://link.aps.org/doi/10.1103/PhysRevX.5.021025.

[91] A. Metelmann and A. A. Clerk. Nonreciprocal quantum interactions and devices via autonomous feedforward. *Phys. Rev. A*, 95:013837, Jan 2017. doi:10.1103/PhysRevA.95.013837. URL https://link.aps.org/doi/10.1103/PhysRevA.95.013837.

[92] A. Metelmann and H. E. Türeci. Nonreciprocal signal routing in an active quantum network. *Phys. Rev. A*, 97:043833, Apr 2018. doi:10.1103/PhysRevA.97.043833. URL https://link.aps.org/doi/10.1103/PhysRevA.97.043833.

[93] A. Metelmann and H. E. Türeci. Nonreciprocal signal routing in an active quantum network. *Phys. Rev. A*, 97:043833, Apr 2018. doi:10.1103/PhysRevA.97.043833. URL https://link.aps.org/doi/10.1103/PhysRevA.97.043833.

[94] Fabrizio Minganti, Alberto Biella, Nicola Bartolo, and Cristiano Ciuti. Spectral theory of liouvillians for dissipative phase transitions. *Phys. Rev. A*, 98:042118, Oct 2018. doi:10.1103/PhysRevA.98.042118. URL https://link.aps.org/doi/10.1103/PhysRevA.98.042118.

[95] Fabrizio Minganti, Adam Miranowicz, Ravindra W. Chhajlany, and Franco Nori. Quantum exceptional points of non-hermitian hamiltonians and liouvillians: The effects of quantum jumps. *Phys. Rev. A*, 100:062131, Dec 2019. doi:10.1103/PhysRevA.100.062131. URL https://link.aps.org/doi/10.1103/PhysRevA.100.062131.

[96] Fabrizio Minganti, Adam Miranowicz, Ravindra W. Chhajlany, and Franco Nori. Quantum exceptional points of non-hermitian hamiltonians and liouvillians: The effects of quantum jumps. *Phys. Rev. A*, 100:062131, Dec 2019. doi:10.1103/PhysRevA.100.062131. URL https://link.aps.org/doi/10.1103/PhysRevA.100.062131.

[97] M. Naghiloo, M. Abbasi, Yogesh N. Joglekar, and K. W. Murch. Quantum state tomography across the exceptional point in a single dissipative qubit. *Nat. Phys.*, 15(12):1232–1236, 2019. ISSN 1745-2473, 1745-2481. doi:10.1038/s41567-019-0652-z. URL http://www.nature.com/articles/s41567-019-0652-z.

[98] Masaya Nakagawa, Norio Kawakami, and Masahito Ueda. Non-hermitian kondo effect in ultracold alkaline-earth atoms. *Phys. Rev. Lett.*, 121:203001, Nov 2018.

doi:10.1103/PhysRevLett.121.203001. URL https://link.aps.org/doi/10.1103/PhysRevLett.121.203001.

[99] Masaya Nakagawa, Norio Kawakami, and Masahito Ueda. Exact liouvillian spectrum of a One-Dimensional dissipative hubbard model. *Phys. Rev. Lett.*, 126(11):110404, March 2021.

[100] Nobuyuki Okuma and Masatoshi Sato. Quantum anomaly, non-hermitian skin effects, and entanglement entropy in open systems. *arXiv:2011.08175*, 2020.

[101] Nobuyuki Okuma, Kohei Kawabata, Ken Shiozaki, and Masatoshi Sato. Topological origin of non-hermitian skin effects. *Phys. Rev. Lett.*, 124:086801, Feb 2020. doi:10.1103/PhysRevLett.124.086801. URL https://link.aps.org/doi/10.1103/PhysRevLett.124.086801.

[102] V. Peano, H. G. L. Schwefel, Ch. Marquardt, and F. Marquardt. Intracavity squeezing can enhance quantum-limited optomechanical position detection through deamplification. *Phys. Rev. Lett.*, 115:243603, Dec 2015. doi:10.1103/PhysRevLett.115.243603. URL https://link.aps.org/doi/10.1103/PhysRevLett.115.243603.

[103] V Peinová, V and A Luk. Exact quantum statistics of a nonlinear dissipative oscillator evolving from an arbitrary state. *Phys. Rev. A*, 41(1):414–420, January 1990.

[104] Michael Edward Peskin and Daniel V Schroeder. *An introduction to quantum field theory*. Addison-Wesley, Reading, Mass., 1995.

[105] Klaus Petermann. Calculated spontaneous emission factor for double-heterostructure injection lasers with gain-induced waveguiding. *IEEE Journal of Quantum Electronics*, 15(7):566–570, 1979.

[106] Luca Pezzè, Augusto Smerzi, Markus K. Oberthaler, Roman Schmied, and Philipp Treutlein. Quantum metrology with nonclassical states of atomic ensembles. *Rev. Mod. Phys.*, 90:035005, Sep 2018. doi:10.1103/RevModPhys.90.035005. URL https://link.aps.org/doi/10.1103/RevModPhys.90.035005.

[107] O. Pinel, P. Jian, N. Treps, C. Fabre, and D. Braun. Quantum parameter estimation using general single-mode gaussian states. *Phys. Rev. A*, 88:040102, Oct 2013. doi:10.1103/PhysRevA.88.040102. URL https://link.aps.org/doi/10.1103/PhysRevA.88.040102.

[108] Olivier Pinel, Julien Fade, Daniel Braun, Pu Jian, Nicolas Treps, and Claude Fabre. Ultimate sensitivity of precision measurements with intense gaussian quantum light: A multimodal approach. *Phys. Rev. A*, 85:010101, Jan 2012. doi:10.1103/PhysRevA.85.010101. URL https://link.aps.org/doi/10.1103/PhysRevA.85.010101.

[109] M. B. Plenio and P. L. Knight. The quantum-jump approach to dissipative dynamics in quantum optics. *Rev. Mod. Phys.*, 70:101–144, Jan 1998. doi:10.1103/RevModPhys.70.101. URL https://link.aps.org/doi/10.1103/RevModPhys.70.101.

[110] M. B. Plenio and P. L. Knight. The quantum-jump approach to dissipative dynamics in quantum optics. *Rev. Mod. Phys.*, 70:101–144, Jan 1998. doi:10.1103/RevModPhys.70.101. URL https://link.aps.org/doi/10.1103/RevModPhys.70.101.

[111] Vladislav Popkov and Carlo Presilla. Full spectrum of the liouvillian of open dissipative quantum systems in the zeno limit. *Phys. Rev. Lett.*, 126(19):190402, May 2021.

[112] Tomaž Prosen. Third quantization: a general method to solve master equations for quadratic open fermi systems. *New J. Phys.*, 10(4):043026, apr 2008. doi:10.1088/1367-2630/10/4/043026. URL https://doi.org/10.1088/1367-2630/10/4/043026.

[113] Tomaž Prosen and Thomas H Seligman. Quantization over boson operator spaces. *J. Phys. A: Math. Theor.*, 43(39):392004, sep 2010. doi:10.1088/1751-8113/43/39/392004. URL https://doi.org/10.1088/1751-8113/43/39/392004.

[114] David Roberts and Aashish A. Clerk. Driven-dissipative quantum kerr resonators: New exact solutions, photon blockade and quantum bistability. *Phys. Rev. X*, 10:021022, Apr 2020. doi:10.1103/PhysRevX.10.021022. URL https://link.aps.org/doi/10.1103/PhysRevX.10.021022.

[115] David Roberts, Andrew Lingenfelter, and A.A. Clerk. Hidden time-reversal symmetry, quantum detailed balance and exact solutions of driven-dissipative quantum systems. *PRX Quantum*, 2:020336, Jun 2021. doi:10.1103/PRXQuantum.2.020336. URL https://link.aps.org/doi/10.1103/PRXQuantum.2.020336.

[116] Suropriya Saha, Jaime Agudo-Canalejo, and Ramin Golestanian. Scalar active mixtures: The nonreciprocal cahn-hilliard model. *Phys. Rev. X*, 10:041009, August 2020. doi:10.1103/PhysRevX.10.041009. URL https://link.aps.org/doi/10.1103/PhysRevX.10.041009.

[117] Orazio Scarlatella, Aashish A Clerk, and Marco Schiro. Spectral functions and negative density of states of a driven-dissipative nonlinear quantum resonator. *New J. Phys.*, 21(4):043040, April 2019.

[118] Colin Scheibner, William T. M. Irvine, and Vincenzo Vitelli. Non-hermitian band topology and skin modes in active elastic media. *Phys. Rev. Lett.*, 125:118001, Sep 2020. doi:10.1103/PhysRevLett.125.118001. URL https://link.aps.org/doi/10.1103/PhysRevLett.125.118001.

[119] Colin Scheibner, Anton Souslov, Debarghya Banerjee, Piotr Surówka, William T. M. Irvine, and Vincenzo Vitelli. Odd elasticity. *Nat. Phys.*, 16:475–480, March 2020. doi:10.1038/s41567-020-0795-y.

[120] Henning Schomerus. Nonreciprocal response theory of non-hermitian mechanical metamaterials: Response phase transition from the skin effect of zero modes. *Phys. Rev. Research*, 2:013058, Jan 2020. doi:10.1103/PhysRevResearch.2.013058. URL https://link.aps.org/doi/10.1103/PhysRevResearch.2.013058.

[121] Matteo Seclì, Massimo Capone, and Marco Schirò. Signatures of self-trapping in the driven-dissipative Bose–Hubbard dimer. *New J. Phys.*, 23(6):063056, June 2021.

[122] Matteo Seclì, Massimo Capone, and Marco Schirò. Signatures of self-trapping in the driven-dissipative bose–hubbard dimer. *New Journal of Physics*, 23(6):063056, jun 2021. doi:10.1088/1367-2630/ac04c8. URL https://doi.org/10.1088/1367-2630/ac04c8.

[123] Naoyuki Shibata and Hosho Katsura. Dissipative quantum ising chain as a non-hermitian ashkin-teller model. *Phys. Rev. B*, 99:224432, Jun 2019. doi:10.1103/PhysRevB.99.224432. URL https://link.aps.org/doi/10.1103/PhysRevB.99.224432.

[124] Naoyuki Shibata and Hosho Katsura. Dissipative spin chain as a non-hermitian kitaev ladder. *Phys. Rev. B*, 99:174303, May 2019. doi:10.1103/PhysRevB.99.174303. URL https://link.aps.org/doi/10.1103/PhysRevB.99.174303.

[125] L. M. Sieberer, S. D. Huber, E. Altman, and S. Diehl. Dynamical critical phenomena in driven-dissipative systems. *Physical Review Letters*, 110(19):195301, may 2013. doi:10.1103/physrevlett.110.195301.

[126] L M Sieberer, M Buchhold, and S Diehl. Keldysh field theory for driven open quantum systems. *Rep. Prog. Phys.*, 79(9):096001, September 2016.

[127] Kazuki Sone, Yuto Ashida, and Takahiro Sagawa. Exceptional non-hermitian topological edge mode and its application to active matter. *Nat. Commun.*, 11:5745, Nov 2020. doi:10.1038/s41467-020-19488-0. URL http://www.nature.com/articles/s41467-020-19488-0.

[128] Fei Song, Shunyu Yao, and Zhong Wang. Non-hermitian skin effect and chiral damping in open quantum systems. *Phys. Rev. Lett.*, 123:170401, Oct 2019. doi:10.1103/PhysRevLett.123.170401. URL https://link.aps.org/doi/10.1103/PhysRevLett.123.170401.

[129] K Stannigel, P Rabl, and P Zoller. Driven-dissipative preparation of entangled states in cascaded quantum-optical networks. *New Journal of Physics*, 14(6):063014, jun 2012. doi:10.1088/1367-2630/14/6/063014. URL https://doi.org/10.1088/1367-2630/14/6/063014.

[130] M. H. Szymańska, J. Keeling, and P. B. Littlewood. Nonequilibrium quantum condensation in an incoherently pumped dissipative system. *Phys. Rev. Lett.*, 96:230602, june 2006. doi:10.1103/PhysRevLett.96.230602.

[131] Si-Hui Tan, Baris I. Erkmen, Vittorio Giovannetti, Saikat Guha, Seth Lloyd, Lorenzo Maccone, Stefano Pirandola, and Jeffrey H. Shapiro. Quantum illumination with gaussian states. *Phys. Rev. Lett.*, 101:253601, Dec 2008. doi:10.1103/PhysRevLett.101.253601. URL https://link.aps.org/doi/10.1103/PhysRevLett.101.253601.

[132] Juan Mauricio Torres. Closed-form solution of lindblad master equations without gain. *Phys. Rev. A*, 89:052133, May 2014. doi:10.1103/PhysRevA.89.052133. URL https://link.aps.org/doi/10.1103/PhysRevA.89.052133.

[133] Luis E F Foa Torres and Luis E Foa. Perspective on topological states of non-hermitian lattices. *JPhys: Materials*, 3(1):014002, 2019.

[134] M. Tse et al. Quantum-enhanced advanced ligo detectors in the era of gravitational-wave astronomy. *Phys. Rev. Lett.*, 123:231107, Dec 2019. doi:10.1103/PhysRevLett.123.231107. URL https://link.aps.org/doi/10.1103/PhysRevLett.123.231107.

[135] F. Vollmer, S. Arnold, and D. Keng. Single virus detection from the reactive shift of a whispering-gallery mode. *PNAS*, 105(52):20701–20704, 2008. ISSN 0027-8424. doi:10.1073/pnas.0808988106. URL https://www.pnas.org/content/105/52/20701.

[136] Yu-Xin Wang and A. A. Clerk. Non-hermitian dynamics without dissipation in quantum systems. *Phys. Rev. A*, 99:063834, Jun 2019. doi:10.1103/PhysRevA.99.063834. URL https://link.aps.org/doi/10.1103/PhysRevA.99.063834.

[137] Clara C Wanjura, Matteo Brunelli, and Andreas Nunnenkamp. Topological framework for directional amplification in driven-dissipative cavity arrays. *arXiv:1909.11647*, 2019.

[138] Jan Wiersig. Enhancing the sensitivity of frequency and energy splitting detection by using exceptional points: Application to microcavity sensors for single-particle detection. *Phys. Rev. Lett.*, 112:203901, May 2014. doi:10.1103/PhysRevLett.112.203901. URL https://link.aps.org/doi/10.1103/PhysRevLett.112.203901.

[139] Howard M Wiseman and Gerard J Milburn. *Quantum measurement and control*. Cambridge university press, 2009.

[140] Zhicheng Xiao, Huanan Li, Tsampikos Kottos, and Andrea Alù. Enhanced sensing and nondegraded thermal noise performance based on $\mathcal{PT}$-symmetric electronic circuits with a sixth-order exceptional point. *Phys. Rev. Lett.*, 123:213901, Nov 2019. doi:10.1103/PhysRevLett.123.213901. URL https://link.aps.org/doi/10.1103/PhysRevLett.123.213901.

[141] Ye Xiong. Why does bulk boundary correspondence fail in some non-hermitian topological models. *Journal of Physics Communications*, 2(3):035043, 2018. URL http://stacks.iop.org/2399-6528/2/i=3/a=035043.

[142] Kazuki Yamamoto, Masaya Nakagawa, Kyosuke Adachi, Kazuaki Takasan, Masahito Ueda, and Norio Kawakami. Theory of non-hermitian fermionic superfluidity with a complex-valued interaction. *Phys. Rev. Lett.*, 123:123601, Sep 2019. doi:10.1103/PhysRevLett.123.123601. URL https://link.aps.org/doi/10.1103/PhysRevLett.123.123601.

[143] Kazuki Yamamoto, Yuto Ashida, and Norio Kawakami. Rectification in nonequilibrium steady states of open many-body systems. *Phys. Rev. Research*, 2:043343, Dec 2020. doi:10.1103/PhysRevResearch.2.043343. URL https://link.aps.org/doi/10.1103/PhysRevResearch.2.043343.

[144] Lisa Yamauchi, Tomoya Hayata, Masahito Uwamichi, Tomoki Ozawa, and Kyogo Kawaguchi. Chirality-driven edge flow and non-hermitian topology in active nematic cells, 2020.

[145] Shunyu Yao and Zhong Wang. Edge states and topological invariants of non-hermitian systems. *Phys. Rev. Lett.*, 121(8):086803, 2018. ISSN 0031-9007, 1079-7114. doi:10.1103/PhysRevLett.121.086803. URL https://link.aps.org/doi/10.1103/PhysRevLett.121.086803.

[146] Shunyu Yao, Fei Song, and Zhong Wang. Non-hermitian chern bands. *Phys. Rev. Lett.*, 121:136802, Sep 2018. doi:10.1103/PhysRevLett.121.136802. URL https://link.aps.org/doi/10.1103/PhysRevLett.121.136802.

[147] Zhihong You, Aparna Baskaran, and M. Cristina Marchetti. Nonreciprocity as a generic route to traveling states. *Proceedings of the National Academy of Sciences*, 117(33): 19767–19772, 2020. ISSN 0027-8424. doi:10.1073/pnas.2010318117. URL http://www.pnas.org/lookup/doi/10.1073/pnas.2010318117.

[148] Mengzhen Zhang, William Sweeney, Chia Wei Hsu, Lan Yang, A. D. Stone, and Liang Jiang. Quantum noise theory of exceptional point amplifying sensors. *Phys. Rev. Lett.*, 123:180501, Oct 2019. doi:10.1103/PhysRevLett.123.180501. URL https://link.aps.org/doi/10.1103/PhysRevLett.123.180501.

[149] Zh Zhang, J Tindall, J Mur-Petit, D Jaksch, and B Buča. Stationary state degeneracy of open quantum systems with non-abelian symmetries. *J. Phys. A: Math. Theor.*, 53 (21):215304, May 2020.

[150] Quntao Zhuang, Zheshen Zhang, and Jeffrey H. Shapiro. Distributed quantum sensing using continuous-variable multipartite entanglement. *Phys. Rev. A*, 97:032329, Mar 2018. doi:10.1103/PhysRevA.97.032329. URL https://link.aps.org/doi/10.1103/PhysRevA.97.032329.